



저작자표시-비영리-변경금지 2.0 대한민국

이용자는 아래의 조건을 따르는 경우에 한하여 자유롭게

- 이 저작물을 복제, 배포, 전송, 전시, 공연 및 방송할 수 있습니다.

다음과 같은 조건을 따라야 합니다:



저작자표시. 귀하는 원저작자를 표시하여야 합니다.



비영리. 귀하는 이 저작물을 영리 목적으로 이용할 수 없습니다.



변경금지. 귀하는 이 저작물을 개작, 변형 또는 가공할 수 없습니다.

- 귀하는, 이 저작물의 재이용이나 배포의 경우, 이 저작물에 적용된 이용허락조건을 명확하게 나타내어야 합니다.
- 저작권자로부터 별도의 허가를 받으면 이러한 조건들은 적용되지 않습니다.

저작권법에 따른 이용자의 권리는 위의 내용에 의하여 영향을 받지 않습니다.

이것은 [이용허락규약\(Legal Code\)](#)을 이해하기 쉽게 요약한 것입니다.

[Disclaimer](#)

Doctor of Philosophy

**Glycerol carbonation with urea over Zn-containing
mixed oxide catalysts**

The Graduate School of the University of Ulsan

Department of Chemical Engineering and

Bioengineering

Huy Nguyen-Phu

Glycerol carbonation with urea over Zn-containing mixed oxide catalysts

Advisor: Professor Eun Woo Shin

A Dissertation

Submitted to

The Graduate School of the University of Ulsan

In partial Fulfillment of the Requirements

for the Degree of

Doctor of philosophy

By

Huy Nguyen-Phu

Department of Chemical Engineering and Bioengineering

Ulsan, South Korea

November 2019

Glycerol carbonation with urea over Zn-containing mixed oxide catalysts

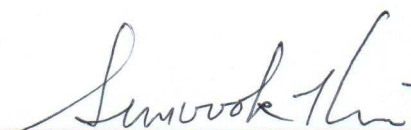
The dissertation of Huy Nguyen-Phu was reviewed
and approved by the following:



Committee Chair Prof. Sung Gu Kang



Committee Vice-chair Prof. Eun Woo Shin



Committee Member Prof. Sunwook Kim



Committee Member Prof. Jung Kyoo Lee



Committee Member Prof. Jeong-Myeong Ha

Department of Chemical Engineering and Bioengineering

Ulsan, South Korea

November 2019

ABSTRACT

In this millennium, climate change is one of the biggest challenges of the human's future. The major aspect of the current climate change is global warming which is the result of human activities. The most influence activity of humans is the emission of greenhouse gas including the carbon dioxide (CO_2) by the burning of fossil fuel. If humans do not have effective actions to control the problem, the impact of climate change can be extended not just in this century but also in the next 10 millennia more. Replacing conventional fossil fuel by other renewable energy (including biofuel, biodiesel) is recognized as a solution to mitigate the impact of climate change. However, one problem of biodiesel is its byproduct- glycerol which is abundant and needs to be converted to a value-added product. In this thesis, I focus on preparing the catalysts for the reaction of glycerol and urea to glycerol carbonate; and investigating the catalysis mechanism of the reaction.

Catalytic conversion to glycerol carbonate (GC) from glycerol and urea was investigated with Zn/Al catalysts supported by activated red mud (ARM), a waste material. Compared to an unsupported catalyst, ARM-supported Zn/Al catalysts exhibited higher GC yields. ARM-supported Zn/Al catalysts showed a volcano curve for the GC yield as a function of the Zn/Al loading. FTIR analysis revealed the ARM-supported Zn/Al catalysts to be more selective, resulting in higher GC yield. The balance of active sites from ARM and Zn/Al was related to rates of each reaction step in GC synthesis, which eventually influenced the selectivity and yield of GC.

In the second research, we prepared ZnO, ZnAl_2O_4 , and ZnAl mixed oxides with different metal molar ratios and applied them for synthesizing glycerol carbonate (GC) from glycerol and urea. The reaction routes related to the Zn species over the ZnAl mixed oxides were investigated. The ZnAl mixed oxides were found to consist of two Zn crystalline phases: ZnO

and ZnAl_2O_4 . From the reaction results, the ZnAl mixed oxides showed much higher glycerol conversion and GC yield than the ZnO and ZnAl_2O_4 . During the reaction, the dissolution of the Zn species from the ZnO phase over the ZnAl mixed oxides was observed while the ZnAl_2O_4 phase remained insoluble. The ZnO phase provided a homogeneous reaction route *via* the dissolved Zn species, resulting in the formation of a Zn complex containing the isocyanate (NCO) and zinc glycerolate. In contrast, the insoluble ZnAl_2O_4 phase was responsible for not only a heterogeneous reaction route, but also adsorption of the Zn NCO complex on the catalyst. We proposed that the adsorbed Zn NCO complex could play a role as an active site for an additional heterogeneous reaction route. Therefore, the ZnAl mixed oxides exhibited high GC yields through the dual catalysis routes: the homogeneous reaction route over the ZnO phase and the heterogeneous reaction route over the ZnAl_2O_4 phase.

To understand the reaction mechanism, two different Zn-based catalysts - ZnO, and ZnAl mixed oxide (ZnAlO or Zn_7Al_3) - were employed to investigate Zn-phase-dependent catalysis in the reaction of glycerol with urea as a function of reaction times. Zn_7Al_3 catalyst exhibited higher selectivity and yield of glycerol carbonate (GC) over a wide range of glycerol conversion than the ZnO catalyst. The time-dependent Zn species and reaction intermediates were observed in the solid and liquid phases at various reaction times through FTIR and XRD measurements in order to understand Zn-containing intermediates and corresponding reaction routes over each catalyst. The low GC selectivity in the reaction over the ZnO catalyst was closely connected to the formation of zinc glycerolate (ZnGly) in the solid phase. For the ZnO catalyst, ZnGly was formed in the solid phase even at an initial reaction time by the reaction between Zn NCO complex and glycerol, resulting in the loss of GC selectivity. Alternatively, over a Zn_7Al_3 catalyst, the formation of the Zn isocyanate (NCO) complex was dominant up to 2 hr of reaction time in both the liquid and solid phases. After 2 hr of reaction time, ZnGly was observed in the spent Zn_7Al_3 catalyst along with decreasing GC selectivity. The relative

formation rates of Zn-containing reaction intermediates (ZnGly and Zn NCO complex) over the Zn_7Al_3 catalyst were affected by the Zn phases over the solid catalysts and the ratio of urea to glycerol in the liquid phase during the reaction time.

The effect of a disordered $ZnAl_2O_4$ spinel structure on the reaction of glycerol with urea was investigated with pure $ZnAl_2O_4$ (c- $ZnAl_2O_4$) and ZnAl mixed oxide (c- $ZnAlO$) prepared by a citrate complex method, and ZnAl physically mixed oxide (p- $ZnAlO$). During catalysts preparation, a disordered bulk $ZnAl_2O_4$ phase generated disordered sites on the surface: the Al^{3+} cations substituting for Zn^{2+} cations at the tetrahedral sites, and the surface oxygen vacancy corresponding to the Zn^{2+} cations substituting for Al^{3+} cations at the octahedral sites. The disordered surface sites increased in order of p- $ZnAlO$ < c- $ZnAlO$ < c- $ZnAl_2O_4$, which was proportional to the surface acidity. c- $ZnAlO$ exhibited the best reaction performance due to the existence of a solid zinc isocyanate (Zn NCO) complex on the disordered sites. Here, we proposed that the solid Zn NCO complex preferentially generated glycerol carbonate (GC), while the liquid Zn NCO complex produced both GC and zinc glycerolate.

Finally, we investigated the glycerolysis of urea over various ZnMeO (Me = Co, Cr, and Fe) mixed oxide catalysts. ZnMeO mixed oxide catalysts were prepared by a co-precipitation method for two Zn/Me ratios, resulting in Zn-rich mixed oxide (Zn_2MeO) and Zn-poor mixed oxide ($ZnMe_2O$). In the glycerolysis of urea, the Zn_2MeO catalysts exhibited higher glycerol conversion and glycerol carbonate yields than the $ZnMe_2O$ catalysts due to the predominance of homogeneous catalysis through Zn isocyanate (NCO) complexes from the Zn_2MeO catalysts. Specifically, Zn_2CrO was the best catalyst, with the highest yield of glycerol carbonate. Fourier transform infrared (FT-IR) and thermogravimetric analysis (TGA) results of the spent catalysts clearly demonstrated the dominant formation of a solid Zn NCO complex over the spent Zn_2CrO catalyst, a unique feature indicating that the better catalytic performance

of Zn_2CrO was due to the additional heterogeneous reaction route through the solid Zn NCO complex.

ACKNOWLEDGMENTS

I would like to send my deep appreciation to my advisor, Professor Eun Woo Shin who helps me with his invaluable constructions during the scheduling, implementing and developing of this research work as well as the preparation of all manuscripts for publication.

I would like to thank all members of my committee, Professor Sung Gu Kang, Professor Sunwook Kim, Professor Jung Kyoo Lee, Professor Jeong-Myeong Ha, for spending their valuable time to review this dissertation and contribute useful recommendations to this research.

I wish to thank all my former and present lab mates, Dr. Chinh Nguyen-Huy, Dr. Thanh Truc Pham, Lien Do-Thi, Chan-Yi Park, Haewon Jung, Hongyan Yu, Kaiming Jiang, Kim Anh Nguyen Thi, Wang Mingyan, Dao Duc Quang for all their cooperation and their help during my study. Special thanks should be given to Ms. Kyong Cho Lim for her assistance to help me use the analysis instruments in the department. And, I also want to thank all office staff in the department for their support in the administration jobs.

Finally, I would like to express my deep gratitude to my family, my mother, my father and my brother who always have encouraged and believed me throughout my study course. Specials thanks should be given to my beloved wife, Lien Do-Thi, a person who spends her love, care, advice, and helps to me by heart. She shares with me every happiness and always beside me in the most difficult moments. That helps me have full energy to complete my integrated Master and Ph.D. course at University of Ulsan.

“If I have seen further it is by standing on the shoulders of Giants.”

- Isaac Newton-

TABLE OF CONTENTS

ABSTRACT.....	i
ACKNOWLEDGMENTS	v
TABLE OF CONTENTS	vi
LIST OF FIGURES	ix
LIST OF SCHEMES	xii
LIST OF TABLES	xiii
NOMENCLATURES	xiv
CHAPTER 1. INTRODUCTION	1
1.1. Background and motivation	1
1.2. Research objectives	9
1.3. Outline of the dissertation	11
CHAPTER 2. OBSERVE THE ACTIVATION OF RED MUD-SUPPORTED ZN/AL CATALYSTS ON THE REACTION STEPS OF THE GLYCEROLYSIS OF UREA..	13
2.1. Introduction	13
2.2. Experimental.....	13
2.2.1. Catalyst preparation	13
2.2.2. Reaction tests	14
2.2.3. Catalyst characterization.....	15
2.3. Results and discussion.....	15
2.3.1. Catalyst characterization.....	15
2.3.2. Catalyst reaction activity	19
2.4. Conclusion.....	25
CHAPTER 3. INVESTIGATE THE ROLE OF ZNO PHASE AND ZN ₂ AL ₂ O ₄ PHASE IN ZN/AL MIXED OXIDE CATALYSTS TO THE DUAL REACTION ROUTE (HOMOGENEOUS AND HETEROGENEOUS) OF THE GLYCEROLYSIS OF UREA. INVESTIGATE TIME-DEPENDENT ZN SPECIES - THEIR ROLES IN THE REACTION MECHANISM.	27
3.1. Introduction	27
3.2. Experimental.....	28
3.2.1. Catalyst preparation	28
3.2.2. Reaction test.....	29
3.2.3. Catalyst characterization.....	29
3.3. Results and discussion.....	30
3.3.1. Catalyst characterization.....	30

3.3.2.	<i>Catalytic tests</i>	37
a.	<i>The catalytic reaction test results for the Zn/Al mixed oxide catalysts in different ratio of Zn:Al</i>	37
b.	<i>The catalytic reaction test results for the Zn/Al mixed oxide catalysts in different reaction time</i>	40
3.3.3.	<i>Analysis of the Zn species by XRD and FTIR measurements</i>	43
3.3.4.	<i>Effect of the ZnO and ZnAl₂O₄ phases in dual catalysis</i>	51
3.3.5.	<i>Characterizations of spent catalysts and liquid products</i>	53
3.3.6.	<i>Evolution of Zn-containing reaction intermediates as a function of the reaction time and their roles in the catalytic reaction routes</i>	61
3.4.	Conclusion	71
CHAPTER 4. INVESTIGATE THE EFFECT OF DISORDERED SPINEL ZNAL₂O₄ PHASE TO THE ACIDITY AND THE GLYCEROLYSIS OF UREA		73
4.1.	Introduction	73
4.2.	Experimental	74
4.2.1.	<i>Catalyst preparation</i>	74
4.2.2.	<i>Reaction test</i>	75
4.2.3.	<i>Catalyst characterization</i>	76
4.3.	Results and discussion	76
4.3.1.	<i>Interactions between the ZnO and ZnAl₂O₄ phases - the disordered ZnAl₂O₄ spinel lattice</i>	76
4.3.2.	<i>Relationship between the disordered spinel structure and the surface acidity</i>	88
4.3.3.	<i>Reaction performance over the catalysts</i>	92
4.3.4.	<i>Catalytic reaction routes through Zn NCO complexes</i>	102
4.4.	Conclusion	109
CHAPTER 5. INVESTIGATION OF GLYCEROLYSIS OF UREA OVER VARIOUS ZNMEO (ME = CO, CR, AND FE) MIXED OXIDE CATALYSTS		110
5.1.	Introduction	110
5.2.	Experimental	111
5.2.1.	<i>Catalyst preparation</i>	111
5.2.2.	<i>Reaction tests</i>	111
5.2.3.	<i>Catalyst characterization</i>	111
5.3.	Results and discussion	112
5.3.1.	<i>Catalyst characterization: ZnO phase and ZnMe₂O₄ spinel phase</i>	112

5.3.2. <i>Glycerolysis of urea over various ZnMeO catalysts: the formation of Zn isocyanate complex in the liquid phase and on the solid catalysts</i>	119
5.3.3. <i>Catalytic reaction routes through different NCO complexes</i>	131
5.4. Conclusion	133
CHAPTER 6. SUMMARY AND RECOMMENDATIONS FOR FUTURE WORK ...	134
6.1. Summary	134
6.2. Recommendations for future work	135
REFERENCES	137
LIST OF PUBLICATIONS	145

LIST OF FIGURES

Fig. 1- 1. U.S. Biodiesel & Renewable diesel market	2
Fig. 1- 2. Worldwide use of vegetable oil for biofuel production	3
Fig. 1- 3. Projection of global glycerol production and prices.	4
Fig. 1- 4. Number of publications on glycerol carbonate in the period 2001–2017 (from Web of Science).	4
Fig. 1- 5. The sketch of the reactor system	9
Fig. 1- 6. The structure of the thesis corresponding to the objectives	12
Fig. 2- 1. N ₂ adsorption-desorption isotherms of a) ARM, b)5%-Zn ₇ Al ₃ O _x /ARM, c)25%-Zn ₇ Al ₃ O _x /ARM, d)40%-Zn ₇ Al ₃ O _x /ARM, e)50%-Zn ₇ Al ₃ O _x ARM, f)60%-Zn ₇ Al ₃ O _x /ARM and g) Zn ₇ Al ₃ O _x	17
Fig. 2- 2. XRD patterns of a) ARM, b)5%-Zn ₇ Al ₃ O _x /ARM, c)25%-Zn ₇ Al ₃ O _x /ARM, d)40%-Zn ₇ Al ₃ O _x /ARM, e)50%-Zn ₇ Al ₃ O _x ARM, f)60%-Zn ₇ Al ₃ O _x /ARM and g) Zn ₇ Al ₃ O _x	18
Fig. 2- 3. SEM images of a) ARM, b) 5%-Zn ₇ Al ₃ O _x /ARM, c) 40%-Zn ₇ Al ₃ O _x /ARM, d) 50%-Zn ₇ Al ₃ O _x /ARM, e) 60%-Zn ₇ Al ₃ O _x /ARM and f) Zn ₇ Al ₃ O _x	19
Fig. 2- 4. Typical gas chromatography graph, (2): 2,3-dihydroxypropyl carbamate, (4): 4-(hydroxymethyl) oxazolidin-2-one, (5): (2-oxo-1,3-dioxolan-4-yl) methyl carbamate.	20
Fig. 2- 5. GC yield as a function of Zn/Al loading amounts. (Reaction conditions: Glycerol/urea molar ratio = 1, P = 3kPa, T = 140°C, 5 wt.% catalyst (of glycerol), at 5h of reaction time.)	22
Fig. 2- 6. FTIR spectra of a) glycerol, b) urea, c) product with catalyst Zn ₇ Al ₃ , d) product with catalyst ARM, e) product with catalyst 5%-Zn ₇ Al ₃ O _x /ARM, f) product with catalyst 25%-Zn ₇ Al ₃ O _x /ARM, g) product with catalyst 40%-Zn ₇ Al ₃ O _x /ARM, h) product with catalyst 50%-Zn ₇ Al ₃ O _x /ARM, and i) product with catalyst 60%-Zn ₇ Al ₃ O _x /ARM.....	23
Fig. 2- 7. Byproducts selectivity calculated from gas chromatography peak area, (2): 2,3-dihydroxypropyl carbamate, (4): 4-(hydroxymethyl) oxazolidin-2-one, (5): (2-oxo-1,3-dioxolan-4-yl)methyl carbamate.....	25
Fig. 3- 1. FE-SEM images of fresh ZnAl mixed oxide catalysts. a) Zn ₆ Al ₄ b) Zn ₇ Al ₃ , c) Zn ₈ Al ₂	33
Fig. 3- 2. N ₂ adsorption-desorption isotherms for the prepared catalysts. a) ZnAl ₂ O ₄ , b) Zn ₆ Al ₄ , c) Zn ₇ Al ₃ , d) Zn ₈ Al ₂ , e) co- Zn ₇ Al ₃ and f) ZnO.....	34
Fig. 3- 3. XRD patterns of fresh catalysts: a) ZnAl ₂ O ₄ , b) Zn ₆ Al ₄ , c) Zn ₇ Al ₃ , d) Zn ₈ Al ₂ , e) co-Zn ₇ Al ₃ and f) ZnO.....	34
Fig. 3- 4. CO ₂ -TPD profiles for the prepared catalysts.....	35
Fig. 3- 5. NH ₃ -TPD profiles for the prepared catalysts.	35
Fig. 3- 6. A) XRD patterns, B) N ₂ adsorption-desorption isotherms curves, C) NH ₃ -TPD profiles and D) CO ₂ -TPD profiles of fresh ZnO and Zn ₇ Al ₃ catalysts.....	37
Fig. 3- 7. Glycerol carbonate (GC) selectivity as a function of the glycerol conversion for ZnO and Zn ₇ Al ₃ catalysts.....	42
Fig. 3- 8. XRD patterns of spent catalysts: a) ZnAl ₂ O ₄ , b) Zn ₆ Al ₄ , c) Zn ₇ Al ₃ , d) Zn ₈ Al ₂ , e) co-Zn ₇ Al ₃ and f) ZnO.....	44
Fig. 3- 9. Trend of the XRD peak ratio ZnO/ZnAl ₂ O ₄ in the fresh catalyst and the relative intensity of the zinc glycerolate XRD peak (011) in the spent catalyst (normalized with Zn ₇ Al ₃)	44

Fig. 3- 10. DTGA profiles of the spent catalysts after 3h reaction. a) $ZnAl_2O_4$, b) Zn_6Al_4 , c) Zn_7Al_3 , d) Zn_8Al_2 , e) co- Zn_7Al_3 and f) ZnO	45
Fig. 3- 11. Enlarged XRD patterns of each catalyst: (a) Zn_6Al_4 -fresh, (b) Zn_6Al_4 -spent, (c) Zn_7Al_3 -fresh, (d) Zn_7Al_3 -spent (e) Zn_8Al_2 -fresh, and (f) Zn_8Al_2 -spent.	46
Fig. 3- 12. FTIR spectra of the liquid products obtained from the carbonylation of glycerol with urea over different catalysts: a) $ZnAl_2O_4$, b) Zn_6Al_4 , c) Zn_7Al_3 , d) Zn_8Al_2 , e) co- Zn_7Al_3 and f) ZnO	47
Fig. 3- 13. FTIR spectra of the spent catalysts: (a) $ZnAl_2O_4$, b) Zn_6Al_4 , c) Zn_7Al_3 , d) Zn_8Al_2 , e) co- Zn_7Al_3 and f) ZnO	48
Fig. 3- 14. A) The trend of the intensity ratio of the NCO/ $ZnGly$ FTIR peak in the spent catalyst and the NCO FTIR peak intensity in the liquid product, and B) trend of the XRD peak ratio $ZnO/ZnAl_2O_4$ in the fresh catalyst and the intensity ratio of the NCO/ $ZnGly$ FTIR peak in the spent catalyst.	50
Fig. 3- 15. XRD patterns of fresh and spent catalysts run at the different reaction time: a) $t = 0$ hr (fresh), b) $t = 0.25$ hr, c) $0.5 t =$ hr, d) $t = 1$ hr, e) $t = 2$ hr, f) $t = 3$ hr, and g) $t = 4$ hr. ZnO catalyst (A) and Zn_7Al_3 catalyst (B).	55
Fig. 3- 16. FTIR spectra of fresh and spent catalysts run at the different reaction time: a) $t = 0$ hr (fresh), b) $t = 0.25$ hr, c) $0.5 t =$ hr, d) $t = 1$ hr, e) $t = 2$ hr, f) $t = 3$ hr, and g) $t = 4$ hr. ZnO catalyst (A) and Zn_7Al_3 catalyst (B).	58
Fig. 3- 17. DTGA patterns of spent catalysts run at the different reaction time: a) $t = 0.25$ hr, b) $0.5 t =$ hr, c) $t = 1$ hr, d) $t = 2$ hr, e) $t = 3$ hr, and f) $t = 4$ hr. ZnO catalyst (A) and Zn_7Al_3 catalyst (B).	59
Fig. 3- 18. FTIR spectra of liquid products obtained the reaction of glycerol with urea running at the different reaction time: a) $t = 0.25$ hr, b) $0.5 t =$ hr, c) $t = 1$ hr, d) $t = 2$ hr, e) $t = 3$ hr, and f) $t = 4$ hr. ZnO catalyst (A) and Zn_7Al_3 catalyst (B).....	60
Fig. 3- 19. The reaction time-dependent evolution of Zn-containing species (ZnO , $ZnGly$ and Zn NCO complex) over catalysts: A) ZnO and C) Zn_7Al_3 . The sketch depicting the evolution of Zn-containing species over catalysts: B) ZnO and D) Zn_7Al_3	62
Fig. 3- 20. FTIR spectra of liquid products obtained the reaction of glycerol with urea over co- Zn_7Al_3 catalyst run at the different reaction t time: a) $t = 0.25$ hr, b) $0.5 t =$ hr, c) $t = 1$ hr, d) $t = 2$ hr, e) $t = 3$ hr, and f) $t = 4$ hr.	65
Fig. 3- 21. FTIR spectra of spent co- Zn_7Al_3 catalysts run at the different reaction time: a) $t = 0.25$ hr, b) $0.5 t =$ hr, c) $t = 1$ hr, d) $t = 2$ hr, e) $t = 3$ hr, and f) $t = 4$ hr..	65
Fig. 3- 22. DTGA patterns of spent catalysts run over co- Zn_7Al_3 at the different reaction time: a) $t = 0.25$ hr, b) $0.5 t =$ hr, c) $t = 1$ hr, d) $t = 2$ hr, e) $t = 3$ hr, and f) $t = 4$ hr.	66
Fig. 3- 23. XRD patterns (A) and FTIR spectra (B) of fresh and spent Zn_7Al_3 catalysts for 3 hr reaction under different initial urea/glycerol ratios: a) fresh, b) urea/glycerol = 1.5, c) urea/glycerol = 1, and d) urea/glycerol = 0.5.....	69
Fig. 4- 1. XRD patterns of fresh catalysts: a) c- $ZnAl_2O_4$, b) c- $ZnAlO$, and c) p- $ZnAlO$	77
Fig. 4- 2. A) Raman and B) FTIR spectra of fresh catalyst: a) ZnO , b) c- $ZnAl_2O_4$, c) c- $ZnAlO$, and d) p- $ZnAlO$. C) Enlarged Raman and D) Enlarged FTIR spectra.....	80
Fig. 4- 3. A) TPD- NH_3 and B) TPD- CO_2 analysis results of fresh catalysts: a) c- $ZnAl_2O_4$, b) c- $ZnAlO$, and c) p- $ZnAlO$	83

Fig. 4- 4. Deconvoluted XPS results of fresh catalysts: a) c-ZnAl ₂ O ₄ , b) c-ZnAlO, and c) p-ZnAlO. A) Al2p XPS results, B) Zn2p _{3/2} XPS results and C) O1s XPS results.	87
Fig. 4- 5. The relationship between the disordered structure of the partially inversed ZnAl ₂ O ₄ phase and the acidity of the catalyst. A) The acidic sites – the inversion parameter. B) The O1s XPS intensity (oxygen vacancy) – the Zn2p XPS intensity (ZnO ₆).	90
Fig. 4- 6. FTIR spectra of liquid products obtained at the reaction time of a) 1 h and b) 3 h. A) c-ZnAl ₂ O ₄ , B) c-ZnAlO and C) p-ZnAlO.....	94
Fig. 4- 7. FTIR results of fresh catalysts and spent catalysts: a) fresh, b) 1 h and c) 3 h. A) c-ZnAl ₂ O ₄ , B) c-ZnAlO, and C) p-ZnAlO.	96
Fig. 4- 8. (A) TGA and (B, C, D) DTGA of spent catalysts: a) 1h and b) 3h. B) DTGA results of c-ZnAl ₂ O ₄ , C) DTGA results of c-ZnAlO and D) DTGA results of p-ZnAlO.	97
Fig. 4- 9. XRD patterns of fresh catalysts and spent catalysts: a) fresh, b) 1 h and c) 3 h. A) c-ZnAlO, B) p-ZnAlO.....	100
Fig. 4- 10. Deconvoluted N1s XPS data of spent c-ZnAlO after 3 h reaction time.	105
Fig. 5- 1. A) XRD patterns of fresh catalysts. a) Zn ₂ CoO, b) Zn ₂ FeO, c) ZnCo ₂ O, d) Zn ₂ CrO, e) ZnFe ₂ O and f) ZnCr ₂ O. B, C, D) Compare the position of (311) peaks (spinel phase ZnMe ₂ O ₄) between the rich-Zn Zn ₂ MeO catalyst and the corresponding poor-Zn ZnMe ₂ O catalyst.	113
Fig. 5- 2. FTIR spectra of fresh catalyst: a) Zn ₂ CoO, b) ZnCo ₂ O, c) Zn ₂ FeO, d) ZnFe ₂ O, e) Zn ₂ CrO and f) ZnCr ₂ O.	115
Fig. 5- 3. TPD-CO ₂ profiles of fresh catalysts: a) Zn ₂ CoO, b) Zn ₂ FeO, c) Zn ₂ CrO, d) ZnCo ₂ O, e) ZnFe ₂ O and f) ZnCr ₂ O.	116
Fig. 5- 4. TPD-NH ₃ profiles of fresh catalysts: a) Zn ₂ CoO, b) Zn ₂ FeO, c) Zn ₂ CrO, d) ZnCo ₂ O, e) ZnFe ₂ O and f) ZnCr ₂ O.	117
Fig. 5- 5. The relationship of glycerol conversion (%) and GC yield (%) by the glycerolysis of urea over various ZnMe (Me = Co, Cr, and Fe) mixed oxide catalysts and in various reaction time	122
Fig. 5- 6. FTIR spectra of the liquid products obtained from the glycerolysis of urea over different catalysts and different reaction times. A): a) Zn ₂ CoO-1h, b) Zn ₂ CoO-3h, c) Zn ₂ FeO-1h, d) Zn ₂ FeO-3h, e) Zn ₂ CrO-1h and f) Zn ₂ CrO-3h. B): a) ZnCo ₂ O-3h, b) ZnCo ₂ O-5h, c) ZnFe ₂ O-3h, d) ZnFe ₂ O-5h, e) ZnCr ₂ O-3h and f) ZnCr ₂ O-5h.	123
Fig. 5- 7. FTIR spectra of spent catalysts. A): a) Zn ₂ CoO-1h-spent, b) Zn ₂ CoO-3h-spent, c) Zn ₂ FeO-1h-spent, d) Zn ₂ FeO-3h-spent, e) Zn ₂ CrO-1h-spent and f) Zn ₂ CrO-3h-spent. B): a) ZnCo ₂ O-3h-spent, b) ZnCo ₂ O-5h-spent, c) ZnFe ₂ O-3h-spent, d) ZnFe ₂ O-5h-spent, e) ZnCr ₂ O-3h-spent and f) ZnCr ₂ O-5h-spent.	124
Fig. 5- 8. XRD patterns of spent catalysts: a) Zn ₂ CoO-3h-spent, b) Zn ₂ FeO-3h-spent, c) ZnCo ₂ O-3h-spent, d) Zn ₂ CrO-3h-spent, e) ZnFe ₂ O-3h-spent and f) ZnCr ₂ O-3h-spent.	129
Fig. 5- 9. DTGA profiles of spent catalysts. A): a) Zn ₂ CoO-3h-spent, b) Zn ₂ CoO-5h-spent, c) Zn ₂ FeO-3h-spent, d) Zn ₂ FeO-5h-spent, e) Zn ₂ CrO-3h-spent and f) Zn ₂ CrO-5h-spent. B): a) ZnCo ₂ O-3h-spent, b) ZnCo ₂ O-5h-spent, c) ZnFe ₂ O-3h-spent, d) ZnFe ₂ O-5h-spent, e) ZnCr ₂ O-3h-spent and f) ZnCr ₂ O-5h-spent	130

LIST OF SCHEMES

Scheme 1- 1. Main routes to glycerol carbonate synthesis [28]	6
Scheme 1- 2. The reaction of glycerol and urea to glycerol carbonate.....	6
Scheme 2- 1. The reaction mechanism for catalytic conversion to glycerol carbonate.....	23
Scheme 3- 1. A simplified reaction mechanism for the reaction of glycerol with urea. One reactant (Glycerol) and four reaction products can be detected by the gas chromatography in this study.	38
Scheme 3- 2. Dual catalysis over the ZnAl mixed oxide catalysts: homogeneous reaction route over the ZnO phase and heterogeneous reaction routes over the ZnAl ₂ O ₄ phase.....	52
Scheme 3- 3. Evolution of Zn species during glycerolysis of urea. A) ZnO catalyst and B) Zn ₇ Al ₃ catalyst.	70
Scheme 4- 1. The lattice structure of A) ordered and disordered spinel ZnAl ₂ O ₄ phase, B) c-ZnAl ₂ O ₄ , C) c-ZnAlO and D) p-ZnAlO.	91
Scheme 4- 2. An illustration of reaction routes in the reaction of glycerol with urea on the surface of the disordered ZnAl ₂ O ₄ spinel structure.	104
Scheme 5- 1. The reaction routes of the glycerolysis of urea over various ZnMe (Me = Co, Cr, and Fe) mixed oxide catalysts.....	132

LIST OF TABLES

Table 2- 1. Textural properties of $Zn_7Al_3O_x$ and ARM-supported Zn/Al catalysts.....	16
Table 2- 2. Composition of the RM and ARM samples measured by EDX (wt. %).	18
Table 2- 3. Reaction results of $Zn_7Al_3O_x$ and ARM-supported Zn/Al catalysts (Reaction conditions: Glycerol/urea molar ratio = 1, P = 3kPa, T = 140°C, 5 wt.% catalyst (of glycerol), at 5h of reaction time.)	20
Table 2- 4. Reaction results of Zn/Al mixed oxide catalysts (Reaction conditions: Glycerol/urea molar ratio = 1, P = 3kPa, T = 140°C, 5 wt.% catalyst (of glycerol), at 5h of reaction time.)	20
Table 3- 1. Physicochemical properties of the prepared catalysts	32
Table 3- 2. Analysis of liquid products obtained from the reaction of glycerol with urea for various catalysts. (Reaction time = 3 h, Urea/glycerol = 1, Reaction temp.= 140°C)	40
Table 3- 3. Analysis of liquid products obtained from the reaction of glycerol with urea over ZnO and Zn_7Al_3 catalysts at the various reaction temperatures. (Reaction Temperature = 140 °C, Reaction Pressure = 3 kPa, Glycerol/Urea Ratio =1:1).	41
Table 4- 1. Properties of the fresh catalysts.	79
Table 4- 2. The surface atomic ratio by XPS analysis of fresh catalyst.	84
Table 4- 3. Analysis of liquid products obtained from the reaction of glycerol with urea over ZnO and ZnAlO catalysts at various reaction times. (Reaction temperature = 140 °C, reaction pressure = 3 kPa, Glycerol/Urea Ratio =1:1). (I) : 2,3-dihydroxypropyl carbamate, (II) : 4-(hydroxymethyl)oxazolidin-2-one, and (III) : (2-oxo-1,3-dioxolan-4-yl)methyl carbamate. .	93
Table 4- 4. Apparent turnover frequency (apparent TOF) of GC and ZnGly for the reaction test at 3 h.....	102
Table 4- 5. Surface atomic ratios of spent p-ZnAlO and c-ZnAlO (3 h reaction time) measured by XPS	105
Table 4- 6. The reaction performance of reaction of glycerol with urea over several published catalysts in the literature	108
Table 4- 7. Catalytic performance of the reaction and the recovery of the re-used catalyst over two reaction cycles. (Reaction temperature = 140 °C, reaction pressure = 3 kPa, Glycerol/Urea Ratio =1:1).	109

NOMENCLATURES

AAS	Atomic absorption spectroscopy
ARM	Activated red mud
BET	Brunauer-Emmett-Teller method
DTGA	Derivative thermogravimetry analysis
FE-SEM	Field Emission Scanning Electron Microscopes
FID	Flame ionization detector
FTIR	Fourier-transform infrared spectroscopy
GC	Glycerol carbonate
ICP-OES	Inductively coupled plasma - optical emission spectrometry
JCPDS	Joint Committee on Powder Diffraction Standards
Me	Metal
NCO	Isocyanate group
PS	Polystyrene
RM	Red mud
TCD	Thermal conductivity detector
TGA	Thermogravimetric analysis
TOF	Turnover frequency
TPD	Temperature programmed desorption
XPS	X-ray photoelectron spectroscopy
XRD	X-ray Powder Diffraction
ZnGly	Zinc glycerolate

CHAPTER 1. INTRODUCTION

1.1. Background and motivation

Nowadays, climate change is considered as one of the greatest threats facing our world [1]. Since the beginning of the Industry Revolution, the major aspect of the current climate change is global warming which is the result of human activities. That finding has been agreed upon by the publishing of almost all the climate researchers [2]. The most influence activity of humans is the emission of greenhouse gas including the carbon dioxide (CO₂) by the burning of the traditional fossil fuel [3–5]. If humans do not have effective actions to control the problem, the impact of climate change can be extended not just in this century but also in the next 10 millennia more [6]. In the future, the reserves of fossil fuel will also be depleted which raises another question for the security of energy [7]. Replacing the conventional fossil fuel by other renewable energy (including biofuel, biodiesel) is recognized as a solution to mitigate the impact of climate change [8] and to ensure the supply of energy.

A renewable and high-compatible energy source like bio-diesel has been received much attention in both research and production [9–11]. In one past decade from 2007 to 2018, the production capacity of biodiesel in the U.S. market increased rapidly by almost 6 times (Fig. 1- 1). The consumed amount of vegetable oil for biofuel production has been grown dramatically especially in the market of Europe (Fig. 1- 2). The world production capacity of biodiesel has also increased rapidly in the last decade [12] with further production potential in the future [13]. The main source for biodiesel production is vegetable oil and one matter of bio-diesel production in that way is the by-product – crude glycerol [14,15]. This crude glycerol has low commercial value, and there is an emerging concern about the environmental impact of this abundant crude glycerol and the sustainability of biodiesel [16,17]. That has made the crude glycerol abundant and inexpensive by-product [18] which needs to be applied for further

product. Although there are some traditional ways to treat or purify crude glycerol, the market for pure glycerol is saturated and the price of crude glycerol has dropped. Fig. 1- 3 shows the opposite trend of the production capacity and the price of both crude and refined glycerol. While the production of glycerol has increased, the corresponding price of glycerol has decreased. Instead of disposal, many alternative methods to utilize glycerol have been researched, including the chemical process to convert glycerol to value-added components. It's necessary to find an efficient approach to upgrade the existing crude glycerol.

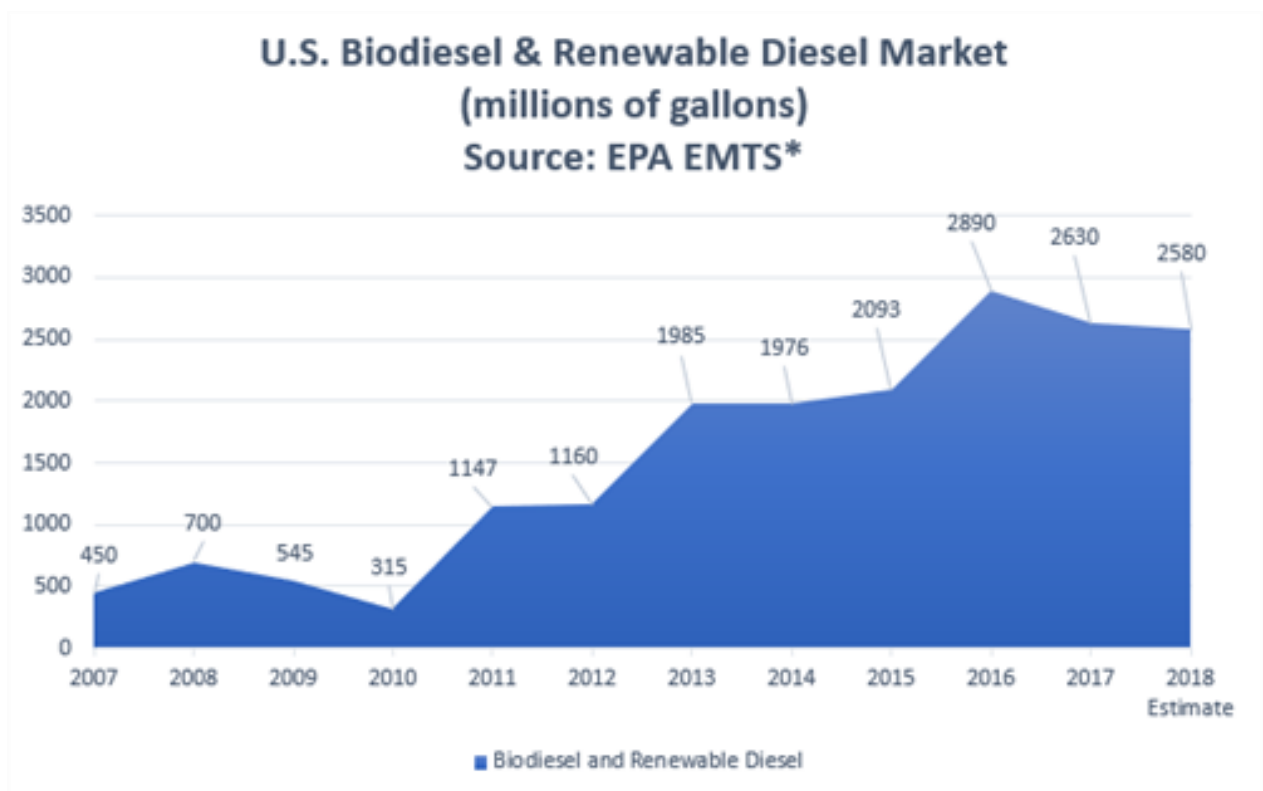


Fig. 1- 1. U.S. Biodiesel & Renewable diesel market [19]

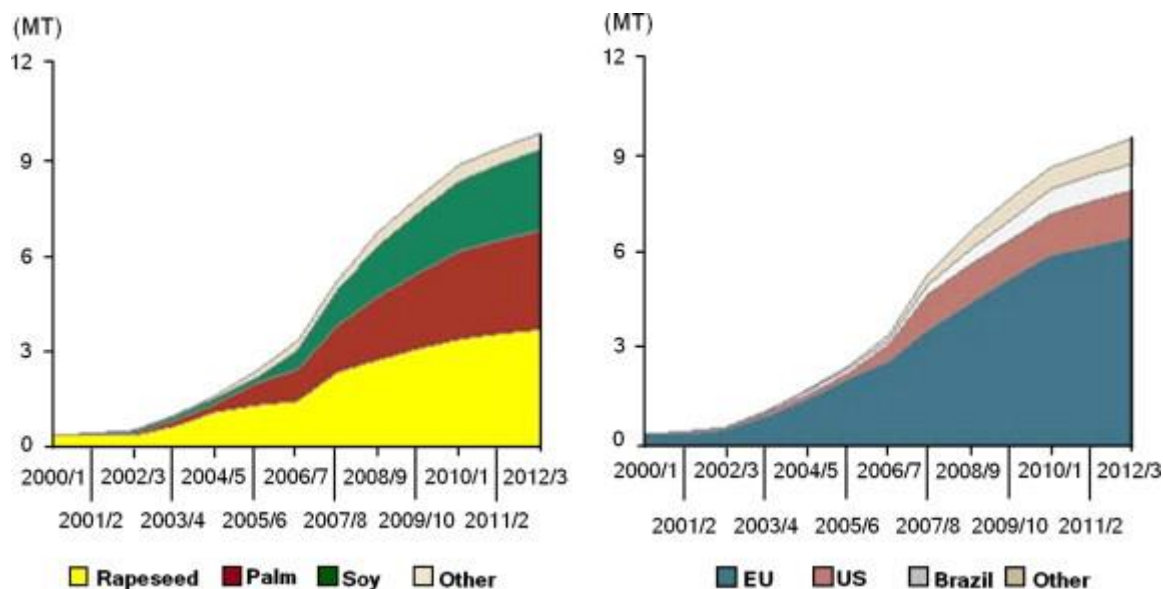


Fig. 1- 2. Worldwide use of vegetable oil for biofuel production [9]

To produce value-added products and optimize the benefit biodiesel manufacturing, the crude glycerol can be converted via several chemical pathway [20]: the selective oxidation [21–23], reduction to 1,3-propanediol [24], glycerol transformation into fuel additives [25] and carboxylation or glycerolysis into glycerol carbonate (or 4-hydroxymethyl-1,3-dioxolan-2-one). Glycerol carbonate (GC) is one attractive added-value chemical from glycerol. Glycerol carbonate has the excellent properties of high boiling point (110–115°C at 0.1 mmHg) [26]), low volatility (vapor pressure 0.008 bar at 177°C [27]), low flammability (flash point 190°C [28]), low toxicity and good biodegradability, and it has potential ability to widely employ in marketable industries such as cosmetics, batteries, polymers and pharmaceutical synthesis [29,30].

More attention for the glycerol carbonate (GC) can be proved by an increasing number of published paper year by year from 2001 to 2017 (Fig. 1- 4), especially since 2009. The period around the 2009 year also is the starting point for the expanding of the biodiesel industry in the U.S and Europe (Fig. 1- 1 and Fig. 1- 2). We can imply that the demand to process by-product glycerol of the biodiesel industry has triggered the glycerol carbonate research trend.

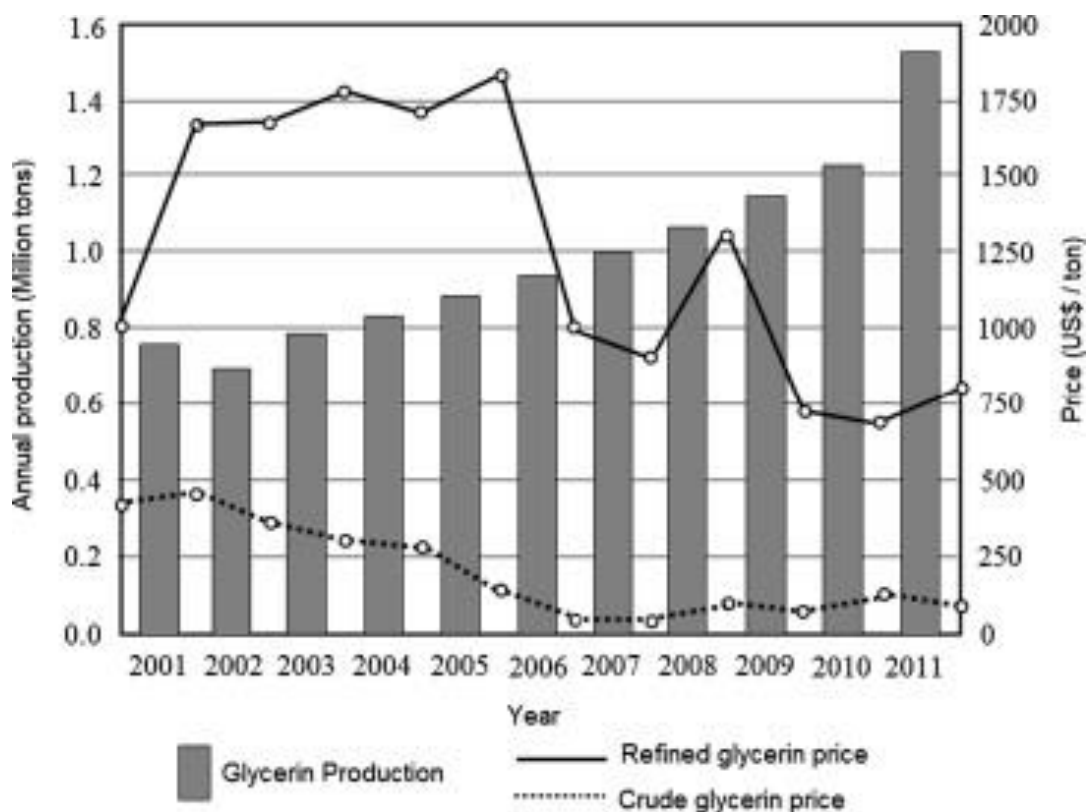


Fig. 1- 3. Projection of global glycerol production and prices. [9]

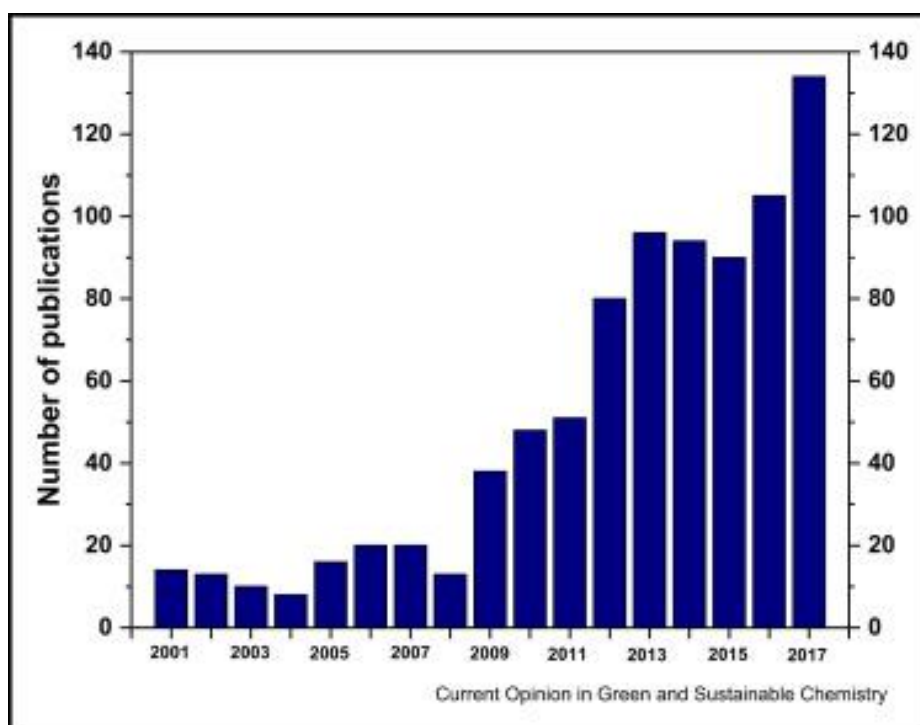
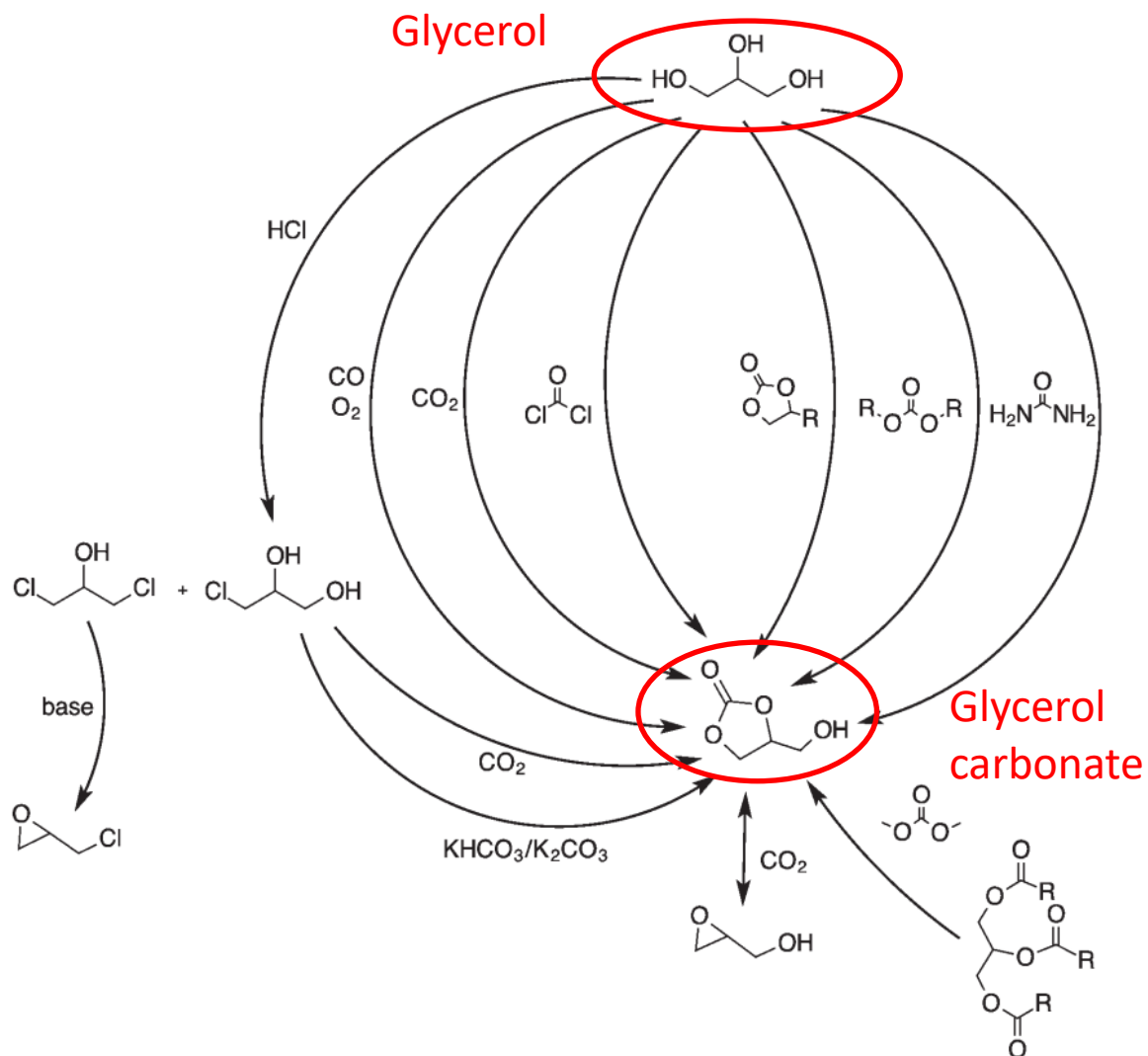


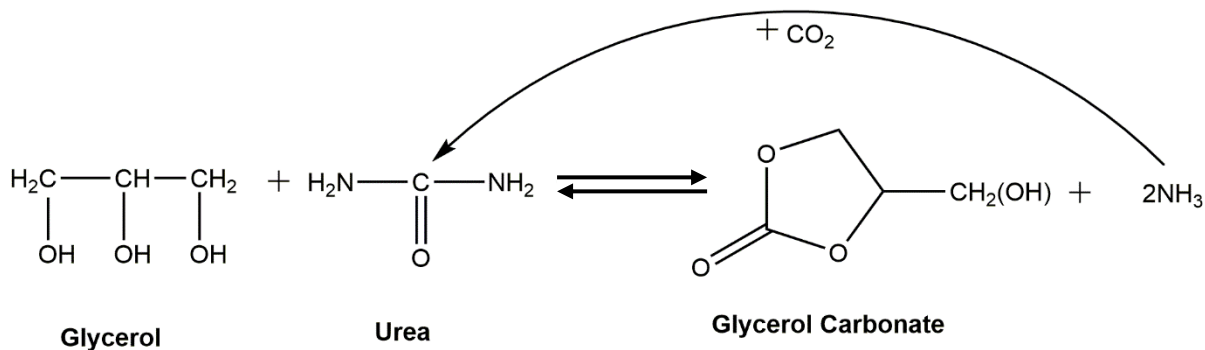
Fig. 1- 4. Number of publications on glycerol carbonate in the period 2001–2017 (from Web of Science). [30]

Scheme 1- 1 shows the main routes to GC through glycerol, oxirane and polycarbonate decomposition. It's clear to realize that the reaction route from glycerol contributes to the greatest number of possible reactions. There are several methods to synthesize GC from glycerol using the transcuration reaction with different carbonate sources: alkylene carbonate [31], dialkyl carbonate [32–38], CO/CO₂ [39–45], and urea [46,47,56–58,48–55]. In particular, GC synthesis using glycerol and urea has attracted attention for several reasons: i) urea is an inexpensive and readily available source, ii) the use of a solvent is unnecessary, and iii) the by-product NH₃ can be easily removed from a reactor by vacuuming or flowing nitrogen, which accelerates the forward reaction to GC. The idea of reaction between glycerol and urea can be summarized in Scheme 1- 2: one molecule of glycerol can react with one molecule of urea to produce one molecule glycerol carbonate and two molecules of by-product ammonia. If considering the economic benefit, the sided ammonia can be recovered and react again with carbon dioxide to produce urea which can carry by a normal urea production process.

The glycerolysis of urea can be accelerated by various kinds of catalysts: zinc salts [46], zinc glycerolate [48], calcined Zn hydrotalcite [49], γ -zirconium phosphate [52], La₂O₃ [53], and Co₃O₄/ZnO [54] and ZnO [37]. In this thesis, we focus on applying the mixed oxide catalysts (mostly the mixed oxide of Zn and Al) for the glycerolysis of urea.



Scheme 1- 1. Main routes to glycerol carbonate synthesis [28]



Scheme 1- 2. The reaction of glycerol and urea to glycerol carbonate

However, the reaction of glycerol and urea to glycerol carbonate meets two main problems: demand to remove ammonia byproduct to push the reversible reaction forward and the

thermodynamic limit of a reversible reaction. According to Li et al. [59], the change of standard molar Gibbs free energy of this reaction was quite small at the standard conditions ($\Delta G_o = 32.43 \text{ kJ.mol}^{-1}$, $T = 25 \text{ }^\circ\text{C}$ and $P = 101,325 \text{ Pa}$). The chemical equilibrium constants K of the reaction are displayed in Table 1- 1 and Table 1- 2. It can conclude that the reaction will be more favorable at a higher temperature and low pressure. However, the temperature cannot be increased too much, because the selectivity of glycerol carbonate decreases due to the catalytic conversion of glycerol carbonate to further by-products. Aresta et al. [52] confirmed that the best reaction performance can be achieved at a temperature $T = 140 \text{ }^\circ\text{C}$.

Table 1- 1. Effect of reaction pressure on chemical equilibrium constants K [59]

Pressure P/P_o ($T = 140 \text{ }^\circ\text{C}$)	Equilibrium constants K
0.000197	3.705×10^7
0.001	1.434×10^6
0.01	1.428×10^5
0.1	1.423×10^2
1	1.417
10	1.411×10^{-2}
20	3.525×10^{-3}
30	1.566×10^{-3}
40	0.88×10^{-3}
50	0.563×10^{-3}

P/P_o is the ratio of reaction pressure to the standard pressure ($P_o = 101,325 \text{ Pa}$).

Table 1- 2. Chemical equilibrium constants K at different temperatures [59].

Temperature (°C)	Equilibrium constants K (20 Pa)
25	0.516×10^2
40	0.575×10^3
60	9.611×10^3
80	1.11×10^5
100	9.547×10^5
120	6.491×10^6
140	3.658×10^7
160	1.78×10^8
180	7.67×10^8

To perform the reaction test at low pressure, a reactor system was installed and connected with a vacuum pump to reduce pressure to 3 kPa (Fig. 1- 5). An acid trap (nitric acid solution) was used to capture ammonia gas (NH₃) so this corrosive gas could not enter the vacuum pump and not damage the pump. The reaction temperature was controlled at 140 °C by a temperature controller. The vapor pressure of glycerol at certain temperatures is listed in Table 1- 3 [60], and we can estimate that at the reaction pressure (3 kPa), the boiling point of glycerol is above the reaction temperature (140 °C). Therefore, it can be assumed that the reaction occurs in the liquid phase. However, to ensure that the vacuum pump only removes ammonia gas, a condenser was installed on the outlet of the reactor so the vapor of every reactant and product is returned to the reactor.

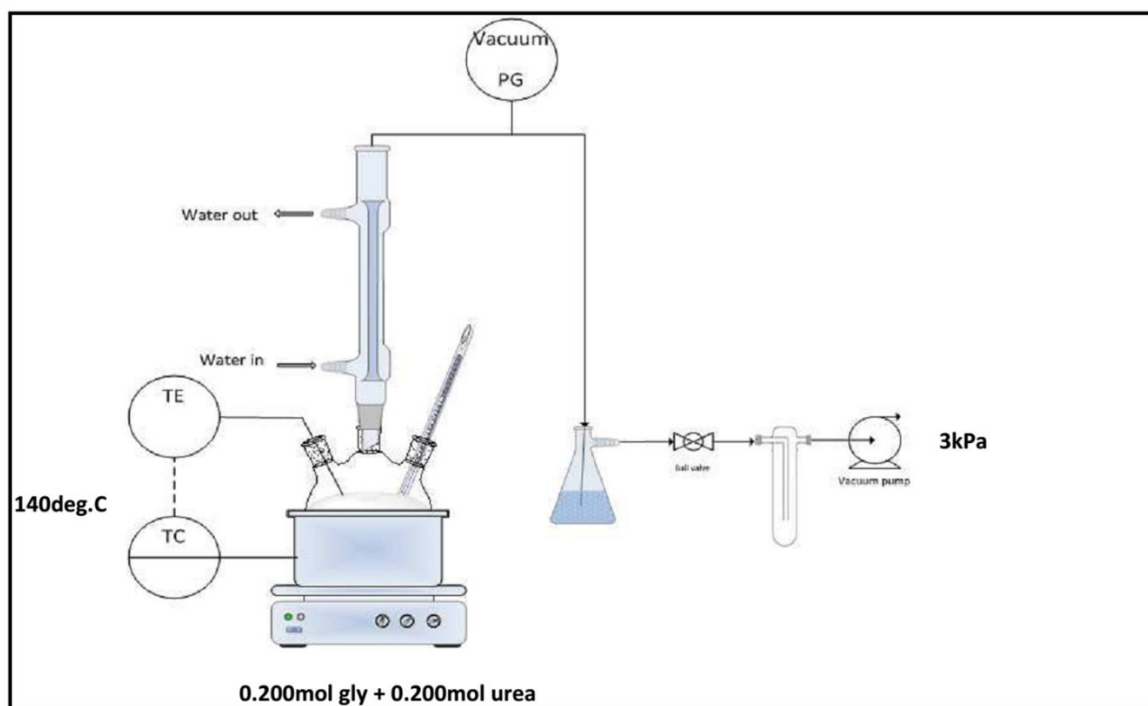


Fig. 1- 5. The sketch of the reactor system

Table 1- 3. Vapor pressure of glycerol [60]

Vapor pressure	Temperature (°C)
1 Pa	96
10 Pa	113
100 Pa	136
1 kPa	168
10 kPa	213.4
100 kPa	287

1.2. Research objectives

The target of this thesis is to discover how and which active site of the mixed oxide catalysts (especially Zn/Al mixed oxide catalysts) catalyzes the reaction of glycerol and urea. This reaction can follow the homogeneous reaction route or heterogeneous reaction route. It was proposed a heterogeneous reaction route through the interaction of reactants (glycerol and urea)

with a pair of Lewis acid-base sites. In addition, the reaction of glycerol and urea can also be catalyzed by homogeneous reaction route: zinc isocyanate (NCO) complex formed in the liquid phase as a main active site for the homogeneous reaction route. Also, the Zn species in the solid phases can leach into the liquid phase, providing evidence for the homogeneous reaction route in the heterogeneous Zn-based catalysts. This zinc isocyanate complex in the liquid phase also can be adsorbed on the surface acidic site of the spinel ZnAl_2O_4 phase and acts as an additional heterogeneous reaction route. The acidity of spinel phase can be monitored by the disorder of distribution of Zn and Al cations in the tetrahedral sites and octahedral sites of a spinel lattice structure. Moreover, the dual reaction route (homogeneous reaction route and heterogeneous reaction route) can be applied for other Zn-containing mixed oxide catalysts (with other metals like Cr, Co, Fe).

Specified objectives are:

- Objective 1: Set up reaction & simply investigate reaction steps. This is the first time this reaction was applied in the laboratory; therefore, a new reactor system needs to be successfully installed and simple reaction steps need to be observed.
- Objective 2: Reaction mechanism - Dual homogeneous & heterogeneous routes over Zn/Me mixed oxide (ZnO & spinel phase). A detailed explanation was given to clarify the reaction routes of reaction over the Zn-containing mixed oxide catalysts (the catalysts with the best reaction performance).
- Objective 3: Effect of disordered spinel phase to surface properties (acidity...) & to reaction mechanism. The relationship between the structure of the spinel phase and the surface properties (especially the acidity) and the relationship between those surface properties and the reaction mechanism were investigated.

The final objective can open more research approaches and can be more completed by other future studies.

1.3. Outline of the dissertation

This dissertation is composed of five chapters that study the application of Zn-containing catalysts for the reaction of glycerol with urea; the reaction routes and the reaction mechanisms are also discussed. In the first Introduction chapter, the current climate change by CO₂ emission with its consequences and the solution to use bio-fuel are presented. Glycerol carbonate is an approach to utilize the abundant amount of crude glycerol which is the by-product of bio-diesel production. In the second chapter, Zn/Al mixed oxide was impregnated on the red mud to observe the effect of the composition of activated red mud-supported Zn/Al catalysts to the reaction steps of the glycerolysis of urea. In the third chapter, a series of Zn/Al mixed oxides were prepared in different ratio of Zn:Al. The two phases ZnO and ZnAl₂O₄ were detected in every catalyst and these two phases take part in a dual reaction route (homogeneous and heterogeneous) of the glycerolysis of urea. Further, the Zn/Al mixed oxides continue to be investigated in the different reaction times to determine the role of Zn species (zinc isocyanate complexes and zinc glycerolate) in the reaction mechanism. The fourth chapter investigates the effect of disordered spinel ZnAl₂O₄ phase to the acidity and the glycerolysis of urea. And in the fifth chapter, the zinc-containing catalysts were prepared with not only Al but also other metals (Co, Cr, Fe); and the reaction routes of these catalysts follows the homogeneous/heterogeneous reaction route or both reaction routes.

A simple structure of the thesis was depicted in Fig. 1- 6. The first objective is discussed in Chapter 1. The second objective is discussed in Chapter 3 and Chapter 5. The third objective is discussed in Chapter 4, Chapter 5 and can be more completed by the current studies and future studies.

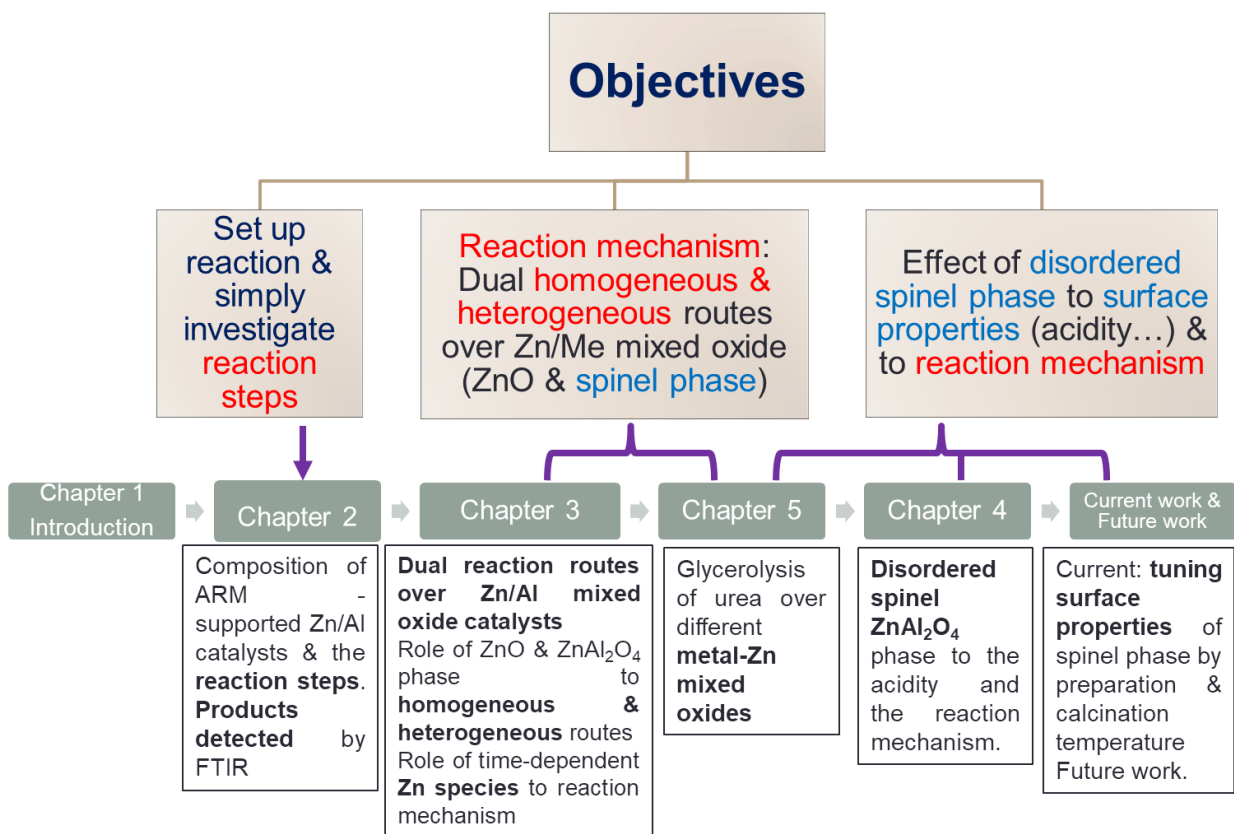


Fig. 1- 6. The structure of the thesis corresponding to the objectives

CHAPTER 2. OBSERVE THE ACTIVATION OF RED MUD-SUPPORTED ZN/AL CATALYSTS ON THE REACTION STEPS OF THE GLYCEROLYSIS OF UREA.

2.1.Introduction

For the heterogeneous catalysts, Climent et al. [49] indicated that the balance between acid-base sites of calcined Zn/Al hydrotalcite catalysts acted an important role in the reaction mechanism. Based on that idea, Ryu et al. [55] investigated the optimal Zn:Al ratio and obtained a better conversion. However, there has been no report to improve the catalytic performance by dispersing the active sites into supports. Red mud (RM) is a by-product from the manufacture of alumina by the Bayer process, specifically the solid residue of the caustic leaching of bauxite. RM has been studied as a catalyst or support for several catalytic reactions [61–64]. Although RM has less activity than the noble metals and metal oxides, its lower price makes it more desirable economically. In this work, we introduced calcined Zn/Al active sites onto activated RM (ARM) to improve its catalytic performance in the synthesis of GC with urea. The ARM-supported Zn/Al mixed oxide catalysts showed higher GC yield than the unsupported Zn/Al catalyst.

2.2.Experimental

2.2.1. Catalyst preparation

The Zn/Al catalyst with molar ratio Zn:Al=7:3 ($Zn_7Al_3O_x$) was prepared by the coprecipitation method [49,55]. An aqueous solution of $Zn(NO_3)_2 \cdot 6H_2O$ and $Al(NO_3)_3 \cdot 9H_2O$ was precipitated by a basic solution of NaOH and $NaNO_3$ under constant pH=6 and vigorous stirring. The mixed solution was then filtered and washed by deionized water. The resulting solid was dried at 100°C and finally calcined at 450°C in 6h. The sample was used as a control catalyst for comparison to the new catalysts.

The ARM-supported Zn/Al catalysts were prepared by the impregnation method. Typically, $\text{Zn}(\text{NO}_3)_2 \cdot 6\text{H}_2\text{O}$ and $\text{Al}(\text{NO}_3)_3 \cdot 9\text{H}_2\text{O}$ were dissolved in 100ml of deionized water, and 5g of ARM was added. The resulted solution was mixed by stirring and the solution temperature was kept at 80°C until all water was evaporated completely. The remaining solid was dried overnight at 110°C and calcined at 450°C in 6h. The prepared catalysts were designated as m%- $\text{Zn}_7\text{Al}_3\text{O}_x/\text{ARM}$. The loading weight of Zn/Al (m%) changed from 5% to 60%.

2.2.2. Reaction tests

Glycerol (0.2 mol) was added to a round-bottom 100 ml flask at 80 °C under stirring by a magnetic bar to reduce the high viscosity of glycerol. The flask was connected to a vacuum pump through an acid solution trap (to remove ammonia) and a cold trap (to remove other volatiles). After glycerol became less viscous, 0.2 mol of urea was poured into the flask and mixed to dissolve in the glycerol. When the solution was transparent, catalyst (5 weight% of the glycerol mass) was added to the flask. The reaction was carried out under vacuum (3 kPa) at 140 °C with constant stirring.

Ethanol was poured into the final product, and the liquid product was filtered away from a spent catalyst. The liquid product was quantitatively analyzed using a gas chromatography machine (Acme 6100 GC, YL Instrument Co., Ltd., Dongan-gu, South Korea) with a flame ionization detector and a capillary column, DB-Wax (30 m × 0.25 mm × 0.25 μm). The molar amount of each component was calculated using the internal standard method (the internal standard is tetraethylene glycol). The glycerol conversion, glycerol carbonate selectivity, glycerol carbonate yield, and byproduct selectivity were calculated using the equations below. The amount of each chemical is on the mole unit.

Glycerol conversion (%)

$$= \frac{\text{Initial amount of glycerol} - \text{Residual amount of glycerol}}{\text{Initial amount of glycerol}} \times 100$$

$$\text{Glycerol carbonate yield (\%)} = \frac{\text{Amount of glycerol carbonate}}{\text{Initial amount of glycerol}} \times 100$$

$$\text{Glycerol carbonate selectivity (\%)} = \frac{\text{Glycerol carbonate yield (\%)}}{\text{Glycerol conversion (\%)}} \times 100$$

Byproduct (except for ZnGly) selectivity (%)

$$= \frac{\text{Amount of byproduct}}{\text{Initial amount of glycerol} - \text{Residual amount of glycerol}} \times 100$$

The FTIR vibration spectra of liquid products were obtained using a Thermo Scientific™ Nicolet™ iS™5 FT-IR Spectrometer (Thermo Fisher Scientific, Waltham, MA, USA). The amount of Zn in the liquid phase was measured using an Agilent Technologies 5110 ICP-OES (Agilent, Santa Clara, CA, USA) instrument.

2.2.3. Catalyst characterization

The surface characterizations were measured by N₂ adsorption isotherm analysis on a Micromeritics ASAP 2020 (USA) apparatus. The surface area was calculated by the Brunauer–Emmett–Teller method. X-ray diffraction (XRD) patterns were obtained using a Rigaku RAD-3C diffractometer (Japan) with Cu K α radiation ($\lambda = 1.5418\text{\AA}$) at a scattering angle (2θ) scan rate of 2°/min, operated at 35 kV and 20 mA. Surface morphology images were obtained by field-emission scanning electron microscopy (FE-SEM, JEOL JSM-7600F, Japan).

2.3. Results and discussion

2.3.1. Catalyst characterization

The textural properties of the catalysts are summarized in Table 2- 1. The surface area of ARM and $Zn_7Al_3O_x$ are 136 and 43 m^2/g , respectively. When Zn/Al was impregnated into ARM, the surface areas of the catalysts were significantly decreased to 56 ~ 95 m^2/g , implying that the impregnation of Zn/Al changed the pore structure of ARM. Fig. 2- 1 shows N_2 adsorption-desorption isotherm plots of the catalysts. All the samples belong to type IV isotherm by IUPAC classification with a hysteresis loop [65]. The catalysts can be separated into two classes according to the hysteresis loop shapes. ARM and 5%- $Zn_7Al_3O_x/ARM$ samples can be grouped to type H4 hysteresis loop, implying a lack of additional phase of Zn and Al or incorporation of metal ions into ARM structure. The samples with 25% to 60% weight loading exhibit H2 hysteresis loop, representing the 'ink bottle' pores with narrow necks and wide bodies [66]. The additional patterns may be due to the existence of the new phase of ZnO and $ZnAl_2O_4$.

Table 2- 1. Textural properties of $Zn_7Al_3O_x$ and ARM-supported Zn/Al catalysts

Catalyst	Surface area (m^2/g)	Pore volume (cm^3/g)	Pore size (nm)
$Zn_7Al_3O_x$	46	0.164	11.6
ARM	136	0.246	6.4
5%- $Zn_7Al_3O_x/ARM$	84	0.148	7.6
25%- $Zn_7Al_3O_x/ARM$	91	0.130	4.8
40%- $Zn_7Al_3O_x/ARM$	95	0.147	5.3
50%- $Zn_7Al_3O_x/ARM$	72	0.145	6.4
60%- $Zn_7Al_3O_x/ARM$	56	0.110	6.6

The main constituents of RM and ARM had been reported in our previous research [64] (Table 2- 2). The main elements of ARM are Fe (22.8%), Al (12.2%) and a small amount of Si (4.1%) and Ti (3.8%). Fig. 2- 2 shows the XRD patterns of the catalysts. The XRD pattern of

$Zn_7Al_3O_x$ has two main phases: white zinc zincite ZnO (JCPDS No. 36-1451) and spinel $ZnAl_2O_4$ (JCPDS No. 05-0669) [67]. In the XRD pattern of ARM, the most important phase is hematite Fe_2O_3 (JCPDS 33-0664) [61], bayerite $Al(OH)_3$ (JCPDS 02-0197), gibbsite $Al(OH)_3$ (JCPDS 02-0249) and brookite TiO_2 (JCPDS 76-1937). The high crystallinity of the ZnO phase is proven by the sharp peaks at 31.8° , 34.4° , 36.3° , 47.5° , 56.7° , and 62.9° . In contrast, the $ZnAl_2O_4$ phase has less crystalline property, proven by the broad and short peaks. At lower Zn/Al loading (5%), there is no evidence of the existence of ZnO and $ZnAl_2O_4$ phases. From 25% to 60% Zn/Al loading, the XRD peak intensities of ZnO and $ZnAl_2O_4$ phases increase with the Zn/Al loading.

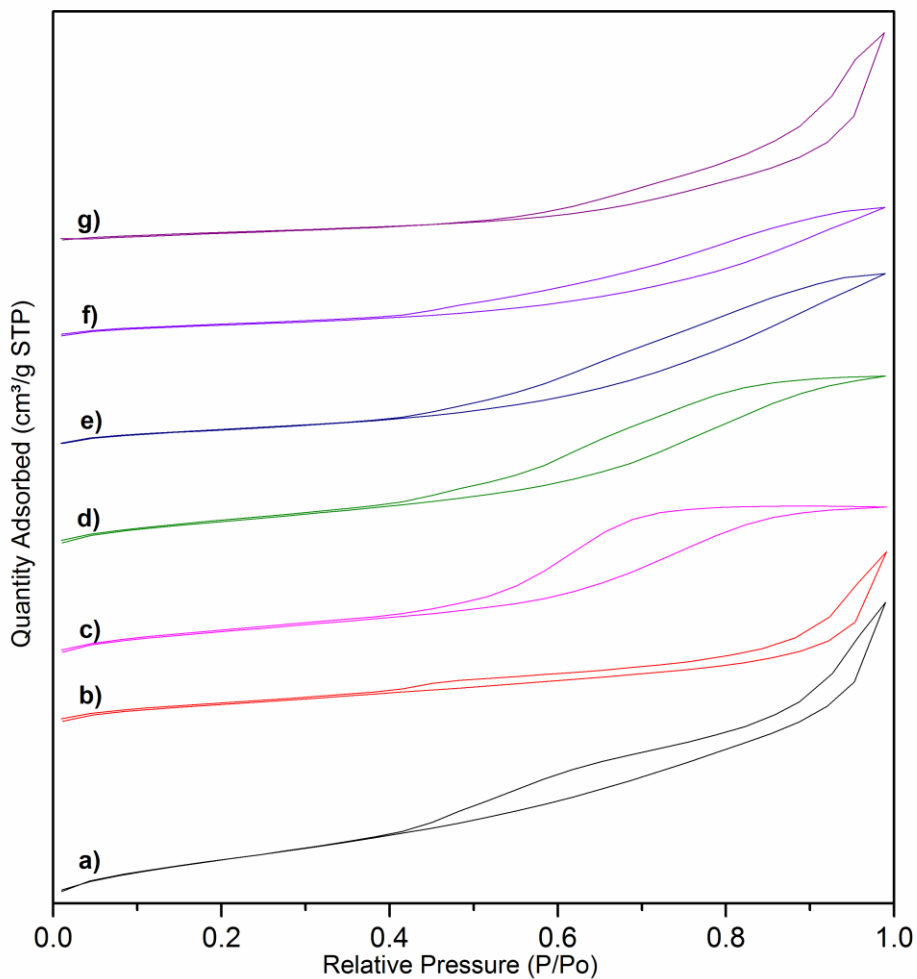


Fig. 2- 1. N_2 adsorption-desorption isotherms of a) ARM, b) 5%- $Zn_7Al_3O_x/ARM$, c) 25%- $Zn_7Al_3O_x/ARM$, d) 40%- $Zn_7Al_3O_x/ARM$, e) 50%- $Zn_7Al_3O_x/ARM$, f) 60%- $Zn_7Al_3O_x/ARM$ and g) $Zn_7Al_3O_x$.

Table 2- 2. Composition of the RM and ARM samples measured by EDX (wt. %).

Element	RM	ARM
Fe	23.32	22.84
O	42.78	50.38
Al	10.39	12.2
Si	4.73	4.1
Na	6.18	0.29
Ca	4.03	1.47
Ti	4.25	3.82
P	—	—

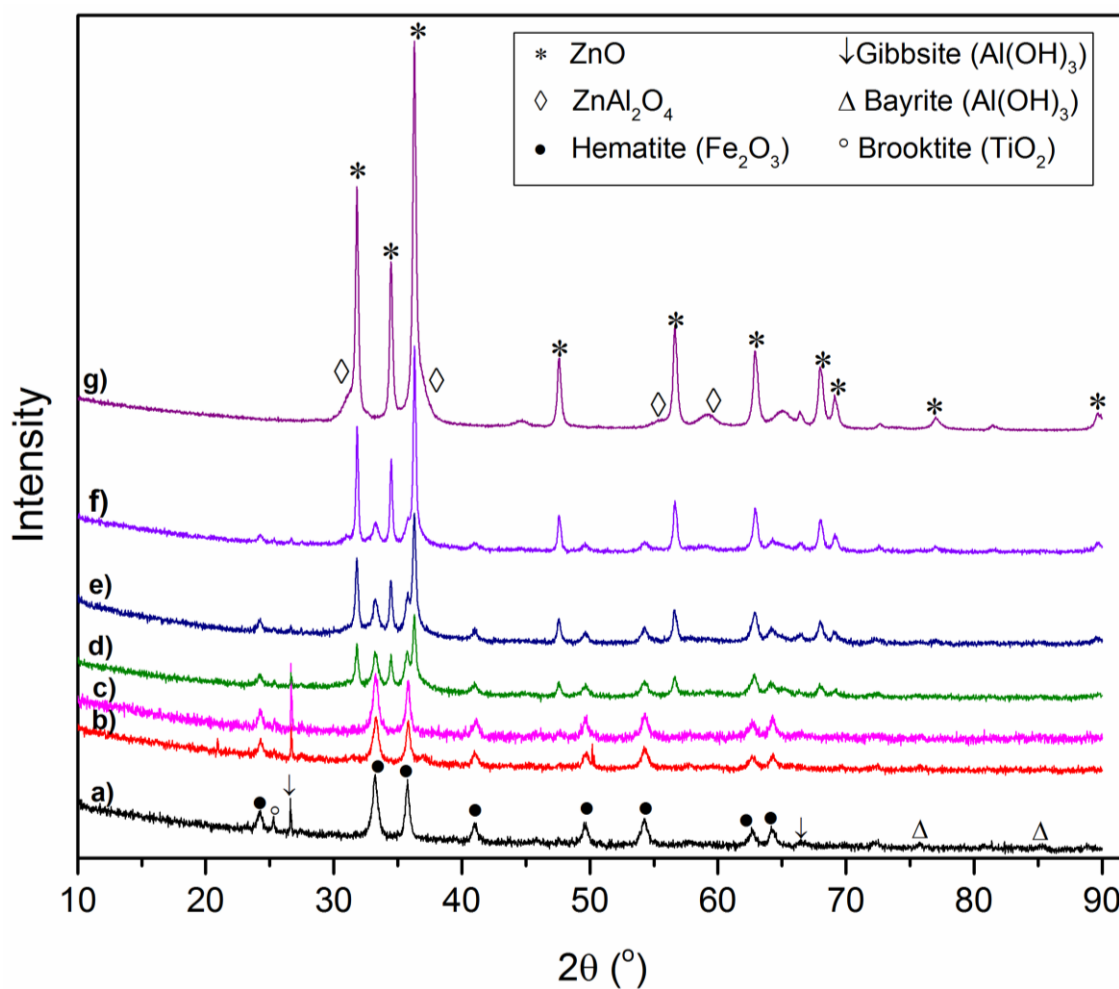


Fig. 2- 2. XRD patterns of a) ARM, b)5%- $\text{Zn}_7\text{Al}_3\text{O}_x/\text{ARM}$, c)25%- $\text{Zn}_7\text{Al}_3\text{O}_x/\text{ARM}$, d)40%- $\text{Zn}_7\text{Al}_3\text{O}_x/\text{ARM}$, e)50%- $\text{Zn}_7\text{Al}_3\text{O}_x/\text{ARM}$, f)60%- $\text{Zn}_7\text{Al}_3\text{O}_x/\text{ARM}$ and g) $\text{Zn}_7\text{Al}_3\text{O}_x$.

To investigate the morphology of the catalysts, FE-SEM images were obtained (Fig. 2- 3). The ARM is composed of fine and rounded shapes of aggregates. At 5% Zn/Al weight loading, the surface morphology is almost similar to that of the ARM sample. At 40% weight loading, additional crystals of ZnO and ZnAl₂O₄ are distributed between the ARM particles. As the Zn/Al weight loading is increased to 50% and 60%, the phases of ZnO and ZnAl₂O₄ agglomerated to bigger particles and mixed with ARM.

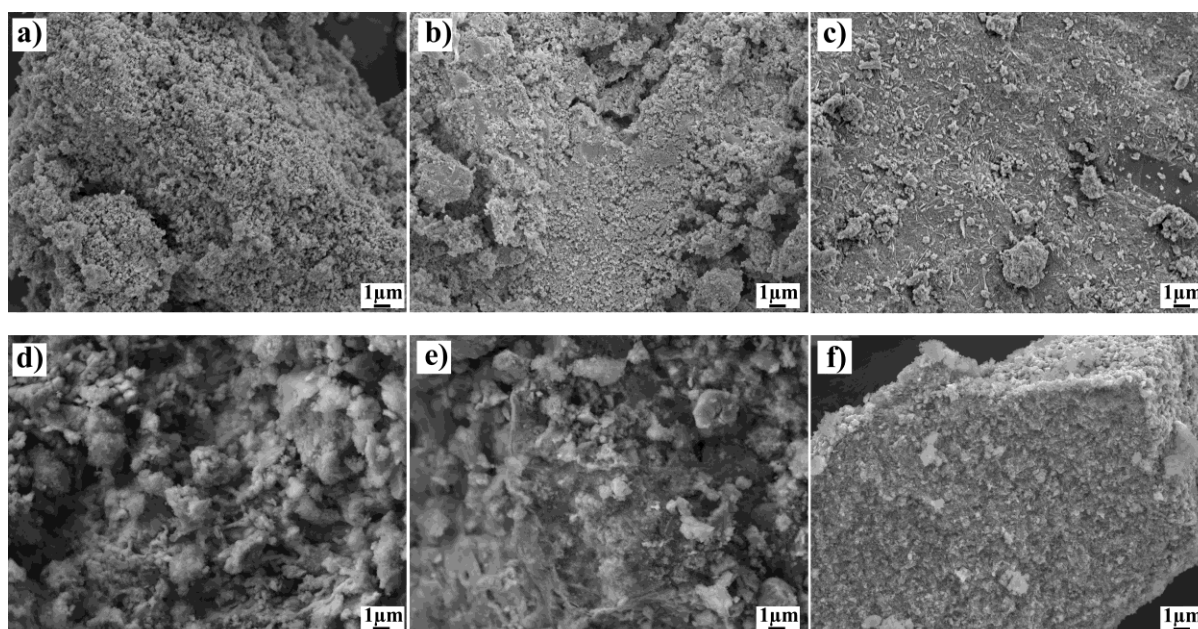


Fig. 2- 3. SEM images of a) ARM, b) 5%-Zn₇Al₃O_x/ARM, c) 40%-Zn₇Al₃O_x/ARM, d) 50%-Zn₇Al₃O_x/ARM, e) 60%-Zn₇Al₃O_x/ARM and f) Zn₇Al₃O_x.

2.3.2. Catalyst reaction activity

The reaction results (yield, conversion, and selectivity) are calculated by gas chromatography results (a typical gas chromatography graph is displayed in Fig. 2- 4) and summarized in Table 2- 3. Following Ryu. et al [55], as for unsupported Zn/Al oxide catalysts, the GC yields showed a volcano-like curve along with the Zn/Al molar ratio and Zn₇Al₃O_x catalyst was selected as a control sample since it had the best performance of unsupported Zn/Al oxide catalysts. A series of Zn/Al oxide were prepared and tested, the reaction results (Table 2- 4) confirmed Zn₇Al₃O_x having the best performance.

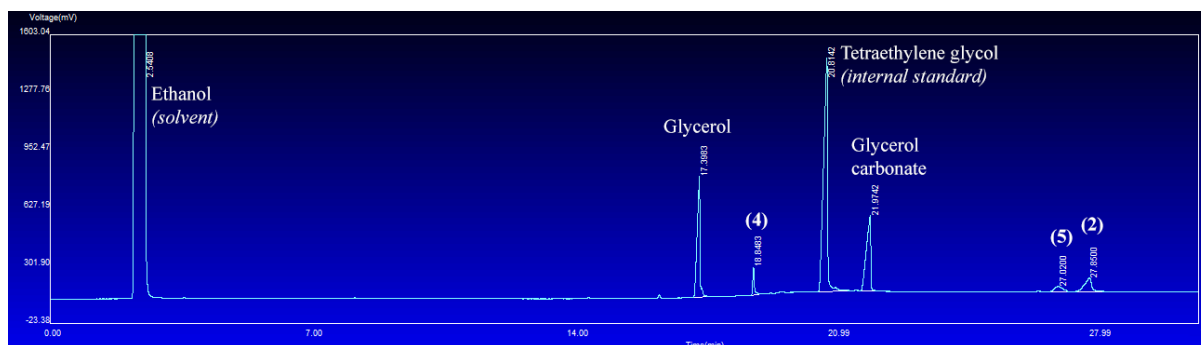


Fig. 2- 4. Typical gas chromatography graph, (2): 2,3-dihydroxypropyl carbamate, (4): 4-(hydroxymethyl) oxazolidin-2-one, (5): (2-oxo-1,3-dioxolan-4-yl) methyl carbamate.

Table 2- 3. Reaction results of $Zn_7Al_3O_x$ and ARM-supported Zn/Al catalysts (Reaction conditions: Glycerol/urea molar ratio = 1, P = 3kPa, T = 140°C, 5 wt.% catalyst (of glycerol), at 5h of reaction time.)

	Yield (%)	Conversion (%)	Selectivity (%)
$Zn_7Al_3O_x$	49.6±0.4	62.8±0.4	78.9±1.3
ARM	30.9±0.5	51.4±0.6	60.1±1.8
5%- $Zn_7Al_3O_x$ /ARM	32.5±0.4	48.9±0.3	66.6±1.7
25%- $Zn_7Al_3O_x$ /ARM	50.7±0.7	62.0±0.8	81.8±2
40%- $Zn_7Al_3O_x$ /ARM	57.6±0.4	64.0±0.6	90.0±1.3
50%- $Zn_7Al_3O_x$ /ARM	58.1±0.3	69.0±0.7	84.2±0.9
60%- $Zn_7Al_3O_x$ /ARM	55.0±0.6	68.3±0.4	80.7±1.6

Table 2- 4. Reaction results of Zn/Al mixed oxide catalysts (Reaction conditions: Glycerol/urea molar ratio = 1, P = 3kPa, T = 140°C, 5 wt.% catalyst (of glycerol), at 5h of reaction time.)

	Yield (%)	Conversion (%)	Selectivity (%)
$Zn_9Al_1O_x$	42.7	59.5	71.7
$Zn_8Al_2O_x$	44.4	61.3	72.5
$Zn_7Al_3O_x$	49.6	62.8	78.9
$Zn_6Al_4O_x$	40.9	58.4	70.0

Adding Zn/Al to the ARM structure gradually improved the conversion and the selectivity. When increasing the Zn/Al loading from 0 to 50%, the conversion increases from 51.4% to 69.0%, and the selectivity increases of 60.1% to 90.0%, thus the yield increases from 30.9% to a maximum of 58.1% at a 50% Zn/Al loading. The relation between the GC yield and the Zn/Al loading is clearly shown in Fig. 2- 5. When the Zn/Al loading increases to 60%, the GC yield drops to 55.0% and continues to decrease to 49.6% with the $Zn_7Al_3O_x$ catalyst (corresponding to 100% loading of Zn/Al). In Table 2- 3, compared to GC yield of $Zn_7Al_3O_x$ (49.6%), the highest GC yield was obtained at 58.1% with 50%- $Zn_7Al_3O_x$ /ARM where the weight percent of active components (Zn/Al) is only 50%. Therefore, the impregnation of Zn/Al onto ARM remarkably increased the catalytic performance. This improvement can be explained by the reaction mechanism through the FTIR analysis.

The FTIR spectra of the products obtained with $Zn_7Al_3O_x$ and 50%- $Zn_7Al_3O_x$ /ARM are compared to the FTIR spectra of two reactants, glycerol, and urea (Fig. 2- 6). Important absorption bands can be assigned to functional groups as follows: 1788 cm^{-1} for C=O stretching of the 5-membered cyclic carbonate of GC, 1736 cm^{-1} for C=O stretching of (2-oxo-1,3-dioxolan-4-yl)methyl carbamate [52,68], and 1712 cm^{-1} for C=O stretching of 2,3-dihydroxypropyl carbamate.

A reaction mechanism was proposed through glycerolysis with urea, as shown in Scheme 2- 1 [52,55]. Firstly, in **Step 1**: one amine group ($-NH_2$) of urea combines with one hydroxyl group ($-OH$) of glycerol (**1**) to form the carbamate intermediate compound $NH_2-(C=O)-(2,3\text{-dihydroxypropyl carbamate})$ (**2**) and one ammonia molecule is released. In **Step 2**, carbamate intermediate (**2**) takes part in the ring-closing reaction to form GC (**3**) and eliminate the second ammonia molecule. The ring-closing reaction can occur by the interaction between the hydroxyl group ($-CH(OH)-$) and the amine ($-NH_2$) to create byproduct 4-

(hydroxymethyl)oxazolidin-2-one (**4**) and a water molecule. In **Step 3**, GC can react with one more urea to achieve byproduct (2-oxo-1,3-dioxolan-4-yl)methyl carbamate (**5**).

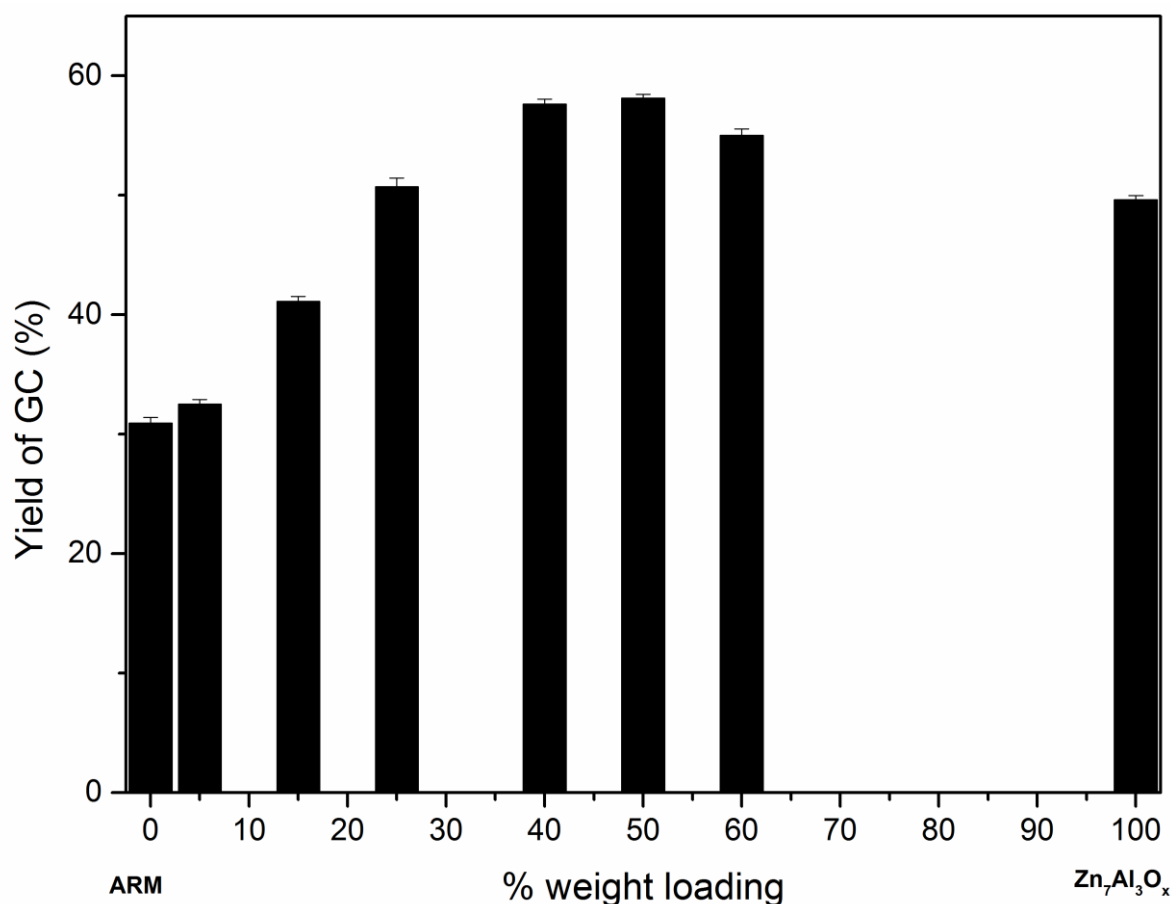


Fig. 2- 5. GC yield as a function of Zn/Al loading amounts. (Reaction conditions: Glycerol/urea molar ratio = 1, P = 3kPa, T = 140°C, 5 wt.% catalyst (of glycerol), at 5h of reaction time.)

The FTIR spectrum of the products with the Zn₇Al₃O_x catalyst presents a shoulder peak of byproduct (**5**) at 1736 cm⁻¹ and a sharp peak of the main product (**3**) at 1788 cm⁻¹. However, the FTIR spectrum of products with 50%-Zn₇Al₃O_x/ARM shows a main peak of GC at 1788 cm⁻¹ a small peak of intermediate carbamate at 1712 cm⁻¹, which is the product of **Step 1**. Here, the ratio between the byproduct peaks is interesting: the main byproduct peak of 50%-Zn₇Al₃O_x/ARM is smaller than that of Zn₇Al₃O_x, and thus the selectivity and the GC yield of the reaction with ARM-supported catalyst are higher than those of the Zn/Al catalysts.

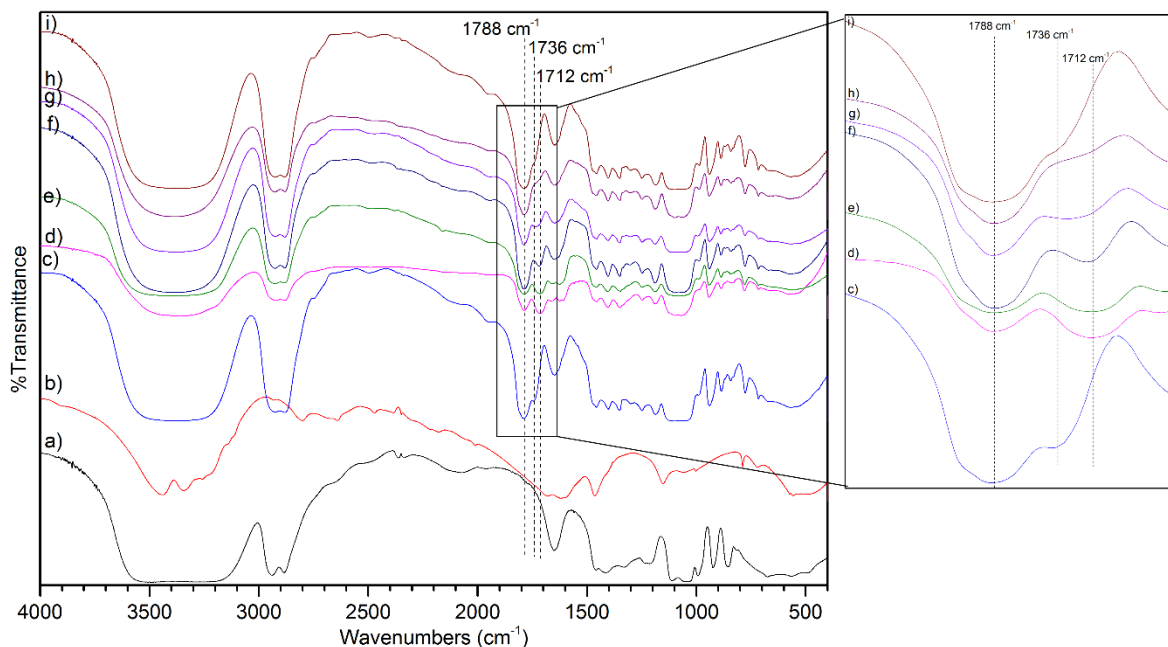
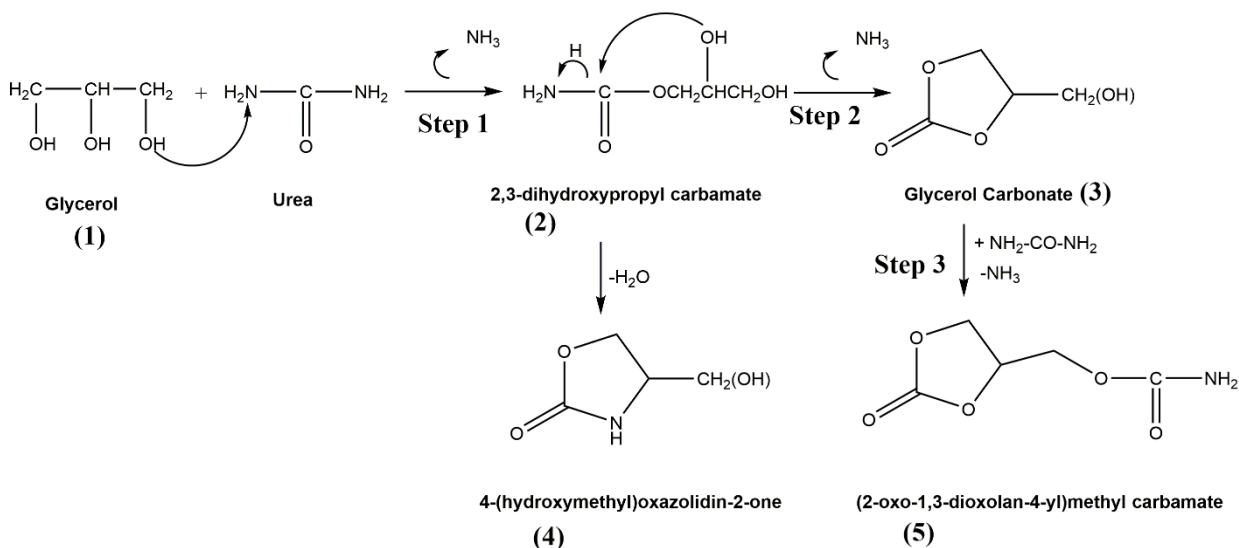


Fig. 2- 6. FTIR spectra of a) glycerol, b) urea, c) product with catalyst Zn_7Al_3 , d) product with catalyst ARM, e) product with catalyst 5%- $Zn_7Al_3O_x/ARM$, f) product with catalyst 25%- $Zn_7Al_3O_x/ARM$, g) product with catalyst 40%- $Zn_7Al_3O_x/ARM$, h) product with catalyst 50%- $Zn_7Al_3O_x/ARM$, and i) product with catalyst 60%- $Zn_7Al_3O_x/ARM$.



Scheme 2- 1. The reaction mechanism for catalytic conversion to glycerol carbonate.

A reaction mechanism is connected with the role of acid and base active sites over the catalysts [52,55]. Fig. 2- 6 shows the FTIR spectra of products with $m\%$ - $Zn_7Al_3O_x/ARM$. ARM was proven to contain high Fe species [64] and Fe affected the reaction from urea to carbamate [69]. The dual acidity and basicity of ARM [64,70] enabled it to accelerate **Step 1** (from

glycerol and urea to carbamate) with pairs of adjacent Lewis acid-base sites. Iron oxide has less basicity than zinc oxide [71], implying that ARM has less activity in **Step 2**. With ARM, small FTIR peaks of the main product (**3**) and intermediate (**2**) appear equally. Catalyst 5%-Zn₇Al₃O_x/ARM has no phase of ZnO and ZnAl₂O₄, and therefore shows a similar FTIR spectrum to ARM, causing no improvement in catalytic performance. From the 25% Zn/Al loading, there are ZnO/ZnAl₂O₄ phases which can accelerate all steps: **1**, **2** and **3**. An increase of **Step 1** makes more glycerol take part in the reaction and increases the conversion from 48.9% (with catalyst 5%-Zn₇Al₃O_x/ARM) to 69.0% (with catalyst 50%-Zn₇Al₃O_x/ARM). In the case, the reaction of **Step 1** occurs over both ARM and ZnO/ZnAl₂O₄ phases. The presence of ZnO/ZnAl₂O₄ phases promotes the reaction of **Step 2** to form more GC and to consume more of (**2**). Decreasing (**2**) is confirmed by FTIR spectra (Fig. 2- 6): when the Zn/Al loading increases from 5% to 50%, the intensity ratio of peak (**2**) decreases, improving the selectivity of GC (Table 2- 3).

At 50% Zn/Al loading, there is a shoulder FTIR band of (**5**) and at 60% Zn/Al loading the peak of (**2**) is replaced with (**5**) (Fig. 2- 6). Since the effect of ZnO/ZnAl₂O₄ phase on the reaction rates is higher than that of ARM, intermediate (**2**) is completely consumed and **Step 3** is relatively accelerated, which creates more byproduct (**5**) and hence decreases the selectivity from 90.0% (40%-Zn₇Al₃O_x/ARM) to 84.2% (50%-Zn₇Al₃O_x/ARM) and 80.7% (60%-Zn₇Al₃O_x/ARM). As the Zn/Al loading increases from 40% to 50%, the selectivity decreases from 90.0% to 84.2% but the conversion increases from 64.0% to 69.0%, hence slightly increasing the GC yield from 57.6% to 58.1%. Fig. 2- 7 shows the selectivities of byproducts which are calculated by the ratio of gas chromatography peak area. The trend of these selectivities is consistent with the conclusion from FT-IR results. With ARM, the amount of (**2**) is much larger than the amount of (**5**), so (**2**) has a significantly higher peak in the FT-IR result. In the case of the catalysts 50%-Zn₇Al₃O_x/ARM and 60%-Zn₇Al₃O_x/ARM, the

selectivity of (5) increases which is reflected in the increasing of FTIR peaks of (5), the increasing of (5) is considered as the reason of decreasing of glycerol carbonate selectivity and the glycerol carbonate yield.

It can be concluded that the balance between the two components ARM and ZnO/ZnAl₂O₄ is closely connected with a good balance between the three reaction steps: 1, 2 and 3 in Scheme 2- 1, which determines the reaction performance: conversion, selectivity, and GC yield.

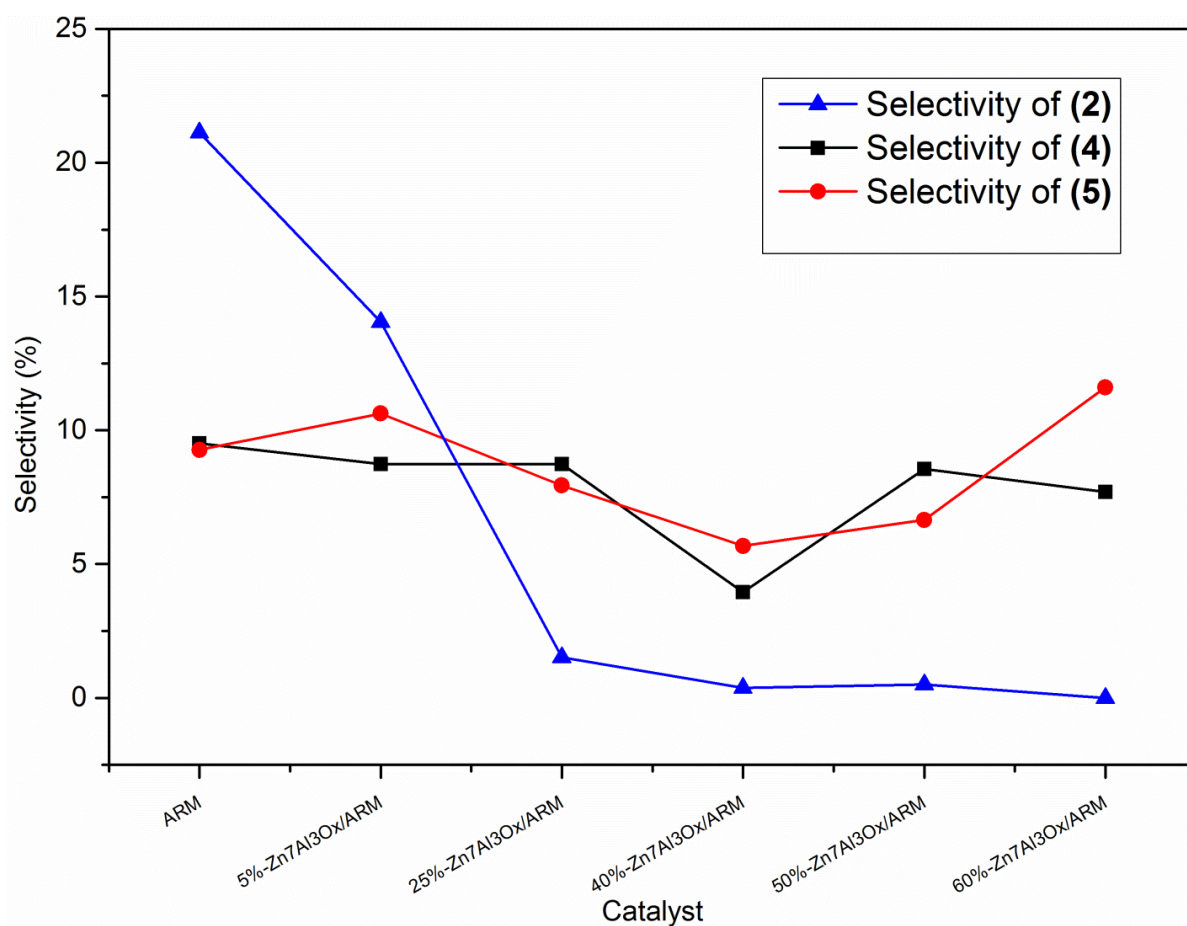


Fig. 2- 7. Byproducts selectivity calculated from gas chromatography peak area, (2): 2,3-dihydroxypropyl carbamate, (4): 4-(hydroxymethyl) oxazolidin-2-one, (5): (2-oxo-1,3-dioxolan-4-yl)methyl carbamate.

2.4. Conclusion

The Zn/Al mixed oxide was successfully impregnated into ARM by the hot wet impregnation method and the catalysts were applied to the synthesis of GC. The catalyst with

50% of Zn/Al loaded on ARM attained a GC yield of 59.8%, which is higher than that (49.6%) of the unsupported catalyst, $Zn_7Al_3O_x$. FTIR analysis of the reaction products indicated that ARM had the activity for the reaction of **Step 1** while Zn/Al showed activity for all the reaction steps: **1, 2, and 3**. With the ARM-supported Zn/Al catalyst, the balance of active sites between the ARM and ZnO/ZnAl₂O₄ phases strongly influenced the catalytic performance.

CHAPTER 3. INVESTIGATE THE ROLE OF ZNO PHASE AND ZNAL₂O₄ PHASE IN ZN/AL MIXED OXIDE CATALYSTS TO THE DUAL REACTION ROUTE (HOMOGENEOUS AND HETEROGENEOUS) OF THE GLYCEROLYSIS OF UREA. INVESTIGATE TIME-DEPENDENT ZN SPECIES - THEIR ROLES IN THE REACTION MECHANISM.

3.1.Introduction

The glycerolysis of urea can be accelerated by heterogeneous catalysts, which are mostly metallic oxides: γ -zirconium phosphate [52], calcined Zn hydrotalcite [49], La_2O_3 [53], and $\text{Co}_3\text{O}_4/\text{ZnO}$ nanodispersions [54]. By investigating the catalytic performance of several metallic oxides and calcinated hydrotalcite, Climent et al. [49] proposed a heterogeneous reaction route through the interaction of reactants (glycerol and urea) with a pair of Lewis acid-base sites. In addition, the reaction of glycerol and urea can also be catalyzed by homogeneous catalysts like zinc salts [46]. The zinc isocyanate (NCO) complex formed in the liquid phase was suggested as a main active site for the homogeneous reaction route. The existence of the Zn NCO complex was also confirmed in the cases of Zn-containing solid catalysts [51], ZnO [37], and zinc glycerolate [48]. This is because the Zn species in the solid phases can leach into the liquid phase, providing evidence for the homogeneous reaction route in the heterogeneous Zn-based catalysts. However, there has not been a report describing dual catalysis that includes homogeneous and heterogeneous reaction routes at the same time over ZnAl mixed oxide catalysts.

In this work, we prepare ZnAl mixed oxide catalysts (in the different molar ration of Zn:Al) via a co-precipitation method using a polystyrene (PS) template, and we apply the catalysts for the glycerolysis of urea in order to investigate the catalytic behavior of the homogeneous and heterogeneous reaction routes. The XRD patterns of the prepared ZnAl mixed oxide catalysts

show the existence of two Zn phases: ZnO and ZnAl₂O₄. The ZnO phase follows the homogeneous reaction route through the dissolution of Zn species into the reaction liquid and the subsequent formation of the Zn NCO complex. In addition, the Zn NCO complex is adsorbed on the ZnAl₂O₄ phase and we propose that it can create an additional heterogeneous reaction route. The reaction route taking place over the Zn NCO complex in the liquid and solid phases enhances the catalytic performance of the ZnAl mixed oxide catalysts along with the conventional heterogeneous reaction route over the ZnAl₂O₄ phase.

For a more detailed study, the observation of the reaction intermediates possessing the Zn species can provide essential information to understand the reaction mechanism for the reaction of glycerol with urea over the Zn-based heterogeneous catalysts. To identify the role of the Zn NCO complex over the ZnAl mixed oxide catalysts, it is necessary to investigate the reaction intermediates possessing the Zn species as a function of the reaction time. We used two typical Zn phase catalysts — ZnO and ZnAl mixed oxide (ZnAlO or Zn₇Al₃)— to investigate the reaction routes in the reaction of glycerol with urea as a function of reaction times. Time-dependent Zn species and reaction intermediates were observed in solid and liquid phases at various reaction times through FTIR, TGA, and XRD measurements in order to understand the evolution of Zn species and reaction intermediates over each catalyst. Eventually, the reaction routes were proposed based on the observation that the Zn-containing reaction intermediates in the liquid and solid phases in this study.

3.2.Experimental

3.2.1. Catalyst preparation

In this study, the ZnAl mixed oxide catalysts were prepared by a co-precipitation method using PS templates in a PS-water suspension environment [72]. Emulsion polymerization was used to synthesize nano-sized PS particles, and the detailed procedure is described elsewhere

[61]. PS powder was used as a hard template to prepare the ZnAl mixed oxide catalysts in various ratios of Zn and Al precursors. Typically, certain amounts of $\text{Zn}(\text{NO}_3)_2 \cdot 6\text{H}_2\text{O}$ and $\text{Al}(\text{NO}_3)_3 \cdot 9\text{H}_2\text{O}$ were dissolved in a 1:1 water:ethanol solution. Another solution of $(\text{NH}_4)_2\text{CO}_3$ in a 1:1 water:ethanol solution was prepared as the precipitation agent. These solutions were dropped into a suspension of PS powder in a 1:1 water:ethanol solution under vigorous stirring at 60°C while the pH was maintained at 6. The mixture was aged for 18 h at constant pH and with continuous stirring. Then, the precipitate was filtered and washed by deionized water. The resultant solid was dried overnight at 70°C and calcined at 600°C for 6 h with a ramping rate of $1^\circ\text{C}/\text{min}$. The prepared catalysts were designated as Zn_aAl_b , where a:b is the molar ratio of the Zn:Al precursors.

Conventional ZnAl mixed oxide with a molar ratio of Zn:Al=7:3 (designated as co- Zn_7Al_3), ZnO and the ZnAl_2O_4 catalysts were prepared by the co-precipitation method [3]. In the case of ZnO, an aqueous solution of $\text{Zn}(\text{NO}_3)_2 \cdot 6\text{H}_2\text{O}$ was precipitated by a basic solution of NaOH and NaNO_3 under a constant pH of 6 and vigorous stirring. The mixed solution was then filtered and washed by deionized water. The resultant solid was dried at 100°C and finally calcined at 450°C for 6 h. The ZnAl_2O_4 catalyst was prepared by the same method except using $\text{Al}(\text{NO}_3)_3 \cdot 9\text{H}_2\text{O}$ as an Al precursor and ammonia solution as a basic solution. The solution pH was adjusted to 7.5. The co- Zn_7Al_3 catalyst was also prepared using the aqueous solution of $\text{Zn}(\text{NO}_3)_2 \cdot 6\text{H}_2\text{O}$ and $\text{Al}(\text{NO}_3)_3 \cdot 9\text{H}_2\text{O}$ (the molar ratio of Zn:Al=7:3) for comparison.

3.2.2. *Reaction test*

The detailed procedure for the glycerolysis of urea to produce glycerol carbonate over the catalysts can be found in the part 2.2.2 of Chapter 2.

3.2.3. *Catalyst characterization*

The surface characterizations were measured by N₂ adsorption isotherm analysis on a Micromeritics ASAP 2020 (USA) apparatus. The surface area was calculated by the Brunauer–Emmett–Teller method. X-ray diffraction (XRD) patterns were obtained using a Rigaku RAD-3C diffractometer (Japan) with Cu K α radiation ($\lambda = 1.5418\text{\AA}$) at a scattering angle (2θ) scan rate of 2°/min and operated at 35 kV and 20 mA. Surface morphology images were obtained via field-emission scanning electron microscopy (FE-SEM, JEOL JSM-7600F, Japan). The spent catalyst for the characterizations was additionally prepared via filtration from the liquid phase and drying overnight at 70 °C in an oven. The spent catalysts were analyzed by a Thermo Scientific™ Nicolet™ iS™ 5 FTIR Spectrometer (USA) using the KBr pellet method. The amount of the Zn species in the liquid phase was measured by an Atomic Absorption Spectrophotometer (AAS, Shimadzu AA-7000, Japan). The amounts of acidic and basic sites were collected using the temperature-programmed method of NH₃ and CO₂ (TPD-NH₃/CO₂) (MicrotracBEL BELCAT-M, Japan). The thermogravimetric analysis (TGA) of the spent catalysts was measured by a TGA Q50 machine (TA Instruments, USA).

3.3. Results and discussion

3.3.1. Catalyst characterization

Table 3- 1 shows the physicochemical properties of the prepared catalysts. Three ZnAl mixed oxide catalysts prepared by the PS-template method have higher surface areas (52 - 86 m²/g) than the catalysts prepared by the co-precipitation method (7 m²/g for ZnO, 17 m²/g for ZnAl₂O₄ and 46 m²/g for co-Zn₇Al₃). This can be explained by the higher density of mesopores inside the thin walls formed by calcining the precipitate around the combusted polystyrene beads [72]. The thin-walled structure of the PS-templated ZnAl mixed oxide catalysts can be confirmed by the FE-SEM images (Fig. 3- 1); the morphology is not an ordered honeycomb shape, which can be built by arrays of the polystyrene beads, but instead, a nanoleaves shape is observed, which is a result of the destruction of the macroporous framework. The porosity

of the materials is measured by considering the N₂ adsorption-desorption isotherm curves (Fig. 3- 2). The ZnO catalyst has an unremarkable hysteresis loop that can be classified as a Type II isotherm [65], implying a non-porous material. Its characteristics of very low surface area (7 m²/g) and low average pore volume (0.017 cm³/g) are also confirmed in the literature [73]. In contrast, ZnAl₂O₄ and the ZnAl mixed oxide catalysts are mesoporous materials with the N₂ adsorption-desorption isotherm curves that are Type IV and type H3 hysteresis loops, which indicate slit-shaped pores. The addition of more Zn into the catalysts creates a larger hysteresis loop, higher BET surface area, and higher average pore volume in the order of Zn₆Al₄ < Zn₇Al₃ < Zn₈Al₂.

Fig. 3- 3 shows the XRD patterns of the prepared catalysts. Two main phases for Zn species can be identified: white zinc zincite ZnO and spinel ZnAl₂O₄, which is consistent with previously reported result [47]. The ZnO phase with a *P6₃mc* space group (JCPDS No. 36-1451) is confirmed by the peaks at 31.8°, 34.4°, 36.3°, 47.5°, 56.7°, and 62.9°, while the ZnAl₂O₄ phase has an *Fd3m* space group (JCPDS No. 05-0669), whose main peaks appear at 31.2°, 36.8°, 44.8°, 49.1°, 55.7°, 59.3°, 65.2°, 74.1°, and 77.3°. The intensity ratio of the crystalline phases of ZnO and ZnAl₂O₄ is simply estimated on the basis of the peak deconvolution in the XRD patterns [74,75] and summarized in Table 3- 1. When increasing the Zn:Al ratio of the precursors for the ZnAl mixed oxide catalysts from 6:4 to 8:2, the phase fractions of ZnO and ZnAl₂O₄ (ZnO:ZnAl₂O₄) also increase from 0.86 to 2.34, respectively. Hence, the PS-template method can provide tunability to synthesize the ZnAl mixed oxide catalysts with a higher ratio of the ZnAl₂O₄ phase. The ZnAl mixed oxides with different phase fractions are employed in order to identify the role of each Zn phase in the catalytic reaction routes for the glycerolysis of urea.

Table 3- 1. Physicochemical properties of the prepared catalysts

Samples	BET Surface Area (m ² /g)	Pore Volume (cm ³ /g)	Pore Size (nm)	Intensity Ratio of ZnO/ZnAl ₂ O ₄ in XRD *	Acidic Sites (mmol/g)	Basic Sites (mmol/g)	Acidic Sites/Basic Sites
ZnAl ₂ O ₄	17	0.137	32.6	0	0.112	0.089	1.258
Zn ₆ Al ₄	52	0.189	13.3	0.86	0.342	0.274	1.248
Zn ₇ Al ₃	77	0.301	17.0	1.29	0.375	0.383	0.979
Zn ₈ Al ₂	86	0.353	13.6	2.34	0.364	0.293	1.242
co-Zn ₇ Al ₃	46	0.164	11.6	8.78	0.305	0.365	0.844
ZnO	7	0.017	10.3	∞	0.015	0.025	0.600

**Intensity ratios of the ZnO/ZnAl₂O₄ phases were obtained from the deconvolution in XRD patterns using the X Powder software.*

The number of acidic and basic sites and their ratios for each catalyst are shown in Table 3- 1. ZnO has very low acidity and basicity. Both CO₂ and NH₃ desorption curves for ZnO are almost flat and it is hard to find a specific peak (Fig. 3- 4 and Fig. 3- 5), which is similar to previous results reported in the literature [31]. The amount of acidic and basic sites for ZnAl₂O₄ is moderate. However, when both ZnO and ZnAl₂O₄ phases co-exist as seen in the ZnAl mixed oxide catalysts, the acidity and basicity are significantly increased, resulting from the synergistic effect of the two phases [76,77]. The acidity and basicity are altered when Al³⁺ cations are substituted for Zn²⁺ cations on the surface. In the series of ZnAl mixed oxide catalysts, the minimum ratio of acidic and basic sites is found for Zn₇Al₃ (acidic sites/basic

sites = 0.979), representing an almost equal balance between acidic and basic sites. This result is consistent with the acid/base ratio previously reported [55].

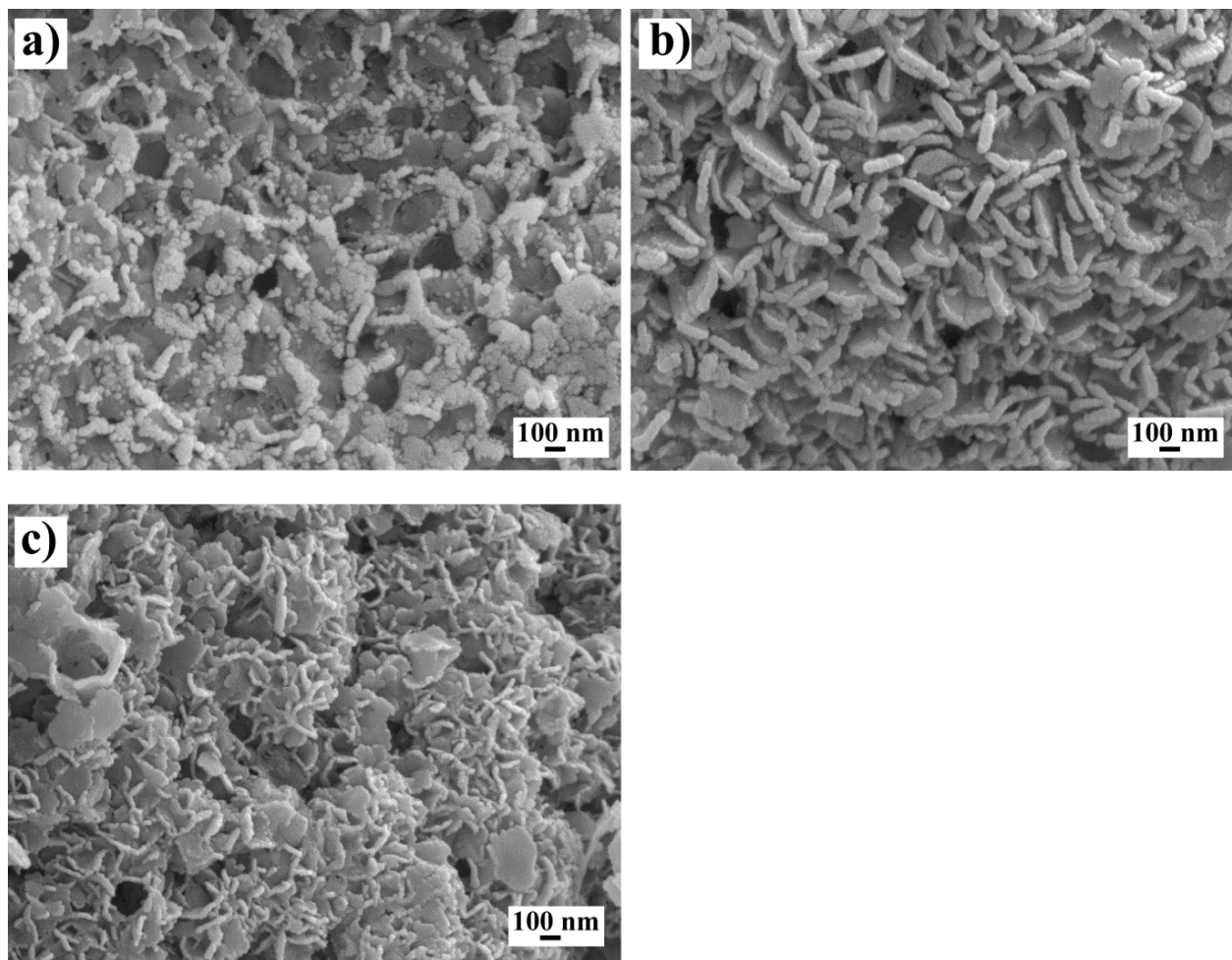


Fig. 3- 1. FE-SEM images of fresh ZnAl mixed oxide catalysts. a) Zn_6Al_4 b) Zn_7Al_3 , c) Zn_8Al_2 .

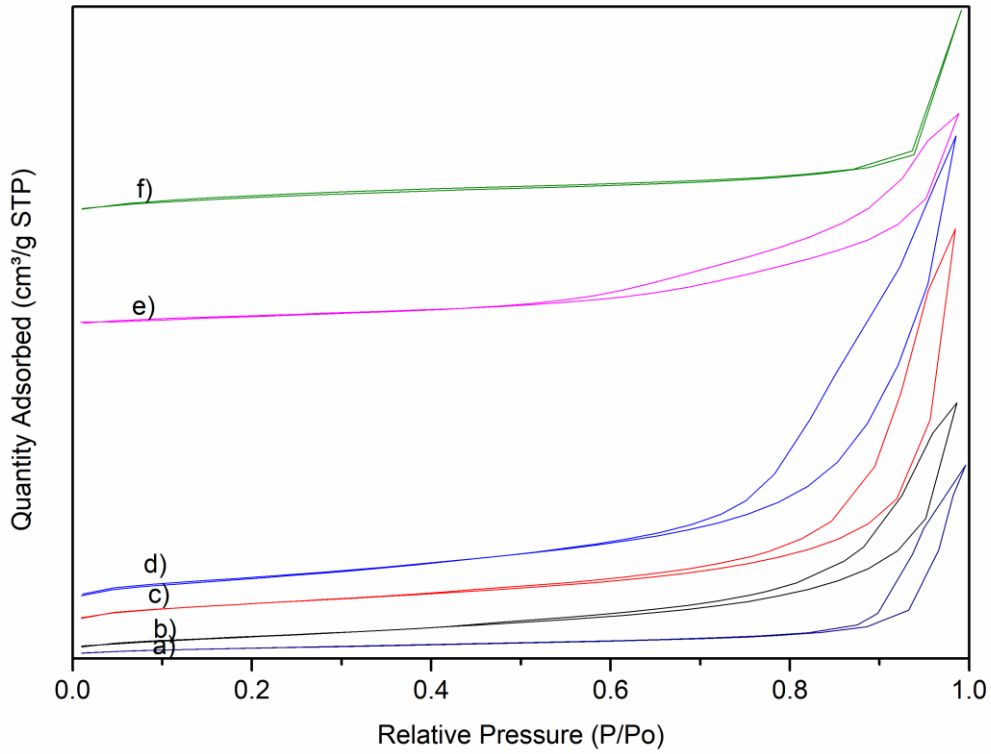


Fig. 3- 2. N₂ adsorption-desorption isotherms for the prepared catalysts. a) ZnAl₂O₄, b) Zn₆Al₄, c) Zn₇Al₃, d) Zn₈Al₂, e) co- Zn₇Al₃ and f) ZnO.

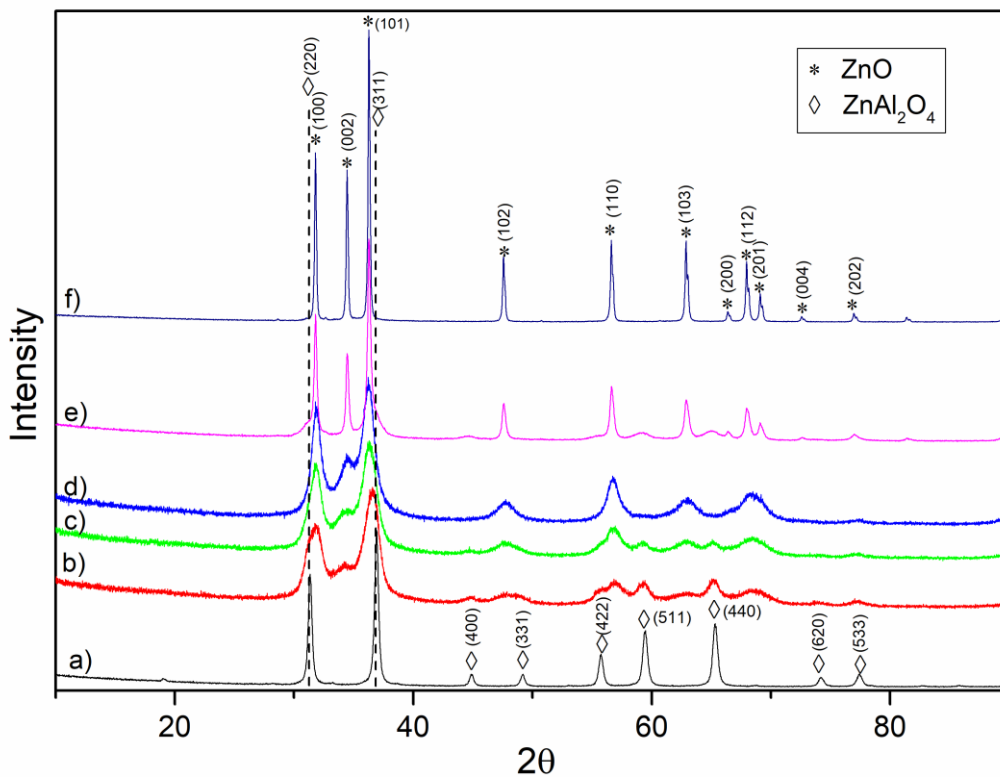


Fig. 3- 3. XRD patterns of fresh catalysts: a) ZnAl₂O₄, b) Zn₆Al₄, c) Zn₇Al₃, d) Zn₈Al₂, e) co- Zn₇Al₃ and f) ZnO.

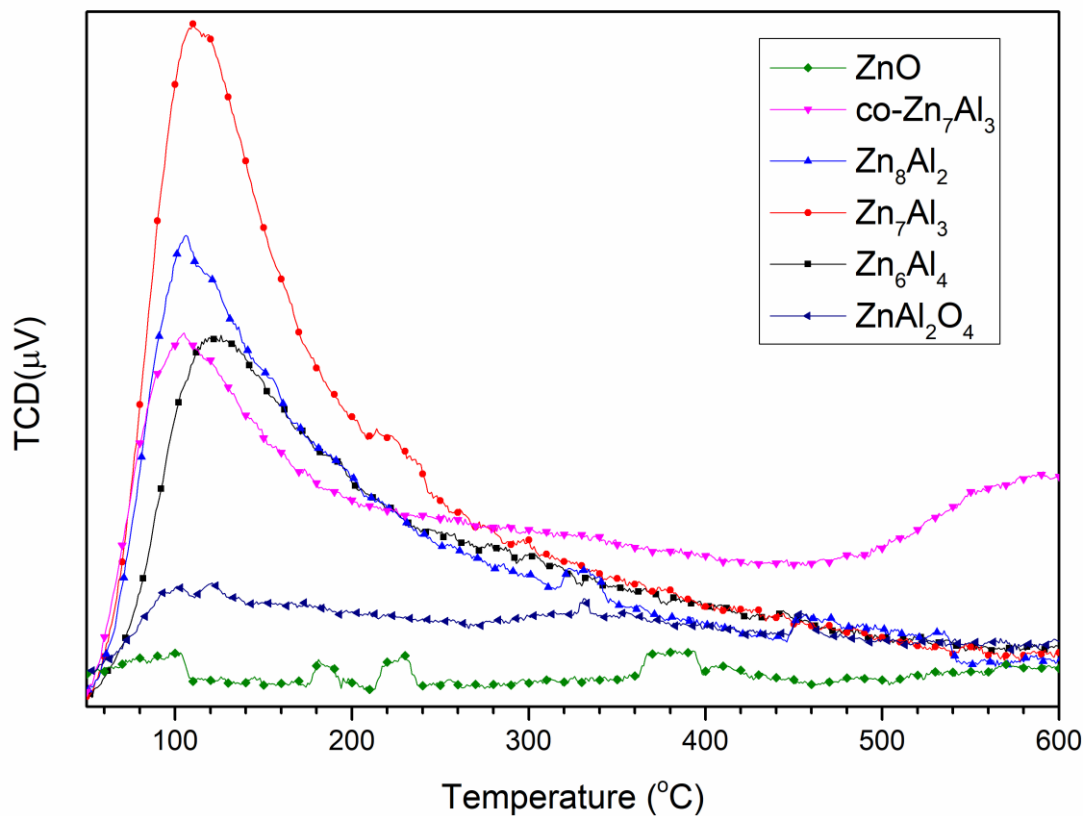


Fig. 3- 4. CO₂-TPD profiles for the prepared catalysts.

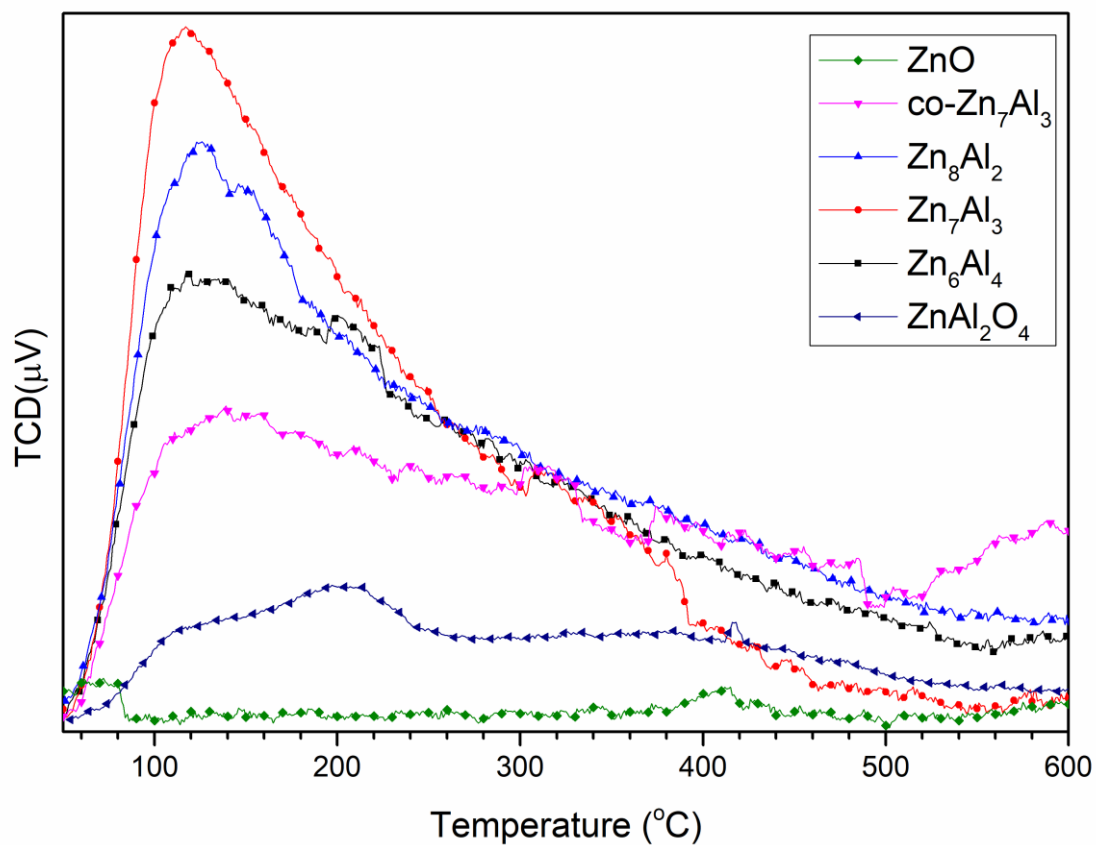


Fig. 3- 5. NH₃-TPD profiles for the prepared catalysts.

The main physicochemical properties of fresh ZnO and Zn₇Al₃ catalysts are summarized in Fig. 3- 6. The main phases of each catalyst were identified via X-ray diffraction (Fig. 3- 6A). While the ZnO catalyst exhibited a pure ZnO phase, the Zn₇Al₃ catalyst was composed of both ZnO and ZnAl₂O₄ phases. The ZnO phase with a *P6₃mc* space group was confirmed by the peaks at 31.8°, 34.4°, 36.3°, 47.5°, 56.7°, and 62.9° (JCPDS No. 36-1451), while the ZnAl₂O₄ phase had an *Fd3m* space group where its main XRD peaks appeared at 31.2°, 36.8°, 44.8°, 49.1°, 55.7°, 59.3°, 65.2°, 74.1°, and 77.3° (JCPDS No. 05-0669). The porosity of the catalysts was measured using the N₂ adsorption-desorption isotherm curves (Fig. 3- 6B). The ZnO catalyst had an unremarkable hysteresis loop that can be classified as a Type II isotherm [65], implying a non-porous material characteristic of a very low surface area ($S_{\text{BET}} = 7 \text{ m}^2/\text{g}$). In contrast, the Zn₇Al₃ catalyst was a mesoporous material that exhibited a Type IV N₂ adsorption-desorption isotherm curve with a hysteresis loop of type H3. The Zn₇Al₃ catalyst had a much higher surface area ($S_{\text{BET}} = 77 \text{ m}^2/\text{g}$). Interestingly, compared to the ZnO catalyst, the Zn₇Al₃ catalyst had much higher amounts of acidic and basic sites based on the TPD-NH₃ and TPD-CO₂ experiments (Fig. 3- 6C and D). The substitution of Zn²⁺ cations with Al³⁺ cations can enhance the acidic and basic properties on the surface of the Zn₇Al₃ catalyst [49,76].

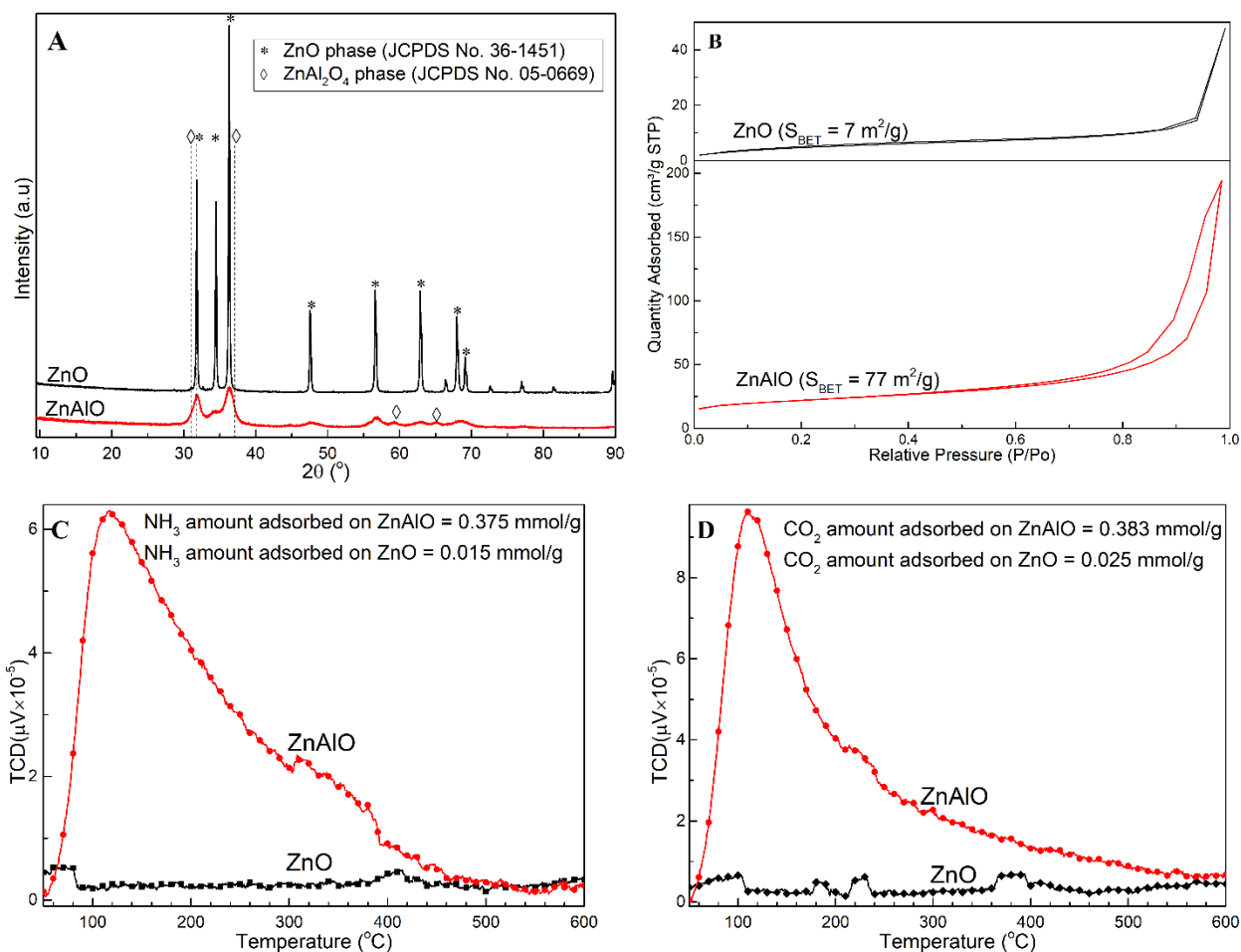


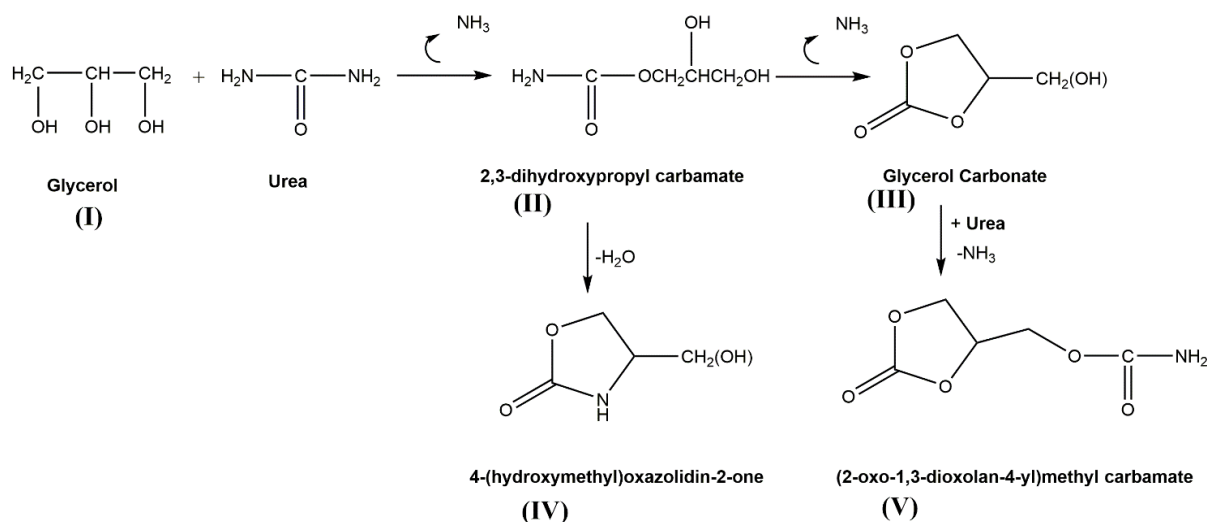
Fig. 3- 6. **A**) XRD patterns, **B**) N₂ adsorption-desorption isotherms curves, **C**) NH₃-TPD profiles and **D**) CO₂-TPD profiles of fresh ZnO and Zn₇Al₃ catalysts.

3.3.2. Catalytic tests

a. The catalytic reaction test results for the Zn/Al mixed oxide catalysts in different ratio of Zn:Al

The reaction results (glycerol conversion, product selectivity, GC yield, and turnover frequency (TOF)) are summarized in Table 3- 2. Identified products including by-products (via gas chromatography analysis) in this reaction are symbolized as follows: **(II)**, 2,3-dihydroxypropyl carbamate; **(III)**, glycerol carbonate; **(IV)**, 4-(hydroxymethyl)oxazolidin-2-one; and **(V)**, (2-oxo-1,3-dioxolan-4-yl)methyl carbamate [47,48]. Related to the chemicals, the simplified reaction routes of the glycerolysis of urea are illustrated in Scheme 3- 1 [47,49]. Initially, glycerol reacts with urea to form the intermediate **(II)** and one molecule of NH₃ is released. The intermediate **(II)** can take part in the ring-closing reaction and release one more

NH₃ to form glycerol carbonate (**III**). Alternatively, one molecule of H₂O can be detached from (**II**) to form the by-product (**IV**) [47,78]. Glycerol carbonate can react with one more urea and release NH₃ to achieve another by-product (**V**).



Scheme 3- 1. A simplified reaction mechanism for the reaction of glycerol with urea. One reactant (Glycerol) and four reaction products can be detected by the gas chromatography in this study.

According to the literature [55], in the case of the ZnAl mixed oxide catalysts prepared by the conventional co-precipitation method, the catalyst with Zn:Al = 7:3 not only has the lowest ratio of acidic and basic sites, but also the highest GC yield; the role of the acidic and basic sites in the catalysts is explained through the heterogeneous reaction mechanism. Interestingly, in this work, the ZnAl mixed oxide catalysts prepared by the PS-template method show the same trend in the ratio of acidic and basic sites, having the lowest value at Zn:Al = 7:3. However, the reaction results of the PS-templated ZnAl mixed oxide catalysts are different from those of the conventional ZnAl mixed oxide catalysts; the GC yield of Zn₇Al₃ is lower than those of Zn₈Al₂ and Zn₆Al₄, implying that the reaction routes over the PS-templated ZnAl mixed oxide catalysts follow a different mechanism.

To examine the role of each Zn phase (ZnO and ZnAl₂O₄) in the glycerolysis of urea, ZnO and ZnAl₂O₄ solid materials are also employed for the reaction tests. In Table 3- 2, the AAS analysis results of the Zn species in the liquid phase are also presented since the Zn species dissolved from ZnO interacts with urea and forms the complex Zn(NH₃)₂(NCO)₂ in the liquid phase, which is involved in a homogeneous reaction route to produce GC [37,48,51,79]. In the case of ZnO and the ZnAl mixed oxide catalysts, the Zn species is detected in the liquid phase. However, there is no Zn species dissolved from the ZnAl₂O₄ catalyst in the liquid phase, implying that the ZnAl₂O₄ catalyst follows the heterogeneous reaction route [52]. The ZnAl₂O₄ catalyst shows relatively low glycerol conversion (48%), low GC selectivity (48%), and low GC yield (23%) through the heterogeneous reaction route. The ZnO catalyst following the homogeneous reaction route shows a higher glycerol conversion (67%), but still has relatively low GC selectivity (73%) and low GC yield (49%). In contrast, the PS template ZnAl mixed oxide catalysts composed of both ZnO and ZnAl₂O₄ phases exhibit high glycerol conversion (83-90%) and high GC yield (68-73%), implying that the combination of homogeneous and heterogeneous catalysis over two different Zn phases has an effect to improve the catalytic reaction performance. This result is clearer in terms of TOF. ZnO and ZnAl₂O₄ have similar and relatively low TOF values (2.9 and 3.1, respectively), while the ZnAl mixed oxide catalysts have significantly higher TOF values ranging from 4.7-6.1.

Table 3- 2. Analysis of liquid products obtained from the reaction of glycerol with urea for various catalysts. (Reaction time = 3 h, Urea/glycerol = 1, Reaction temp.= 140°C)

Sample	Glycerol	GC	Selectivity (%)				Amounts of Zn * (mmol)	TOF ** (h ⁻¹)
	Conv. (%)	Yield (%)	GC	(II)	(IV)	(V)		
ZnAl ₂ O ₄	48±0.8	23±0.7	48±0.7	30±2.4	18±2.1	4±0.3	n.d.	3.1±0.09
Zn ₆ Al ₄	83±0.3	73±0.7	88±0.5	3±1.3	8±0.2	0±0.1	1.2	6.1±0.06
Zn ₇ Al ₃	87±0.8	68±0.4	78±1.1	5±0.9	16±1.6	1±0.1	0.9	5.1±0.03
Zn ₈ Al ₂	90±0.7	69±0.8	77±1.5	10±0.5	13±0.5	1±0.1	0.6	4.7±0.05
co-Zn ₇ Al ₃	89±0.8	52±0.7	59±1.3	14±0.3	26±1.8	1±0.1	1.5	3.9±0.05
ZnO	67±0.2	49±0.8	73±1.0	5±1.6	14±1.5	2±0.2	1.1	2.9±0.04

*Amounts of Zn dissolved into the liquid phase as measured by the AAS method.

**Apparent turnover frequency = moles of glycerol carbonate formed / (moles of Zn used × reaction time).

One more interesting point related to the homogeneous and heterogeneous reaction routes is the surface area. Even though the ZnO catalyst has the lowest surface area (7 m²/g), ZnO still shows a higher reaction performance than the ZnAl₂O₄ catalyst (17 m²/g). While the heterogeneous reaction route requires a high surface area to increase the number of active sites for the reaction, the homogeneous reaction route does not. Therefore, it seems that the catalytic behavior of the three PS template ZnAl mixed oxide catalysts does not match their surface areas in this study.

b. The catalytic reaction test results for the Zn/Al mixed oxide catalysts in different reaction time

The reaction test results of the ZnO and Zn₇Al₃ catalysts are summarized in Table 3- 3. The glycerol conversion of ZnO catalyst at the initial time (t = 0.25 hr) was twice (26%) as much

as that of the Zn_7Al_3 catalyst (11%) but increased slower. After $t = 2$ hr, the trend was reversed; the glycerol selectivity of the Zn_7Al_3 catalyst (73%) started to overcome that of the ZnO catalyst (60%). Finally, after $t = 4$ hr, the glycerol conversion of the Zn_7Al_3 catalyst (91%) was much greater than that of the ZnO catalyst (78%). The GC yields of both catalysts were in the same range. The Zn_7Al_3 catalyst achieved a maximum of GC yield at 68% ($t = 3$ hr), then the yield decreased to 64% at $t = 4$ hr. The ZnO catalyst reached a maximum GC yield at 60% after $t = 4$ hr since the GC yields of the ZnO catalyst continuously increased along with the glycerol conversion. The trends in GC selectivity of both catalysts were also different; the GC selectivity of the ZnO catalyst continuously increased from 52% ($t = 0.25$ hr) to 76% ($t = 4$ hr) and the GC selectivity of the Zn_7Al_3 catalyst had a volcano-curved trend with a maximum at 92% ($t = 2$ h).

Table 3- 3. Analysis of liquid products obtained from the reaction of glycerol with urea over ZnO and Zn_7Al_3 catalysts at the various reaction temperatures. (Reaction Temperature = 140 °C, Reaction Pressure = 3 kPa, Glycerol/Urea Ratio =1:1).

Catalyst	Reaction time (hr)	Glycerol Conversion (%)	GC Yield (%)	Selectivity (%) [*]			
				GC	(II)	(IV)	(V)
ZnO	0.25 hr	26	13	52	31	17	0
	0.5 hr	49	27	54	27	19	0
	1 hr	53	30	56	23	17	3
	2 hr	60	43	72	11	13	5
	3 hr	67	49	73	6	18	3
	4 hr	78	60	76	2	13	9
Zn_7Al_3	0.25 hr	11	8	79	16	5	0
	0.5 hr	17	14	83	8	9	0
	1 hr	48	39	81	7	11	1
	2 hr	73	67	92	2	5	1
	3 hr	87	68	78	1	16	5
	4 hr	91	64	70	1	17	12

^{*} Selectivities of products are the results of gas chromatography analysis of the liquid products.

The relation of the GC selectivity and glycerol conversion for both catalysts are plotted in Fig. 3- 7. The relation for the Zn_7Al_3 catalyst exhibited a volcano curve with a maximum at 92%, then decreased with increasing glycerol conversions. The GC selectivity of the ZnO catalyst was proportional to the glycerol conversion. However, the most important behavior observed in Fig. 3- 7 is that the GC selectivities of the Zn_7Al_3 catalysts were greater than those of the ZnO catalyst overall conversion ranges, indicating a better catalytic performance of Zn_7Al_3 catalyst in the reaction of glycerol with urea. The high GC selectivity at the same glycerol conversion was directly related to the catalytic reaction routes, with more GC generation than the other reaction products.

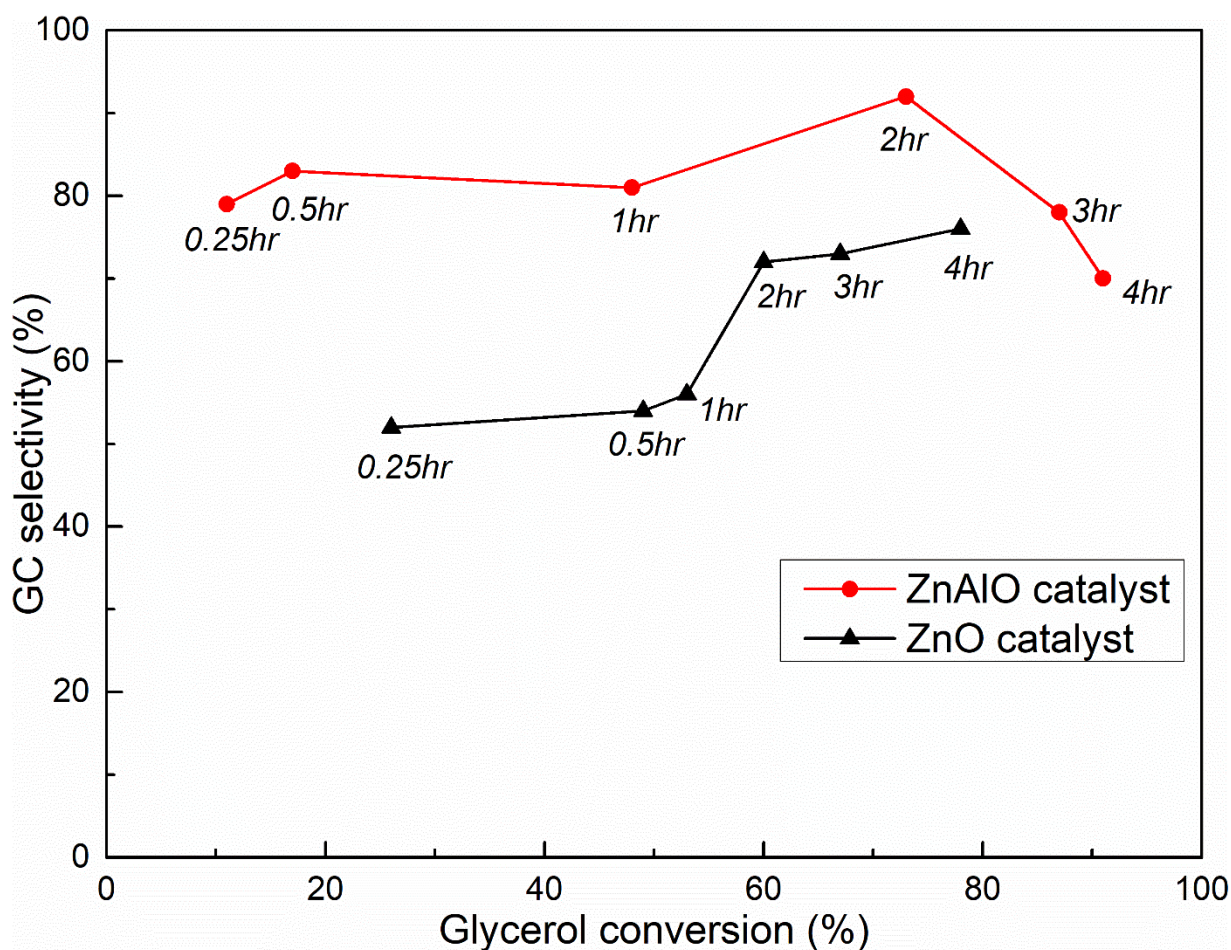


Fig. 3- 7. Glycerol carbonate (GC) selectivity as a function of the glycerol conversion for ZnO and Zn_7Al_3 catalysts

3.3.3. Analysis of the Zn species by XRD and FTIR measurements

The XRD patterns of spent catalysts are displayed in Fig. 3- 8, where three main Zn phases - ZnO, ZnAl₂O₄, and zinc glycerolate (ZnGly) are detected. Typical peaks of ZnGly with the space group *P2₁/c* (JCPDS No. 23-1975) can be observed at the positions of 10.9°, 17.1°, 20.5°, 23.8°, 24.7°, 27.6°, 27.7°, 36.4°, and 38.2° in the XRD patterns. ZnGly is not observed in the case of the spent Zn₆Al₄ and ZnAl₂O₄ catalysts. In contrast, the XRD pattern of the spent ZnO catalyst remarkably shows the characteristic peaks for ZnGly, representing the dissolution of ZnO in the fresh catalysts and its transformation into ZnGly during the reaction since ZnO can be readily transformed into ZnGly in a glycerol medium [40,80,81]. Fig. 3- 9 represents the correlation between the ratios of the Zn crystalline phases (ZnO/ZnAl₂O₄) over the fresh catalysts and the formation of ZnGly over the spent catalysts. When increasing the Zn:Al ratios, the Zn phases ratio (ZnO/ZnAl₂O₄) in the fresh catalysts increases in the order of ZnAl₂O₄ < Zn₆Al₄ < Zn₇Al₃ < Zn₈Al₂ < co-Zn₇Al₃ < ZnO. No XRD characteristic peak of ZnGly appears in the case of ZnAl₂O₄ and Zn₆Al₄, which contain a much low portion of the ZnO phase in the fresh catalysts. When increasing the ratio of the ZnO phase in the fresh catalysts, the peak intensity of ZnGly in the spent catalysts correspondingly increases and reaches the maximum with the ZnO catalyst, which consists of 100% of the ZnO phase. The TGA measurements confirm the trend in ZnGly formation over the spent catalysts. A peak created at 340°C in the DTGA graphs belongs to the decomposition of ZnGly to ZnO [82] (Fig. 3- 10). The peak intensity of ZnGly decomposition in the DTGA profiles increases in the order of ZnAl₂O₄ < Zn₆Al₄ < Zn₇Al₃ < Zn₈Al₂ < co-Zn₇Al₃ < ZnO. Accordingly, it is apparent that the greater the amount of the ZnO phase over the fresh catalysts, the greater the ZnGly formation in the spent catalyst.

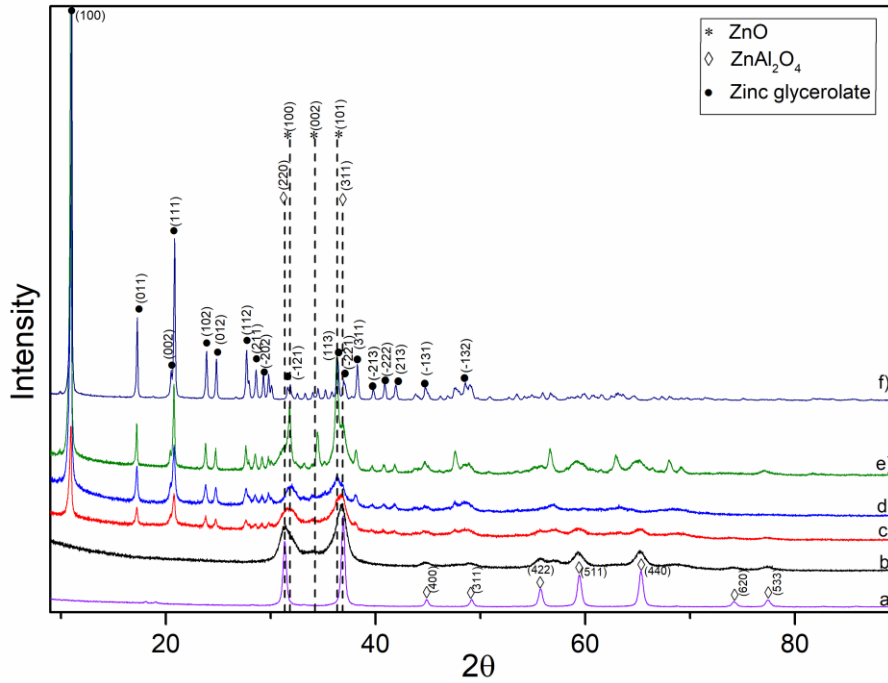


Fig. 3- 8. XRD patterns of spent catalysts: a) ZnAl₂O₄, b) Zn₆Al₄, c) Zn₇Al₃, d) Zn₈Al₂, e) co-Zn₇Al₃ and f) ZnO.

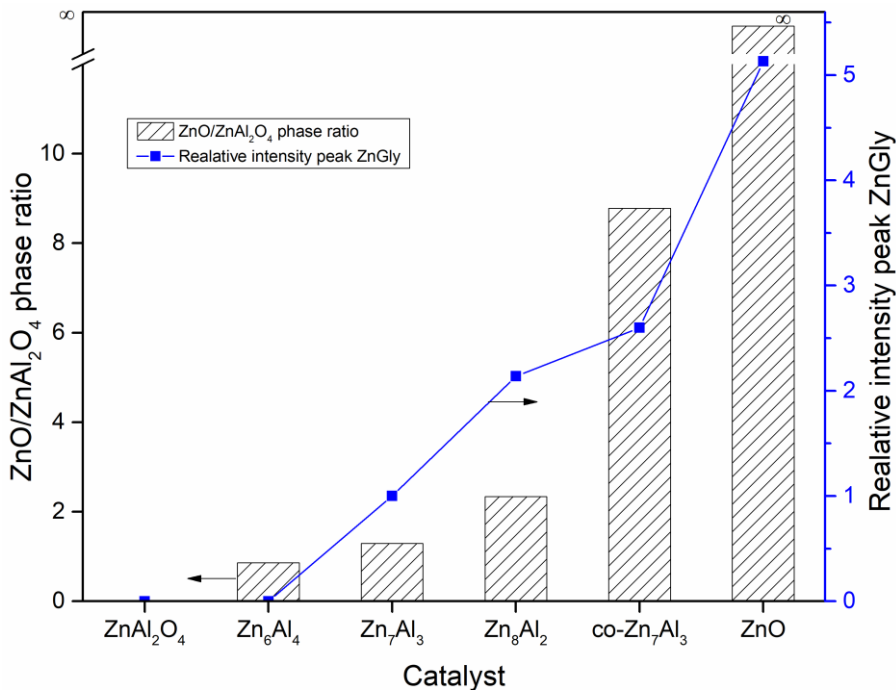


Fig. 3- 9. Trend of the XRD peak ratio ZnO/ZnAl₂O₄ in the fresh catalyst and the relative intensity of the zinc glycerolate XRD peak (011) in the spent catalyst (normalized with Zn₇Al₃)

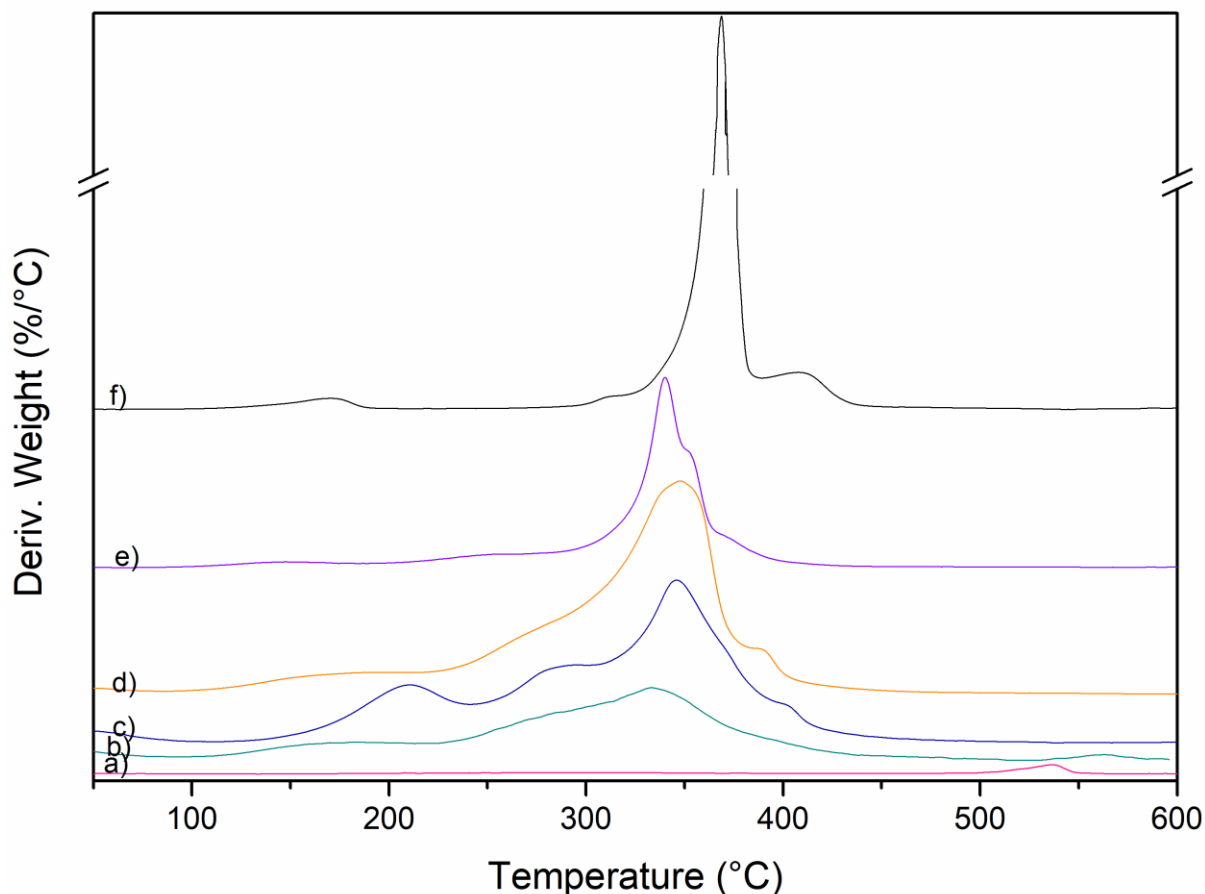


Fig. 3- 10. DTGA profiles of the spent catalysts after 3h reaction. a) ZnAl_2O_4 , b) Zn_6Al_4 , c) Zn_7Al_3 , d) Zn_8Al_2 , e) co- Zn_7Al_3 and f) ZnO .

To clarify the change of the Zn crystalline structure from ZnO to ZnGly during the reaction, the enlarged XRD patterns (in the range of 2θ from 25° to 40°) for the fresh and spent catalysts are shown in Fig. 3- 11. The overlapped peaks of the two ZnO and ZnAl_2O_4 phases in the 2θ range are separated by deconvolution. Two pairs of overlapping peaks, which belong to ZnO and ZnAl_2O_4 , can be deconvoluted: 31.2° (ZnAl_2O_4) and 31.8° (ZnO), and 36.3° (ZnO) and 36.8° (ZnAl_2O_4). For all of the catalysts, the intensity ratios of the ZnO to ZnAl_2O_4 phases over the spent catalysts become smaller compared to the fresh catalysts, which clearly indicates that the ZnO phase is dissolved into the liquid medium during the reaction while the ZnAl_2O_4 phase remains an insoluble solid. The different behavior of the two Zn phases during the reaction is strongly connected with the dual catalysis over the ZnAl mixed oxide catalysts: the

homogeneous reaction route over the ZnO phase and the heterogeneous reaction route over the ZnAl₂O₄ phase.

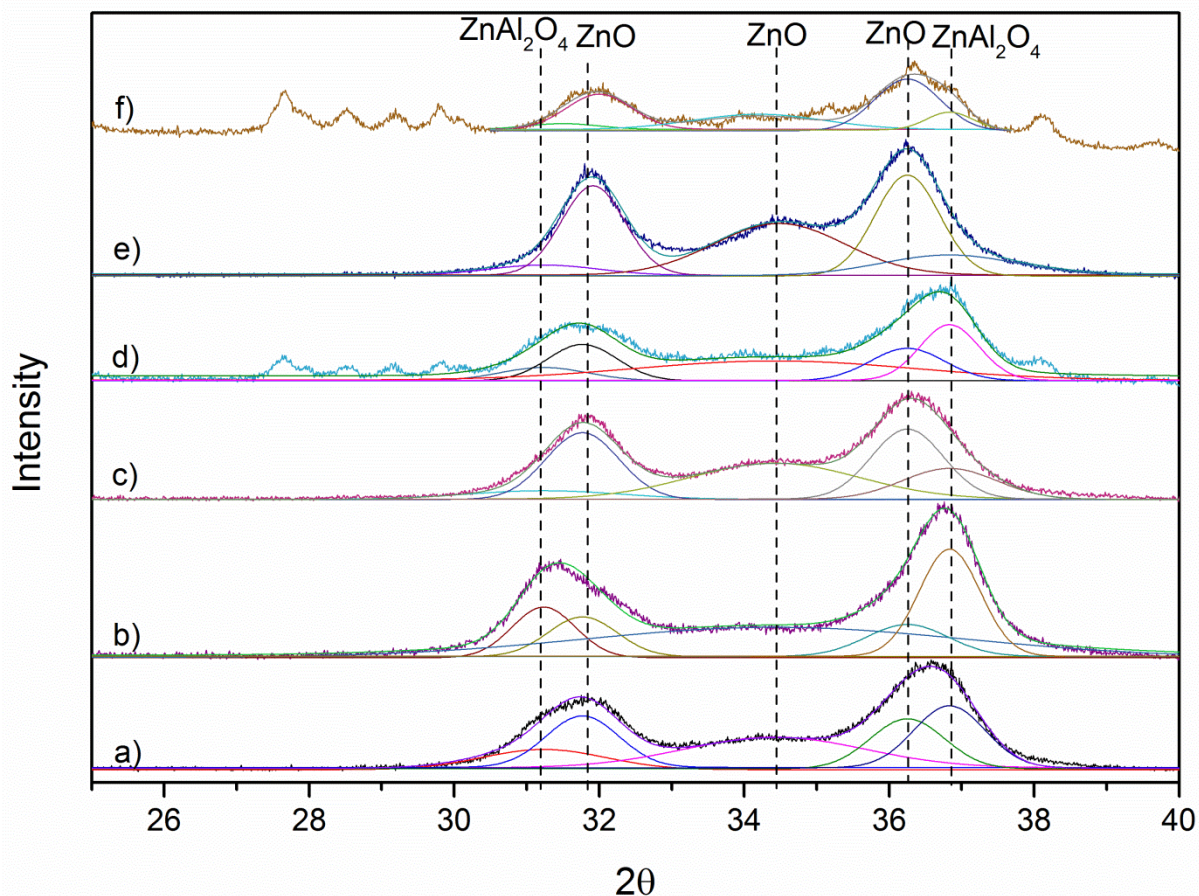


Fig. 3- 11. Enlarged XRD patterns of each catalyst: (a) Zn₆Al₄-fresh, (b) Zn₆Al₄-spent, (c) Zn₇Al₃-fresh, (d) Zn₇Al₃-spent (e) Zn₈Al₂-fresh, and (f) Zn₈Al₂-spent.

Fig. 3- 12 shows the FTIR spectra of the liquid products obtained from the 3 h reaction with the catalysts. The peak at 2213 cm⁻¹ can be assigned as the N=C stretching vibration of the isocyanate functional group (-NCO), which belongs to the Zn(NCO)₂(NH₃)₂ complex formed in the liquid phase [37,51]. This complex is a product of the dissolved Zn with urea, which then acts as an intermediate for the reaction to GC. The NCO peak intensity in Fig. 3- 12 decreases in the order of Zn₆Al₄ > Zn₇Al₃ > Zn₈Al₂, which is consistent with the trend of the Zn amounts dissolved in the liquid phase. The peaks at 1788 cm⁻¹ and 1712 cm⁻¹ correspond to the C=O vibration of GC and the by-product (**II**), respectively [47]. As a whole, the relative

intensity ratio of the two peaks in the FTIR measurements is related to the selectivity of GC and the main by-product (**II**). The ZnAl_2O_4 catalyst gives the lowest selectivity of glycerol carbonate (48%) and the highest selectivity of (**II**) (30%). Correspondingly, the peak intensity ratio of GC to (**II**) for ZnAl_2O_4 is the lowest (Fig. 3- 12a). Conversely, the Zn_6Al_4 catalyst shows the highest GC selectivity (88%) and the lowest (**II**) selectivity, resulting in the highest peak intensity ratio of GC to (**II**) (Fig. 3- 12b).

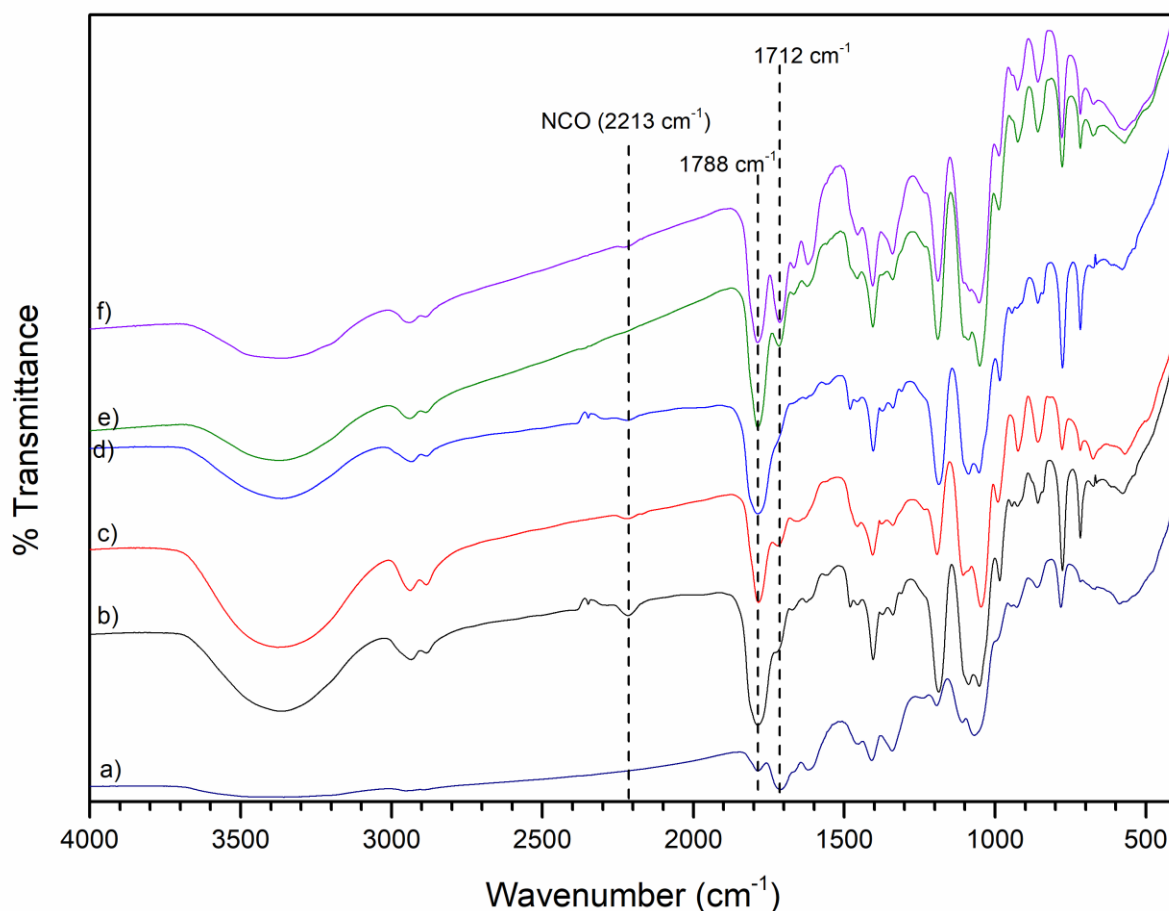


Fig. 3- 12. FTIR spectra of the liquid products obtained from the carbonylation of glycerol with urea over different catalysts: a) ZnAl_2O_4 , b) Zn_6Al_4 , c) Zn_7Al_3 , d) Zn_8Al_2 , e) co- Zn_7Al_3 and f) ZnO .

FTIR results of the spent catalysts are plotted in Fig. 3- 13. The strong peak at 1950 cm^{-1} can be assigned to the C-O stretching vibration, in which the O atom contributes to the hydrogen bonding ($\text{H-O}\cdots\text{H}$) to form the ZnGly crystalline phase [83]. Other peaks for ZnGly

can be found at 2844 cm^{-1} , 2879 cm^{-1} , and 2932 cm^{-1} (C-H stretching vibrations) [84] and especially the broad peak at 2508 cm^{-1} , which corresponds to the hydrogen bonding vibration mode of the ZnGly phase [85]. Another important peak appears at 2222 cm^{-1} and belongs to the vibration mode of the NCO functional groups of the Zn complex in the solid phase, which is blue-shifted compared to that in the liquid phase [86]. The FTIR spectrum of the spent ZnAl_2O_4 catalyst is completely identical to that of the fresh catalyst, implying that no substance remains on the catalyst surface and there is no change in the solid structure. In Fig. 3- 13, the NCO peak of the solid Zn complex appears at 2222 cm^{-1} along with the existence of the ZnO phase in the ZnAl mixed oxide catalysts. When increasing the amount of the ZnO phase in the ZnAl mixed oxide catalysts (from Zn_6Al_4 to Zn_8Al_2), the NCO peak intensity decreases and instead, the peak for ZnGly appears in the spent Zn_7Al_3 and Zn_8Al_2 catalysts. The spent co- Zn_7Al_3 shows a smaller intensity of NCO peak than that of ZnGly peak. For the spent ZnO catalyst, only the peaks for ZnGly can be clearly detected with no appearance of the NCO peak.

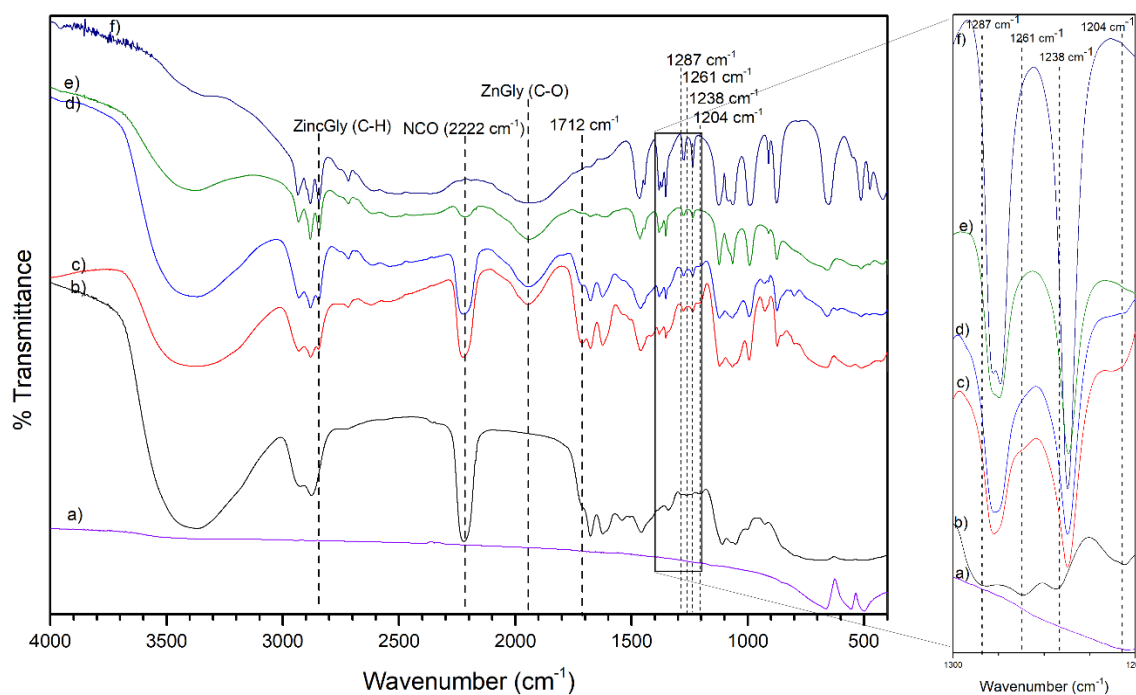


Fig. 3- 13. FTIR spectra of the spent catalysts: (a) ZnAl_2O_4 , b) Zn_6Al_4 , c) Zn_7Al_3 , d) Zn_8Al_2 , e) co- Zn_7Al_3 and f) ZnO.

To clarify the relationship of the Zn phases (ZnO and ZnAl₂O₄ phases) in the fresh catalysts to the formation of solid substances on the spent catalysts and the Zn complex containing the NCO group in the liquid phase, we make a plot of the FTIR peak intensity ratio of NCO and ZnGly in the spent catalysts vs. the FTIR peak intensity of NCO in the liquid phase in Fig. 3-14A. We make another plot of the relative ratio of ZnO/ZnAl₂O₄ in the fresh catalysts vs. the FTIR peak intensity ratio of NCO and ZnGly in the spent catalysts in Fig. 3-14B. First, the relative amounts of NCO in the solid spent catalysts and the liquid phase are strongly correlated since both values decrease in the same order of Zn₆Al₄ > Zn₇Al₃ > Zn₈Al₂ > co-Zn₇Al₃ > ZnO, as shown in Fig. 3-14A. In the literature [23], the Zn NCO complex can be synthesized and precipitated in the form of an isolated solid. There was an equilibrium of the Zn complex with the NCO group between the solid and liquid phases. Second, in Fig. 3-14B, the relative ratios of ZnO/ZnAl₂O₄ in the fresh catalysts are well-matched with the FTIR peak intensity ratios of NCO and ZnGly in the spent catalysts, resulting in the same decreasing trends: Zn₆Al₄ > Zn₇Al₃ > Zn₈Al₂ > co-Zn₇Al₃ > ZnO. In the case of ZnO, the spent catalyst shows the existence of only the ZnGly phase without the Zn NCO complex. When increasing the ZnAl₂O₄ phase in the fresh ZnAl mixed oxide catalysts, the formation of the Zn NCO complex relatively increases in the solid spent catalysts and the liquid phase at the same time. Therefore, it can be concluded that the formation of ZnGly prefers the ZnO phase, whereas the formation of the solid Zn NCO complex prefers the ZnAl₂O₄ phase. The formation of the NCO group in the spent catalysts is strongly related to the ZnAl₂O₄ phase, but there is no formation of the NCO complex in the case of the ZnAl₂O₄ catalyst, implying that the solid NCO complex is formed by selective adsorption onto the solid ZnAl₂O₄ phase in the ZnAl mixed oxide catalysts under the effect of ZnO.

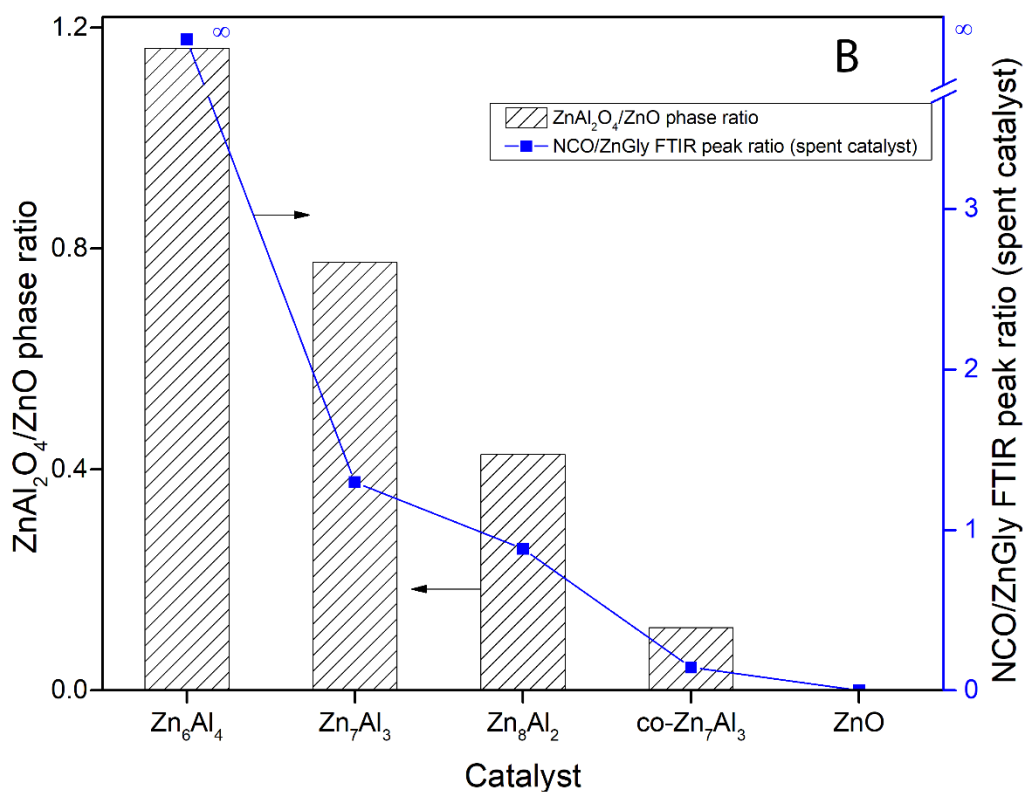
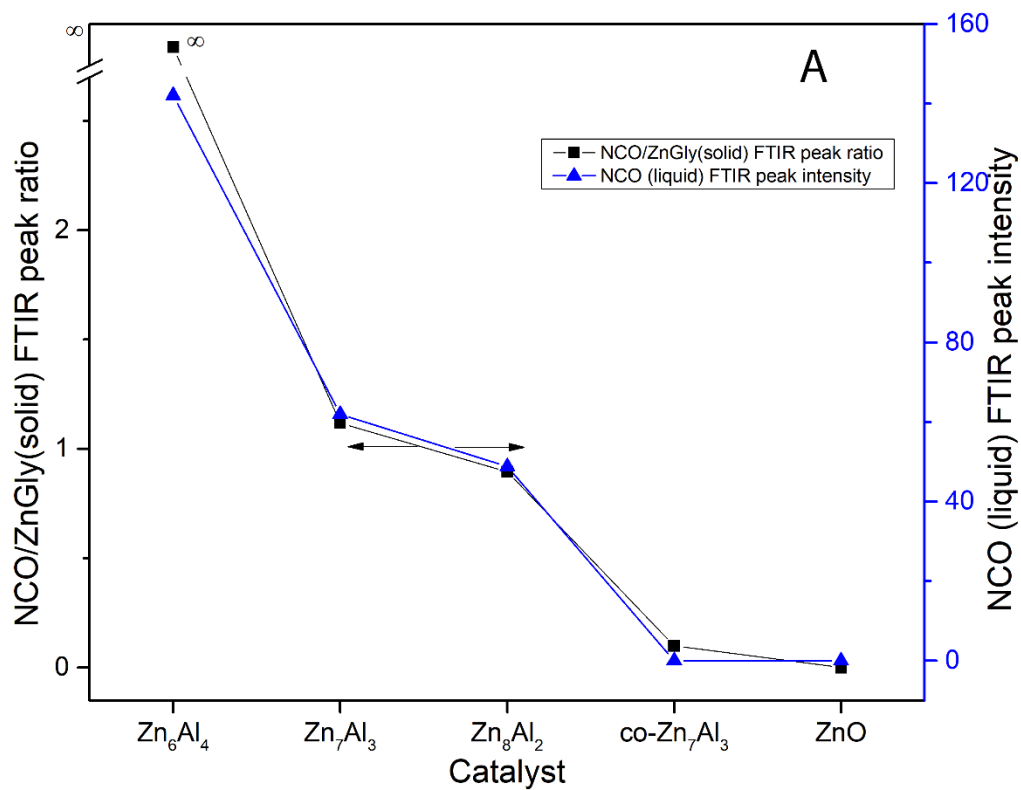


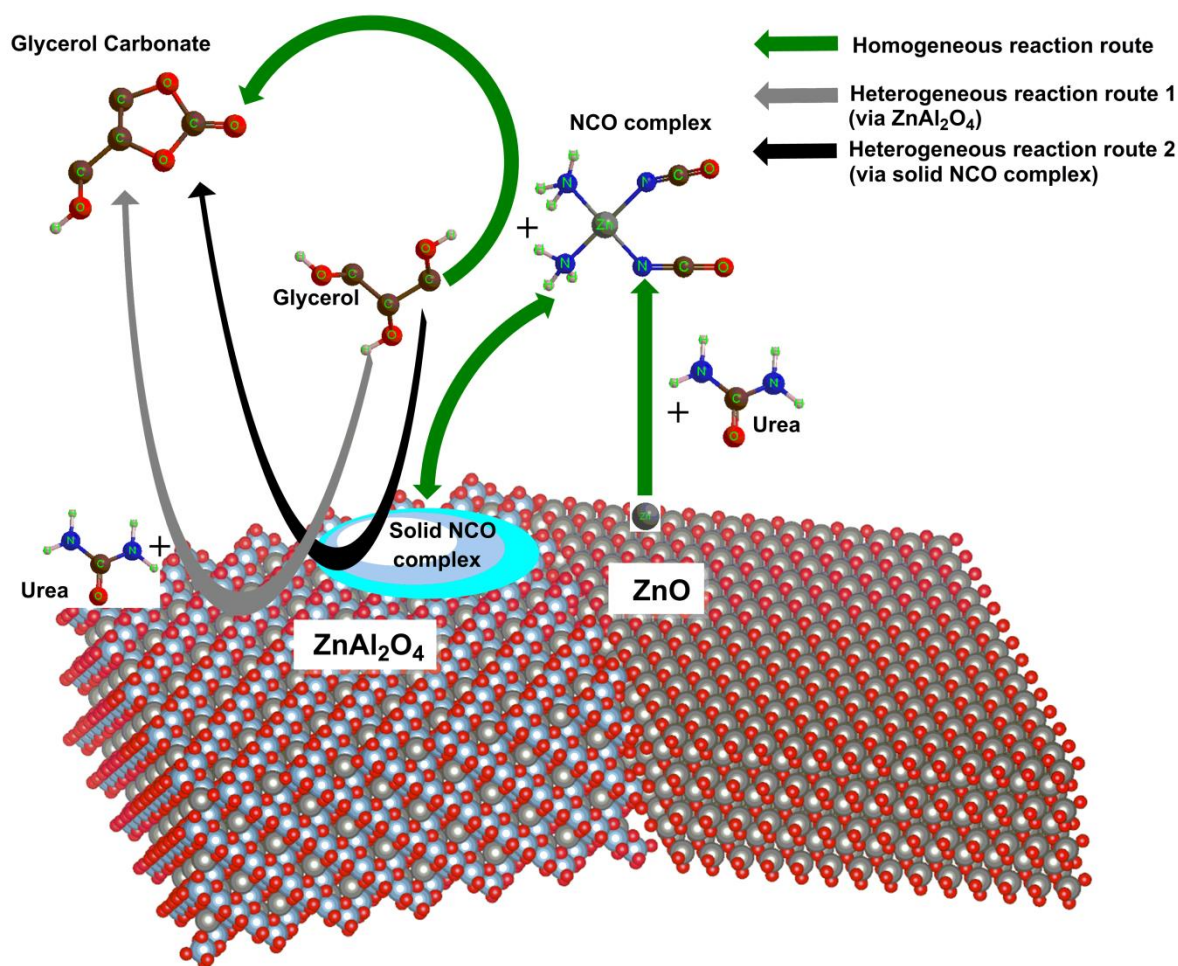
Fig. 3- 14. A) The trend of the intensity ratio of the NCO/ZnGly FTIR peak in the spent catalyst and the NCO FTIR peak intensity in the liquid product, and B) trend of the XRD peak ratio $ZnO/ZnAl_2O_4$ in the fresh catalyst and the intensity ratio of the NCO/ZnGly FTIR peak in the spent catalyst.

3.3.4. Effect of the ZnO and ZnAl₂O₄ phases in dual catalysis

Scheme 3- 2 summarizes the reaction routes of the dual catalysis over the ZnAl mixed oxide catalysts containing two Zn phases: ZnO and ZnAl₂O₄. First, under the reaction condition, ZnO reacts with urea to release the complex Zn(NCO)₂(NH₃)₂ into the liquid medium. This complex acts as a reactive intermediate for the homogeneous reaction route, where glycerol is converted to GC and the complex is recycled by the reaction with urea [51]. As seen in the NH₃-TPD, the ZnAl mixed oxide catalysts generate more acidic sites and can adsorb more NH₃ molecules, indicating that the combination of both ZnO and ZnAl₂O₄ phases in the ZnAl mixed oxide catalysts can create the higher capacity of NH₃ adsorption. This phenomenon was quantitatively researched by Shen [77]. In the case of the ZnO catalyst, there is no formation of the complex on the catalyst surface due to almost zero ability for NH₃ adsorption. Even in the case of ZnAl₂O₄, the complex cannot be formed due to no dissolution of the Zn species into the liquid phase from ZnAl₂O₄.

The complex Zn(NCO)₂(NH₃)₂ can adsorb onto the catalyst surface by the interaction of NH₃ molecules with the Lewis acidic sites (Zn and Al sites). FTIR of the spent catalysts shows evidence for this interaction (Fig. 3- 13). A set of small peaks in the range of 1200-1330 cm⁻¹ relates to the formation of the complex. The peaks at 1261 cm⁻¹ and 1238 cm⁻¹ relate to the structures of the NCO complex (NCO deformation and ZnNH deformation, respectively) [86]. The two peaks at 1204 cm⁻¹ and 1287 cm⁻¹ represent the adsorption of NH₃ coordinated to different Lewis sites (Zn and Al, respectively), corresponding to the ZnAl₂O₄ phase [77,87]. This strongly supports the ability of the NCO complex to adsorb on the ZnAl₂O₄ phase through the Zn species dissolved from the ZnO phase. The set of these four peaks can be clearly observed only with Zn₆Al₄ due to the absence of ZnGly. In the case of Zn₇Al₃, Zn₈Al₂, and ZnO, three peaks of the Zn(NCO)₂(NH₃)₂ complex at 1238 cm⁻¹, 1261 cm⁻¹, and 1287 cm⁻¹ overlap with two peaks at 1236 cm⁻¹ and 1275 cm⁻¹ assigned as the C-O stretching vibrations

of ZnGly, resulting in shoulders of the peaks for ZnGly [84,85]. One of the most important peaks in the FTIR analysis of the spent catalysts is the peak at 1712 cm^{-1} , corresponding to the C=O vibration of the by-product (II) [51]. Because of the formation of (II) on the catalyst surface, we suggest that the complex on the catalyst surface acts as an active site to accelerate the reaction to produce by-product (II) and then GC. Finally, GC can desorb back to the liquid phase as the main product.



Scheme 3- 2. Dual catalysis over the ZnAl mixed oxide catalysts: homogeneous reaction route over the ZnO phase and heterogeneous reaction routes over the ZnAl₂O₄ phase.

As illustrated in Scheme 3- 2, in the case of the ZnAl mixed oxide catalysts, the homogeneous and heterogeneous reactions can be described through three pathways: i) the NCO complex in the liquid phase acts as an active site for homogeneous reaction, ii) in the

ordinary heterogeneous reaction route, glycerol and urea adsorb on the Lewis acidic and basic sites, and then promote GC production, and iii) the NCO complex adsorbing on the catalyst surface acts as an additional active site for the extra heterogeneous reaction route. Compared to the ZnO catalyst (homogeneous reaction route only) and the ZnAl₂O₄ catalyst (heterogeneous reaction route only), the ZnAl mixed oxide catalysts exhibit greater catalytic performance, including high selectivity and yield of GC, through dual catalysis, which is a combination of the homogeneous and heterogeneous reaction routes.

For other Zn-containing mixed oxides, the combination of oxide phases might also enhance the reaction performance. Rubio-Marcos et al. [54] prepared the mixed oxide of ZnO and Co₃O₄; the combination of two oxides achieved better reaction performance than separated ZnO or Co₃O₄ catalyst. The interaction between ZnO and Co₃O₄ showed an effect on the reaction activity even though there was no clear explanation for the reaction routes. Fujita et al. [51] synthesized some solid Zn-containing catalysts and proved a homogeneous reaction route with the solid catalysts. However, the amount of Zn in the liquid phase was decreased by the reaction time, which was assigned as the redeposition/precipitation on the solid catalysts. Interestingly, the behavior of spent ZnO and SM(Zn) (smectite-like material of Zn, Si, Al, O) catalysts was different; on the basis of the XRD patterns, the spent ZnO showed the characteristic XRD peaks of ZnGly while the spent SM(Zn) did not have any ZnGly structure. The redeposition of Zn species in the spent SM(Zn) could relate to the Zn complex on the solid surface of the catalyst, which could provide active sites for the heterogeneous reaction route as we suggest.

3.3.5. Characterizations of spent catalysts and liquid products

The XRD patterns of the spent catalysts are shown in Fig. 3- 15. With the characteristic XRD peaks for the ZnO and ZnAl₂O₄ phases, the XRD peaks for an additional Zn species, ZnGly, were clearly detected. Typical XRD peaks for the ZnGly phase with the space group

P2₁/c were observed at 10.9°, 17.1°, 20.5°, 23.8°, 24.7°, 27.6°, 27.7°, 36.4°, and 38.2° (JCPDS No. 23-1975). In the XRD pattern of the spent ZnO catalyst, the XRD peak intensity for ZnGly is remarkably high even at the initial reaction time (t = 0.25 hr), implying the fast formation of ZnGly. The ZnGly phase was then slowly produced to a saturation state. The XRD peak intensities of the ZnO phase continuously decreased to a trace amount after t = 3 hr. In contrast, the XRD patterns of the spent Zn₇Al₃ catalyst show a different behavior, specifically the characteristic XRD peaks of ZnGly appeared only after t = 2 hr and then the intensities increased continuously (Fig. 3- 15B).

The FTIR spectra of the spent catalysts (Fig. 3- 16) were consistent with the XRD results. In the case of the spent ZnO catalyst, a typical FTIR peak for ZnGly (C-O stretching vibration at 1950 cm⁻¹) appeared with a high intensity even at the initial reaction stage (t = 0.25 hr). Similar to the XRD results, the peak intensities of the typical FTIR peak for ZnGly reached saturation and remained unchanged (Fig. 3- 16A). In contrast to the spent ZnO catalyst, the spent Zn₇Al₃ catalyst did not show any typical FTIR peaks for ZnGly up to t = 1 hr. Beginning at t = 2 hr, the typical FTIR peak for ZnGly at 1950 cm⁻¹ appeared and continuously increased.

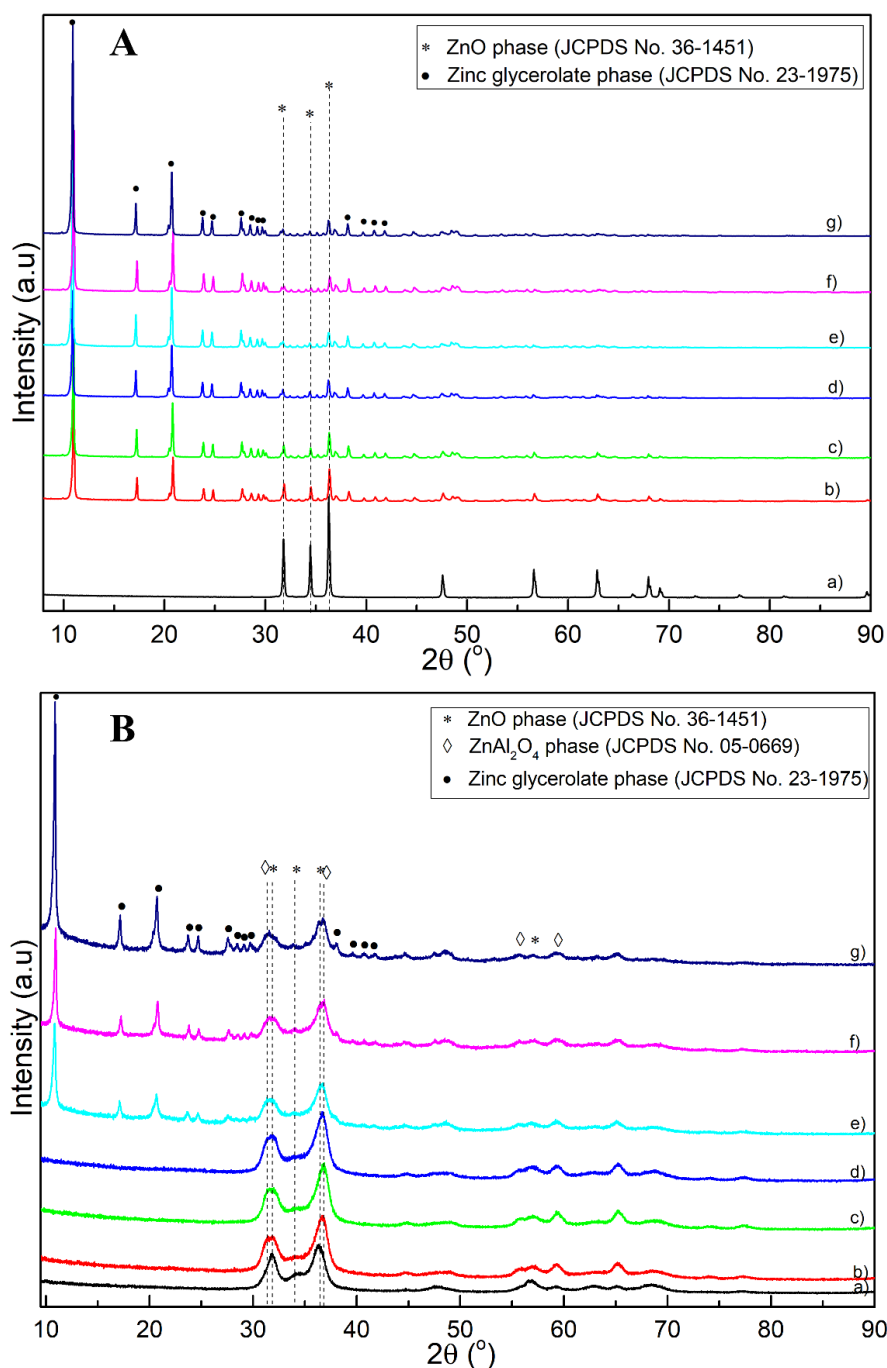


Fig. 3- 15. XRD patterns of fresh and spent catalysts run at the different reaction time: a) $t = 0$ hr (fresh), b) $t = 0.25$ hr, c) $0.5 t =$ hr, d) $t = 1$ hr, e) $t = 2$ hr, f) $t = 3$ hr, and g) $t = 4$ hr. ZnO catalyst (**A**) and Zn₇Al₃ catalyst (**B**).

In addition to ZnGly, the FTIR spectra of the spent Zn₇Al₃ catalyst contained some noticeable peaks: a peak at 2222 cm^{-1} for the NCO vibration, a peak at 1261 cm^{-1} for the NCO deformation, a peak at 1238 cm^{-1} relating to ZnNH deformation, a peak at 1712 cm^{-1} for the C=O vibration of the by-product (**II**), peaks at 1677 cm^{-1} , 1664 cm^{-1} , and 1623 cm^{-1} relating to

N-H deformation, and peaks at 3445 cm^{-1} , 3351 cm^{-1} , and 3190 cm^{-1} for the N-H stretching vibrations [50,86]. The FTIR peaks for the NCO vibration, N-H deformation, NCO deformation, ZnNH deformation and N-H stretching vibration reflect the existence of an NCO complex related to Zn [37,50,51,88,89]. Especially, we found the existence of vibration at 1201 cm^{-1} which belongs to the adsorption of NH_3 coordinated to Zn Lewis sites [77] and proved the adsorption of Zn NCO complex to the solid catalyst, which was discussed in our previous research [50]. In Fig. 3- 16B, the Zn NCO complex was detected at a very early stage of $t = 0.25\text{ hr}$ over the spent Zn_7Al_3 catalyst and was still available even after the appearance of the ZnGly phase ($t = 2\text{ hr}$). Interestingly, over the spent ZnO catalyst, there was no FTIR peak for the NCO functional group for all tested reaction times. Formation of the Zn NCO complex on solid phase only occurred over the spent Zn_7Al_3 catalyst, implying that the existence of the ZnAl_2O_4 phase in the Zn_7Al_3 catalyst influenced the formation of the Zn NCO complex on the solid phase. This phenomenon was confirmed by the results in a previous study [50]: formation of the Zn NCO complex on the solid phase was proportional to the relative ratio of ZnAl_2O_4 to the ZnO phase in the Zn_7Al_3 catalyst. The ZnO phase tended to produce ZnGly on the spent catalyst while the ZnAl_2O_4 phase preferred the Zn NCO complex on the solid catalyst. Fig. 3- 17 displays the DTGA profiles of the spent catalysts. The DTGA profiles of the spent ZnO catalyst for all reaction times exhibited a very high and sharp peak at $360\text{-}370\text{ }^\circ\text{C}$, corresponding to the decomposition of ZnGly [41,90], which properly matched the results obtained by the XRD and FTIR measurements. The peaks for the ZnGly decomposition remained nearly unchanged, reaching saturation (Fig. 3- 17A). However, the DTGA profiles of the spent Zn_7Al_3 catalyst were much more complicated. Before $t = 2\text{ hr}$, the DTGA profiles showed several peaks that might relate to the formation of the Zn NCO complex on the catalyst surface. After $t = 2\text{ hr}$, the DTGA profiles of the spent Zn_7Al_3 catalyst clearly showed an additional peak at $360\text{ }^\circ\text{C}$, corresponding to the decomposition of ZnGly. This DTGA result

was in a good agreement with other measurements of the spent catalysts. Based on the observation of the spent catalysts by XRD, FTIR, and TGA measurements, we concluded that over the ZnO catalyst, ZnGly was dominantly formed, even at the initial reaction time ($t = 0.25$ hr), without formation of the Zn NCO complex, whereas the Zn_7Al_3 catalyst mainly generated the Zn NCO complex on the surface at the initial time ($t = 0.25$ hr) with the delayed formation of ZnGly after $t = 2$ hr.

FTIR spectra of the liquid products obtained from the reactions are shown in Fig. 3- 18. For the both ZnO and Zn_7Al_3 catalysts, and even in the liquid products, typical FTIR peaks for the Zn NCO complex [37,48,51] were detected: a peak at 2213 cm^{-1} (NCO vibration), a peak at 1712 cm^{-1} (C=O vibration of by-product **(II)**), a peak at 1788 cm^{-1} (C=O vibration of main product GC), peaks at 1666 cm^{-1} and 1623 cm^{-1} (N-H deformation), and the N-H stretching vibration peaks in the range $3190\text{-}3480\text{ cm}^{-1}$. Additionally, the peaks at 1712 cm^{-1} (C=O vibration of by-product **(II)**) and 1788 cm^{-1} (C=O vibration of main product GC) corresponded to the generation of the main product and intermediate in the reaction. The Zn NCO complex existed in both catalysts from the initial time and did not disappear after 4 hr of reaction time.

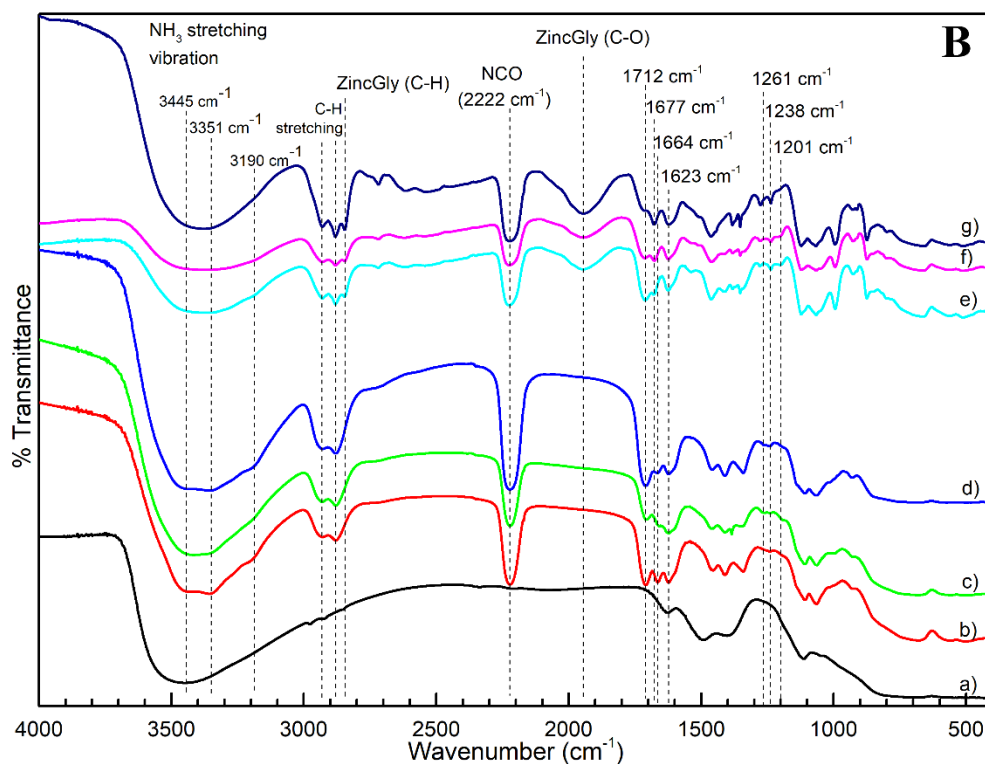
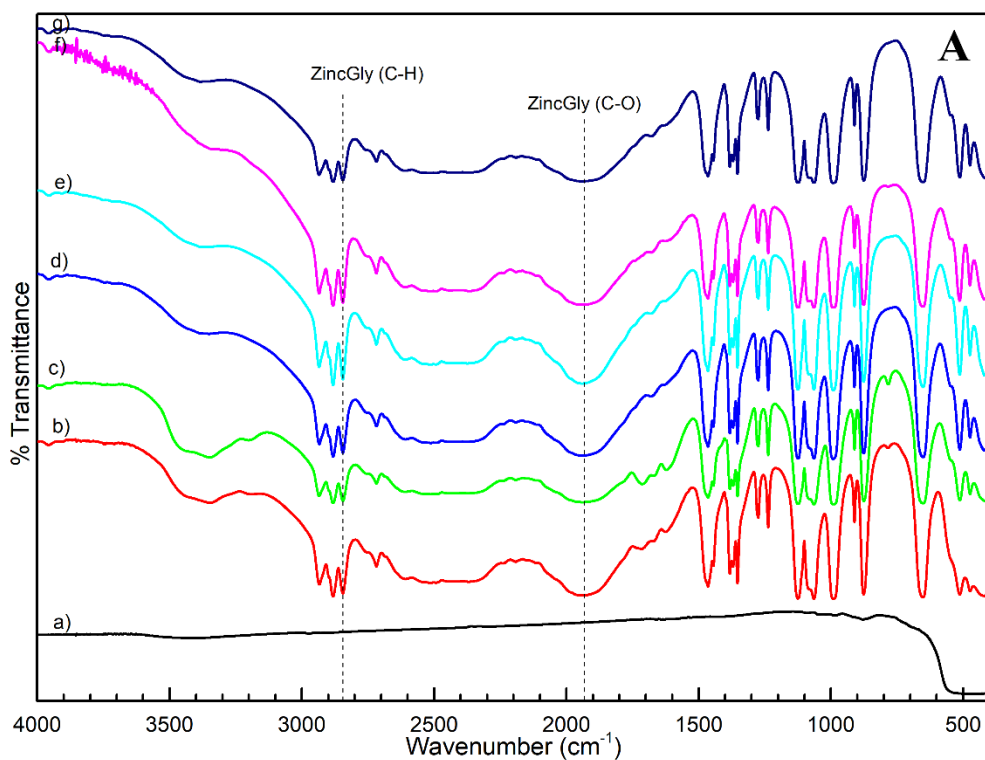


Fig. 3- 16. FTIR spectra of fresh and spent catalysts run at the different reaction time: a) $t = 0$ hr (fresh), b) $t = 0.25$ hr, c) $0.5 t =$ hr, d) $t = 1$ hr, e) $t = 2$ hr, f) $t = 3$ hr, and g) $t = 4$ hr. ZnO catalyst (A) and Zn₇Al₃ catalyst (B).

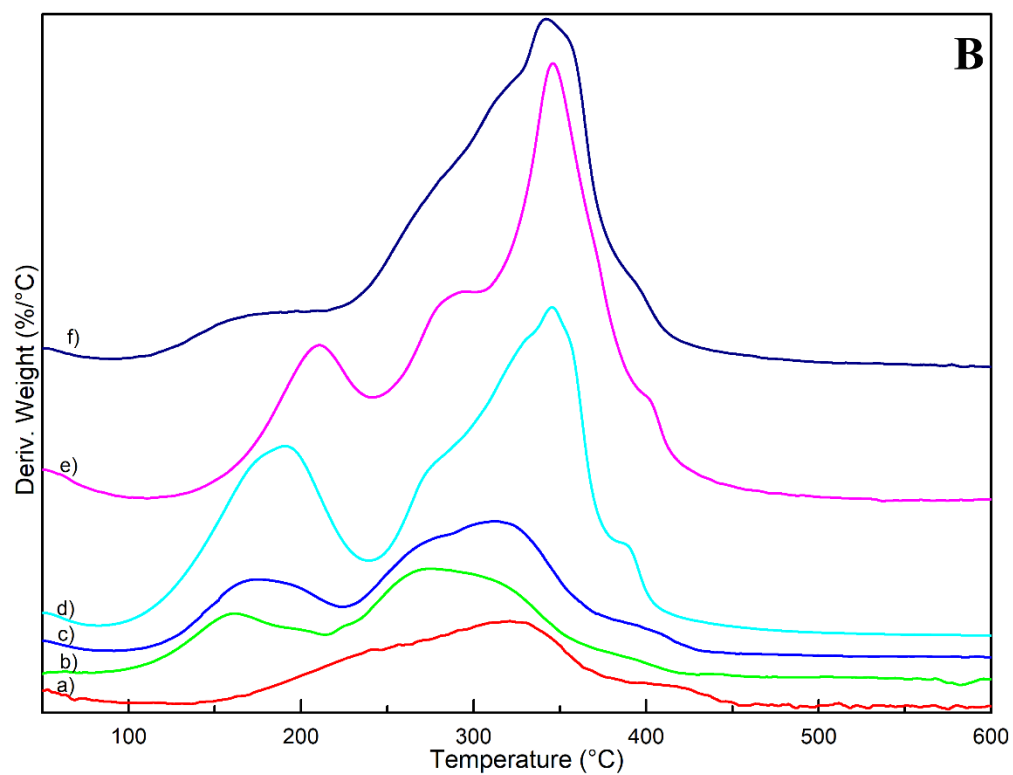
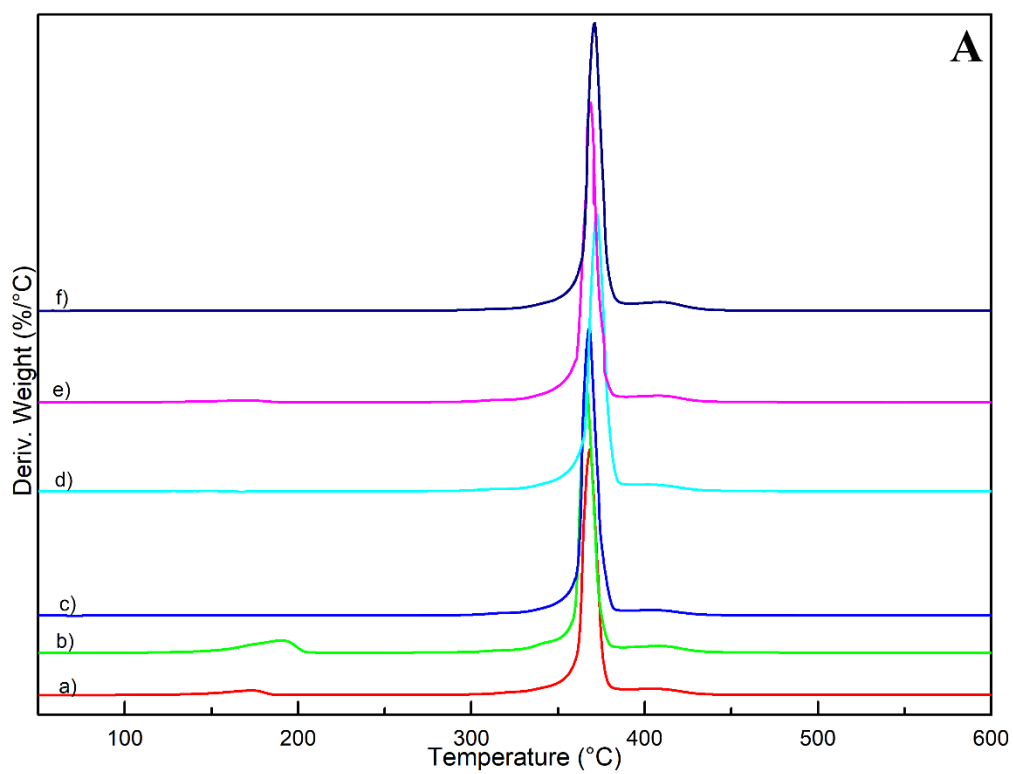


Fig. 3- 17. DTGA patterns of spent catalysts run at the different reaction time: **a)** $t = 0.25$ hr, **b)** 0.5 $t =$ hr, **c)** $t = 1$ hr, **d)** $t = 2$ hr, **e)** $t = 3$ hr, and **f)** $t = 4$ hr. ZnO catalyst (**A**) and Zn₇Al₃ catalyst (**B**).

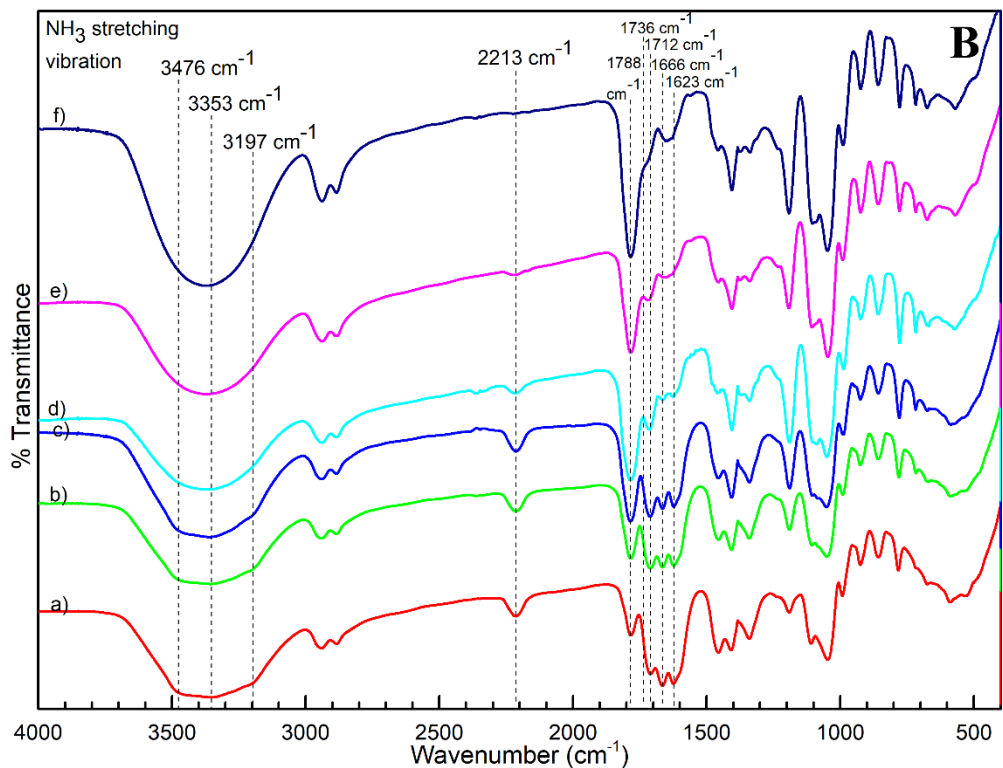
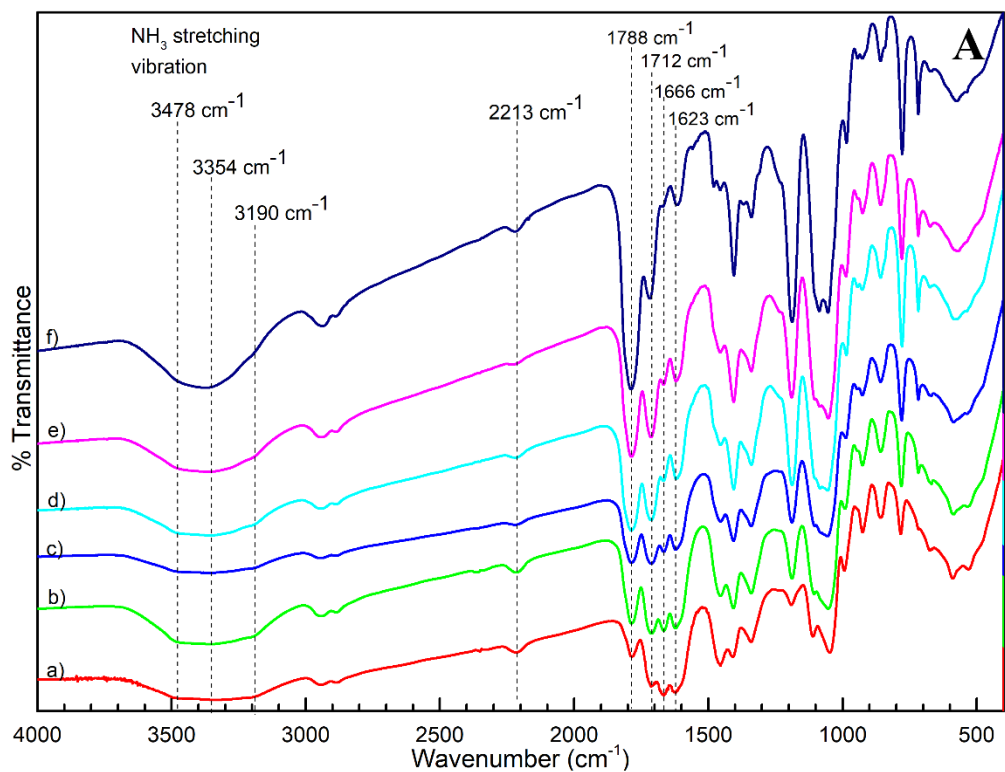
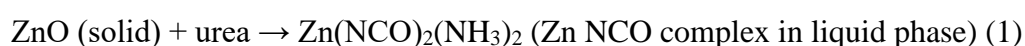


Fig. 3- 18. FTIR spectra of liquid products obtained the reaction of glycerol with urea running at the different reaction time: **a)** $t = 0.25$ hr, **b)** $t = 0.5$ hr, **c)** $t = 1$ hr, **d)** $t = 2$ hr, **e)** $t = 3$ hr, and **f)** $t = 4$ hr. ZnO catalyst (**A**) and Zn₇Al₃ catalyst (**B**).

3.3.6. Evolution of Zn-containing reaction intermediates as a function of the reaction time and their roles in the catalytic reaction routes

In this study, two main Zn-containing reaction intermediates (ZnGly and Zn NCO complex) were observed on the solid surface of the spent catalysts. Here, we focused on the evolution of two Zn-containing reaction intermediates during the reaction as a function of reaction time. The XRD, TGA, and FTIR results of the spent ZnO catalyst indicated that the ZnGly production over the ZnO catalyst was dominant, reaching a saturation state soon as suggested by the high intensity of ZnGly at $t = 0.25$ hr and the subsequent and fast saturation of ZnGly intensities. To quantitatively measure the Zn species, the intensity of the ZnGly (011) peak and the intensity of ZnO (002) peak in the XRD patterns of the spent catalysts was employed to represent the ZnGly production and the ZnO consumption, while the relative intensity of the NCO peak to the C-H peak in the FTIR spectra represents the amount of Zn NCO complex in the liquid phase and on the spent catalysts (Fig. 3- 19). In Fig. 3- 19A, on the spent ZnO catalyst, the NCO complex was not observed for any of the reaction times, implying no generation of Zn NCO complex on the spent ZnO catalyst. The Zn NCO complex existed in the liquid phase through the reaction between ZnO and urea [36,37,51]. However, a large amount of ZnGly was formed even at the initial reaction time ($t = 0.25$ hr) and the ZnGly formation reached a saturation state after $t = 2$ hr. M. Arai et al. suggested the formation of ZnGly from the reaction of Zn NCO complex and glycerol [51]. Fig. 3- 19B illustrates a consecutive reaction route of Zn species, which starts with the reaction of ZnO and urea to form Zn NCO complex in the liquid phase and finalize with a consecutive reaction between the complex and glycerol to form ZnGly. The Zn NCO complex in the liquid phase acts as the main active site to produce GC. Meanwhile, there is no route to form Zn NCO complex on the solid phase.



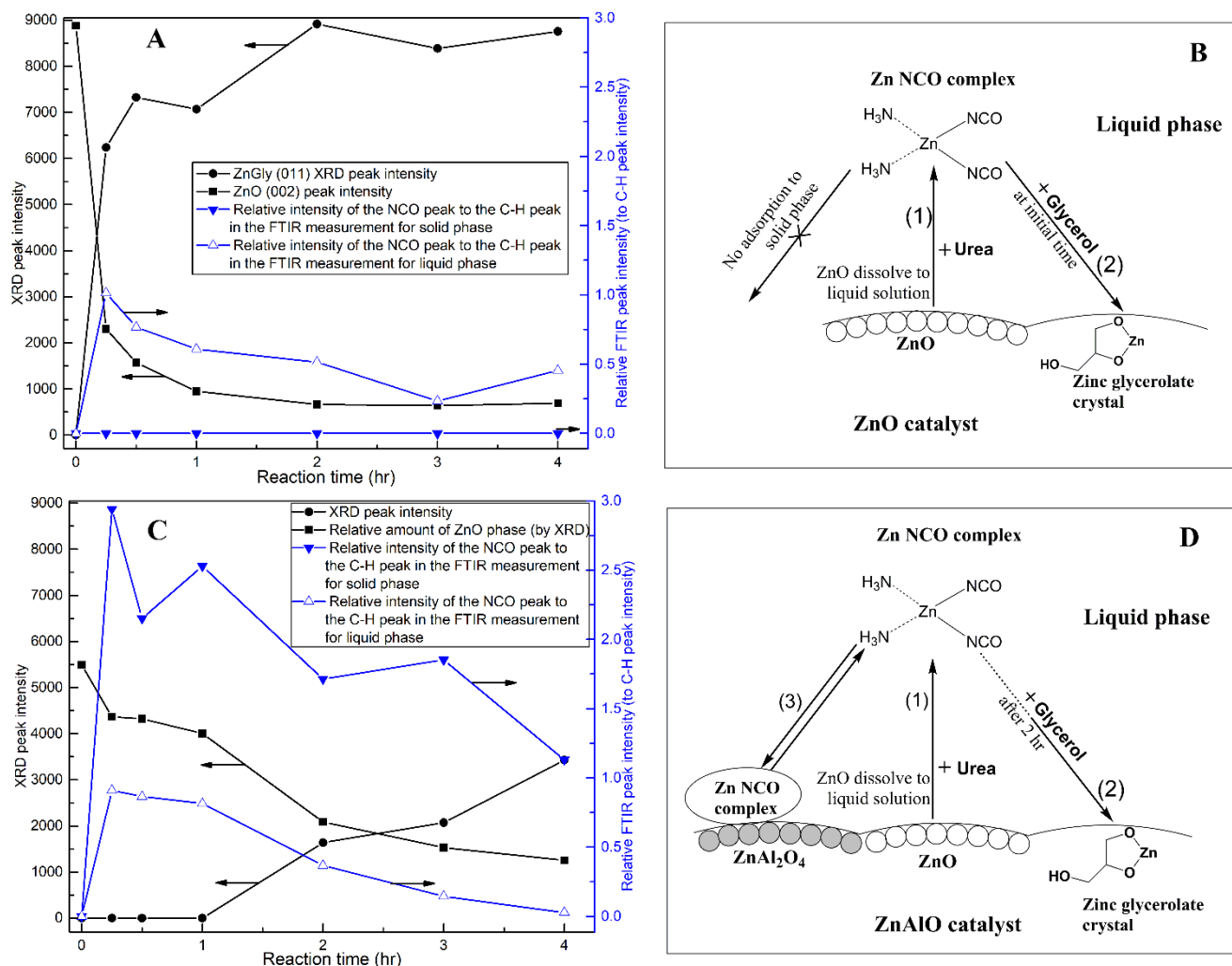
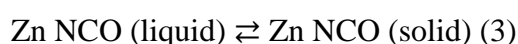


Fig. 3- 19. The reaction time-dependent evolution of Zn-containing species (ZnO, ZnGly and Zn NCO complex) over catalysts: **A)** ZnO and **C)** Zn₇Al₃. The sketch depicting the evolution of Zn-containing species over catalysts: **B)** ZnO and **D)** Zn₇Al₃.

The trends in the relative amounts of Zn species in Fig. 3- 19A proves that consecutive reaction route. The relative amounts of ZnO and ZnGly show two opposite trends, while the relative amount of Zn NCO complex (acted as the intermediate compound in the consecutive reaction route) follows a volcano curve trend. From the beginning of reaction test to 0.25 hr, the relative amounts of ZnGly and Zn NCO complex rapidly increased; at the same time, the relative amount of ZnO fell quickly, implying that, in the very initial time, reaction (1) and (2) occurred fast and consumed most amount of the reactant (ZnO). From 0.25 hr to 2 hr, because

of less amount of the reactant ZnO, reaction (1) was slower than reaction (2), then the Zn NCO complex amount decreased. The amount of ZnO slightly decreased and the amount of ZnGly slightly increased, correspondingly. From $t = 2$ hr, the amount of all three compounds kept almost unchanged. The amount of ZnO was very low and the amount of ZnGly was saturated. Interestingly, the Zn NCO complex was not detected at all in all of the spent ZnO catalysts.

The evolution of Zn species over the Zn_7Al_3 catalyst basically follows the consecutive reaction route (the reaction (1) and reaction (2)) as that over ZnO catalyst. However, unlike the ZnO catalyst, ZnGly over the spent Zn_7Al_3 catalyst was formed from $t = 2$ hr, and its amount increased with reaction time. Besides the Zn NCO complex in the liquid phase and ZnGly in the solid phase, there was the additional contribution of Zn NCO complex in the solid phase. Both the relative amounts of the NCO complex over the spent Zn_7Al_3 catalyst and the relative amounts of the NCO complex in the liquid phase (Fig. 3- 19C) were the highest at the initial reaction time ($t = 0.25$ hr), and then decreased continuously along with the reaction time. This was consistent with our previous conclusion [50] that there was specific adsorption of the NCO complex in the liquid phase onto the spent Zn_7Al_3 catalyst.



From the beginning to 0.25h, by the reaction (1) and (3), the relative amounts of both Zn NCO complex (liquid) and Zn NCO complex (solid) quickly increased together while the relative amount of ZnO decreased and there was no existence of ZnGly. From $t = 0.25$ hr to 2hr, because there was still no formation of ZnGly, the Zn NCO complex acted as the active site for the reaction to GC and was not consumed to make ZnGly, so that both the amounts of the Zn NCO complex in the liquid and solid phases remained unchanged. From $t = 2$ hr, the formation of ZnGly started and its relative amount increased continuously while the relative amounts of the Zn NCO complex in the liquid and solid phases and ZnO were continuously

decreased. Interestingly, the behavior of the relative amount of the Zn NCO complex (liquid) was nearly opposite that of ZnGly, indicating that the ZnGly production over the Zn_7Al_3 catalyst was strongly related to the disappearance of the Zn NCO complex in the liquid phase. Specifically, ZnO reacted with urea to make the Zn NCO complex (liquid) by reaction (1), ZnGly over the spent Zn_7Al_3 catalyst was formed via transformation of the Zn NCO complex (liquid) by reaction (2), resulting in a decrease in the NCO complex in the liquid phase and on the solid catalyst (reaction (3)). Fig. 3- 19D summarizes the transformation of ZnO over Zn_7Al_3 catalyst. Initially, ZnO dissolved to the liquid phase by reacting with urea to form Zn NCO complex. This complex could adsorb on the surface of the $ZnAl_2O_4$ phase. The formation of ZnGly crystal only occurred after 2 hr reaction time by the reaction of the Zn NCO complex in the liquid phase and glycerol.

The same phenomena were observed in the case of co- Zn_7Al_3 , which was prepared by a different method, but the two main phases of ZnO and $ZnAl_2O_4$ were kept as described elsewhere [50]. The intensities of the NCO peaks in the liquid phase (Fig. 3- 20) decreased with reaction time, while the peak representing ZnGly on the solid phase did not exist at the initial time but appeared from $t = 2$ hr (Fig. 3- 21). A similar result was found in the TGA analysis of the spent co- Zn_7Al_3 catalyst; the decomposition peak of ZnGly at 360-370 °C only appeared from $t = 2$ hr (Fig. 3- 22). This evidence supports the conclusion that in the case of the Zn_7Al_3 catalyst (including two phases of ZnO and $ZnAl_2O_4$), ZnGly was generated by the transformation of the Zn NCO complex.

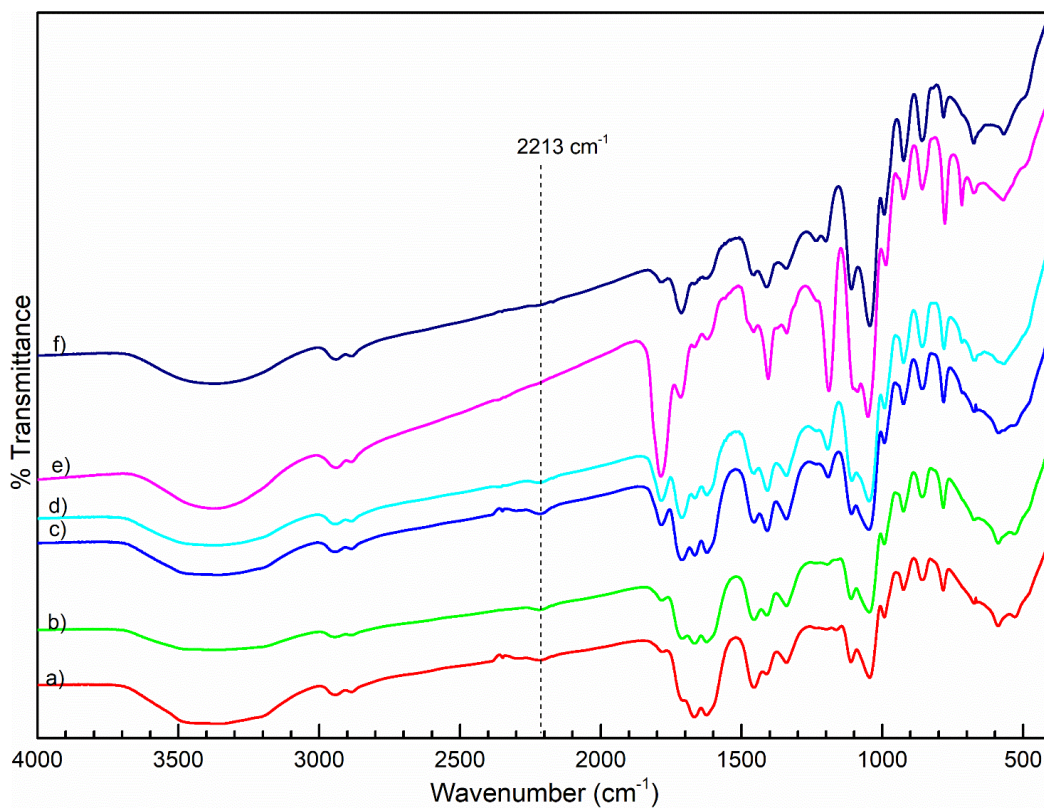


Fig. 3- 20. FTIR spectra of liquid products obtained the reaction of glycerol with urea over co- Zn_7Al_3 catalyst run at the different reaction time: a) $t = 0.25$ hr, b) $0.5 t =$ hr, c) $t = 1$ hr, d) $t = 2$ hr, e) $t = 3$ hr, and f) $t = 4$ hr.

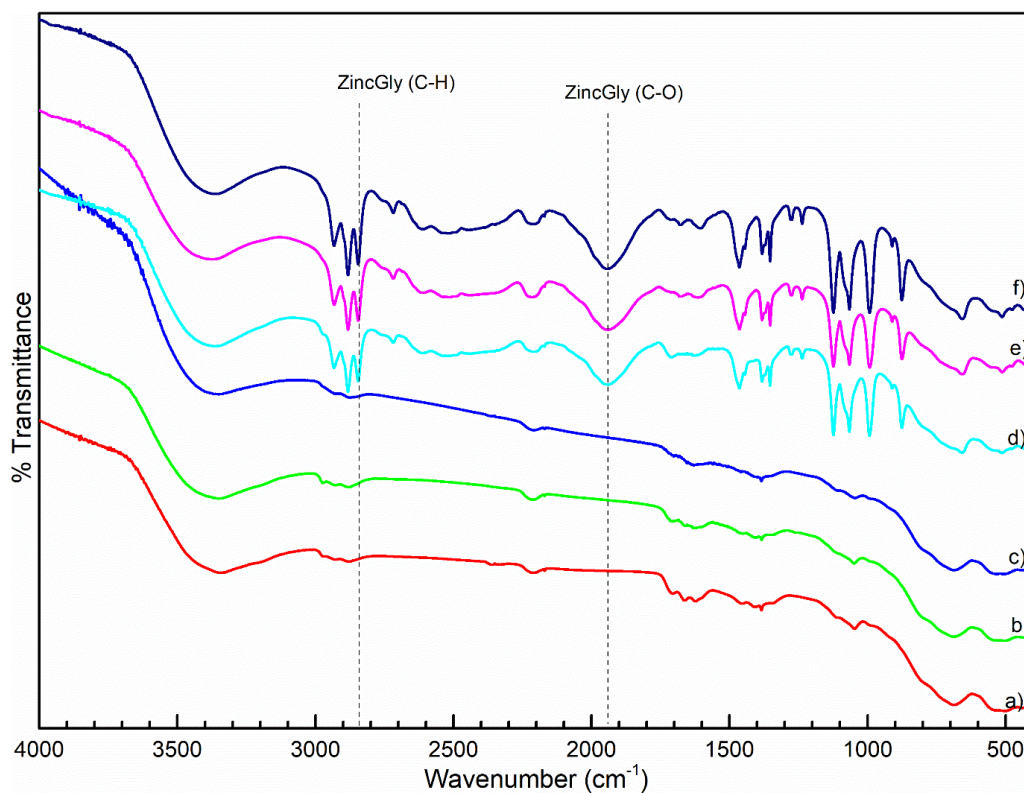


Fig. 3- 21. FTIR spectra of spent co- Zn_7Al_3 catalysts run at the different reaction time: a) $t = 0.25$ hr, b) $0.5 t =$ hr, c) $t = 1$ hr, d) $t = 2$ hr, e) $t = 3$ hr, and f) $t = 4$ hr..

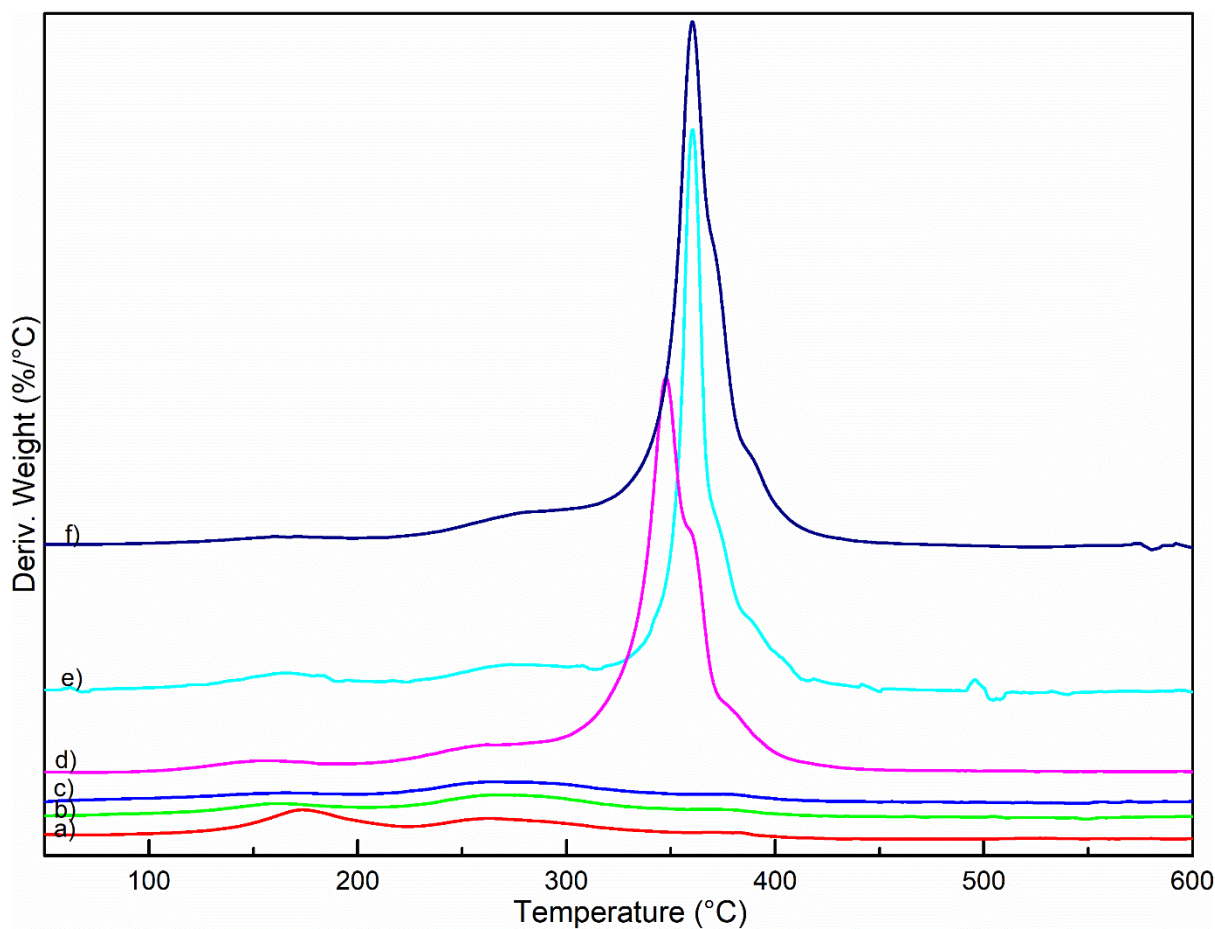


Fig. 3- 22. DTGA patterns of spent catalysts run over co- Zn_7Al_3 at the different reaction time: a) $t = 0.25$ hr, b) 0.5 t = hr, c) $t = 1$ hr, d) $t = 2$ hr, e) $t = 3$ hr, and f) $t = 4$ hr.

To further investigate a factor that affects the formation rate of ZnGly from the Zn NCO complex in the liquid phase, additional reaction tests for the Zn_7Al_3 catalyst were conducted under the reaction conditions of the different urea/glycerol (u/g) ratios ($t = 3$ hr, $u/g = 0.5, 1,$ and 1.5). The spent catalysts were characterized by the FTIR and XRD measurements, whose data are displayed in Fig. 3- 23. The XRD results show that with a high ratio of urea/glycerol ($u/g = 1.5$, urea-rich condition), ZnGly was not formed over the solid catalyst at all. When decreasing the ratio of urea/glycerol to 1 and 0.5, the ZnGly phase appeared and its XRD peak intensity became higher. The FTIR spectra of the spent Zn_7Al_3 catalyst followed the same trend: under the urea-rich condition ($u/g = 1.5$), there was no characteristic peak of ZnGly, but the characteristic FTIR peak for the NCO complex appeared. Under the urea-poor conditions ($u/g = 1$ and 0.5), the FTIR peaks for both ZnGly and the NCO complex were observed and the

relative peak intensity of ZnGly to the Zn NCO complex increased with decreasing u/g ratio (Fig. 3- 23B). Therefore, the formation of ZnGly over the Zn_7Al_3 catalyst depended on not only the Zn phase in the solid catalysts but also the ratio of urea/glycerol in the liquid phase. The urea-poor condition in the liquid phase induced more ZnGly. In other words, the NCO complex in the liquid phase was transformed into the ZnGly phase with the formation of the Zn NCO complex over Zn_7Al_3 catalyst under the urea-poor condition. Under the urea-rich condition, the formation of ZnGly over the Zn_7Al_3 catalyst was inhibited due to less glycerol in the liquid phase. An interesting point is that the formation of the Zn NCO complex over the Zn_7Al_3 catalyst was preferred to the transformation to ZnGly. In Fig. 3- 19C, over the Zn_7Al_3 catalyst, ZnGly was produced from $t = 2$ hr with the presence of the Zn NCO complex on the solid. The generation of the Zn NCO complex on the solid catalyst consumed Zn and urea in the liquid phase, resulting in the urea-poor condition in the liquid phase. Then, the liquid condition induced ZnGly production. Consequently, ZnGly produced over Zn_7Al_3 catalyst was a final by-product due to the reaction of glycerol and the Zn NCO complex in the liquid phase, indicating that the ZnGly production influenced glycerol conversion and GC selectivity. It is suggested that the formation of ZnGly consumes glycerol to produce an extra glycerol-containing by-product, decreasing the selectivity of main product GC. As a result, in the case of the ZnO catalyst, due to the generation of a large amount of ZnGly at the initial time, the selectivity of GC was much lower than that of the Zn_7Al_3 catalyst. In the case of Zn_7Al_3 catalyst, after 2h of reaction, the production of ZnGly began, thus decreasing the selectivity of GC (Fig. 3- 7). The proposed reaction routes over ZnO and Zn_7Al_3 catalysts are illustrated in Scheme 3- 3. The ZnO catalyst follows the homogeneous reaction route (Scheme 3- 3A). The ZnO phase was consumed by the dissolution into the liquid phase and formation of the Zn NCO complex and then the Zn NCO complex could react further with glycerol to make ZnGly. ZnGly was detected from the initial reaction time ($t = 0.25$ h), which soon reached a saturation state at $t =$

2 hr. The reaction route to produce ZnGly contributed positively to glycerol conversion but negatively to GC selectivity. For ZnO catalyst, since $t = 2$ hr, glycerol was consumed only for the reaction that generates GC and by-products in the liquid phase, increasing the GC selectivity. The activity role belonged to the NCO complex (containing Zn) in the liquid phase. This complex reacted with glycerol to produce the main product, GC, and with other by-products, (II) and (IV), in the liquid phase. Since ZnGly is a solid by-product that consumes glycerol, the formation of ZnGly resulted in low GC selectivity. For ZnO catalyst, the ZnGly production occurred at earlier reaction times ($t = 0.25$ and 1 hr) and saturated at $t = 2$ hr. As a result, GC selectivity increased after $t = 2$ hr whereas it was lower at the initial time.

Over the Zn_7Al_3 catalyst, the reaction routes were more complicated due to dual catalysis: the homogeneous reaction route via the Zn NCO complex in the liquid phase and the heterogeneous reaction route via $ZnAl_2O_4$ and the Zn NCO complex in the solid phase. The homogeneous reaction route with Zn_7Al_3 catalyst was the same as that with the ZnO catalyst, except the pathway where the Zn NCO complex in the liquid phase can be adsorbed on the $ZnAl_2O_4$ phase. The transformation of the Zn NCO complex into ZnGly influenced the glycerol conversion and GC selectivity in the reaction performance because of the involvement of glycerol in the transformation and the existence of ZnGly as a solid by-product, whereas the adsorption of Zn NCO complex on the $ZnAl_2O_4$ phase did not affect the product distribution (Scheme 3- 3B). The heterogeneous reaction route proceeded via the $ZnAl_2O_4$ phase or the Zn NCO complex on the solid. The active sites of the latter provided the same reaction route with the Zn NCO complex in the liquid, implying a similar product distribution in the liquid phase. The active sites of the former worked largely based on the relationship between the acidic and basic properties.

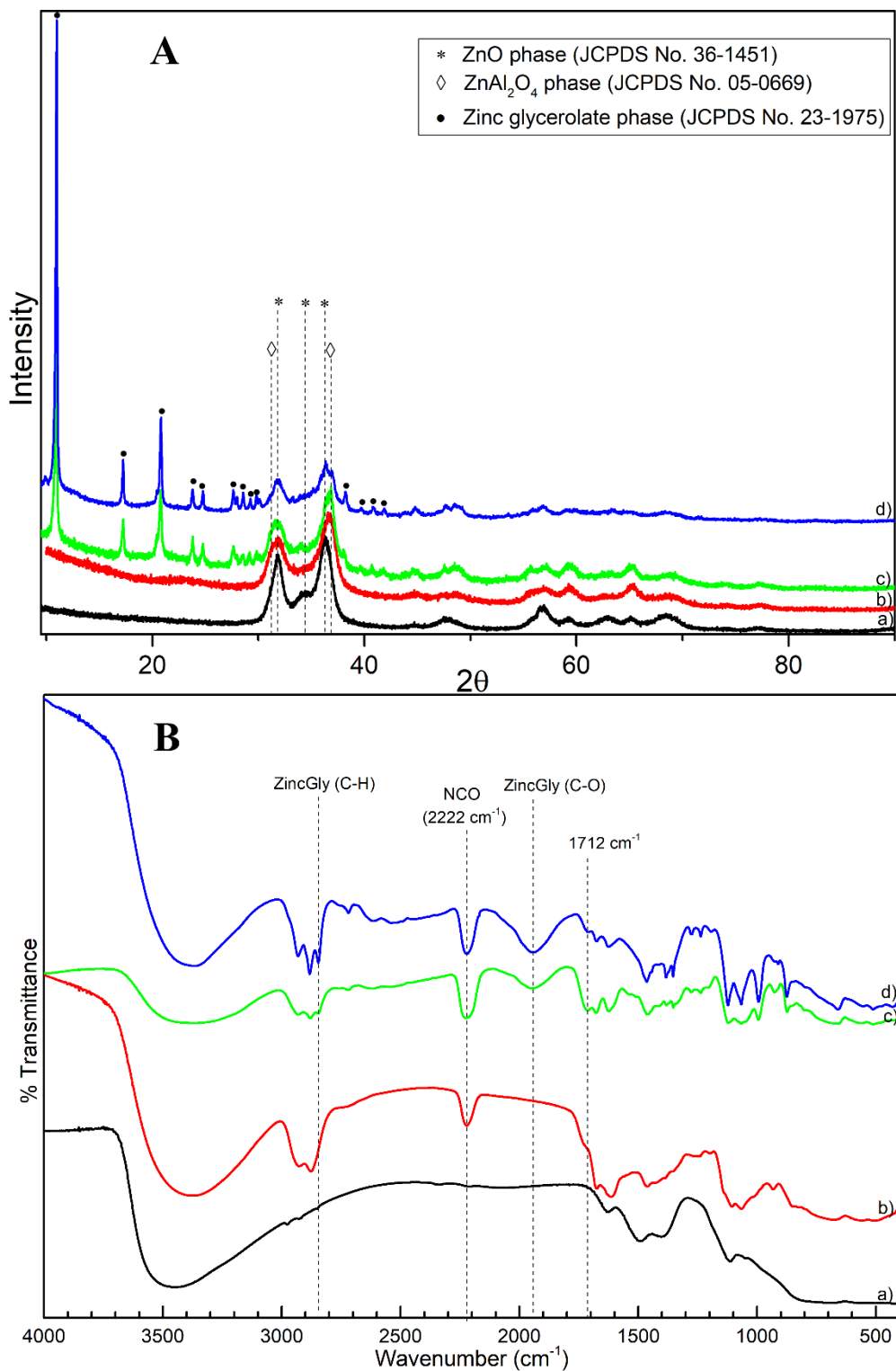
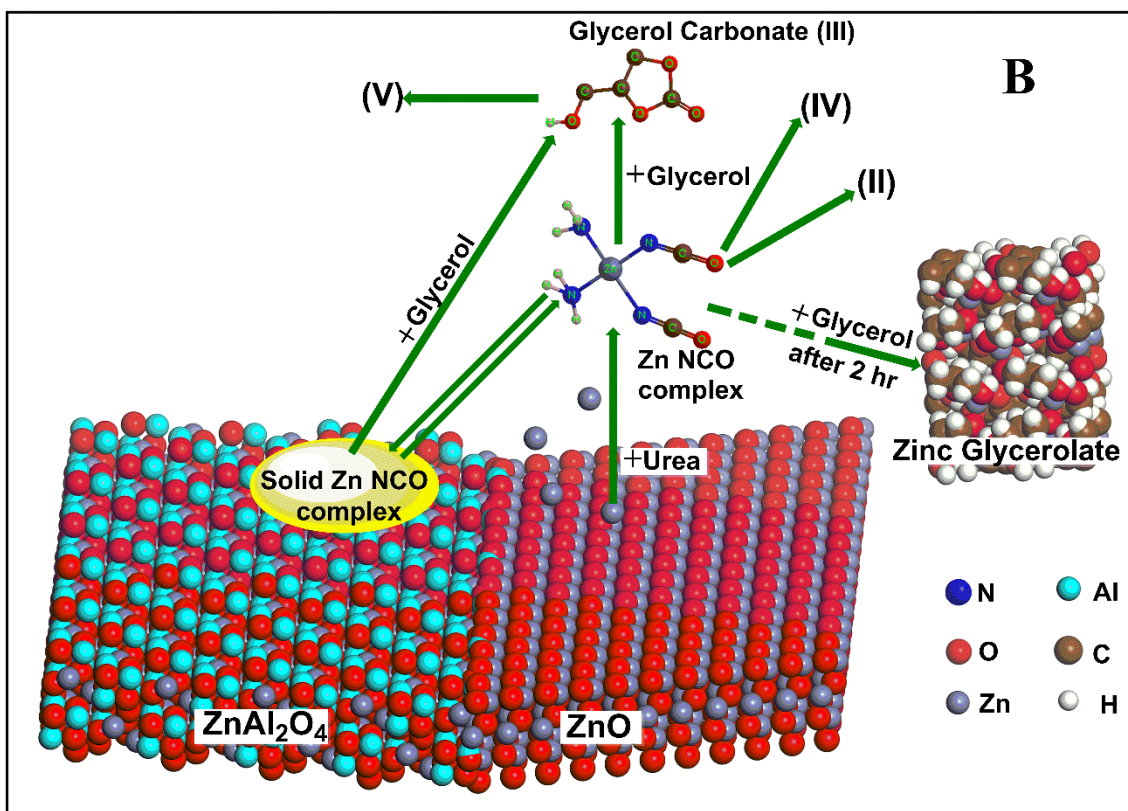
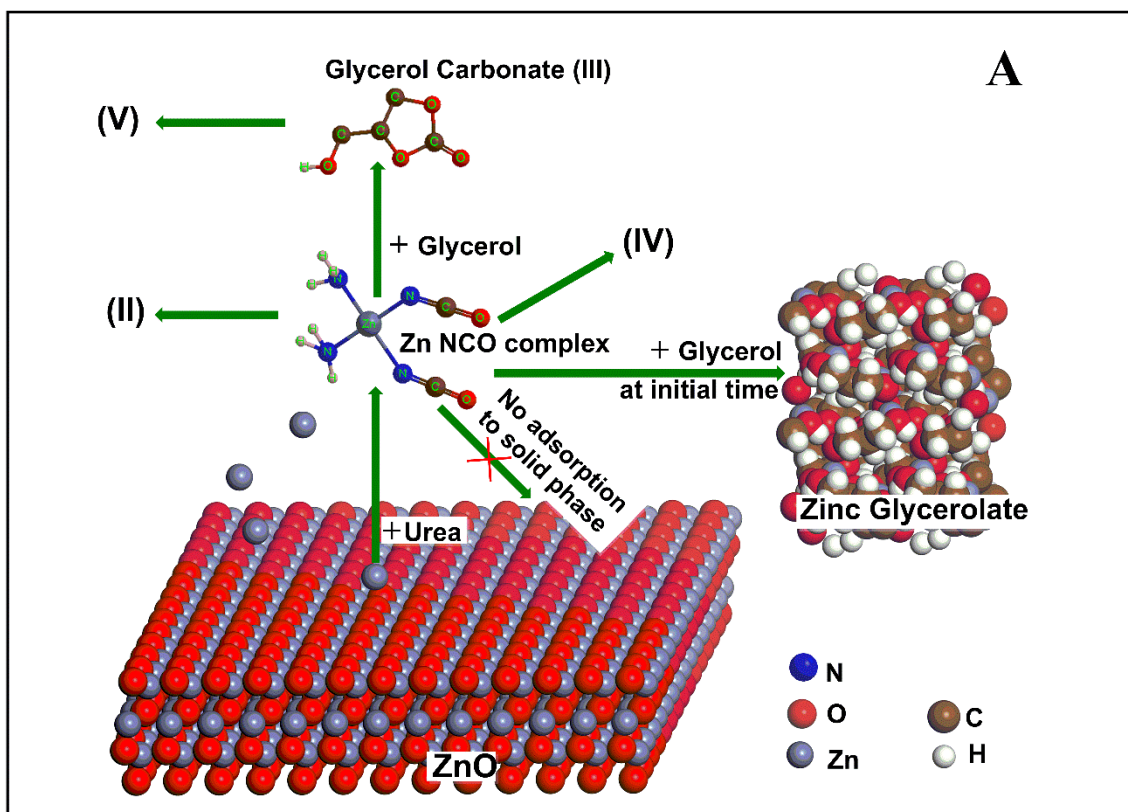


Fig. 3- 23. XRD patterns (A) and FTIR spectra (B) of fresh and spent Zn₇Al₃ catalysts for 3 hr reaction under different initial urea/glycerol ratios: a) fresh, b) urea/glycerol = 1.5, c) urea/glycerol = 1, and d) urea/glycerol = 0.5.



Scheme 3- 3. Evolution of Zn species during glycerolysis of urea. A) ZnO catalyst and B) Zn₇Al₃ catalyst.

The different behaviors in GC selectivity of the two catalysts can be explained by the reaction routes, including the Zn-containing reaction intermediates. The formation of ZnGly automatically caused low GC selectivity in the reaction performance because ZnGly is a solid by-product acquired from the consumption of a certain amount of glycerol. As seen in Fig. 3-7, ZnO catalysts showed lower GC selectivity than the Zn₇Al₃ catalyst since the ZnO catalyst produced a high amount of ZnGly even at the initial reaction time ($t = 0.25$ hr), while there was no ZnGly over the Zn₇Al₃ catalyst at the initial stage of the reaction. However, after $t = 2$ hr, there was no further formation of ZnGly over the ZnO catalyst, resulting in a slight increase in GC selectivity. In contrast, the GC selectivity of the ZnAlO catalyst decreased after $t = 2$ hr due to the generation of ZnGly from the Zn NCO complex in the liquid phase.

3.4. Conclusion

The ZnAl mixed oxide catalysts prepared by the PS template method in this work consist of ZnO and ZnAl₂O₄ phases and show much better catalytic performance in the glycerolysis of urea (high glycerol conversion and GC yield) compared to the pure ZnO and ZnAl₂O₄ catalysts. On the basis of the results from catalyst characterizations, we propose a reaction mechanism of dual catalysis, which includes both homogeneous and heterogeneous reaction routes. ZnO dissolves to the liquid phase to form a Zn NCO complex, which acts as a reactive site for the homogeneous reaction mechanism. This NCO complex also adsorbs on the ZnAl₂O₄ phase and acts as a supplementary heterogeneous active site, in addition to the original Lewis acid-base active site of ZnAl₂O₄. The combination of these homogeneous and heterogeneous reaction routes enhances the catalytic performance of the ZnAl mixed oxide catalysts, resulting in high GC yield.

The Zn-containing reaction intermediates play an important role in the catalytic reaction routes of the reaction of glycerol with urea over ZnO and Zn₇Al₃ catalysts. However, the time-

dependent evolution of these Zn species is different and depends on the composition of the catalysts and the liquid phase conditions. For ZnO catalyst, the ZnGly phase appears from the beginning of the reaction test ($t = 0.25$ hr), resulting in lower GC selectivity than that of the Zn₇Al₃ catalyst. The Zn₇Al₃ catalyst composed of the ZnO and ZnAl₂O₄ phases does not prefer the formation of ZnGly at the initial stage (before $t = 2$ hr), whereas the solid Zn NCO complex is strongly detected in the spent Zn₇Al₃ catalysts. The formation of the solid Zn NCO complex is closely connected with the existence of the ZnAl₂O₄ phase. However, even over the Zn₇Al₃ catalyst, the ZnGly phase is produced after $t = 2$ hr via transformation of the Zn NCO complex in the liquid phase, decreasing the GC selectivity of the Zn₇Al₃ catalyst

CHAPTER 4. INVESTIGATE THE EFFECT OF DISORDERED SPINEL ZnAl_2O_4 PHASE TO THE ACIDITY AND THE GLYCEROLYSIS OF UREA.

4.1.Introduction

In the reaction mechanism over the Zn-based catalysts, zinc diamine diisocyanate ($\text{Zn}(\text{NH}_3)_2(\text{NCO})_2$, abbreviated as a Zn NCO complex) can be formed by the dissolution of Zn from a Zn-containing catalyst into a liquid phase, where it can act as an active site for the homogeneous reaction route. In our previous studies [50,91], we found that the ZnAl mixed oxide catalysts followed dual catalytic reaction routes resulting in better catalytic reaction performance than a ZnO catalyst alone. In the dual catalytic reaction routes, the catalytic performance was affected by the existence of two Zn-containing intermediates — zinc glycerolate (ZnGly) and Zn NCO complex. The formation of ZnGly in the reaction consumed glycerol but decreased the GC selectivity, whereas the Zn NCO complex in solid and liquid phases enhanced the GC yield. The formation of a solid Zn NCO complex over a ZnAl_2O_4 phase brought additional benefits including: i) serving as an active site for a heterogeneous reaction route producing GC, ii) interacting selectively with an insoluble ZnAl_2O_4 phase [50], and iii) suspending the formation of ZnGly which reduced the GC selectivity [91]. It was also found that the formation of Zn NCO complex on the insoluble ZnAl_2O_4 phase related to the surface acidity. Therefore, to clearly understand how the catalytic properties of Zn-containing catalysts influence the catalytic reaction mechanism in the reaction of glycerol with urea, it is necessary to ascertain how the molecular structure of the catalysts can change the catalytic properties related to the surface acidity.

ZnAl_2O_4 is a well-known spinel structure with a typical formula $(\text{A}^{2+})[\text{B}^{3+}_2]\text{O}_4$, where A^{2+} (Zn^{2+}) and B^{3+} (Al^{3+}) are the divalent and trivalent metal cations, respectively [92]. A spinel structure is composed of two types of sites: tetrahedral sites expressed by the () symbol and

octahedral sites represented by the [] symbol when viewed in a formula. In a typical normal spinel structure, A^{2+} cations occupy one-eighth of the tetrahedral sites and B^{3+} cations occupy half of the octahedral sites. In contrast, an inverse spinel structure is a different spinel group having the formula $(B^{3+})[A^{2+}B^{3+}]O_4$, which contains not only half of the B^{3+} cations occupying the tetrahedral sites but also all of A^{2+} cations and half of the B^{3+} cations occupying the octahedral sites [93]. A normal spinel structure can be partially disordered by changing the distribution of A^{2+} and B^{3+} cations occupying these two sites. The disordered structure is called a partially inversed structure. In partially inversed $ZnAl_2O_4$, the main cations of Zn^{2+} and Al^{3+} occupy the tetrahedral and octahedral sites, respectively. Even so, some Zn^{2+} cations substitute for Al^{3+} cations in the octahedral sites and some Al^{3+} cations substitute for Zn^{2+} in the tetrahedral sites.

In this research, we investigated the relationship between the disordered $ZnAl_2O_4$ spinel lattice structure in ZnAl mixed oxide catalysts, the acidity of the catalysts and the formation of a Zn NCO complex over the catalysts. Moreover, we discussed the differences between Zn NCO complexes on the solid catalyst or in the liquid phase, which induced different catalytic behavior in the reaction of glycerol with urea. The formation of a Zn NCO complex over the $ZnAl_2O_4$ phase improved the GC yield by inhibiting the catalytic reaction route to produce ZnGly.

4.2. Experimental

4.2.1. Catalyst preparation

The physically mixed ZnAl catalyst (denoted as p-ZnAlO) was prepared by simple mixing of each powder of ZnO and $ZnAl_2O_4$ precipitated at room temperature. The molar ratio of Zn to Al in p-ZnAlO was 7:3. The precipitated ZnO and $ZnAl_2O_4$ powders were prepared using a conventional precipitation method. To prepare the precipitated $ZnAl_2O_4$, an aqueous solution

of $\text{Zn}(\text{NO}_3)_2 \cdot 6\text{H}_2\text{O}$ (Sigma-Aldrich Korea, Gyeonggi, South Korea) and $\text{Al}(\text{NO}_3)_3 \cdot 9\text{H}_2\text{O}$ (Sigma-Aldrich Korea, Gyeonggi, South Korea) with a molar ratio of 1:2 was simultaneously mixed with a basic solution of NaOH and NaNO_3 under constant $\text{pH} = 6$ and vigorous stirring. The solution was filtered and washed with deionized water several times. Finally, the solid powder was dried at $100\text{ }^\circ\text{C}$ overnight and calcined at $600\text{ }^\circ\text{C}$ for 6 h. The precipitated ZnO was prepared in the same way using only $\text{Zn}(\text{NO}_3)_2 \cdot 6\text{H}_2\text{O}$ as a precursor.

The citrate complex ZnAl mixed oxide catalyst (denoted c-ZnAlO) and citrate complex ZnAl_2O_4 (denoted as c- ZnAl_2O_4) were prepared using a modified citrate complex technique [94]. To synthesize c-ZnAlO, an aqueous solution of $\text{Zn}(\text{NO}_3)_2 \cdot 6\text{H}_2\text{O}$ and $\text{Al}(\text{NO}_3)_3 \cdot 9\text{H}_2\text{O}$ at the same molar ratio with p-ZnAlO (Zn:Al = 7:3) was prepared at room temperature, then citric acid powder (ratio of citric acid to metal = 2:1) was added to the solution followed by stirring with a magnetic bar. Stirring was continued at $70\text{ }^\circ\text{C}$ to evaporate water until a yellow viscous gel solution was formed. The gel was dried at $140\text{ }^\circ\text{C}$ and spontaneously solidified by the emission of NO_x gases. The resulting solid powder was ground and calcined at $600\text{ }^\circ\text{C}$ for 4 h. c- ZnAl_2O_4 was prepared in the same way with a molar ratio of Zn and Al in the precursor of 1:2.

4.2.2. Reaction test

The detailed procedure for the glycerolysis of urea to produce glycerol carbonate over the catalysts can be found in the part 2.2.2 of Chapter 2.

The recyclability of catalysts also was inspected. The spent catalysts used for the characterizations and recycle tests were additionally prepared via filtration from the liquid phase, washing with ethanol and drying at $70\text{ }^\circ\text{C}$. The spent catalysts (without any further calcination process) were re-used over 2 catalytic cycles under a similar reaction condition with the fresh catalysts.

4.2.3. Catalyst characterization

X-ray diffraction (XRD) patterns for fresh and spent catalysts were obtained using a Rigaku RAD-3C diffractometer (Rigaku Corp., Tokyo, Japan) with Cu K α radiation ($\lambda = 1.5418 \text{ \AA}$) at a scattering angle (2θ) scan rate of $2^\circ/\text{min}$ operated at 35 kV and 20 mA. The spent catalysts were analyzed using a Thermo Scientific Nicolet iS5 FT-IR spectrometer (Thermo Fisher Scientific, Waltham, MA, USA). Raman signals of the fresh catalysts were examined using a Thermo Scientific DXR Raman microscope (Thermo Fisher Scientific, Waltham, MA, USA). XPS data and the surface atomic ratios were surveyed using a Thermo Scientific K-Alpha XPS spectrometer (Thermo Fisher Scientific, Waltham, MA, USA). The nitrogen adsorption/desorption isotherms were measured by a QUADRASORB evo Gas Sorption Surface Area and Pore Size Analyzer (Quantachrome Instruments, Boynton Beach, FL, USA) and the surface areas of the fresh catalysts were calculated by the Brunauer-Emmett-Teller (BET) equation.

The number of acidic and basic sites was measured using the temperature-programmed desorption method of NH_3 and CO_2 (TPD- NH_3/CO_2) on a MicrotracBEL BELCAT-M (MicrotracBEL Corp., Osaka, Japan). Ordinarily, an amount of 100 ~ 200 mg of fresh catalyst was put into the quartz sample tube of the BELCAT-M instrument. Initially, the sample was pretreated under the helium flow (100 mL/min) at 600 °C in 1 h. After that, a flow of NH_3 or CO_2 (50 mL/min) was applied to the sample at 50 °C for the adsorption step. Finally, the temperature was slowly increased from 50 °C to 600 °C at the rate of 1.5 °C/min; the desorbed species were removed by helium flow (30 mL/min) and analyzed by the TCD detector.

4.3. Results and discussion

4.3.1. Interactions between the ZnO and ZnAl₂O₄ phases - the disordered ZnAl₂O₄ spinel lattice

The XRD patterns of the fresh catalysts are shown in Fig. 4- 1. Characteristic diffraction peaks of the ZnO phase and ZnAl₂O₄ phase are clearly detected in the XRD patterns of the ZnAl mixed oxide catalysts (p-ZnAlO and c-ZnAlO). Typical peaks are observed at 31.8°, 34.4°, 36.3°, 47.5°, 56.7°, and 62.9° positions for the ZnO phase with the P6₃mc space group (JCPDS No. 36-1451) [95]. Characteristic peaks are observed at 31.2°, 36.8°, 44.8°, 49.1°, 55.7°, 59.3°, 65.2°, 74.1°, and 77.3° positions for the ZnAl₂O₄ phase with the Fd3m space group (JCPDS No. 05-0669) [96]. Meanwhile, the XRD pattern of c-ZnAl₂O₄ catalyst apparently shows only the characteristic peaks of a single ZnAl₂O₄ phase, confirming that c-ZnAl₂O₄ contains a pure ZnAl₂O₄ phase.

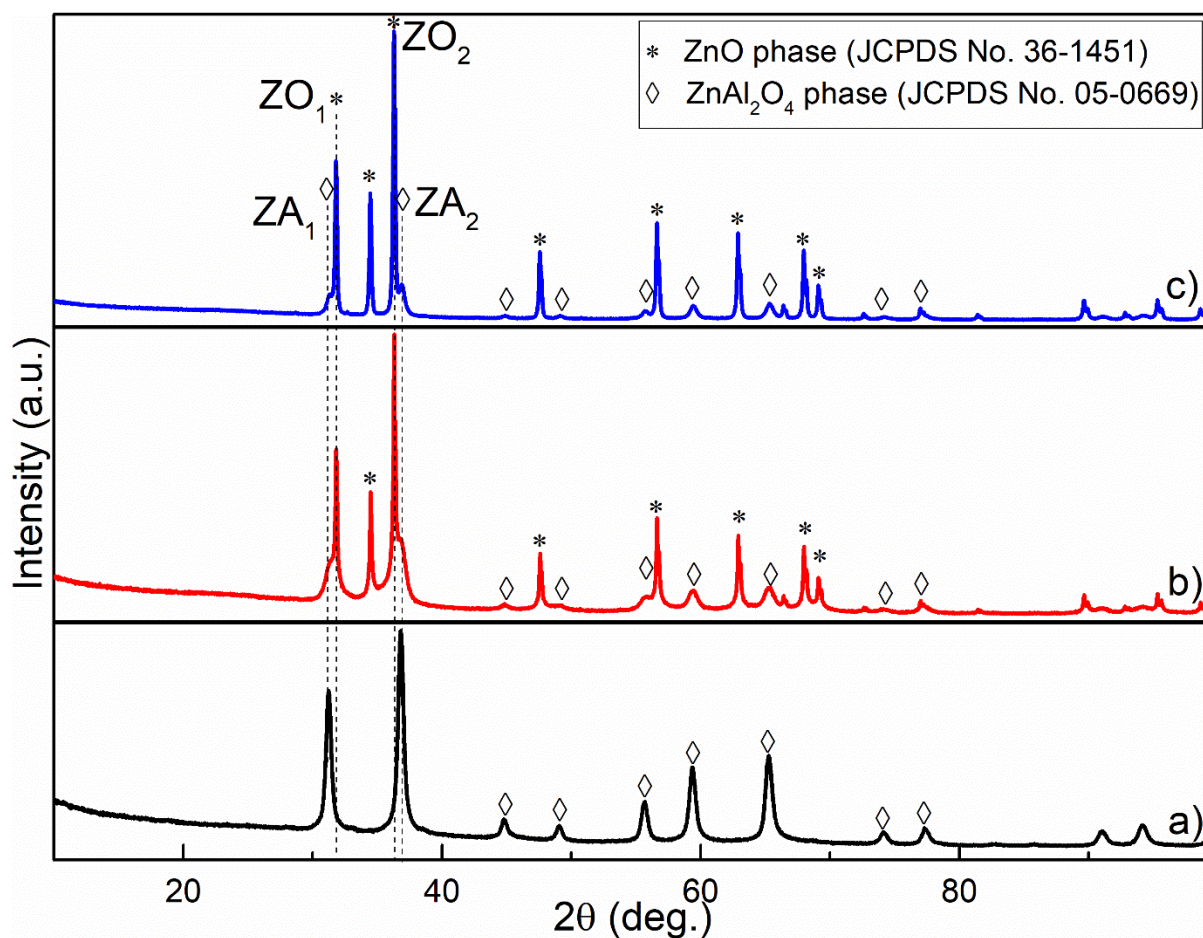


Fig. 4- 1. XRD patterns of fresh catalysts: a) c-ZnAl₂O₄, b) c-ZnAlO, and c) p-ZnAlO.

In Fig. 4- 1, the characteristic ZnAl₂O₄ XRD peaks for c-ZnAlO and p-ZnAlO are not as sharp as those for c-ZnAl₂O₄ catalyst. The peaks at 31.2° (ZA₁) and 36.8° (ZA₂) for c-ZnAlO

are broad enough to look like a shoulder of the dominant ZnO phase peaks at 31.8° (ZO_1) and 36.3° (ZO_2). This behavior is different from that of p-ZnAlO, whose XRD peaks at 31.2° (ZA_1) and 36.8° (ZA_2) are observed as separate peaks because the difference in the peak positions between ZO_1 and ZA_1 (or ZO_2 and ZA_2) for p-ZnAlO is larger than that for c-ZnAlO. Moreover, the peaks of ZA_1 and ZA_2 for the $ZnAl_2O_4$ phase in p-ZnAlO are relatively easier to detect than those in c-ZnAlO, although the relative peak intensities in p-ZnAlO are much smaller than those in c-ZnAlO. This implies that there are strong interactions between the ZnO and $ZnAl_2O_4$ phases during the preparation of c-ZnAlO (citrate complex method). The high-temperature heat treatment (600°C) of the mixed precursors induces solid phase diffusion and strong interactions between the two phases [97]. In contrast, there are no strong interactions between two phases in p-ZnAlO due to the simple mixing of the pre-synthesized precipitated powders of ZnO and $ZnAl_2O_4$ without any further thermal treatment. As a result, the ZnO/ $ZnAl_2O_4$ XRD intensity ratio of p-ZnAlO (9.8) is much higher than that of c-ZnAlO (4.8), which is listed in Table 4- 1. Although p-ZnAlO and c-ZnAlO have the same molar ratio of Zn:Al, the ZnO amount detected in c-ZnAlO is smaller than that in the physically mixed p-ZnAlO sample. Del Piero et al. [98] and Errani et al. [99] explained that the undetected ZnO could go inside the spinel structure of $ZnCr_2O_4$ to make a Zn-rich non-stoichiometric Zn–Cr spinel structure. This may also explain the spinel structure of $ZnAl_2O_4$ observed in this study.

Raman and FTIR spectra of fresh catalysts and conventional precipitated ZnO (co-ZnO) (for comparison) are presented in Fig. 4- 2. In the Raman scattering signals, only the ZnO phase shows significant bands [100,101]. A band at 382 cm^{-1} is assigned to the transverse optical A_1 mode (A_1 (TO)). Bands at 410 cm^{-1} , 583 cm^{-1} , and 437 cm^{-1} correspond to a transverse optical E_1 mode (E_1 (TO)), a longitudinal optical E_1 mode (E_1 (LO)), and an E_2 (high) mode, respectively, while the band at 330 cm^{-1} can be assigned to multi-phonon processes. The E_2 (high) mode in the Raman spectra is a characteristic mode for the lattice oxygen displacement

of the ZnO lattice [102]. The intensities of the E₂ (high) bands of both co-ZnO and p-ZnAlO samples are very similar, indicating that the ZnO phase in p-ZnAlO is unchanged when the ZnO phase is simply mixed with the ZnAl₂O₄ phase. The E₂ (high) vibration is also IR active, corresponding to a band at 434 cm⁻¹ in the FTIR spectra (Fig. 4- 2B) [103]. The E₂ mode IR intensities for co-ZnO and p-ZnAlO are so strong that this band overwhelms any IR band of the ZnAl₂O₄ phase in p-ZnAlO. Meanwhile, the E₂ (high) bands of c-ZnAlO in the Raman and FTIR spectra have relatively lower intensity than those of p-ZnAlO and co-ZnO. In the FTIR spectra, the fraction of the ZnO phase in c-ZnAlO (Fig. 4- 2B(c)) is lower than that in p-ZnAlO (Fig. 4- 2B(d)) even though they have the same molar ratios of Zn to Al in the precursors. The undetected ZnO in c-ZnAlO may go inside the ZnAl₂O₄ spinel lattice structure due to the strong interactions between ZnO and ZnAl₂O₄ phases. This is consistent with the XRD results in this study.

Table 4- 1. Properties of the fresh catalysts.

Catalyst	Intensity ratio of ZnO/ZnAl ₂ O ₄ in XRD *	Inversion parameter (Intensity Ratio of AlO ₄ /(AlO ₆ +AlO ₄) by XPS) **	Acidic Sites (mmol/g)	Basic Sites (mmol/g)	Surface area (m ² /g)
c-ZnAl ₂ O ₄	0	0.466	0.687	0.287	156
c-ZnAlO	4.8	0.278	0.464	0.200	29
p-ZnAlO	9.8	0.059	0.204	0.052	13

* Intensity ratios of the ZnO/ZnAl₂O₄ phases were obtained from the deconvolution in XRD patterns using the X Powder software.

*** Intensity ratios of the AlO_4 (tetrahedral site) and AlO_6 (octahedral site) were obtained from the deconvolution of XPS results using the Origin software.*

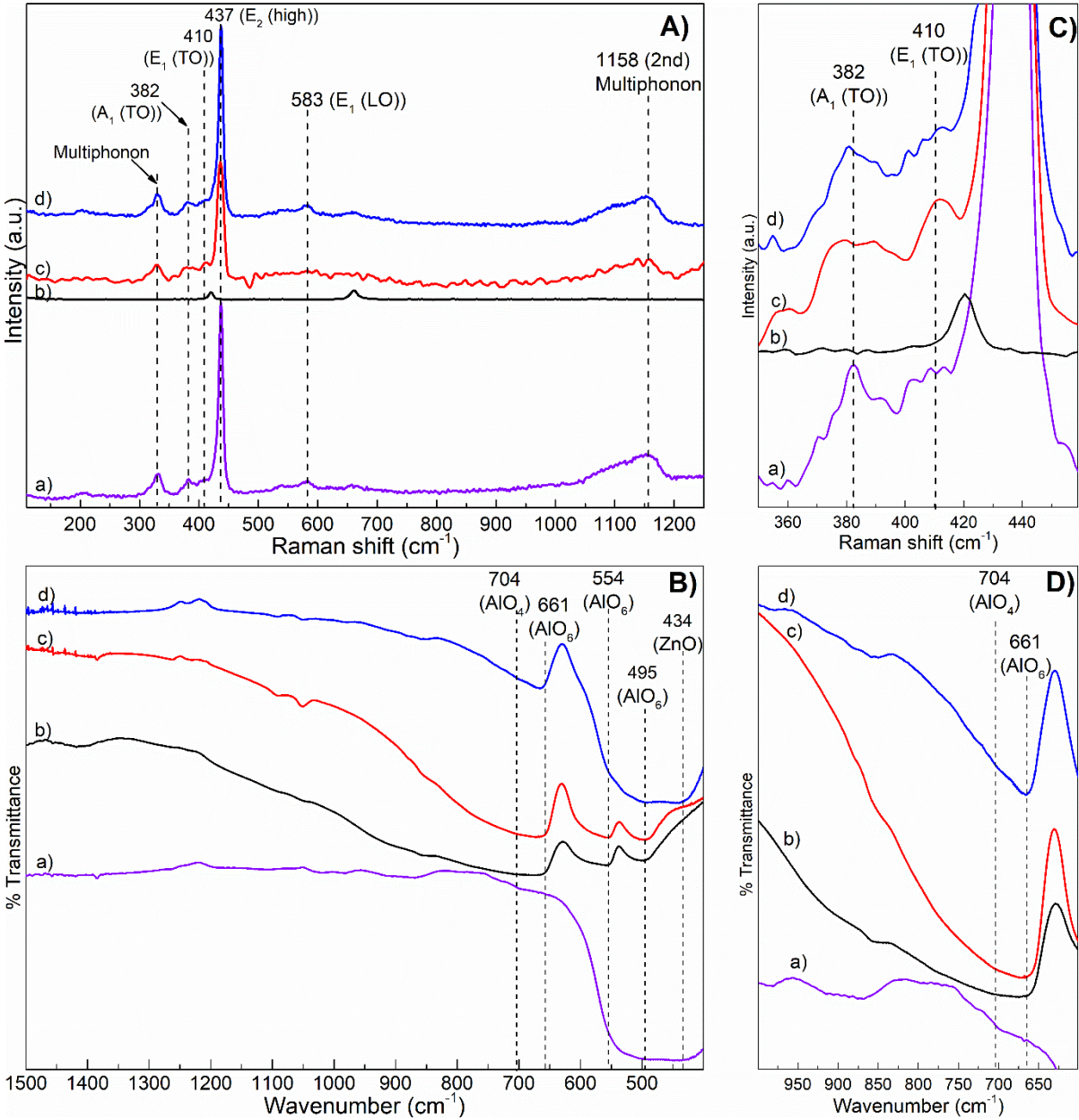


Fig. 4- 2. A) Raman and B) FTIR spectra of fresh catalyst: a) ZnO, b) c-ZnAl₂O₄, c) c-ZnAlO, and d) p-ZnAlO. C) Enlarged Raman and D) Enlarged FTIR spectra.

Fig. 4- 2C is enlarged Raman spectra in the range of 350-500 cm⁻¹, which is used to compare the relative intensity between A₁ (TO) and E₁ (TO) modes. The A₁ (TO) mode is due to the displacement of ions parallel to the z-axis, and the E₁ (TO) is ascribed to the displacement of ions parallel to the xy-plane. The wurtzite hexagonal lattice of ZnO can be described as

alternating close-packed layers of Zn and O stacked along the z-axis. Therefore, the lattice disorder along with the z-axis would have more of an effect on the displacement of ions in the A_1 (TO) than E_1 (TO), resulting in a decreased relative intensity of A_1 (TO) to E_1 (TO) [100]. The intensity ratios of A_1 (TO)/ E_1 (TO) can be calculated, and they follow the order of c-ZnAlO (0.7) < p-ZnAlO (0.9) < co-ZnO (1.0), implying a higher disordered structure of the ZnO phase in c-ZnAlO compared to those in p-ZnAlO and co-ZnO. This disordered structure in c-ZnAlO may be caused by the strong interactions between the ZnO and $ZnAl_2O_4$ phases in the citrate complex method. Pan et al. [104] investigated the formation of ZnO and concluded that removing the inter-layer organic by high-temperature calcination produced more defects or distortions along the z-axis.

As shown in Fig. 4- 2B, various vibration modes for the $ZnAl_2O_4$ phase can be detected at 661 cm^{-1} , 554 cm^{-1} (assigned for the stretching mode of AlO_6 - octahedrally coordinated Al-O), 495 cm^{-1} (assigned for the bending mode of AlO_6), and a broad shoulder was observed from 704 cm^{-1} to 900 cm^{-1} (assigned to AlO_4 - tetrahedral coordinated Al-O) [105–107]. FTIR spectra focusing on the vibration modes of AlO_4 and AlO_6 are shown in Fig. 4- 2D. The relative intensities of AlO_4 to AlO_6 increased in the order of co-ZnO < p-ZnAlO < c-ZnAlO < c- $ZnAl_2O_4$. While the AlO_4 vibration for p-ZnAlO is weak, the shoulder of the AlO_4 vibration for c-ZnAlO and c- $ZnAl_2O_4$ is visible and strong. The tetrahedrally coordinated AlO_4 reflects a partial inversion of the $ZnAl_2O_4$ spinel structure, and the FTIR results are consistent with the inversion parameter from the XPS data, which is described later.

The normal spinel structure of $ZnAl_2O_4$ contains Zn^{2+} cations at the tetrahedral sites and Al^{3+} cations at the octahedral sites of a cubic close-packed crystal. The partially inversed spinel structure is a disordered $ZnAl_2O_4$ structure where some Al^{3+} cations occupy the tetrahedral sites and some Zn^{2+} cations occupy the octahedral sites. The disordered structure of bulk spinel $ZnAl_2O_4$ can be extended to the catalyst surface. Duan et al. [92] defined the inversion

parameter of a spinel structure as a portion of tetrahedrally coordinated trivalent cations (Al^{3+}), or a portion of octahedrally coordinated divalent cations (Zn^{2+}), which can be estimated by the surface XPS measurement. Table 4- 1 displays the inversion parameter of each catalyst by calculating the ratio of $\text{AlO}_4/(\text{AlO}_6 + \text{AlO}_4)$ acquired from the XPS data. AlO_4 and AlO_6 represent the tetrahedrally coordinated Al^{3+} and the octahedrally coordinated Al^{3+} , respectively. In this study, the portion of octahedrally coordinated Zn^{2+} is not used since the octahedrally coordinated Zn^{2+} cations mainly appear on the ZnO phase in the ZnAl mixed oxide catalysts, and it is difficult to distinguish them from Zn^{2+} cations on the ZnAl_2O_4 phase. The inversion parameters of c-ZnAl₂O₄ and c-ZnAlO are higher than those of p-ZnAlO, reflecting the strong interactions between Zn and the spinel structure in the samples prepared using the citrate complex method. In Table 4- 1, the inversion parameters follow the order of p-ZnAlO < c-ZnAlO < c-ZnAl₂O₄, which is the same as the order of surface acidity of the catalysts. Table 4- 1 shows acidic and basic sites for each catalyst, which are calculated from the NH₃ and CO₂ TPD measurements (Fig. 4- 3). The values of acidic and basic sites increase in the order of p-ZnAlO < c-ZnAlO < c-ZnAl₂O₄.

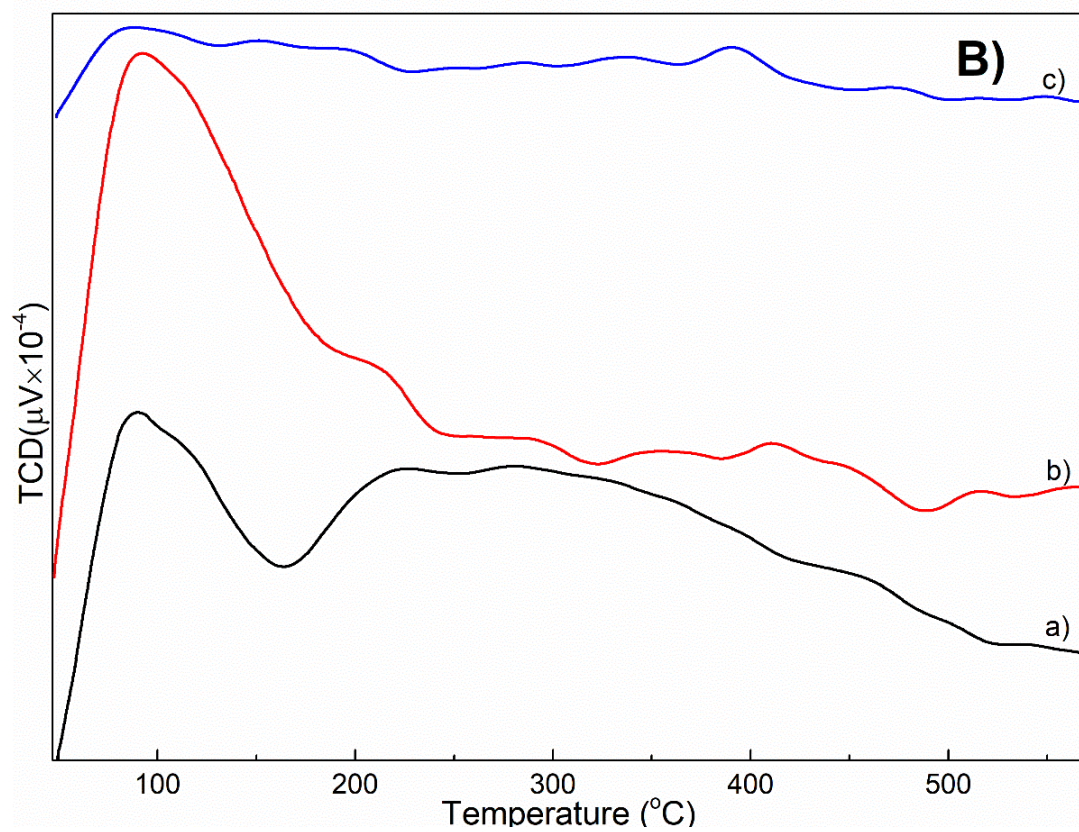
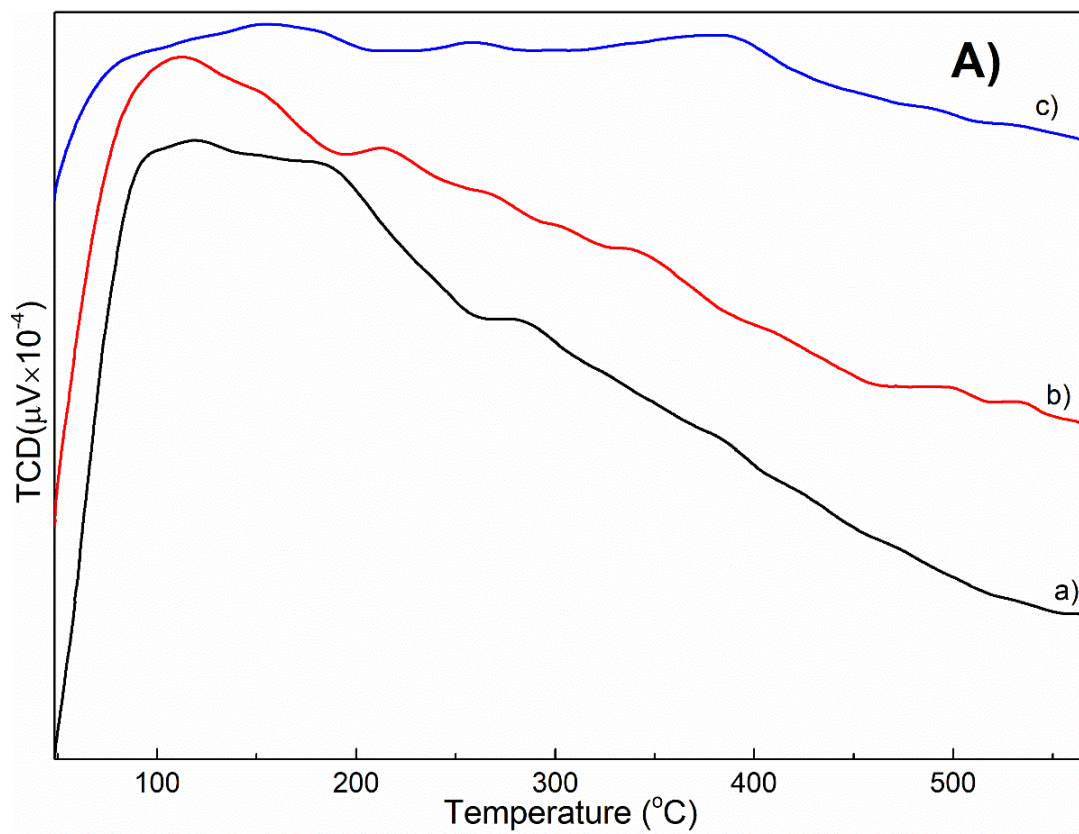


Fig. 4- 3. A) TPD-NH₃ and B) TPD-CO₂ analysis results of fresh catalysts: a) c-ZnAl₂O₄, b) c-ZnAlO, and c) p-ZnAlO.

Additional evidence for a lower intensity ZnO phase in c-ZnAlO than that in p-ZnAlO is obtained from surface atomic ratios from the XPS analysis, which are listed in Table 4- 2. For p-ZnAlO and c-ZnAlO, the atomic ratios of Zn on the outer surface (31.51% for p-ZnAlO and 22.79% for c-ZnAlO) are much higher than c-ZnAl₂O₄ (4.02%). These results imply both that a ZnO phase exists in the ZnAlO mixed oxide samples and that a Zn cation outer layer on the ZnO phase mainly contributes to the higher Zn surface atomic ratio for p-ZnAlO and c-ZnAlO. In addition, the Zn atomic ratio for c-ZnAlO is lower than that for p-ZnAlO, while the Al atomic ratios on the outer surface of the mixed oxide catalysts also decrease from 23.50% for c-ZnAlO to 12.70% for p-ZnAlO. The Zn/Al ratio on the outer surface of p-ZnAlO is 2.48, which is just slightly higher than the nominal bulk ratio of Zn/Al (7/3 or 2.33). In contrast, the outer Zn/Al ratio for c-ZnAlO is 0.97, which is much smaller than that of p-ZnAlO and the bulk ratio. The strong interaction between the ZnO and ZnAl₂O₄ phases in c-ZnAlO induces a lower portion of the ZnO phase on the outer surface, resulting in the corresponding lower Zn/Al ratio for c-ZnAlO. Song et al. [108] suggested that interactions could create a special structure of ZnO layer on the surface of the spinel lattice. Moreover, the coverage of the ZnO phase over the ZnAl₂O₄ phase due to the strong interactions can decrease the surface acidity and basicity.

Table 4- 2. The surface atomic ratio by XPS analysis of fresh catalyst.

Atomic%	c-ZnAl ₂ O ₄	c-ZnAlO	p-ZnAlO
O1s	59.26	53.70	55.79
Zn2p _{3/2}	4.02	22.79	31.51
Al2p	36.72	23.50	12.70

Surface areas of the fresh catalysts are displayed in Table 4- 1. The surface areas follow the order of $c\text{-ZnAl}_2\text{O}_4 > c\text{-ZnAlO} > p\text{-ZnAlO}$. The high surface area of $c\text{-ZnAl}_2\text{O}_4$ at $156 \text{ m}^2/\text{g}$ is consistent with the value reported previously [94]. The lowest surface area of $p\text{-ZnAlO}$ ($13 \text{ m}^2/\text{g}$) reflects the simple mixing of precipitated ZnO and ZnAl_2O_4 whose surface areas are $7 \text{ m}^2/\text{g}$ and $17 \text{ m}^2/\text{g}$, respectively [50,91]. Interestingly, the surface area of $c\text{-ZnAl}_2\text{O}_4$ rapidly decreases to $29 \text{ m}^2/\text{g}$, indicating the strong interaction between ZnO and ZnAl_2O_4 phases in $c\text{-ZnAlO}$, which is in good agreement with the XPS results.

As shown in Table 4- 2, the Zn surface atomic ratio for $c\text{-ZnAl}_2\text{O}_4$ is surprisingly small (only 4.02%), and the Al surface atomic ratio for $c\text{-ZnAl}_2\text{O}_4$ is 36.72%, resulting in a surface atomic molar ratio Zn/Al of only 0.11, which is much smaller than the stoichiometric Zn/Al ratio in the bulk spinel structure (0.5). Wachs and Routray [109] showed that the realistic surface model of a normal spinel crystal was almost covered up with octahedral sites or the Al^{3+} cations in the ZnAl_2O_4 phase. The possibility of having Zn^{2+} on the outer surface was very low due to its weak stability on the spinel surface. In this study, the presence of Zn on the surface of $c\text{-ZnAl}_2\text{O}_4$ indicates the formation of the partially inversed spinel structure [106], which is clearly confirmed by the deconvoluted XPS peak for Zn cations occupying the octahedral sites (ZnO_6).

Fig. 4- 4 displays XPS data for $\text{Al}2p$, $\text{O}1s$, and $\text{Zn}2p_{3/2}$ for all the fresh catalysts with their deconvoluted peaks. The $\text{Al}2p$ XPS can be fitted into a smaller peak around 73.1 eV, assigned to the Al^{3+} occupying the tetrahedral sites (AlO_4), and a peak around 74.3 eV, assigned to the Al^{3+} occupying the octahedral sites (AlO_6) [92,110]. The XPS results of $\text{Zn}2p_{3/2}$ can also be fitted into two peaks: a larger peak at a lower binding energy (around 1021.1-1022.0 eV) corresponding to the Zn^{2+} occupying the tetrahedral sites (ZnO_4), and a smaller peak at a higher binding energy (around 1023.4-1023.7 eV) assigned to the Zn^{2+} occupying the octahedral sites (ZnO_6) [92,111]. It is difficult to distinguish each ZnO_4 site from the ZnO and ZnAl_2O_4 phases

[112], so that there is only one peak assignment for both ZnO_4 sites in this study. Since the ZnO phase includes Zn^{2+} cations only at the tetrahedral sites (i.e., they are not in the octahedral sites), the peak for ZnO_6 indicates that the Zn^{2+} cations occupy the octahedral sites on the ZnAl_2O_4 phase. The distribution on the tetrahedral and octahedral sites of Al^{3+} and Zn^{2+} cations follows the opposite trend. Namely, the main Al^{3+} cations occupy the octahedral sites of the ZnAl_2O_4 spinel structure, while the main Zn^{2+} cations occupy the tetrahedral sites in both ZnO and ZnAl_2O_4 , which corresponds to the model of a normal spinel structure. The deconvoluted patterns of O1s XPS are more complicated and can be fitted by four peaks: O_a at 534.1 eV, O_b in the range of 532.8 – 533.1 eV, O_c in the range of 531.2 – 531.5 eV and O_d in the range of 530.7 – 530.9 eV. Two peaks, O_c and O_d at lower binding energies, belong to the lattice O and can be assigned to the lattice O in the ZnAl_2O_4 and ZnO phase, respectively, since the binding energy of the lattice O in the ZnAl_2O_4 phase is slightly higher than that in the ZnO phase [112,113]. The peak O_a at the highest binding energy can be assigned to the oxygen loosely bonded to the catalyst surface from the atmosphere (such as adsorbed H_2O , O_2 , etc.) [114,115]. Finally, the O1s peak at the intermediate binding energy, O_b , corresponds to the oxygen-deficient regions or the oxygen vacancy (O_v) on the lattice surface of the catalysts [114,115]. One of the main reasons for the oxygen vacancy on the catalyst surface is the substitution of Zn^{2+} (a divalent cation) for Al^{3+} (a trivalent cation) at octahedral sites. As a result, an oxygen vacancy is required to balance the positive charge of cations at the center of octahedral sites [116], which can explain the same trends in the intensities of O_v (oxygen vacancy) and ZnO_6 ($\text{p-ZnAlO} < \text{c-ZnAlO} < \text{c-ZnAl}_2\text{O}_4$). The oxygen vacancy of an octahedral site is shared with a neighboring tetrahedral site. In addition, this oxygen vacancy can indirectly lead to a shift in the ZnO_4 peak positions from 1022.0 eV for p-ZnAlO to 1021.1 eV for $\text{c-ZnAl}_2\text{O}_4$ and 1021.5 eV for c-ZnAlO . Since the oxygen vacancy breaks one or more of four O^{2-} anions tetrahedrally

coordinated with Zn^{2+} cations, the charge transfer from Zn^{2+} cations to O^{2-} anions decreases, resulting in the decrease in the binding energy of ZnO_4 [117].

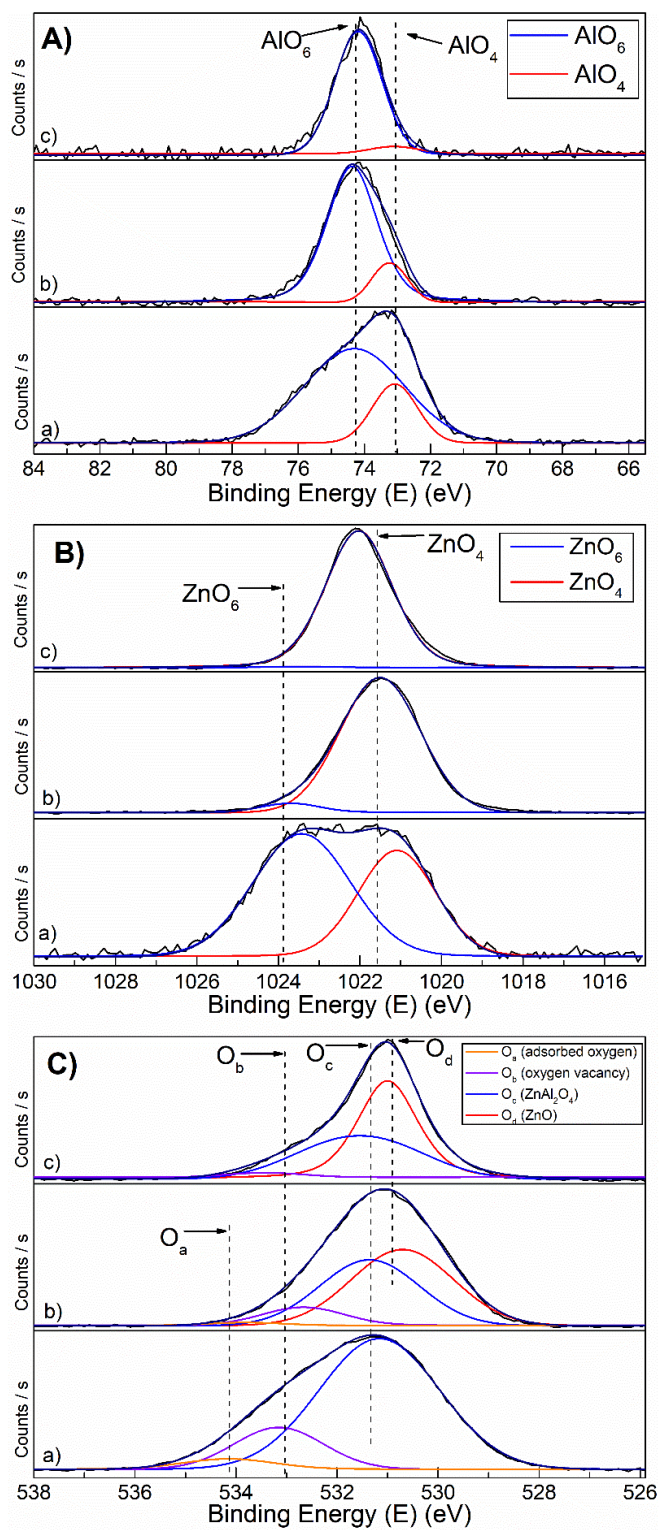


Fig. 4- 4. Deconvoluted XPS results of fresh catalysts: a) c-ZnAl₂O₄, b) c-ZnAlO, and c) p-ZnAlO. **A)** Al2p XPS results, **B)** Zn2p_{3/2} XPS results and **C)** O1s XPS results.

4.3.2. Relationship between the disordered spinel structure and the surface acidity

The existence of ZnO_6 and AlO_4 is an indicator of the partially inverted spinel structure of ZnAl_2O_4 and, in this study, the intensity ratios between two XPS peaks ($\text{AlO}_4/\text{AlO}_6$) are used as the inversion parameter (Table 4- 1). The inversion parameters in Table 4- 1 and the intensities of the AlO_4 FTIR shoulder follow the same trend ($\text{p-ZnAlO} < \text{c-ZnAlO} < \text{c-ZnAl}_2\text{O}_4$), clearly proving the partially inverted ZnAl_2O_4 spinel structure of the catalysts. The inverted ZnAl_2O_4 spinel structure can produce surface acidity on the catalysts, which is related to the XPS intensity of O_a (H_2O or O_2 adsorbed from the atmosphere onto the catalyst surface). The O_a peak intensity is highest for $\text{c-ZnAl}_2\text{O}_4$ and almost negligible for p-ZnAlO .

Fig. 4- 5 clearly shows the relationship between the surface acidity of the catalysts and the inversion parameter (Fig. 4- 5A), the XPS intensity of ZnO_6 and the XPS intensity of oxygen vacancies (Fig. 4- 5B). As explained, the proportional relationship between the XPS intensities of ZnO_6 and oxygen vacancies (O_v) proves that the charge compensated for the substitution of Zn^{2+} cations for Al^{3+} cations at the octahedral sites. The plot also obviously indicates a positive relationship between the inversion parameter and the surface oxygen vacancy with the surface acidity of the catalysts. The inversion parameter relates to the ratio of AlO_6 and AlO_4 sites of the spinel ZnAl_2O_4 . A normal spinel ZnAl_2O_4 having Al^{3+} cations at the octahedral sites (AlO_6) has low acidity, whereas the AlO_4 sites of the partially inverted spinel ZnAl_2O_4 structure can create high surface acidity [106,118–121]. Sohlberg et al. [122] explained the higher Lewis acidity of AlO_4 . When a tetrahedrally coordinated Al cation was exposed to the surface, one of four oxygen atoms bonded with Al could be removed, leaving a three-coordinated Al (termed as “quasi-trihedral” Al) that had lower energy acceptor orbital (or higher Lewis acidity strength) than the AlO_6 exposed to the surface. Another factor that increases the surface acidity is the Lewis acidity of surface oxygen vacancy, which results in surface hydroxyl groups [123]. The evidence for the surface hydroxylation is provided by peaks for OH vibration in the range 3000-

3600 cm^{-1} of the FTIR spectra of fresh c-ZnAlO or c-ZnAl₂O₄ and the XPS O_a peaks of H₂O or O₂ adsorbed from the atmosphere. We conclude that the disordered bulk structure of spinel ZnAl₂O₄ produces disordered sites on the catalyst surface and, as a result, the disordered surface AlO₄ and oxygen vacancies enhance the surface acidity of the catalysts.

Another noticeable point is that the surface basicity of the fresh catalyst follows the same trend with the surface acidity (Table 4- 1). The enhancement of basicity can be attributed to the increase of density of negative charge on the oxygen anion in the lattice [49]. The disordered spinel ZnAl₂O₄ structure produces oxygen vacancies which may induce an increased electronic density on M^{δ+}-O²⁻ sites [124]. Therefore, c-ZnAl₂O₄ has the highest acidity and basicity due to the disordered spinel structure.

The conceptual structures of three catalysts can be illustrated in Scheme 4- 1 based on the previously mentioned explanation. Scheme 4- 1A displays the differences in ordered and disordered bulk spinel lattice structures of ZnAl₂O₄ by exchanging the locations of Al³⁺ and Zn²⁺ cations in the structure. In an ordered structure, a normal spinel ZnAl₂O₄ consists of Zn²⁺ cations at the tetrahedral sites and Al³⁺ cations at the octahedral sites. A partially inversed spinel structure or a disordered structure can be generated by some disarrangements: i) exchange of a Zn²⁺ cation with an Al³⁺ cation to create an octahedrally coordinated Zn²⁺ (ZnO₆, symbolized as Zn* in Scheme 4- 1A) and a tetrahedrally coordinated Al³⁺ (AlO₄ or symbolized as Al* in Scheme 4- 1A), ii) replacement of an Al³⁺ cation with a Zn²⁺ cation at the tetrahedral site to generate an AlO₄ and leave a cation vacancy (symbolized as Al_v in Scheme 4- 1A), and vice versa for Zn²⁺ substitution at octahedral sites, and iii) an oxygen vacancy (symbolized as O_v in Scheme IA) was generated to compensate for the charge imbalance by Zn²⁺ substitution for Al³⁺ at an octahedral site.

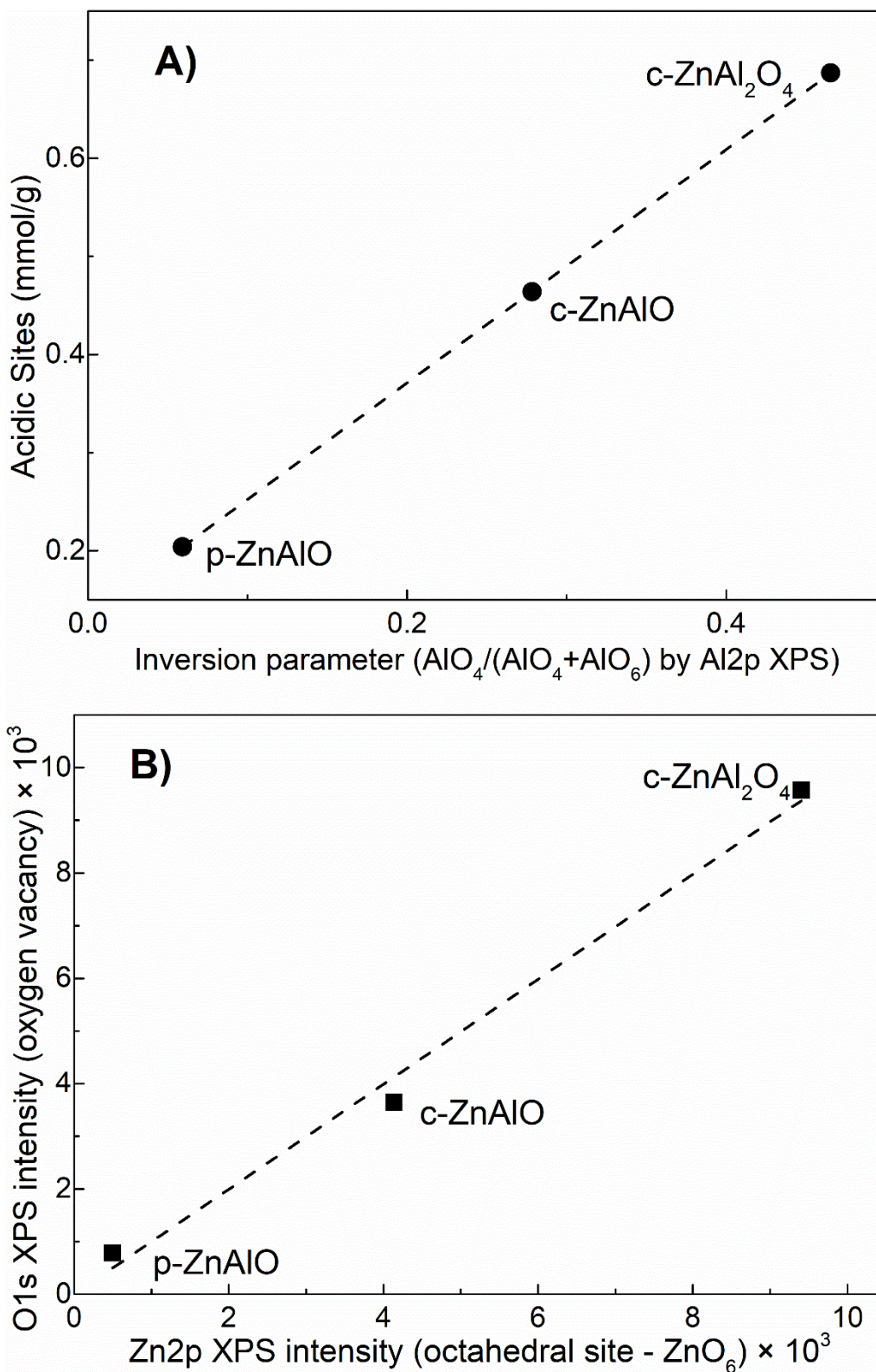
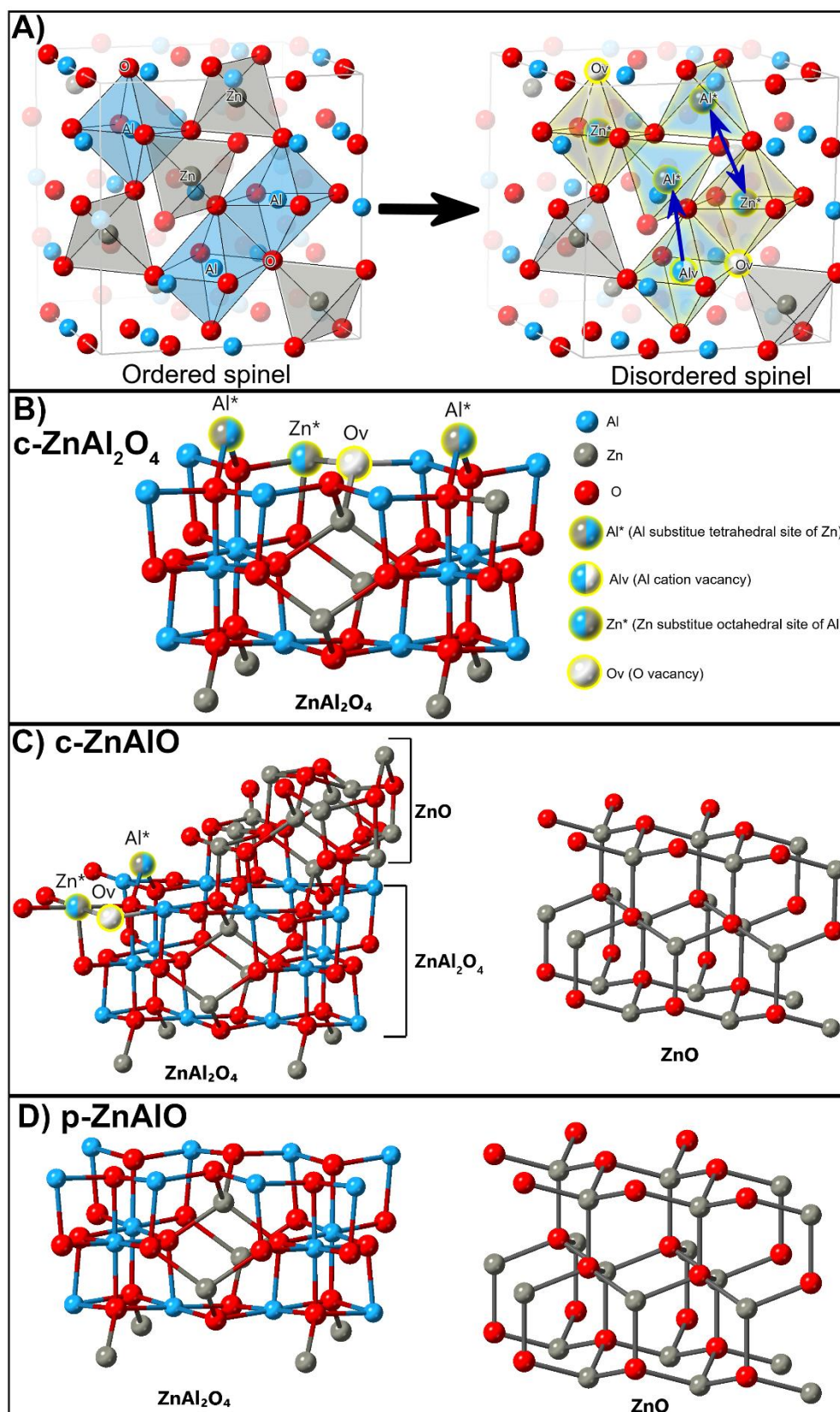


Fig. 4- 5. The relationship between the disordered structure of the partially inverted ZnAl_2O_4 phase and the acidity of the catalyst. **A)** The acidic sites – the inversion parameter. **B)** The O1s XPS intensity (oxygen vacancy) – the Zn2p XPS intensity (ZnO_6).



Scheme 4- 1. The lattice structure of **A)** ordered and disordered spinel ZnAl₂O₄ phase, **B)** c-ZnAl₂O₄, **C)** c-ZnAlO and **D)** p-ZnAlO.

Scheme 4- 1B illustrates the disorder on the surface of c-ZnAl₂O₄ using AlO₄ (Al*), ZnO₆ (Zn*) and oxygen vacancies (O_v). As previously mentioned, the disordered structure may be the result of thermally removing the organic attached onto metal cations in the preparation process of c-ZnAl₂O₄ and c-ZnAlO and the strong interaction between the ZnO and ZnAl₂O₄ phases [97,104], whereas p-ZnAlO was prepared by a precipitation method, and it can produce a perfect structure (Scheme 4- 1C). For p-ZnAlO, there are almost no disordered sites on the surface of both separate ZnO and ZnAl₂O₄ phases. Based on the simple mixing used in the preparation, p-ZnAlO contains two separate ordered structures of ZnO and ZnAl₂O₄ phases without any strong interactions between ZnO and ZnAl₂O₄ phases. However, even though the structure of c-ZnAlO (Scheme 4- 1D) is also composed of ZnO and ZnAl₂O₄ phases, the ZnAl₂O₄ phase in c-ZnAlO is not a pure phase like c-ZnAl₂O₄ or p-ZnAlO. There are strong interactions between the Zn²⁺ cations and the partially inversed spinel lattice of the ZnAl₂O₄ phase, resulting in thin ZnO-stoichiometry layers supported on the ZnAl₂O₄ spinel structure in c-ZnAlO [108]. The surface of the c-ZnAlO can be described by two parts: (1) the surface of the normal ZnO phase with or without a small number of disordered sites, and (2) the surface of the ZnAl₂O₄ phase with exposed disordered sites similar to that of c-ZnAl₂O₄ (AlO₄, ZnO₆, and oxygen vacancy), where the number of disordered sites and the corresponding surface acidity are partially eliminated by the covering of the ZnO layer.

4.3.3. Reaction performance over the catalysts

The reaction results of three catalysts at reaction times of 1 h and 3 h are summarized in Table 4- 3. Besides the production of GC, 2,3-dihydroxypropyl carbamate (I), 4-(hydroxymethyl)oxazolidin-2-one (II), and (2-oxo-1,3-dioxolan-4-yl)methyl carbamate (III), Zn-containing chemicals such as ZnGly and a Zn NCO complex were observed as an intermediate or a product during the reaction. Under the urea environment, ZnO reacts with urea to dissolve and form a Zn NCO complex. The amount of Zn in the liquid phase is the

amount of the Zn NCO complex dissolved in the liquid phase [51]. The existence of the Zn NCO complex in the liquid phase is confirmed by the NCO vibration at 2213 cm^{-1} in the FTIR spectra of liquid products (Fig. 4- 6) [37,48,51]. The Zn amounts in the liquid phase are listed in Table 4- 3. The trend in the values fits the NCO vibration behavior in the FTIR spectra of liquid products; a signal at 2213 cm^{-1} is observed only in the FTIR spectra for p-ZnAlO and c-ZnAlO but does not exist for c-ZnAl₂O₄.

Table 4- 3. Analysis of liquid products obtained from the reaction of glycerol with urea over ZnO and ZnAlO catalysts at various reaction times. (Reaction temperature = 140 °C, reaction pressure = 3 kPa, Glycerol/Urea Ratio =1:1). **(I)**: 2,3-dihydroxypropyl carbamate, **(II)**: 4-(hydroxymethyl)oxazolidin-2-one, and **(III)**: (2-oxo-1,3-dioxolan-4-yl)methyl carbamate.

Sample	Reaction time (h)	Glycerol Conversion (%)	GC Yield (%)	Selectivity (%)				Zn	ZnGly	Zn NCO
				_____				amount	amount on	complex on
				GC	(I)	(II)	(III)	in liquid (mmol) *	solid (mmol) **	solid (mmol) **
c-	1	19	10	50	41	8	1	0.0	0.0	0.00
ZnAl ₂ O ₄	3	34	20	59	25	14	2	0.0	0.0	0.00
c-	1	46	33	73	16	9	2	2.2	0.0	0.24
ZnAlO	3	83	59	70	9	19	1	1.4	2.3	0.94
p-	1	49	27	56	32	9	3	1.3	5.6	0.09
ZnAlO	3	72	46	63	8	17	12	0.9	5.8	0.08

* Amounts of Zn dissolved in the liquid phase as measured by the ICP-OES method.

** The amounts of ZnGly and Zn NCO complex on the solid phase were calculated by the TGA result.

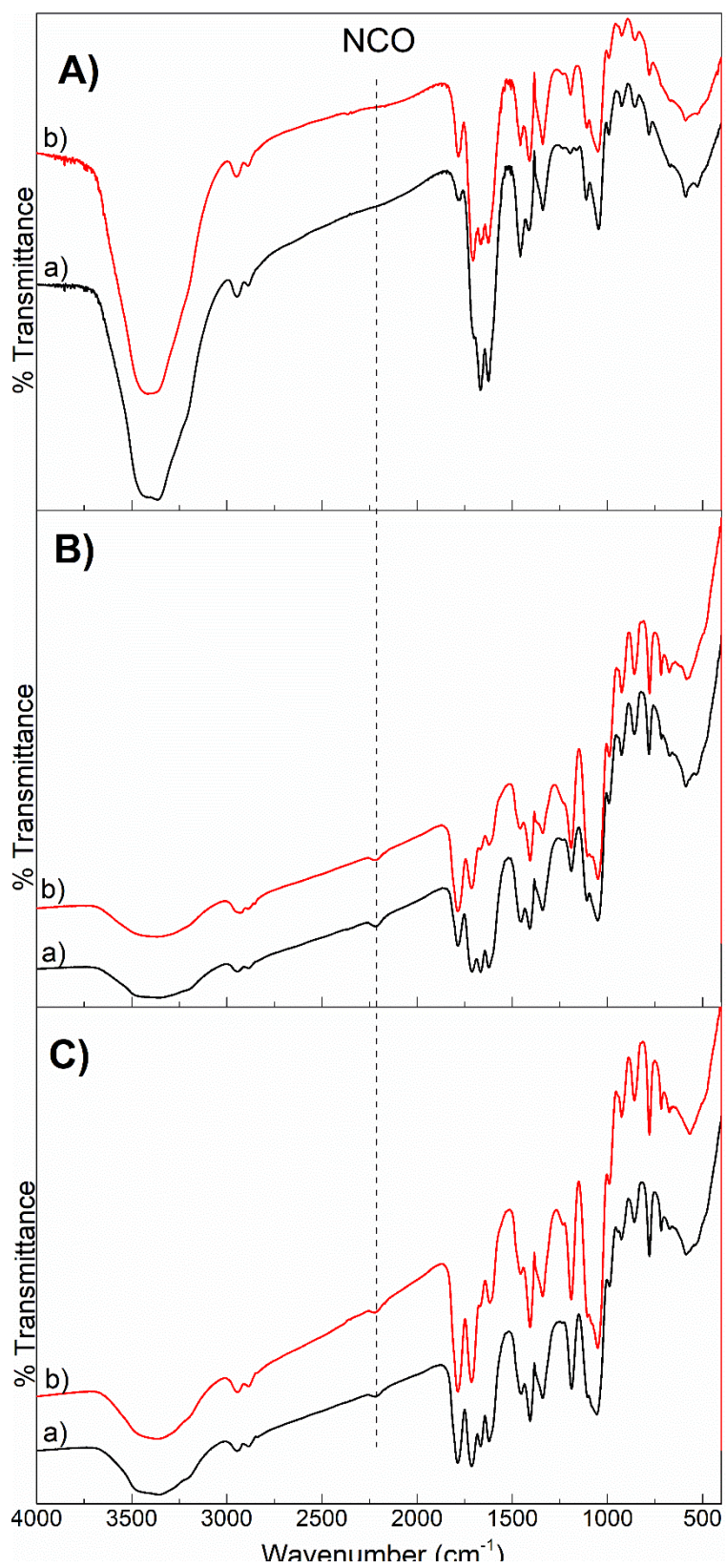


Fig. 4- 6. FTIR spectra of liquid products obtained at the reaction time of a) 1 h and b) 3 h. A) c-ZnAl₂O₄, B) c-ZnAlO and C) p-ZnAlO.

FTIR spectra of spent catalysts are presented in Fig. 4- 7. Besides the bands for AlO_6 (661 cm^{-1} , 554 cm^{-1}), AlO_4 (shoulder around 704 cm^{-1}) and ZnO (434 cm^{-1}) are detected in the FTIR spectra of the fresh catalysts, additional vibrations for ZnGly and Zn NCO complex are assigned as a C-O stretching modes with oxygen in hydrogen bonding (around 1950 cm^{-1}), a C-H stretching mode (2846 cm^{-1}), a Zn-O stretching mode (514 cm^{-1} and 655 cm^{-1}), and the NCO vibration in the Zn NCO complex on the solid phase and in the liquid phase (2220 cm^{-1} for solid phase) [125,126]. Table 4- 3 displays the amounts of Zn calculated from the ICP-OES measurements and the molar amounts of Zn NCO complex and ZnGly on the solid phase calculated from the TGA data (Fig. 4- 8).

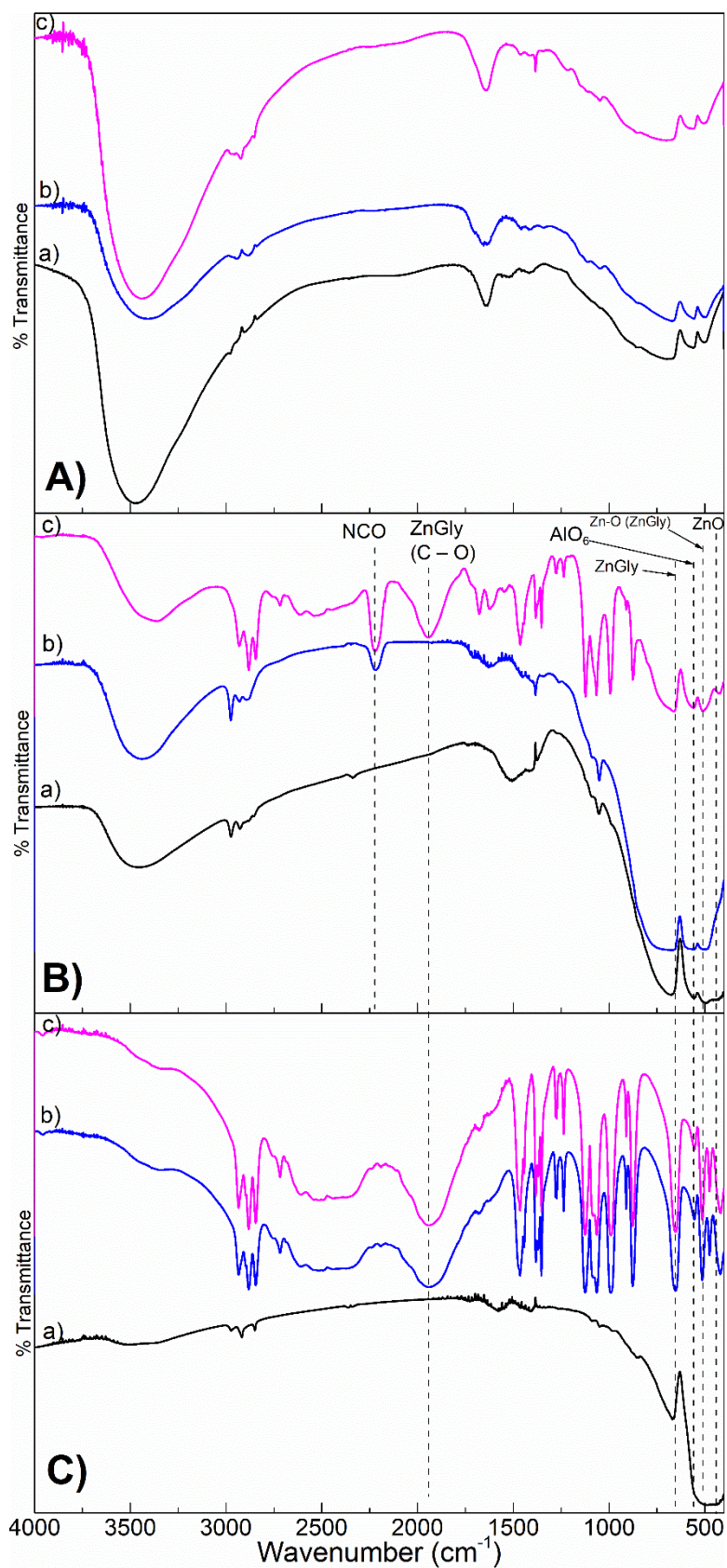


Fig. 4- 7. FTIR results of fresh catalysts and spent catalysts: a) fresh, b) 1 h and c) 3 h. **A)** c-ZnAl₂O₄, **B)** c-ZnAlO, and **C)** p-ZnAlO.

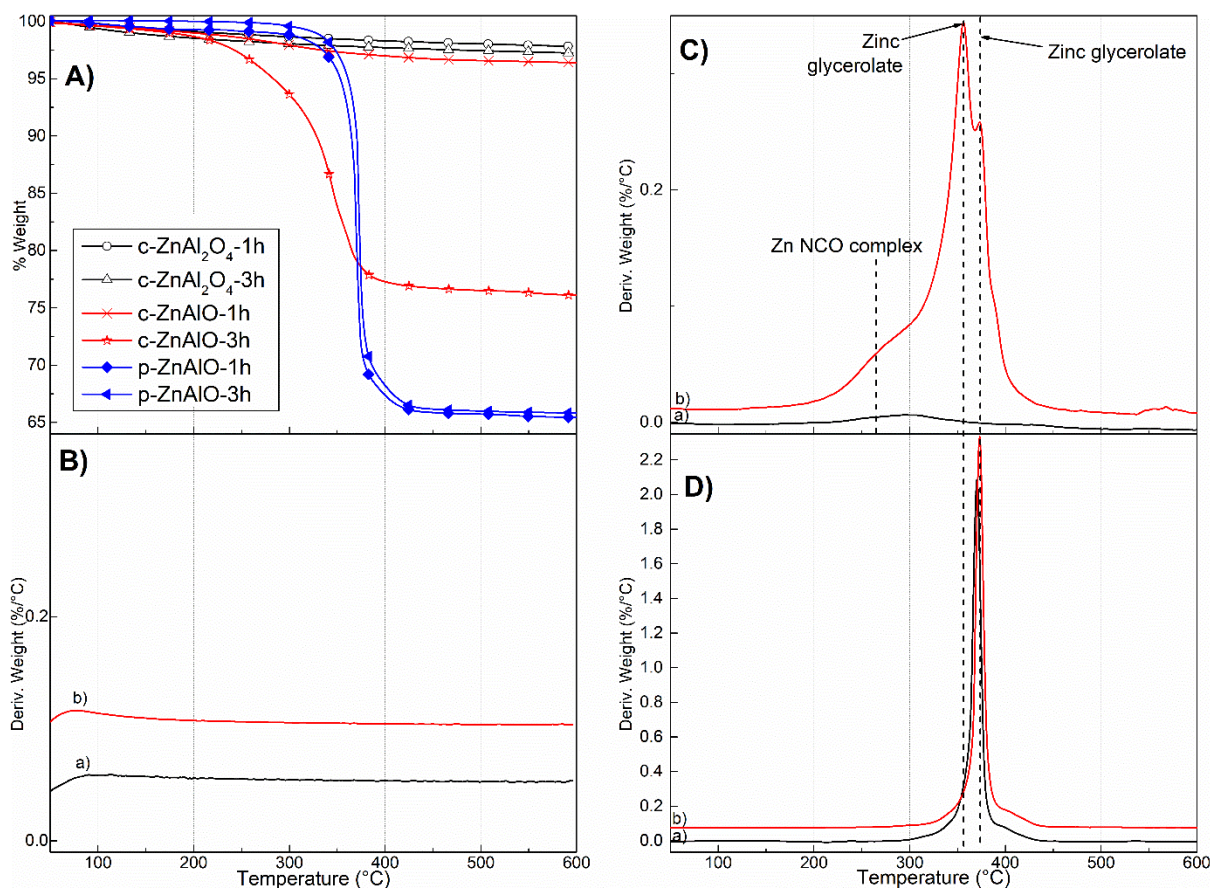


Fig. 4- 8. (A) TGA and (B, C, D) DTGA of spent catalysts: a) 1h and b) 3h. (B) DTGA results of c-ZnAl₂O₄, (C) DTGA results of c-ZnAlO and (D) DTGA results of p-ZnAlO.

c-ZnAl₂O₄ (no ZnO phase in its composition) shows the lowest glycerol conversion and GC yield since GC is produced through only a heterogeneous reaction route by direct adsorption of glycerol and urea onto the catalyst surface, which is in good agreement with the results reported previously [50]. There is no formation of the Zn NCO complex and ZnGly over c-ZnAl₂O₄ (Table 4- 3) because the outer surface of the c-ZnAl₂O₄ phase consists of mostly the Al³⁺ cations and few Zn²⁺ cations. However, the main component of fresh p-ZnAlO is the ZnO phase, so that its reaction result is similar to that of ZnO catalyst in literature, i.e., fast dissolution of the ZnO phase and quick formation of ZnGly at the initial reaction time [50]. c-ZnAlO has similar reaction behavior to that of ZnAl mixed oxide in our previous research, i.e., the strong formation of the Zn NCO complex on the solid phase [91]. The amounts of the Zn NCO complex on the solid phase of spent c-ZnAlO (around 0.2-0.9 mmol) are much higher

than those of spent p-ZnAlO (only around 0.08-0.09 mmol) based on the TGA measurement (Fig. 4- 8 and Table 4- 3). A comparable result is also observed from the FTIR spectra of spent catalyst (Fig. 4- 7), where the NCO peak intensities of spent c-ZnAlO are clearly high, and the NCO peak for spent p-ZnAlO is detected in trace amounts. The formation of the Zn NCO complex on the solid phase is closely related to the catalyst surface acidity and the existence of the ZnO phase, which provides an additional heterogeneous active site in the dual reaction routes. Due to the disordered ZnAl₂O₄ structure, c-ZnAlO has a higher surface acidity than p-ZnAlO, resulting in stronger interactions of the Zn NCO complex on its surface to enhance the dual catalytic reaction routes and achieve better reaction performance at 3 h than p-ZnAlO. In Table 4- 3, c-ZnAlO shows higher glycerol conversion (83% for c-ZnAlO and 72% for p-ZnAlO) and higher GC yield (59% for c-ZnAlO and 46% for p-ZnAlO).

c-ZnAlO shows a higher GC selectivity (70-73%) than p-ZnAlO (56-63%) in Table 4- 3. According to previous research [91], one reason for the lower GC selectivity for p-ZnAlO is the formation of ZnGly from the Zn NCO complex in the liquid phase. Therefore, there is a negative relationship between the formation of ZnGly and the amount of the liquid Zn NCO complex. The formation of ZnGly over p-ZnAlO starts at the initial reaction time and increases to 5.6 mmol after 1 h reaction time and almost reaches a saturated value of ZnGly. The final amount of ZnGly at 3 h is 5.8 mmol. In contrast, the amount of the Zn NCO complex in the liquid phase (or the amount of Zn atom in the liquid phase) continuously decreases along with the reaction time and reaches 1.3 mmol at 1 h and 0.9 mol at 3 h, which supports the formation of ZnGly from the liquid Zn NCO complex. The behavior of the Zn-containing chemicals for c-ZnAlO also corresponds to this behavior. That is, ZnGly appears only at 3 h reaction time (2.3 mmol), where the amount of Zn in the liquid phase for c-ZnAlO decreases from 2.2 mmol (1 h) to 1.4 mmol (3 h), implying the formation of ZnGly from the liquid Zn NCO complex. The formation of ZnGly over the spent catalysts can be supported by the XRD patterns of the

spent catalysts (Fig. 4- 9). The XRD characteristic peaks for the ZnGly phase with space group $P2_1/c$ are observed at 10.9° , 17.1° , 20.5° , 23.8° , 24.7° , 27.6° , 27.7° , 36.4° , and 38.2° (JCPDS No. 23-1975). For p-ZnAlO, the intensity of peaks for ZnGly reaches a saturated value at 1 h and 3 h, whereas those for c-ZnAlO are detected only at 3 h reaction time.

The FTIR bands in the region $400-800\text{ cm}^{-1}$ of the spent catalysts were exploited to further understand the change in the catalyst surface properties during the reaction. The band intensity of ZnO (E_2 mode at 434 cm^{-1}) decreases with increasing reaction time for both c-ZnAlO and p-ZnAlO, which is strong evidence for the collapse of the ZnO phase caused by Zn dissolution into the liquid phase (Fig. 4- 7B and C). The highly disordered c-ZnAlO (with high surface acidity) can lead to more adsorption of the Zn NCO complex on the catalyst surface (0.94 mmol at 3 h while 0.24 mmol at 1 h) during the reaction test. The DTGA plot of spent c-ZnAlO (Fig. 4- 8C) shows the decomposition of the Zn NCO complex formed over spent c-ZnAlO, whose peak appears in the range of $200-350^\circ\text{C}$ with two decomposition peaks of ZnGly at 355°C and 375°C . As shown in Fig. 4- 8C, the decomposition peak of ZnGly over spent c-ZnAlO at a lower temperature (355°C) may relate to an unfinished reaction or a partial polymerization of ZnGly to a complete crystalline structure [127]. The ZnGly decomposition peak at a higher temperature (375°C) can be assigned to a stronger crystalline ZnGly with higher thermal stability. Only one strong and sharp peak for the ZnGly decomposition is observed in the case of spent p-ZnAlO (Fig. 4- 8D). There is a slight shift in the ZnGly decomposition peaks to higher temperatures when comparing the DTGA profiles of spent p-ZnAlO at 1 h and 3 h. This indicates the formation of a stronger ZnGly crystalline structure after 1 h and 3 h reaction times. In contrast, spent c-ZnAlO shows peaks associated with ZnGly decomposition only at a reaction time of 3 h, implying incomplete ZnGly formation.

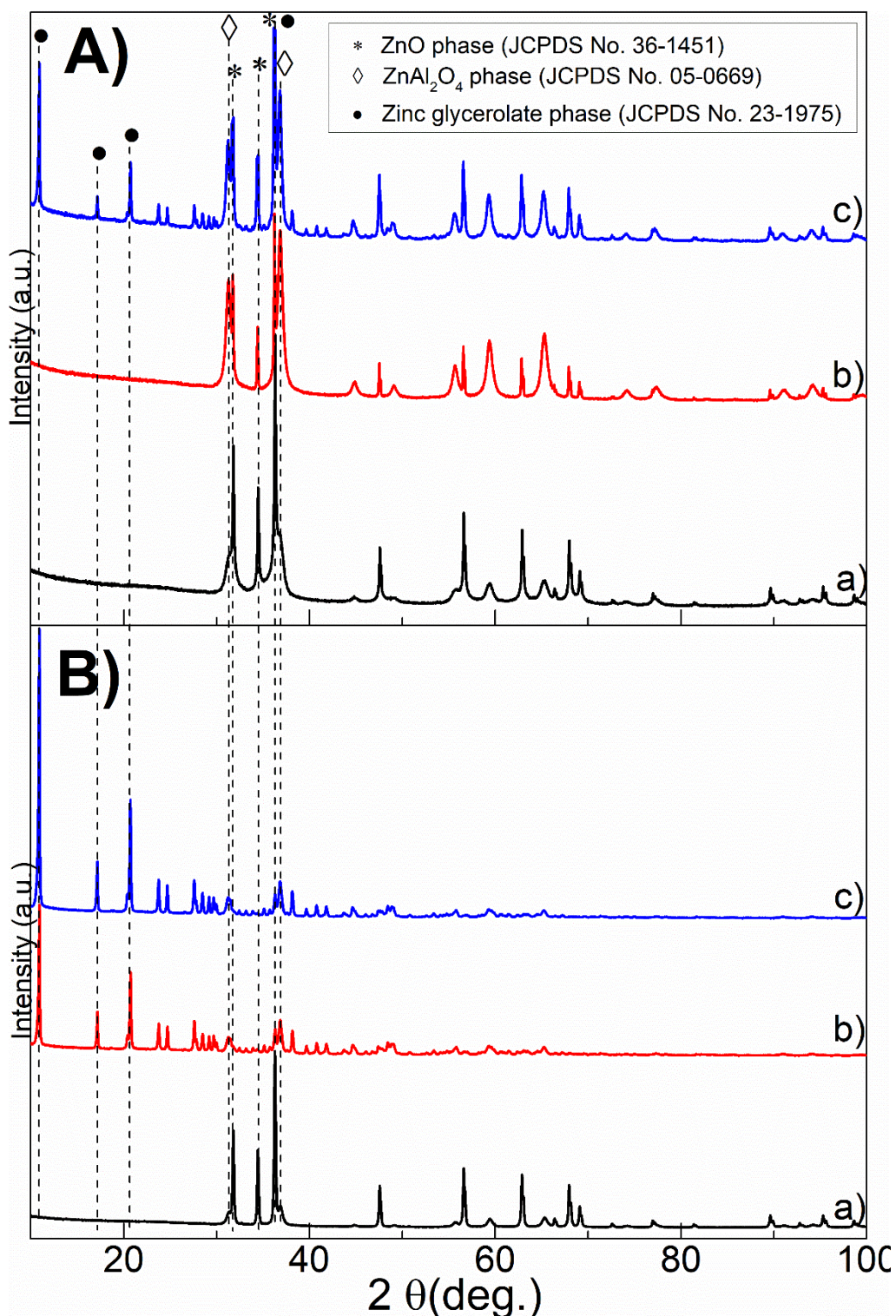


Fig. 4- 9. XRD patterns of fresh catalysts and spent catalysts: a) fresh, b) 1 h and c) 3 h. A) c-ZnAlO, B) p-ZnAlO.

The difference in catalytic reaction performance between c-ZnAl₂O₄, p-ZnAlO, and c-ZnAlO can be clarified by the apparent turnover frequency (TOF) quantity calculated with 3 h reaction time data (Table 4- 4), which was introduced elsewhere [51]. The apparent TOF of

GC was calculated as ‘moles of GC produced’ divided by ‘moles of Zn used \times reaction time’ in this study. The apparent TOF of GC values follow the trend of c-ZnAl₂O₄ (2.7 h⁻¹) < p-ZnAlO (3.4 h⁻¹) < c-ZnAlO (4.4 h⁻¹). c-ZnAl₂O₄ shows the lowest reaction rate for producing GC because it has only a single heterogeneous reaction route, even though it has the highest surface acidity due to the highly disordered ZnAl₂O₄ spinel structure, based on the inversion parameters in Table 4- 1. p-ZnAlO consists of less disordered lattice structures with lower surface acidity, resulting in few Zn NCO complexes adsorbed on the catalyst surface. However, p-ZnAlO exhibits a median value of apparent TOF of GC because the high amount of ZnO dissolves in the liquid environment required to form the liquid Zn NCO complex for the homogeneous reaction route. c-ZnAlO has a disordered ZnAl₂O₄ lattice structure with a high surface acidity, allowing it to adsorb more Zn NCO complex on the surface and catalyze glycerol through both homogeneous and heterogeneous reaction routes, achieving the highest apparent TOF of GC. Meanwhile, the apparent TOF of ZnGly was calculated as ‘moles of ZnGly produced’ divided by ‘moles of the liquid Zn NCO complex \times reaction time’. The apparent TOF of ZnGly for c-ZnAl₂O₄ is zero since there is no formation of the liquid Zn NCO complex (which is an intermediate to generate ZnGly). For p-ZnAlO, the formation of ZnGly occurs at early reaction times due to the fast reaction rate associated with generating the liquid Zn NCO complex; this results in a low ratio of urea to glycerol. Therefore, the apparent TOF of ZnGly value for p-ZnAlO catalyst is very high (2.2 h⁻¹), whereas that for c-ZnAlO is much lower (0.5 h⁻¹). The formation of ZnGly over c-ZnAlO is much slower and starts after 1 h of reaction time.

Table 4- 4. Apparent turnover frequency (apparent TOF) of GC and ZnGly for the reaction test at 3 h.

Sample	Apparent TOF of GC (h ⁻¹) *	Apparent TOF of ZnGly (h ⁻¹) **
c-ZnAl ₂ O ₄	2.7	0.0
c-ZnAlO	4.4	0.5
p-ZnAlO	3.4	2.2

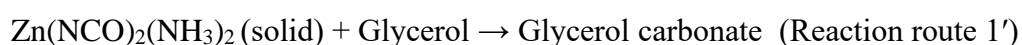
* *Apparent turnover frequency of GC = moles of glycerol carbonate formed/(moles of Zn used × reaction time).*

** *Apparent turnover frequency of ZnGly = moles of zinc glycerolate formed/(moles of Zn NCO complex in the liquid phase × reaction time).*

4.3.4. Catalytic reaction routes through Zn NCO complexes

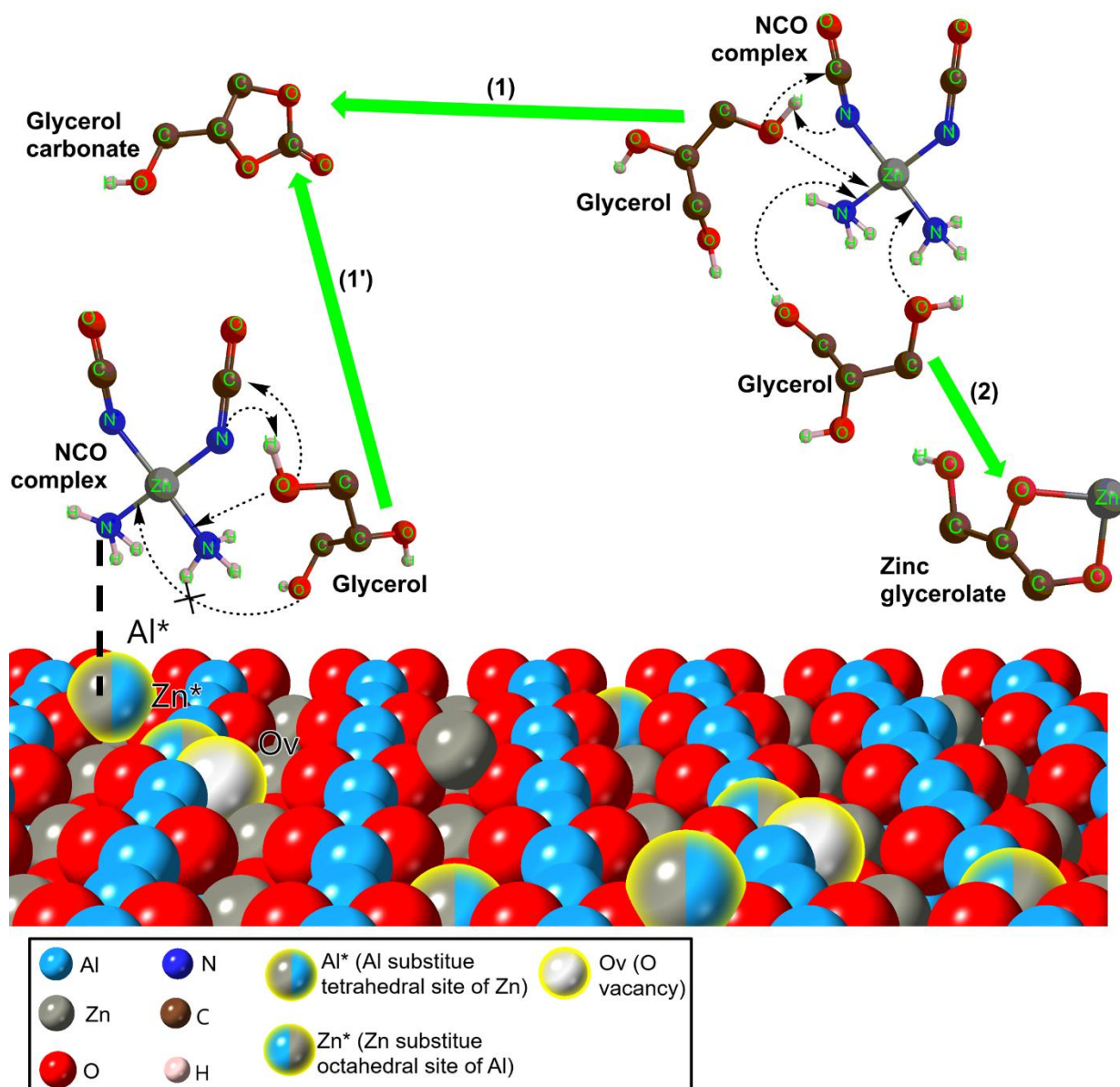
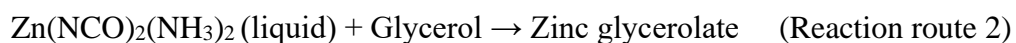
Catalytic reaction routes over a disordered ZnAl₂O₄ spinel structure are illustrated in Scheme 4- 2. As described in Scheme 4- 1, there are some disordered sites over the disordered ZnAl₂O₄ spinel structure: AlO₄ (symbolized as Al*, Al³⁺ cations substituted for Zn²⁺ cations at the tetrahedral site), ZnO₆ (symbolized as Zn*, Zn²⁺ cations substituting for Al³⁺ cations at the tetrahedral site) and oxygen vacancies (symbolized as O_v). The AlO₄ site acts as a Lewis acidic site where the ammonia (NH₃) group of Zn NCO complex can adsorb. The Zn NCO complex adsorbed on the solid phase is detected on N1s XPS of spent c-ZnAlO after 3 h reaction time (Fig. 4- 10). Three deconvoluted peaks of the N1s XPS are observed at 398.7 eV (61%), 399.7 eV (9%) and 400.6 eV (30%). The peaks at 398.7 eV and 400.6 eV are assigned for the ammonia group (Zn-NH₃) and the isocyanate (Zn-NCO) that connect to the center Zn atom of the complex, respectively [128]. The intermediate peak at 399.7 eV can be assigned for the

ammonia group that adsorbs on the defected AlO_4 site ($\text{Zn-NH}_3\cdots\text{Al}$) [129]. This higher binding energy of N1s for the ammonia group adsorbed on the Al site can be explained by a decrease in the electron density of nitrogen atom because the electron pair of this nitrogen atom is shared with the Al atom served as a Lewis acidic site [130]. Two main active complexes to produce GC as shown in Scheme 4- 2: (1) the liquid Zn NCO complex for the homogeneous reaction route and (2) the Zn NCO complex adsorbed on the solid phase for the heterogeneous reaction route.



ZnGly is another solid product of the reaction between the Zn NCO complex in the liquid phase and glycerol (Reaction route 2). It consumes glycerol without generating GC, resulting in lower GC selectivity, whereas the formation of the Zn NCO complex consumes urea and ZnO. The formation of ZnGly should be a deposition process from species in the liquid phase to the solid phase. Table 4- 5 displays the surface atomic ratios of spent p-ZnAlO and c-ZnAlO measured by XPS. For only spent c-ZnAlO, N atoms are detected on the surface at 2.77% of atomic percentage, proving the existence of Zn NCO complex on the surface of spent c-ZnAlO, which is in good agreement with the FTIR and TGA results of spent catalysts. The additional existence of C atoms over the spent catalysts proves the deposition of ZnGly, resulting in a significant reduction in the Al surface ratios. The Al surface atomic ratios for spent c-ZnAlO and p-ZnAlO are 14.53% and almost 0%, respectively, while those for fresh c-ZnAlO and p-ZnAlO are 23.50% and 12.70%, respectively. Therefore, ZnGly is produced by the reaction of the Zn NCO complex and glycerol in the liquid phase, and then its successive deposition results in a layer covering the catalyst surface. After a 3 h reaction, the large amount of ZnGly covers

most of the p-ZnAlO surface. In contrast, spent c-ZnAlO contains a lower amount of ZnGly and is partially covered with the adsorbed Zn NCO complex and ZnGly.



Scheme 4- 2. An illustration of reaction routes in the reaction of glycerol with urea on the surface of the disordered ZnAl₂O₄ spinel structure.

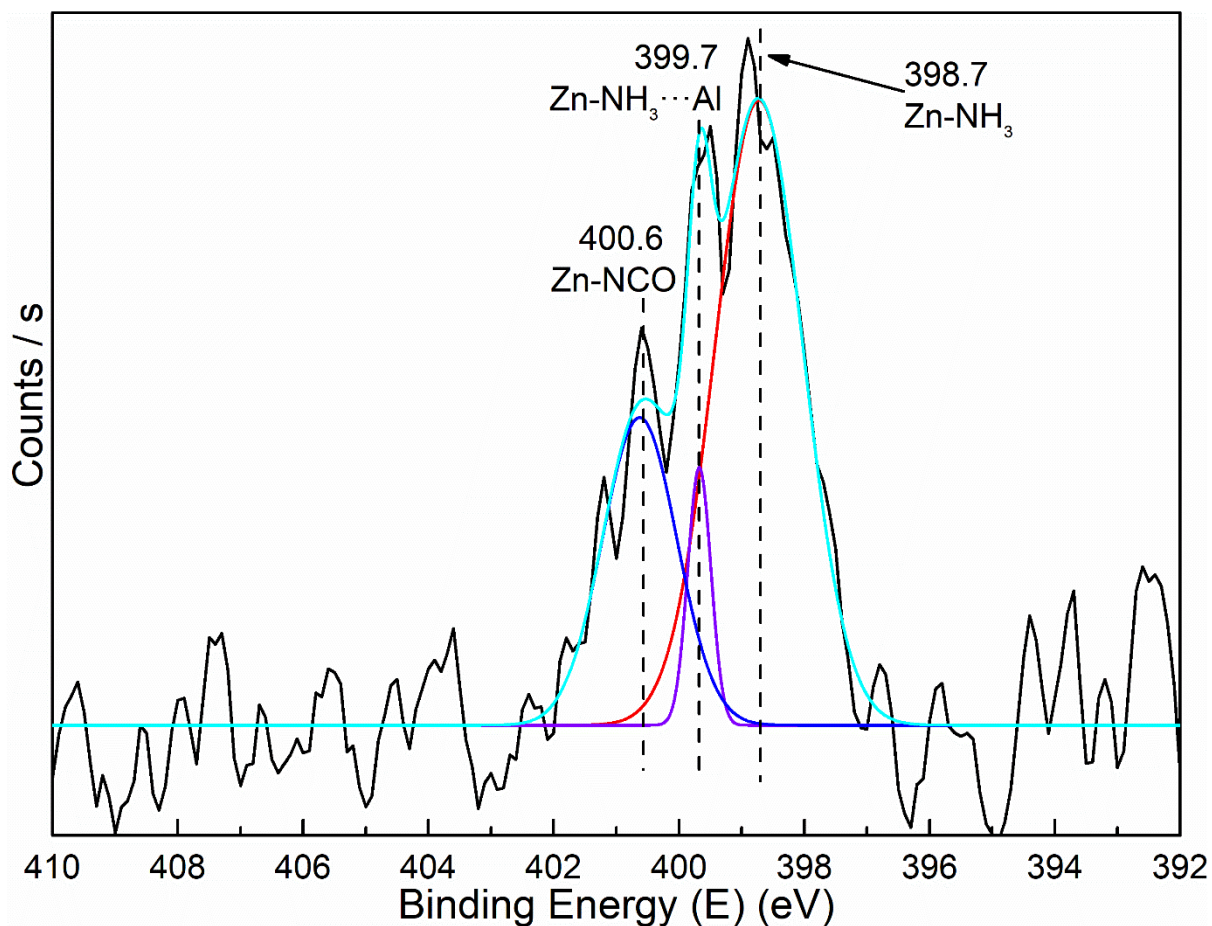


Fig. 4- 10. Deconvoluted N1s XPS data of spent c-ZnAlO after 3 h reaction time.

Table 4- 5. Surface atomic ratios of spent p-ZnAlO and c-ZnAlO (3 h reaction time) measured by XPS

Atomic %	c-ZnAlO-spent	p-ZnAlO-spent
O1s	54.38	54.79
Zn2p3/2	20.47	33.66
Al2p	14.53	0.00
C1s	7.85	11.56
N1s	2.77	0.00

According to Fujita et al. [51], the reaction between the Zn NCO complex and glycerol starts by replacing one weakly-bonded NH_3 in the Zn NCO complex with the hydroxyl group of glycerol to make an active Zn complex. Then, glycerol is attracted to the Zn center by its oxygen, and the hydroxyl group captures an NCO group to produce an active carbamate complex. The carbamate complex continues to participate in the intra-cyclization reaction, reacts with another urea to generate glycerol carbonate, and then returns to the original form of the Zn NCO complex by releasing the second NH_3 group. The hydroxyl group of glycerol interacts with one NH_3 group and one NCO group of the Zn NCO complex, resulting in the conversion of glycerol to GC. If the hydroxyl group of glycerol interacts with two NH_3 groups of the Zn NCO complex, the reaction turns to the cyclization reaction of a Zn center with the formation of ZnGly from glycerol. The Zn NCO complex in the liquid phase with 4 ligands (2 NH_3 and 2 NCO) can easily follow the reaction routes (1) and (2) to generate GC and ZnGly. Otherwise, the adsorbed Zn NCO complex on the solid phase makes a bond between an NH_3 group and an acidic site (AlO_4) on the catalyst surface, which can block the interaction between glycerol with both NH_3 groups of Zn NCO to generate ZnGly. Since the NH_3 ligands bonding with the Zn site is not strong, the adsorbed Zn NCO on the solid phase can lose one or both NH_3 groups and convert to a $\text{Zn}(\text{NCO})_2$ complex [89]. Based on the N1s XPS of spent c-ZnAlO catalyst (Fig. 4- 10), the ratio of NH_3 and NCO group is 3:7, implying that the portion of the NH_3 -rich Zn NCO complex is higher than the NH_3 -poor complex $\text{Zn}(\text{NCO})_2$. In conclusion, the Zn NCO complex on the solid phase tends to react with glycerol to form only GC by reaction route (1') and limits the formation of ZnGly. In contrast, the Zn NCO complex in the liquid phase can react with glycerol to produce both GC and ZnGly through reaction routes (1) and (2).

In Table 4- 6, the catalytic reaction results in this work are simply compared to those reported previously. Following the dual homogeneous and heterogeneous reaction routes, c-

ZnAlO catalyst shows comparable glycerol conversion and GC selectivity. Fujita et al. [51] prepared the hydrotalcite Zn-Al and ZnO catalysts for the same reaction. Glycerol conversion of the hydrotalcite Zn-Al catalyst is similar to that of c-ZnAlO (82-83%). The authors described the leaching of Zn into the liquid phase, the existence of the active NCO complex, and the formation of ZnGly. In this study, we not only explain a negative role of ZnGly as a by-product which consumes glycerol and limits the GC selectivity, but also propose a positive role of the Zn NCO complex on the solid phase. Both ZnO and p-ZnAlO mainly follow the homogeneous reaction route with lower values of glycerol conversion and GC selectivity due to the significant formation of ZnGly over these catalysts. Turney et al. [48] used zinc mono-glycerolate as a catalyst that ultimately dissolved to the liquid phase to form the active NCO complex and resulted in a similar glycerol conversion with p-ZnAlO (71-72%). In this case, the catalyst showed a higher GC selectivity due to a lack of the formation of ZnGly as a by-product than p-ZnAlO. In addition, since the catalysts followed the homogeneous reaction route, they could not be fully recovered and recycled.

We also carried out the recovery and re-using tests for our catalysts following the procedure described elsewhere [48] and the results are summarized in Table 4- 7. The recovery percentage of the spent catalysts matches the reaction route. c-ZnAl₂O₄ follows only the heterogeneous reaction route, resulting in an almost complete recovery (98-100% recovery). In contrast, c-ZnAlO and p-ZnAlO including the homogeneous reaction route cannot be fully recovered and re-used (81-89% recovery for c-ZnAlO and 91-92% for p-ZnAlO, respectively). In Table 4- 3, the amount of Zn in the liquid phase of c-ZnAlO (1.4 mmol) is higher than that of p-ZnAlO (0.9 mmol), which implies that the catalyst recovery of c-ZnAlO (81-89%) is lower than that of p-ZnAlO (91-92%). Therefore, while the catalytic activity of c-ZnAl₂O₄ is maintained even after the recycling, the activities of p-ZnAlO and c-ZnAlO slowly decreases along with the

recycles. However, c-ZnAlO still shows a better catalytic reaction performance than p-ZnAlO in Table 4- 7 (54% GC yield for c-ZnAlO and 44% GC yield for p-ZnAlO, respectively).

Table 4- 6. The reaction performance of reaction of glycerol with urea over several published catalysts in the literature

Entry	Catalyst	Mol glycerol/ mol urea	Weight % catalyst/ glycerol	Recovered (catalyst reusability)	Glycerol conversion (%)	GC selectivity (%)	Reference
1	γ -ZrP calcined	1:1	1	Yes	76	~100	Aresta et al. [52]
2	calcined hydrotalcite HTc-Zn	1:1	5	Yes	82	88	Climent et al. [49]
3	Au/MgO	1:1.5	~1.8	Yes	81	68	Hammond et al. [56]
4	Zinc mono- glycerolates	1:1	5	n/a ^{a,b}	71	92	Turney et al. [48]
5	Co ₃ O ₄ /ZnO nanoparticles	1:1	6	n/a ^a	69	97	Rubio-Marcos et al. [54]
6	ZnO	1:1	~5.4	n/a ^{a,b}	61	69	Fujita et al. [51]
7	Hydrotalcite HT(Zn/Al)	1:1	~5.4	n/a ^{a,b}	82	80	Fujita et al. [51]
8	p-ZnAlO	1:1	5	n/a ^{a,b}	72	63	This research
9	c-ZnAlO	1:1	5	n/a ^{a,b}	83	70	This research

^a There was no data for the reusability of catalyst in the published research.

^b A homogeneous reaction route was described in the published research.

Table 4- 7. Catalytic performance of the reaction and the recovery of the re-used catalyst over two reaction cycles. (Reaction temperature = 140 °C, reaction pressure = 3 kPa, Glycerol/Urea Ratio =1:1).

Sample	Fresh catalyst			1st Recycle			2nd Recycle		
	Glycerol Conv. (%)	GC yield (%)	Catalyst recovery (%) *	Glycerol Conv. (%)	GC yield (%)	Catalyst recovery (%) *	Glycerol Conv. (%)	GC yield (%)	Catalyst recovery (%) *
c-ZnAl ₂ O ₄	34	20	98	34	22	99	35	19	100
c-ZnAlO	83	59	89	82	61	83	71	54	81
p-ZnAlO	72	46	92	66	47	91	68	44	91

* The recovered weight amount of spent catalysts was determined by the TGA analysis.

4.4. Conclusion

In this study, p-ZnAlO with the separate phases of ZnO and ZnAl₂O₄ has the same reaction performance as the ZnO catalyst, whereas the c-ZnAlO shows better catalytic reaction performance due to the dual reaction routes. The citrate complex method can make a more disordered ZnAl₂O₄ structure in the ZnAl mixed oxide catalysts than the precipitation method. The disordered sites of AlO₄ and the oxygen vacancies of the partially inversed ZnAl₂O₄ spinel structure can produce surfaces with high surface acidity for c-ZnAlO and c-ZnAl₂O₄. The high acidity and the strong interactions between ZnO and ZnAl₂O₄ phases in c-ZnAlO showed a higher ability to adsorb the liquid Zn NCO complex on the catalyst surface. In contrast, a lack of a ZnO phase in c-ZnAl₂O₄ means that it only follows the heterogeneous reaction route because there is no Zn NCO complex. The reaction of this solid Zn NCO complex with glycerol prefers GC to ZnGly because of the bonding between the adsorbed Zn NCO complex and the acidic site (AlO₄), while the Zn NCO complex in the liquid can react with glycerol to produce both GC and ZnGly.

CHAPTER 5. INVESTIGATION OF GLYCEROLYSIS OF UREA OVER VARIOUS ZNMEO (ME = CO, CR, AND FE) MIXED OXIDE CATALYSTS

5.1.Introduction

Various Zn-based mixed oxide catalysts have been used for the glycerolysis of urea [46,47,49–51,91,131]. Zn-based mixed oxide catalysts follow a dual catalytic mechanism: a homogeneous reaction route through dissolved Zn species and a heterogeneous reaction route over solid active sites. In previous studies, it was found that ZnAl mixed oxide catalysts exhibit better catalytic performance through the dual mechanism than the ZnO catalyst. The catalytic performance is related to not only the formation of Zn-containing intermediates during the reaction but also the disordered structure of the ZnAl_2O_4 spinel lattice in ZnAl mixed oxide catalysts [50,91,131]. Zn-containing intermediates are produced through Zn species dissolved from ZnAl mixed oxide catalysts, following the homogeneous reaction route in the liquid phase. The homogeneous reactivity is directly related to the amount of Zn species dissolved in the liquid phase from ZnAl mixed oxide catalysts. Moreover, the disordered ZnAl_2O_4 spinel structure influences the catalytic performance *via* the surface acidity of the catalysts and the formation of a Zn-containing complex in the solid phase.

However, the investigation of dual catalysis over Zn-based mixed oxide catalysts has not been extended to Zn-based mixed oxide catalysts containing other metal components that are also favorable to the preparation of Zn-based mixed oxide catalysts [54,108,132–134]. In this study, we investigated the glycerolysis of urea over various ZnMeO (Me = Co, Cr, and Fe) mixed oxide catalysts with two Zn/Me ratios: a high Zn ratio (Zn_2MeO) and a low Zn ratio (ZnMe_2O). The Zn-rich mixed oxide catalysts (Zn_2MeO) are expected to generate more Zn-containing intermediates in the liquid phase and follow both homogeneous and heterogeneous reaction routes; in contrast, the Zn-poor mixed oxide catalysts (ZnMe_2O) are expected to form

a spinel lattice structure with a lower level of dissolved Zn species in the liquid phase and follow a heterogeneous reaction route.

5.2. Experimental

5.2.1. Catalyst preparation

The catalysts used in this study were prepared by a co-precipitation method from metal nitrate salts [$\text{Zn}(\text{NO}_3)_2 \cdot 6\text{H}_2\text{O}$, $\text{Cr}(\text{NO}_3)_3 \cdot 9\text{H}_2\text{O}$, $\text{Co}(\text{NO}_3)_2 \cdot 6\text{H}_2\text{O}$, and $\text{Fe}(\text{NO}_3)_3 \cdot 9\text{H}_2\text{O}$] [108,135,136]. All chemicals were obtained from Sigma–Aldrich Korea (Gyeonggi, South Korea). Typically, an aqueous solution of $\text{Zn}(\text{NO}_3)_2 \cdot 6\text{H}_2\text{O}$ and nitrate salt of Me (Cr, Co, or Fe) with a molar ratio of 1:2 for the ZnMe_2O catalysts or 2:1 for the Zn_2MeO catalysts was gradually mixed with a basic solution of ammonia under constant pH and vigorous stirring. For the preparation of Zn_2CoO and ZnCo_2O , a hydrogen peroxide solution (H_2O_2) was continually added to the mixture to oxidize Co^{2+} to Co^{3+} . After complete mixing, the suspension was filtered, and the remaining precipitate was washed with deionized water several times. Finally, the solid powder was dried at 100 °C overnight and calcined at 600 °C for 6 h.

5.2.2. Reaction tests

The detailed procedure for the glycerolysis of urea to produce glycerol carbonate over the catalysts can be found in the part 2.2.2 of Chapter 2.

5.2.3. Catalyst characterization

X-ray diffraction (XRD) patterns for fresh and spent catalysts were obtained using a Rigaku RAD-3C diffractometer (Rigaku Corp., Tokyo, Japan) with Cu K α radiation ($\lambda = 1.5418 \text{ \AA}$) at a scattering angle (2θ) scan rate of $2^\circ/\text{min}$, operating at 35 kV and 20 mA. The spent catalysts were analyzed by using a Thermo Scientific Nicolet iS5 FTIR spectrometer (Thermo Fisher Scientific, Waltham, MA, USA). The numbers of acidic and basic sites were measured based

on the temperature-programmed desorption of NH_3 and CO_2 (TPD- NH_3/CO_2) on a MicrotracBEL BELCAT-M instrument (MicrotracBEL Corp., Osaka, Japan). TPD- NH_3/CO_2 results were recorded for the temperature range of 50–600 °C by a TCD detector. The detailed procedure for the TPD analysis has been described elsewhere [131]. Thermogravimetric analysis (TGA) of the spent catalysts was measured by a TGA Q50 apparatus (TA Instruments, New Castle, DE, USA).

5.3. Results and discussion

5.3.1. Catalyst characterization: ZnO phase and ZnMe_2O_4 spinel phase

Fig. 5- 1 shows XRD patterns of the fresh catalysts. The Zn-rich catalysts (Zn_2MeO) are composed of two primary phases (ZnO and the corresponding spinel ZnMe_2O_4 phase) while only the spinel ZnMe_2O_4 phase was detected in the Zn-poor catalysts (ZnMe_2O). These crystalline phases can be readily identified in the XRD patterns of the fresh catalysts (Fig. 5- 1A). Typical XRD peaks for the ZnO phase with the $P6_3mc$ space group (JCPDS No. 36-1451) are observed at 31.8°, 34.4°, 36.3°, 47.5°, 56.7°, and 62.9° in the XRD patterns of the Zn_2CoO , Zn_2FeO , and Zn_2CrO catalysts [91]. The spinel ZnCo_2O_4 phase is detected in the XRD patterns of the Zn_2CoO and ZnCo_2O catalysts, with characteristic XRD peaks at 19.0°, 31.2°, 36.8°, 44.7°, 55.6°, 59.3°, and 65.1° (JCPDS No. 23-1390, $Fd3m$ space group) [137]. Similarly, the XRD patterns of the Zn_2FeO and ZnFe_2O catalysts exhibit the spinel ZnFe_2O_4 phase, with typical peaks at 18.2°, 29.9°, 35.2°, 42.8°, 53.1°, 56.6°, and 62.2° (JCPDS No. 82-1049, $Fd3m$ space group) [138]. Characteristic XRD peaks for the spinel ZnCr_2O_4 phase (JCPDS No. 22- 1107, $Fd3m$ space group) appear at 18.8°, 30.3°, 35.7°, 43.4°, 53.9°, 57.6°, and 63.1° in the XRD patterns of the Zn_2CrO and ZnCr_2O catalysts [139]. The lattice structure of all the ZnMe_2O_4 phases belongs to the spinel group. Typically, in a normal spinel ZnMe_2O_4 lattice, the Zn^{2+} cations occupy the tetrahedral sites and Me^{3+} cations occupy the octahedral sites. A disordered property in the spinel structure can generate a partially inversed spinel structure

where some Zn^{2+} cations occupy the octahedral sites and some Me^{3+} cations occupy the tetrahedral sites [140,141].

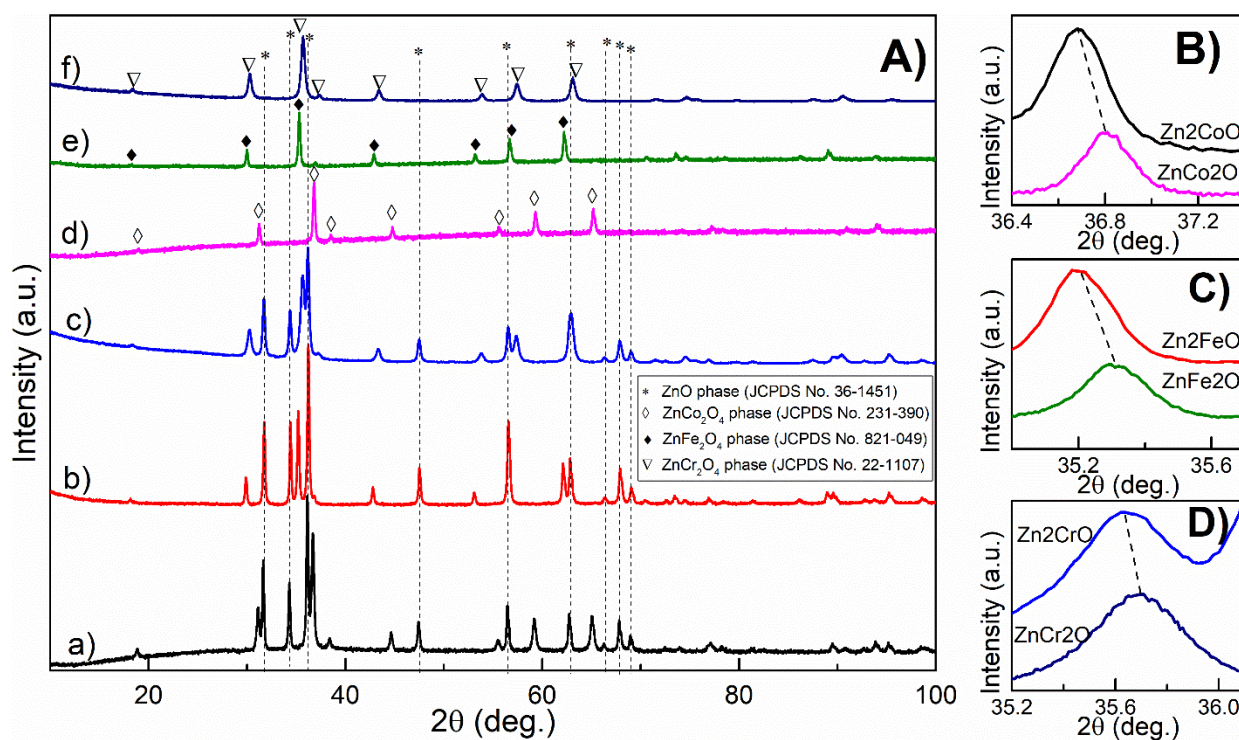


Fig. 5- 1. **A)** XRD patterns of fresh catalysts. a) Zn₂CoO, b) Zn₂FeO, c) ZnCo₂O, d) ZnCrO, e) ZnFe₂O and f) ZnCr₂O. **B, C, D)** Compare the position of (311) peaks (spinel phase ZnMe₂O₄) between the rich-Zn Zn₂MeO catalyst and the corresponding poor-Zn ZnMe₂O catalyst.

The XRD peaks corresponding to the (311) plane of the spinel ZnMe₂O₄ phases are enlarged in Fig. 5- 1.B–D to compare the lattice spacing between the Zn-rich Zn₂MeO and Zn-poor ZnMe₂O catalysts. For the Zn₂MeO catalysts, the position of the characteristic XRD peak for the (311) plane is shifted to a lower 2θ value with respect to the positions for the ZnMe₂O catalysts, indicating that the lattice spacing of Zn₂MeO is greater than that of ZnMe₂O. This peak position shift for the Zn-rich Zn₂MeO catalysts is caused by the interaction between the ZnO and spinel ZnMe₂O₄ phases in the Zn-rich mixed oxide of Zn/Me (Zn₂MeO catalysts in this study), where the excess Zn (of ZnO phase) can generate a layer of amorphous ZnO on the surface of the spinel ZnMe₂O₄ phase. The excess Zn cations in the ZnO phase can migrate into the lattice of the spinel phase to produce a non-stoichiometric spinel phase (Zn/Me ratio >0.5),

indicating more Zn amount in the spinel structure [108,131,142]. In detail, the excessive Zn^{2+} cations can replace the Me^{3+} cations in the octahedral sites of the spinel lattice structure. The Zn migration and substitution cause a distortion in the spinel lattice structure, with consequent changes in the interplanar lattice spacing of the spinel phase due to the different cation radii. For the octahedral sites, the cation radii of the metal cations can be estimated at 88 pm for Zn^{2+} , 68.5 pm for Co^{3+} , 78.5 pm for Fe^{3+} , and 75.5 pm for Cr^{3+} [143]. The radius of the Zn^{2+} cation is much larger than the radii of the other Me^{3+} cations. Therefore, the migration of Zn^{2+} to the octahedral sites of the spinel ZnMe_2O_4 lattice structure can expand the lattice spacing of the spinel structure, with a shift in the corresponding XRD peak position to a lower value [98,108,142]. In summary, the XRD peak shift of the (311) plane indicates an interaction between the ZnO and ZnMe_2O_4 phases in the Zn-rich Zn2MeO catalysts.

FTIR spectra of the fresh catalysts are displayed in Fig. 5- 2. Two vibration bands (ν_1 , and ν_2) of M-O bonds, related to the metal cations at the octahedral sites of the spinel ZnMe_2O_4 lattice, are observed in the FTIR spectra of both Zn2MeO and ZnMe2O in the range of 552–690 cm^{-1} (ν_1) and 425–582 cm^{-1} (ν_2) [132,144]. Because the majority of the octahedral sites in a normal spinel lattice structure are occupied by trivalent Me^{3+} cations [140], the positions of ν_1 and ν_2 may change depending on the nature of Me^{3+} cations. For the Zn2CoO and ZnCo2O catalysts (Fig. 5- 2a and 5- 2b), the ν_1 and ν_2 modes of the spinel ZnCo_2O_4 lattice are found at 676 and 590 cm^{-1} , respectively. For the Zn2CrO and ZnCr2O catalysts, two bands of the spinel ZnCr_2O_4 lattice appear at 623 and 505 cm^{-1} (Fig. 5- 2e and 5- 2f). However, due to the limitation of our FTIR instrument for measurements below 400 cm^{-1} , the FTIR spectra of the Zn2FeO and ZnFe2O catalysts only show the full band of ν_1 vibration of the spinel ZnFe_2O_4 lattice at 544 cm^{-1} (Fig. 5- 2c and 5- 2d). Beside the vibration modes ν_1 and ν_2 of the spinel phase, vibration of the ZnO lattice is detected at 434 cm^{-1} in the FTIR spectra of all of the Zn-rich catalysts (Zn2MeO) [145], providing further evidence for the occurrence of the ZnO phase in

these fresh catalysts. Therefore, the FTIR results are consistent with the XRD data. The Zn-poor ZnMe₂O catalysts are composed of the pure spinel ZnMe₂O₄ phase, whereas both the ZnMe₂O₄ and ZnO phases are dominant in the Zn-rich Zn₂MeO catalysts.

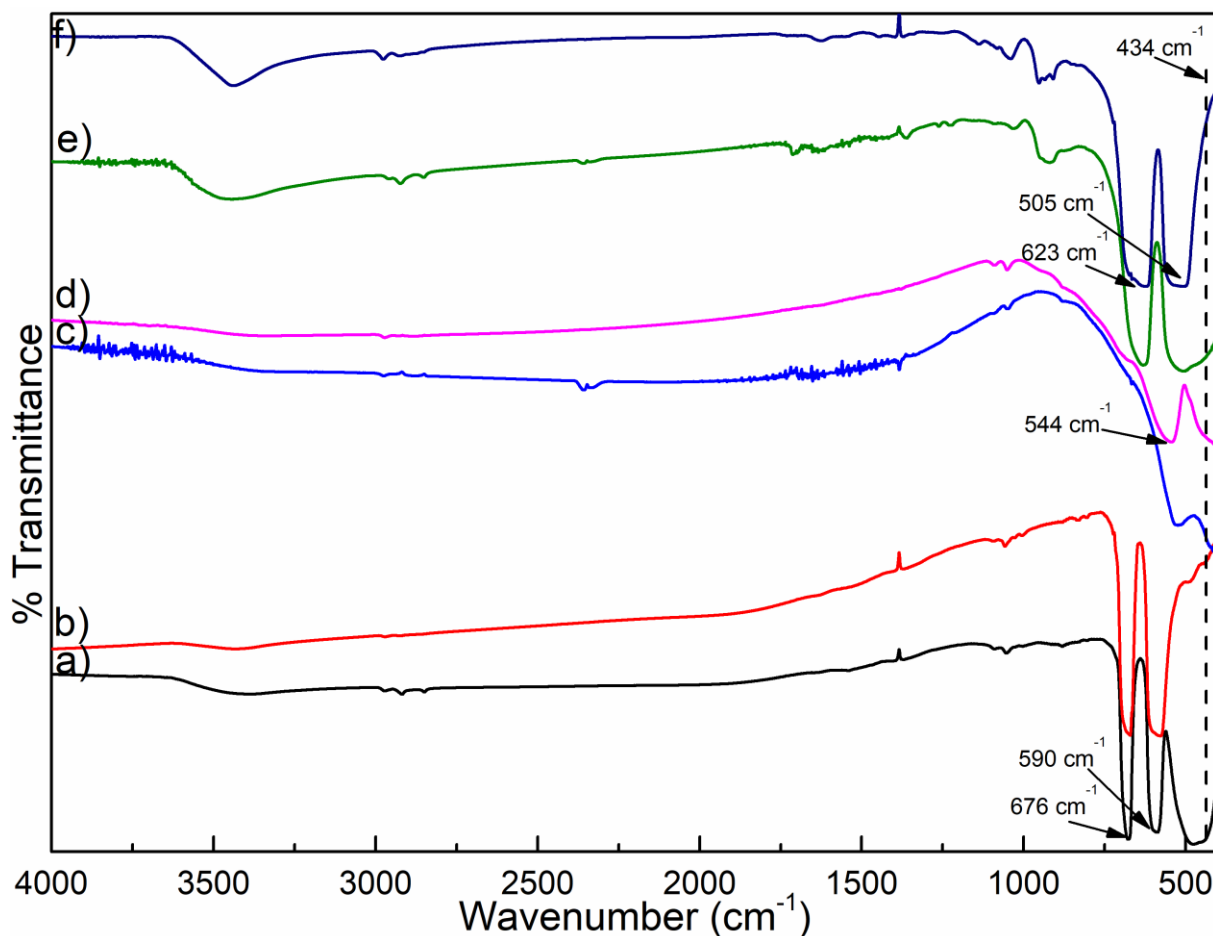


Fig. 5- 2. FTIR spectra of fresh catalyst: a) Zn₂CoO, b) ZnCo₂O, c) Zn₂FeO, d) ZnFe₂O, e) Zn₂CrO and f) ZnCr₂O.

To investigate the chemisorption properties (acidity and basicity) of these fresh catalysts, we determined the number of surface acidic sites and surface basic sites using the TPD- NH₃ and TPD-CO₂ methods, respectively. TPD-CO₂ and TPD- NH₃ profiles of the catalysts are plotted in Fig. 5- 3 and Fig. 5- 4, and the total numbers of acidic and basic sites are summarized in Table 5- 1. Among the Zn-rich Zn₂MeO catalysts, Zn₂CrO has the greatest number of both acidic sites (0.186 mmol/g) and basic sites (0.157 mmol/g), and the numbers of acidic and basic sites follow the same trend: Zn₂CrO > Zn₂CoO > Zn₂FeO. For the Zn-poor ZnMe₂O catalysts,

the numbers of both acidic and basic sites follow the order of $\text{ZnCr}_2\text{O} > \text{ZnFe}_2\text{O} > \text{ZnCo}_2\text{O}$, and the highest values (acidic site amount = 0.259 mmol/g, and basic site amount = 0.140 mmol/g) are observed for ZnCr_2O . In the literature, high amounts of acidic and basic sites in $\text{ZnO}/\text{ZnAl}_2\text{O}_4$ mixed oxides are attributed to the disordered structure of a partially inverted spinel lattice prepared by the polystyrene-template method [50,91] or citrate complex method [131].

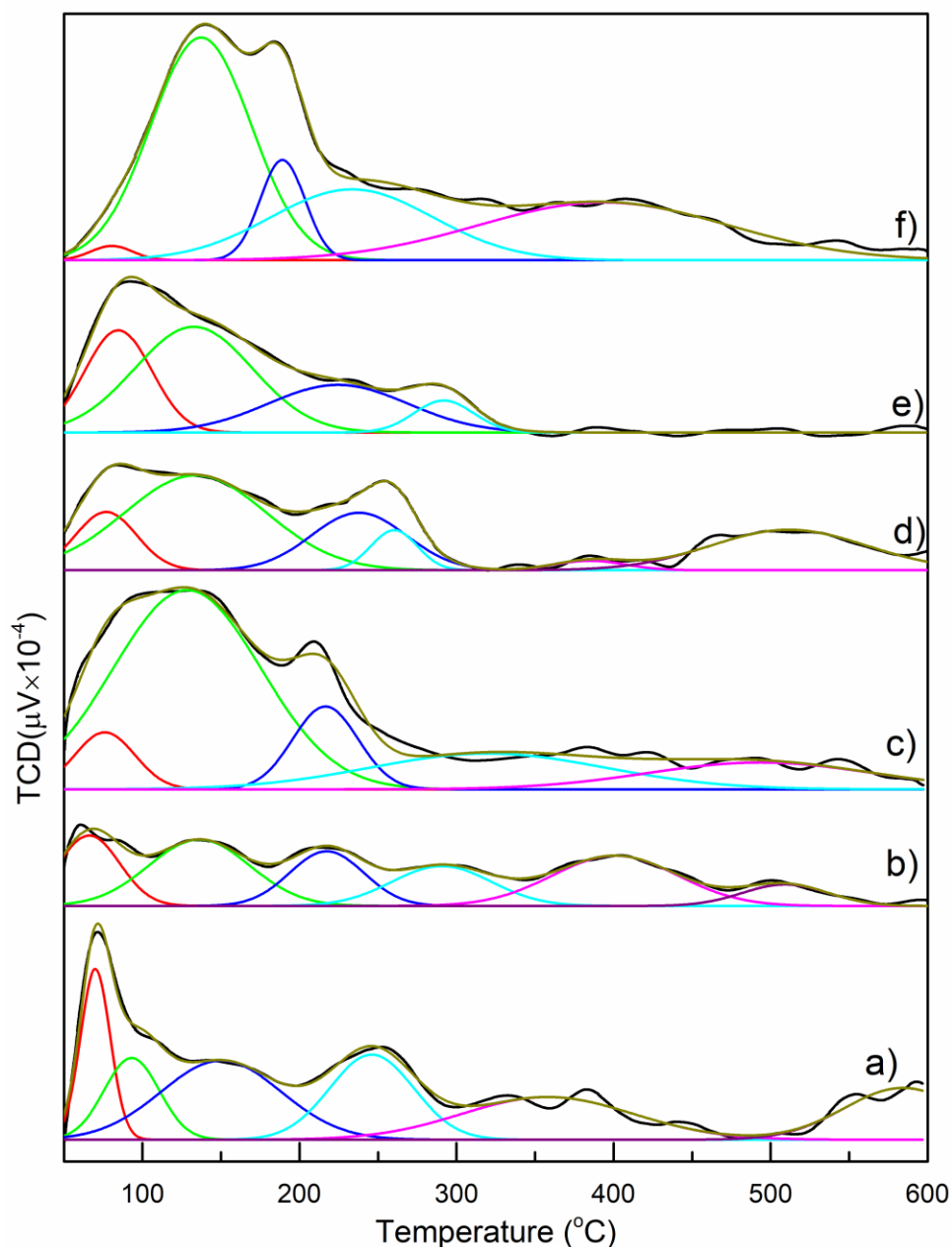


Fig. 5- 3. TPD- CO_2 profiles of fresh catalysts: a) Zn_2CoO , b) Zn_2FeO , c) Zn_2CrO , d) ZnCo_2O , e) ZnFe_2O and f) ZnCr_2O .

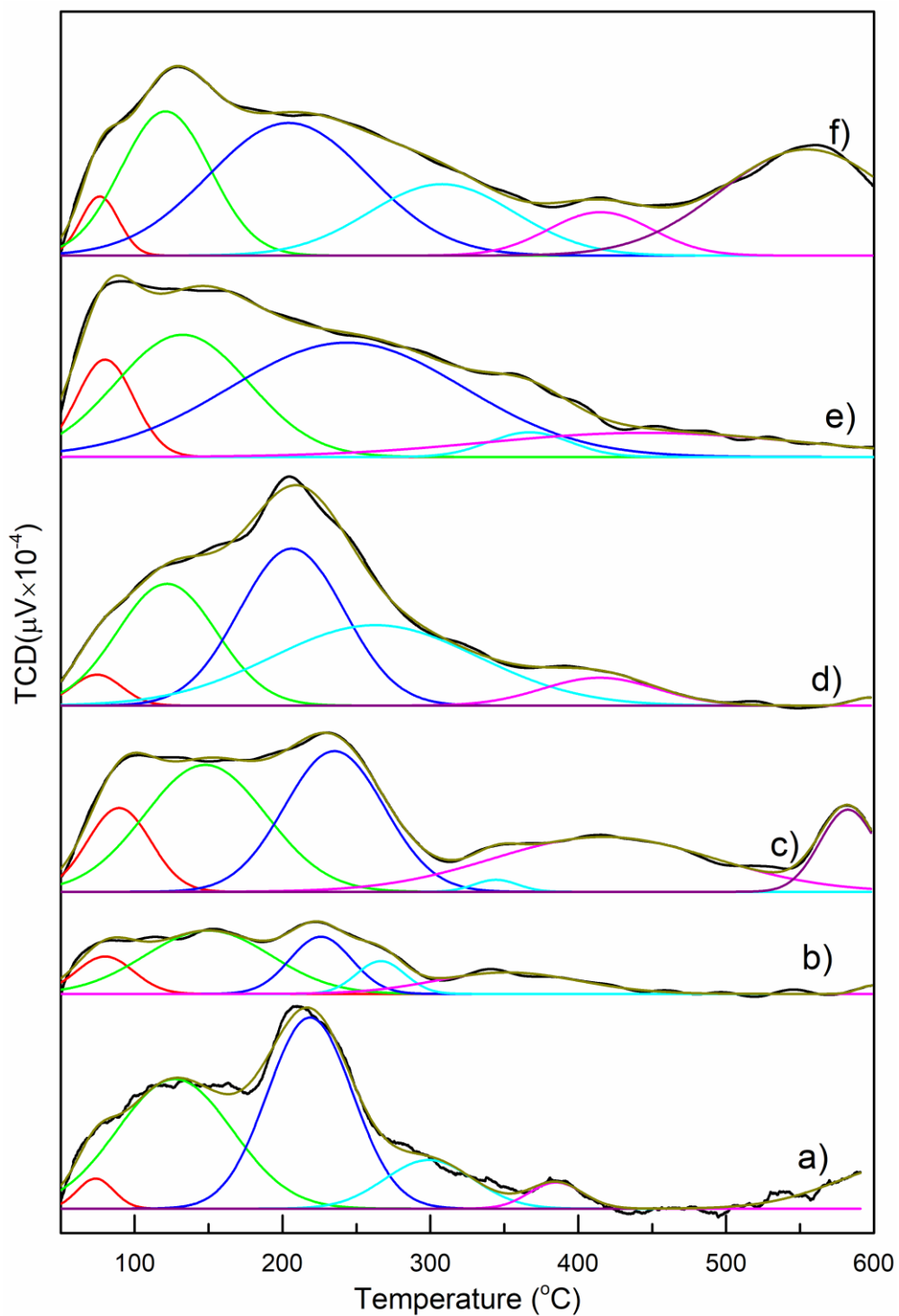


Fig. 5- 4. TPD-NH₃ profiles of fresh catalysts: a) Zn₂CoO, b) Zn₂FeO, c) Zn₂CrO, d) ZnCo₂O, e) ZnFe₂O and f) ZnCr₂O.

Table 5- 1. Acidity and basicity of fresh catalysts

Sample	Acidic Sites (mmol/g)	Basic Sites (mmol/g)
Zn ₂ CoO	0.144	0.113
Zn ₂ FeO	0.081	0.066
Zn ₂ CrO	0.186	0.157
ZnCo ₂ O	0.202	0.082
ZnFe ₂ O	0.225	0.084
ZnCr ₂ O	0.259	0.140

The TPD profiles were deconvoluted to check the relative distributions of acidic sites and basic sites for each catalyst (Fig. 5- 4 and Fig. 5- 3). The strength of deconvoluted acidic and basic sites can be classified as follows: weak strength sites (< 300 °C), medium strength sites (300 – 550 °C) and strong strength sites (> 550 °C) [146–148]. The distributions of individual acidic and basic sites on each fresh catalyst are summarized in Table 5- 2. For the acidity, except the case of Zn₂CrO and ZnCr₂O, other fresh catalysts have a very small amount of strong acidic sites (0.000 – 0.006 mmol/g). The amount of strong acidic sites on Zn₂CrO and ZnCr₂O catalysts are 0.014 and 0.057 mmol/g, respectively. These two Zn₂CrO and ZnCr₂O catalysts also have the highest amount of medium acidic sites (0.046 and 0.059 mmol/g, respectively). As for the basicity, all the catalysts are dominated by the weak and medium basic sites, the strong basic sites only exist on the Zn₂Co catalysts, while the ZnFe₂O catalyst only has the weak basic sites. Comparing to the ZnMe₂O catalysts, the amount of medium acidic sites on Zn₂MeO catalysts is moderately smaller than that on ZnMe₂O catalysts, and the amount of weak acidic sites on Zn₂MeO catalysts is remarkably smaller than that on the ZnMe₂O catalysts. In contrast to the acidity, the amount of medium and strong basic sites on the Zn₂MeO catalysts is slightly larger than that on the ZnMe₂O catalysts. Those results are

relevant to the composition model of the Zn₂MeO catalysts where a layer of amorphous ZnO can partially cover the surface of the ZnMe₂O₄ phase, and relevant to the strength of acidity and basicity on each phase. As the analyzed data in this research, the ZnMe₂O₄ phase is composed of mostly the weak acidic sites and minorly the medium/strong acidic site, that matches the result in the literature [147]. While the ZnO phase is famous for the medium and strong basic sites [148], but not the acidic sites; especially for the ZnO prepared by precipitation method, the total amount of acidic and basic site is small [91]. Therefore, the partial covering of the ZnO phase on the surface of the ZnMe₂O₄ phase of the Zn₂MeO catalysts can cause a decrease in the amount of weak/medium acidic sites and the slight increase of medium/strong basic sites on the Zn₂MeO catalysts comparing to the ZnMe₂O catalysts.

Table 5- 2. Distribution of acidic sites and basic sites on fresh catalysts.

Catalyst	Acidic sites distribution (mmol NH ₃ /g _{cat.})				Basic sites distribution (mmol CO ₂ /g _{cat.})			
	Weak	Medium	Strong	Total	Weak	Medium	Strong	Total
	Zn ₂ CoO	0.133	0.005	0.006	0.144	0.079	0.022	0.012
Zn ₂ FeO	0.067	0.014	0.000	0.081	0.046	0.020	n.d.	0.066
Zn ₂ CrO	0.126	0.046	0.014	0.186	0.115	0.042	n.d.	0.157
ZnCo ₂ O	0.189	0.013	0.001	0.202	0.064	0.018	n.d.	0.082
ZnFe ₂ O	0.189	0.036	n.d.	0.225	0.084	n.d.	n.d.	0.084
ZnCr ₂ O	0.143	0.059	0.057	0.259	0.102	0.038	n.d.	0.140

n.d.: not detected

5.3.2. Glycerolysis of urea over various ZnMeO catalysts: the formation of Zn isocyanate complex in the liquid phase and on the solid catalysts

The reaction results for the glycerolysis of urea over various ZnMe mixed oxide catalysts are summarized in Table 5- 3. The Zn-rich Zn₂MeO catalysts were tested at reaction times of

1 and 3 h while the Zn-poor ZnMe₂O catalysts were investigated at longer reaction times (3 and 5 h) since the ZnMe₂O catalysts exhibit lower catalytic reaction rates than the Zn₂MeO catalysts. The relationship between the glycerol conversion and GC yield for each catalyst is depicted in Fig. 5- 5. Clearly, the data for the Zn₂MeO catalysts correspond to higher positions with a higher glycerol conversion compared to the results for the ZnMe₂O catalysts. In Fig. 5- 5, data points at a higher position indicate that a higher GC yield or selectivity can be achieved at a given glycerol conversion. For all of the Zn₂MeO catalysts, the highest glycerol conversion and GC yield (glycerol conversion = 76%, GC yield = 57%) was observed for Zn₂CrO at a reaction time of 3 h; meanwhile, the results for the Zn₂CoO and Zn₂FeO catalysts are similar, with glycerol conversion = 74% and GC yield = 52% at a reaction time of 3 h. Among the ZnMe₂O catalysts, the glycerol conversion and GC yield follow the order of ZnFe₂O < ZnCr₂O < ZnCo₂O; the best reaction performance was observed for the ZnCr₂O catalyst at a reaction time of 5 h, with glycerol conversion = 63% and GC yield = 40%.

According to Fujita et al. [51] and Turney et al. [48], in the glycerolysis of urea over Zn-containing catalysts, Zn atoms can leach from the ZnO phase into the liquid phase through a reaction with urea to generate an isocyanate (NCO) complex of Zn, which is an active site for the reaction. This phenomenon was also confirmed in our previous studies [50,91,131]. Furthermore, we found that NCO complexes adsorbed on the surface acidic sites of the catalyst (ZnAl₂O₄ phase) act as additional active sites to catalyze the reaction. For this reason, we measured the metal cation levels using an ICP-OES instrument (Table 5- 3) and collected FTIR spectra of both the liquid products (Fig. 5- 6) and the spent catalysts (Fig. 5- 7) to identify the existence of an NCO functional vibration.

Table 5- 3. Analysis of liquid products obtained from the glycerolysis of urea over various ZnMe (Me = Co, Cr, and Fe) mixed oxide catalysts and in various reaction time. (Reaction temperature = 140 °C, reaction pressure = 3 kPa, Glycerol/Urea Ratio =1:1). **(2)**: 2,3-dihydroxypropyl carbamate, **(4)**: 4-(hydroxymethyl)oxazolidin-2-one, and **(5)**: (2-oxo-1,3-dioxolan-4-yl)methyl carbamate.

Sample	Reaction time (h)	Glycerol Conv. (%)	GC Yield (%)	Selectivity (%)				Metallic amount in liquid phase (mmol) *			
				GC	(2)	(4)	(5)	Co	Fe	Cr	Zn
Zn ₂ CoO	1	50	34	67	24	7	2	--	--	--	1.50
	3	74	52	71	9	7	14	--	--	--	0.66
Zn ₂ FeO	1	57	41	72	17	10	1	--	--	--	1.43
	3	74	52	70	7	15	8	--	--	--	0.75
Zn ₂ CrO	1	50	38	75	16	7	1	--	--	0.02	2.07
	3	76	57	74	5	13	8	--	--	--	0.99
ZnCo ₂ O	3	50	29	57	28	10	4	0.09	--	--	0.38
	5	63	40	63	17	6	13	0.13	--	--	0.41
ZnFe ₂ O	3	34	18	53	32	11	4	--	--	--	--
	5	47	27	57	20	8	15	--	--	--	--
ZnCr ₂ O	3	37	21	56	32	7	4	--	--	0.02	--
	5	53	33	62	21	4	13	--	--	0.03	--

* Amounts of Zn dissolved in the liquid phase as measured by the ICP-OES method.

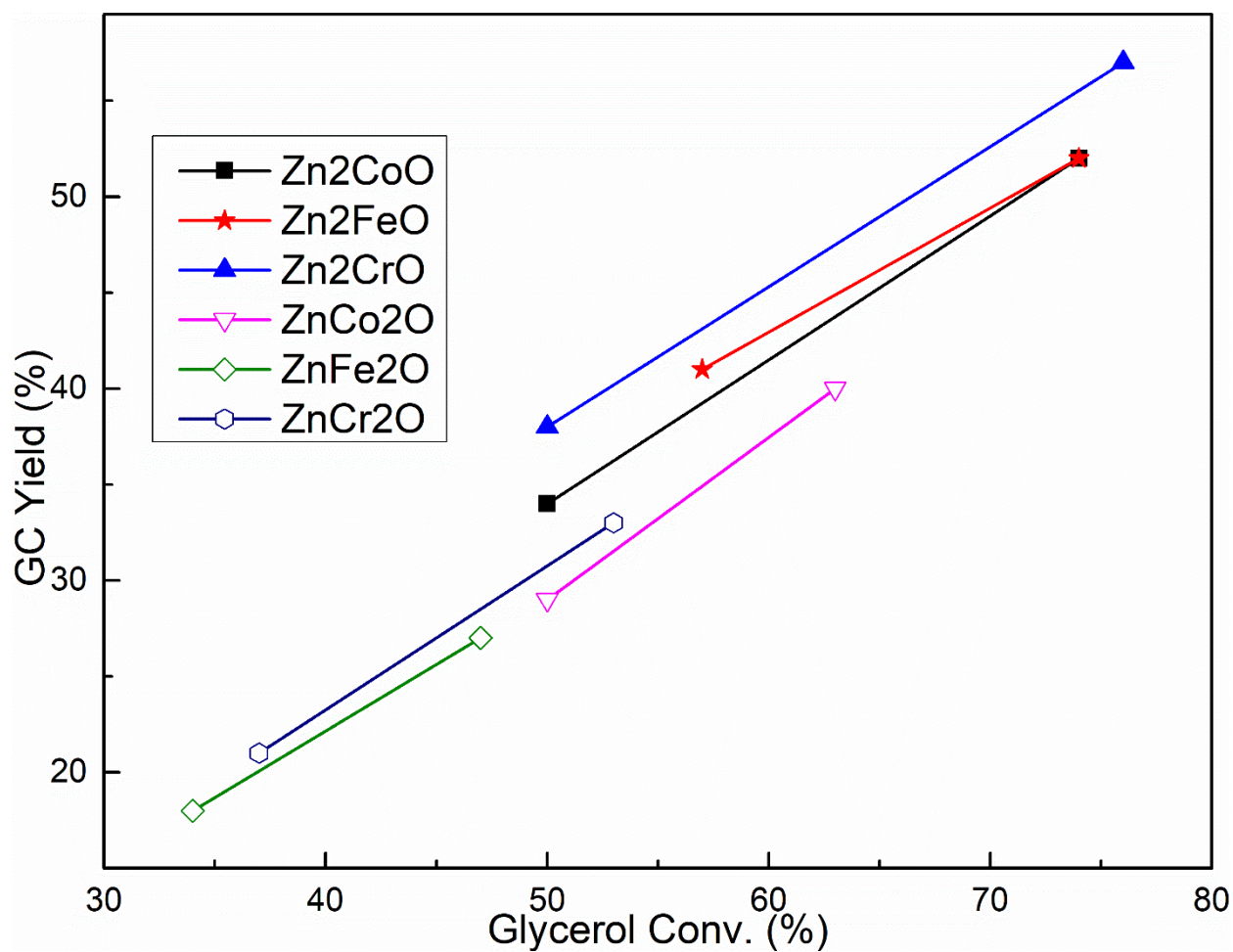


Fig. 5- 5. The relationship of glycerol conversion (%) and GC yield (%) by the glycerolysis of urea over various ZnMe (Me = Co, Cr, and Fe) mixed oxide catalysts and in various reaction time

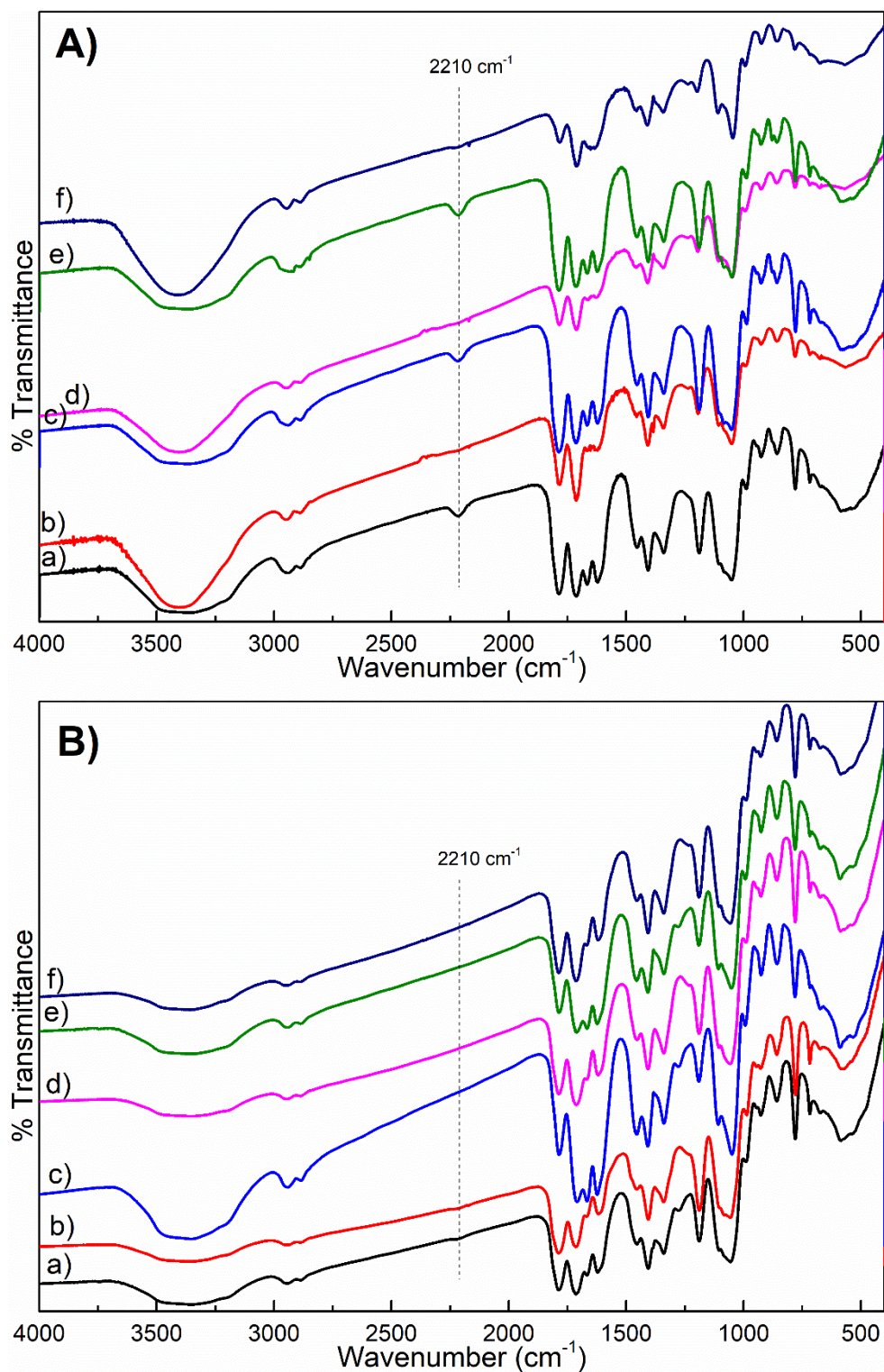


Fig. 5- 6. FTIR spectra of the liquid products obtained from the glycerolysis of urea over different catalysts and different reaction times. **A)**: a) Zn_2CoO -1h, b) Zn_2CoO -3h, c) Zn_2FeO -1h, d) Zn_2FeO -3h, e) Zn_2CrO -1h and f) Zn_2CrO -3h. **B)**: a) ZnCo_2O -3h, b) ZnCo_2O -5h, c) ZnFe_2O -3h, d) ZnFe_2O -5h, e) ZnCr_2O -3h and f) ZnCr_2O -5h.

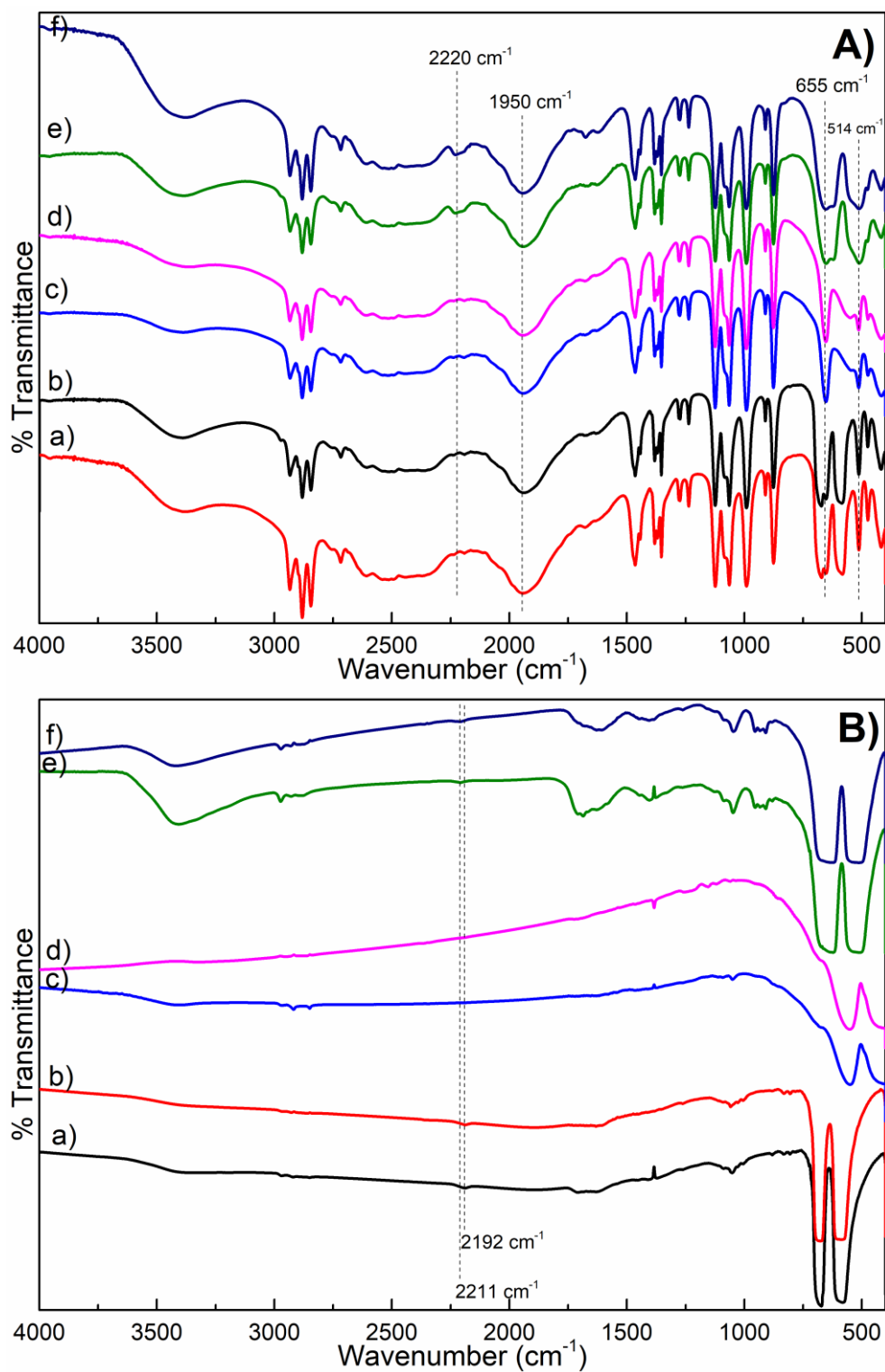


Fig. 5- 7. FTIR spectra of spent catalysts. **A**): a) Zn₂CoO-1h-spent, b) Zn₂CoO-3h-spent, c) Zn₂FeO-1h-spent, d) Zn₂FeO-3h-spent, e) Zn₂CrO-1h-spent and f) Zn₂CrO-3h-spent. **B**): a) ZnCo₂O-3h-spent, b) ZnCo₂O-5h-spent, c) ZnFe₂O-3h-spent, d) ZnFe₂O-5h-spent, e) ZnCr₂O-3h-spent and f) ZnCr₂O-5h-spent.

The ICP results in Table 5- 3 show that Zn atoms are detected in the liquid products for all of the Zn-rich Zn₂MeO catalysts. After a reaction time of 1 h, high levels of Zn are detected: 2.07 mmol for Zn₂CrO, 1.50 mmol for Zn₂CoO, and 1.43 mmol for Zn₂FeO. After a reaction time of 3 h, the level of Zn in the liquid phase for the Zn-rich Zn₂MeO catalysts is lower, resulting from the formation of zinc glycerolate. However, no Fe or Co atoms are detected in the liquid phases of the Zn₂CoO or Zn₂FeO catalysts. Moreover, a negligible amount of Cr (0.02 mmol) is observed in the liquid product of the Zn₂CrO catalyst after a reaction time of 1 h. The level of Cr in the liquid is 100-fold times smaller than the corresponding level of Zn (2.07 mmol) in the liquid and falls to zero after a reaction time of 3 h. The FTIR spectra of the liquid products obtained from the Zn₂MeO catalysts (Fig. 5- 6A) are in good agreement with the ICP results. The peak at 2210 cm⁻¹ can be assigned to the NCO vibration [37,51]. The intensities of the NCO peaks in Fig. 5- 6A follow the same trend as the amount of Zn in the liquid products for the Zn₂MeO catalysts. A peak at 2210 cm⁻¹ is clearly present in the FTIR spectra after a reaction time of 1 h and almost disappears after a reaction time of 3 h. Therefore, we can conclude that for the Zn₂MeO catalysts, the Zn NCO complex exists in the liquid phase for at least 1 h of reaction time.

Fig. 5- 7A displays the FTIR spectra of the spent Zn₂MeO catalysts. All of the typical FTIR peaks of M-O bonding in the spinel ZnMe₂O₄ lattice are detected in the range of 400–680 cm⁻¹. However, the typical peak of Zn-O bonding in the ZnO lattice almost disappears due to the Zn dissolution. Additionally, characteristic peaks for zinc glycerolate appear at 1950 cm⁻¹ (C-O stretching modes with oxygen in hydrogen bonding), 655 cm⁻¹, and 514 cm⁻¹ (Zn-O stretching mode) [126], confirming the formation of zinc glycerolate. Interestingly, the vibration peak of an NCO functional group is detected only in the FTIR spectrum of the spent ZnCr₂O catalyst at 2220 cm⁻¹, which is assigned to the NCO complex adsorbed on the solid surface. These results are consistent with our previous reports on the reaction over

ZnO/ZnAl₂O₄ mixed oxides [50,91,131]. Zn atoms from the ZnO phase can dissolve and react with urea to produce a Zn NCO complex in the liquid phase, providing an active site for a homogeneous reaction route in the glycerolysis of urea. Furthermore, the Zn NCO complex can be adsorbed on the surface acidic sites of the catalyst to form a Zn NCO complex on the surface, which generates another heterogeneous reaction route for the glycerolysis of urea. This interpretation explains the reaction behavior of the Zn-rich Zn₂MeO catalysts (ZnO/ZnMe₂O₄ mixed oxide). The existence of a Zn NCO complex in the liquid phase for all Zn₂MeO catalysts leads to a homogeneous reaction in the liquid phase. In contrast, an additional heterogeneous reaction occurs only over Zn₂CrO *via* the formation of the Zn NCO complex on the solid because the acidity of Zn₂CrO is higher than that of the other Zn₂MeO catalysts (Table 5- 1), and a high surface acidity is necessary for adsorption of the Zn NCO complex on the catalyst surface.

The FTIR spectra of the liquid products from the Zn-poor catalysts (ZnMe₂O) are displayed in Fig. 5- 6B. A vibration band for the NCO functional group at 2210 cm⁻¹ is detected only for the ZnCo₂O catalyst after reaction times of 3 and 5 h. Meanwhile, there is no evidence of an NCO functional group in the FTIR spectra of the liquid products from the ZnFe₂O and ZnCr₂O catalysts. The ICP results in Table 5- 3 reveal an interesting appearance of both Zn and Co atoms in the liquid phase of ZnCo₂O. While the Zn level in the liquid phase of the Zn₂MeO catalysts decreases for longer reaction times, the levels of Zn and Co in the liquid phase of the ZnCo₂O catalyst increase slightly with increasing reaction time. In detail, after a reaction time of 3 h, the levels of Zn and Co in the liquid phase of ZnCo₂O are 0.09 and 0.38 mmol, respectively, and increase to 0.13 and 0.41 mmol for a 5-h reaction time, respectively. In the liquid phase of the ZnFe₂O catalyst, there is no evidence of Zn or Fe atoms in the ICP measurements. For the ZnCr₂O catalyst, only a trace level of Cr atoms is measured in the liquid phase (0.02 mmol at 3 h and 0.03 mmol at 5 h).

Based on the ICP and FTIR results for the liquid products, the ZnFe₂O catalyst does not induce the generation of an NCO complex in the liquid phase. In contrast, for the ZnCo₂O catalyst, both NCO functional groups and Zn/Co atoms are present in the liquid phase, implying an NCO complex of Co and Zn in the liquid phase. In previous works, NCO complexes of Co²⁺ and Co³⁺ have been reported as intermediates of the reduction reaction [149,150] or glycerolysis reaction [48]. Herein, the Co NCO complex can form in the liquid phase in the case of the ZnCo₂O catalyst but not in the case of the Zn₂CoO catalyst because no Co atoms are found in the liquid phase of the Zn₂CoO catalyst, due to the difference in the structures of ZnCo₂O and Zn₂CoO. As previously mentioned, the ZnCo₂O catalyst is composed of a pure normal spinel phase of ZnCo₂O₄ with a predominance of Co³⁺ cations on the outset surface layer. According to the model by Wachs and Routray [109], other layers of Co³⁺ and Zn²⁺ cations can be found below the outset surface layer. In the reaction process over ZnCo₂O, the outer layer of Co³⁺ cations can react with urea and dissolve to the liquid phase, resulting in the further dissolution of Co³⁺ and Zn²⁺ cations in the lower layers. This process renders the ZnCo₂O catalyst unstable and causes a Zn (or Co) NCO complex to appear in the liquid phase. In contrast, the structure of the Zn₂CoO catalyst includes an amorphous layer of ZnO above the spinel phase of ZnCo₂O₄, which can prevent the Co³⁺ cations from leaching into the liquid phase.

The FTIR spectra of the spent Zn-poor ZnMe₂O catalysts are displayed in Fig. 5- 7B. For all three catalysts, the typical vibration peaks of M-O bonding in the spinel ZnMe₂O₄ are unaltered compared to those of the fresh catalysts (even for spent ZnCo₂O, where Zn²⁺ and Co³⁺ cations are dissolved in the liquid phase). However, in the FTIR spectra of spent Zn₂CoO, a small additional vibration band for the NCO functional group is observed at 2192 cm⁻¹, which is redshifted in comparison to the vibration for the spent Zn₂MeO catalysts (2220 cm⁻¹). Turney et al. [48] found that the FTIR vibration of NCO functional groups related to the Co NCO

complex occurred at a lower position compared to that of the NCO functional group related to the Zn NCO complex. Because the NCO functional group of the spent ZnCo₂O catalyst is related to the NCO complexes of both Zn and Co, its vibrational wavenumber is lower than that of Zn₂MeO (NCO functional group of only the Zn NCO complex). In the FTIR spectrum of the spent ZnCr₂O catalyst, a small additional vibration band for the NCO functional group appears at 2211 cm⁻¹, which may be associated with a Cr NCO complex. A reaction between Cr³⁺ and urea to generate an insoluble Cr NCO complex has been previously reported [151,152].

The XRD patterns of the spent catalysts after a reaction time of 3 h are displayed in Fig. 5-8. For the spent Zn-rich Zn₂MeO catalysts, the characteristic peaks for the ZnO phase almost disappear while the peaks for the spinel phase ZnMe₂O₄ remain unchanged. Moreover, typical peaks for the zinc glycerolate phase (JCPDS No. 23-1975, P2₁/c space group) are clearly detected in the XRD patterns of the spent Zn₂MeO catalysts at 10.9°, 17.1°, 20.5°, 23.8°, 24.7°, 27.6°, 27.7°, 36.4°, and 38.2° [104]. Conversely, the XRD patterns of the spent Zn-poor ZnMe₂O catalysts are almost identical to those of the fresh ZnMe₂O catalysts; only typical peaks for the spinel phase ZnMe₂O₄ are detected, without any other phases. The XRD results of the spent catalysts are in good agreement with the FTIR results. That is, the ZnO phase of the Zn₂MeO catalysts disappears with the additional formation of the zinc glycerolate phase after the reaction, whereas the spinel ZnMe₂O₄ phase of the ZnMe₂O catalysts remains unchanged. For the spent ZnCo₂O catalyst, metal glycerolate is not found due to the different oxidation states of the Co cations: Co³⁺ cations in the ZnMe₂O₄ lattice and Co NCO complex and Co²⁺ cations in cobalt glycerolate [85,153].

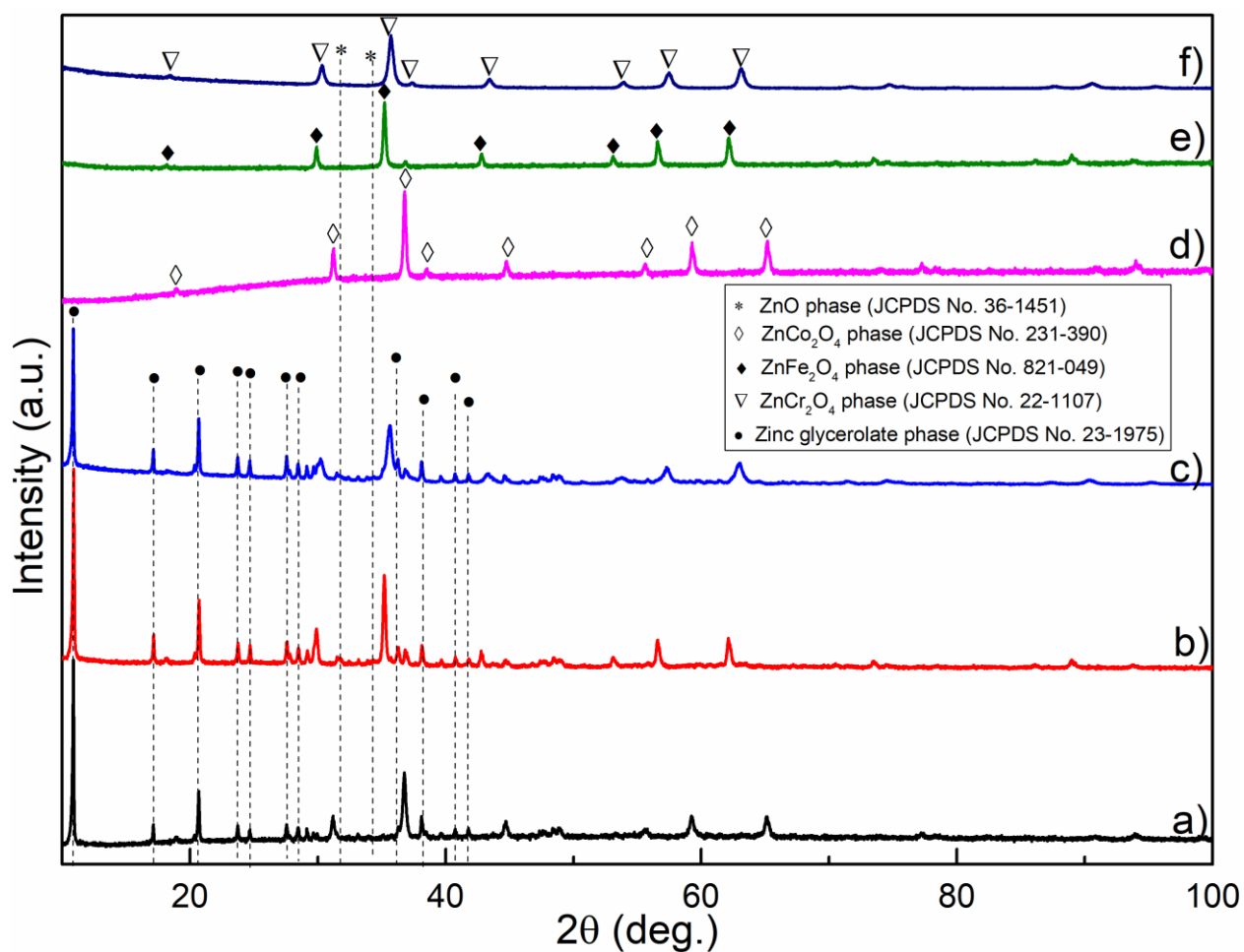


Fig. 5- 8. XRD patterns of spent catalysts: a) Zn₂CoO-3h-spent, b) Zn₂FeO-3h-spent, c) ZnCo₂O-3h-spent, d) Zn₂CrO-3h-spent, e) ZnFe₂O-3h-spent and f) ZnCr₂O-3h-spent.

Based on the TGA analysis, DTGA profiles of the spent catalysts are plotted in Fig. 5- 9 (see Supplementary Data). The DTGA results for the spent catalysts match the XRD and FTIR results. Decomposition peaks of zinc glycerolate are observed in the range of 350–400 °C for the spent Zn₂MeO catalysts [83], and decomposition peaks of metal NCO complex in the range of 200–350 °C are detected for the spent Zn₂CrO, ZnCr₂O, and ZnCo₂O catalysts [131].

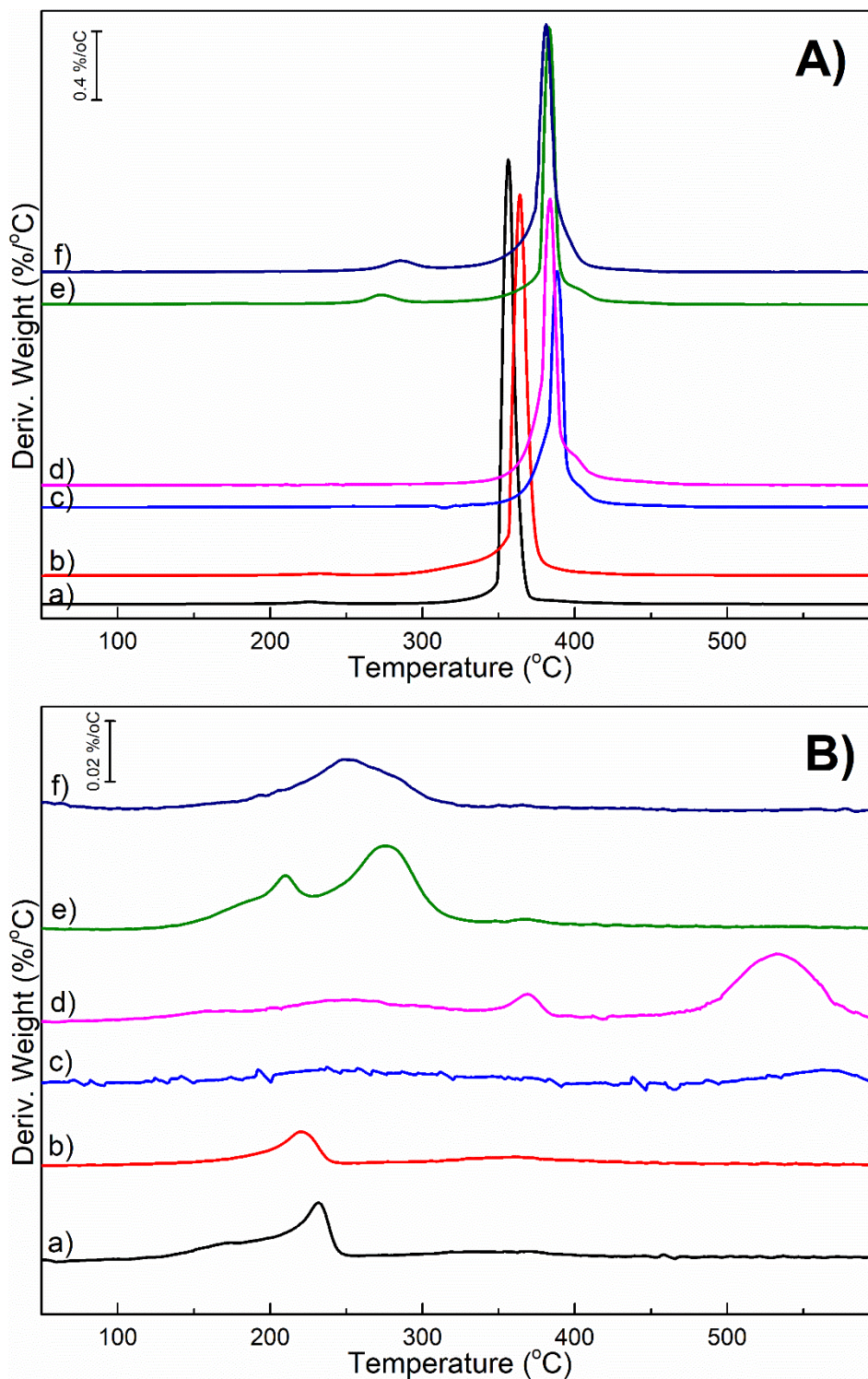


Fig. 5- 9. DTGA profiles of spent catalysts. **A)**: a) Zn_2CoO -3h-spent, b) Zn_2CoO -5h-spent, c) Zn_2FeO -3h-spent, d) Zn_2FeO -5h-spent, e) Zn_2CrO -3h-spent and f) Zn_2CrO -5h-spent. **B)**: a) $ZnCo_2O$ -3h-spent, b) $ZnCo_2O$ -5h-spent, c) $ZnFe_2O$ -3h-spent, d) $ZnFe_2O$ -5h-spent, e) $ZnCr_2O$ -3h-spent and f) $ZnCr_2O$ -5h-spent

5.3.3. Catalytic reaction routes through different NCO complexes

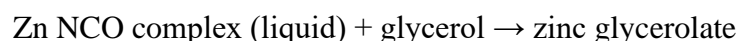
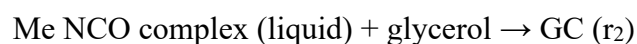
We can summarize the catalytic performance of the various ZnMe mixed oxide catalysts in the glycerolysis of urea in terms of the formation of the NCO complex. Different types of NCO complexes are detected in the liquid phase and on the solid surface of the catalysts, except for the ZnFe₂O catalyst, for which no NCO complex is formed because no metal cations dissolve from the catalyst. In the reaction over the ZnCr₂O catalyst, there is a small amount of Cr NCO complex on the solid phase. For the ZnCo₂O catalyst, NCO complexes of Zn and Co are found in the liquid phase, with a low amount of complexes on the solid surface of the spent catalyst. In contrast, for all of the Zn-rich catalysts, a high level of Zn NCO complexes is clearly detected in the liquid phase for a reaction time of 1 h, indicating Zn dissolution from the ZnO phase in the Zn₂FeO, Zn₂CoO, and Zn₂CrO catalysts. Interestingly, a higher level of Zn NCO complexes is observed on the solid surface only for the Zn₂CrO catalyst, due to its higher surface acidity/basicity and the occurrence of ZnO phases.

Based on the reaction mechanism of urea glycerolysis, which has been described elsewhere [50,91,131], we illustrate three primary catalytic reaction routes (r_1 , r_2 , and r_3) in Scheme 5- 1.

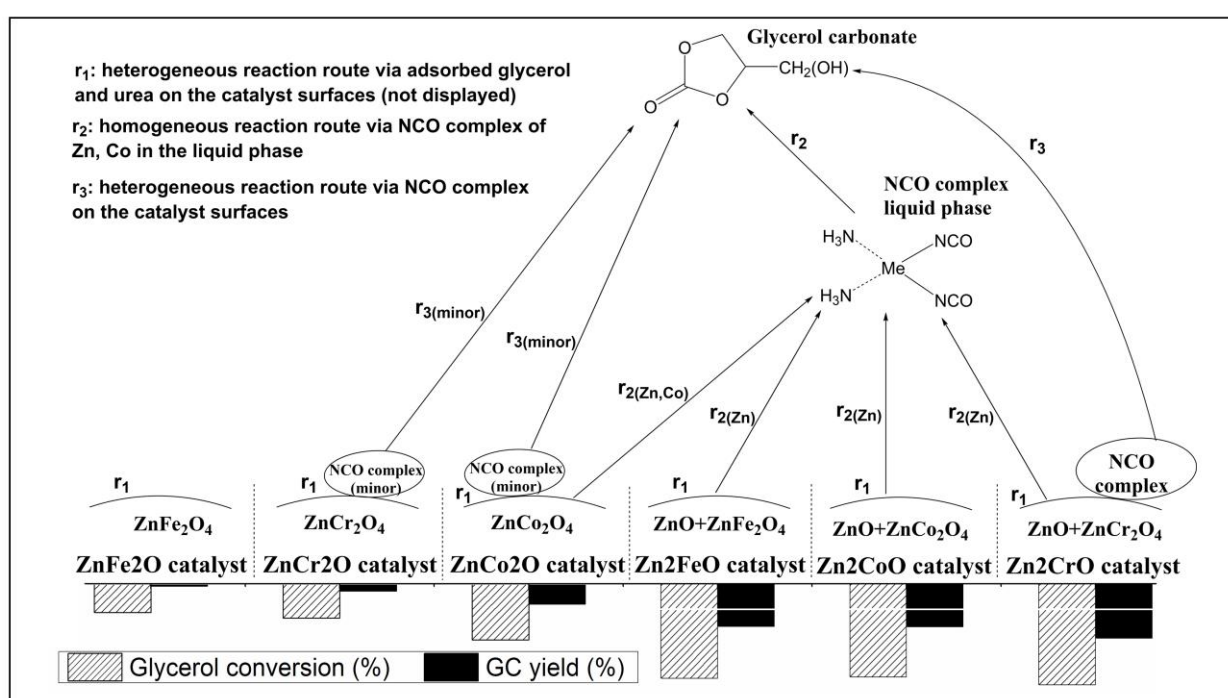
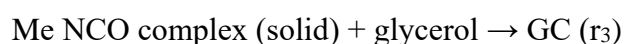
- i) r_1 is a heterogeneous reaction route *via* the adsorption of glycerol and urea on the surface acidic and basic sites of the catalysts [49]. This reaction is the slowest reaction route, resulting in the lowest catalytic performance.



- ii) r_2 is a homogeneous reaction route *via* NCO complexes of Zn or Co in the liquid phase [51,131]. This homogeneous reaction occurs more rapidly than r_1 ; however, the formation of zinc glycerolate as a by-product from the reaction between the Zn NCO complex and glycerol in the liquid phase reduces the number of Zn NCO active sites and the GC selectivity.



- iii) r_3 is another heterogeneous reaction route *via* NCO complexes adsorbed on the surface acidic sites of the catalysts [91,131]. This reaction route can enhance the catalytic reaction performance because there is no formation of zinc glycerolate.



Scheme 5- 1. The reaction routes of the glycerolysis of urea over various ZnMe (Me = Co, Cr, and Fe) mixed oxide catalysts.

The reaction performance of the catalysts can be evaluated on the basis of GC yields, which follow the order of $\text{ZnFe}_2\text{O} < \text{ZnCr}_2\text{O} < \text{ZnCo}_2\text{O} < \text{Zn}_2\text{FeO} < \text{Zn}_2\text{CoO} < \text{Zn}_2\text{CrO}$ in this study. Depending on the NCO complex, different catalytic reaction routes occur for each catalyst. Scheme 5- 1 presents the performance of the catalysts in terms of the catalytic reaction routes (r_1 , r_2 , and r_3) as follows:

- ZnFe₂O (glycerol conversion = 34%, GC yield = 18%): r_1 route only.

- ZnCr₂O (glycerol conversion = 37%, GC yield = 21%): r₁ (main route) + r₃ (minor route).
- ZnCo₂O (glycerol conversion = 50%, GC yield = 28%): r₁ (main route) + r₂ + r₃ (minor route).
- Zn₂FeO and Zn₂CrO (glycerol conversion = 74%, GC yield = 52%): r₁ (minor route) + r₂ (main route).
- Zn₂CrO (glycerol conversion = 76%, GC yield = 57%): r₁ (minor route) + r₂ (main route) + r₃.

5.4. Conclusion

Various Zn-containing mixed oxide catalysts with different secondary metals (Me = Cr, Co, Fe) were successfully prepared by the co-precipitation method with two Zn/Me ratios, resulting in Zn-rich and Zn-poor catalysts. Depending on the Zn content and the nature of the metal ions, the structures of the Zn-containing phases differed, resulting in various types of NCO complexes in the liquid phase and on the solid surface. The formation of the NCO complex strongly influenced the catalytic route in urea glycerolysis. The Zn₂CrO catalyst achieved the best catalytic reaction performance because of the high level of NCO complex in the liquid phase and the unique formation of the adsorbed NCO complex due to the high surface acidity.

CHAPTER 6. SUMMARY AND RECOMMENDATIONS FOR FUTURE WORK

6.1. Summary

My research has focused on the reaction of glycerol with urea over Zn-containing mixed oxide catalysts to produce the heterocycle glycerol carbonate (4-hydroxymethyl-1,3-dioxolan-2-one). Glycerol is a cheap by-product of the biodiesel industry, and glycerol carbonate is a value-added derived product.

The reaction is catalyzed by the mixed oxide catalysts of Zn/Al and follows both the homogeneous and heterogeneous reaction routes. While the heterogeneous reaction route is conducted by the adsorption of glycerol and urea on the surface acidic/basic sites of catalyst, the homogeneous reaction route is catalyzed by an isocyanate (NCO) metal-organic complex of Zn. The homogeneous route achieves a superior reaction performance than the heterogeneous reaction route. Interestingly, the NCO complex of Zn also can be adsorbed and deposited on the Lewis acidic site of surface catalysts and can contribute an additional heterogeneous reaction route which increases the reaction result comparing to the only homogeneous catalyst.

The combined interaction between ligands of complex (the isocyanate (NCO) ligand and the ammine (NH₃) ligand) and glycerol can produce the glycerol carbonate. Therefore, both the complex in the liquid phase and the complex on the surface of the catalyst can catalyze the reaction.

The surface acidity of the ZnAl₂O₄ comes from the inversion of the disordered lattice structure. During catalysts preparation, a disordered bulk ZnAl₂O₄ phase generated disordered sites on the surface: the Al³⁺ cations substituting for Zn²⁺ cations at the tetrahedral sites and the surface oxygen vacancy corresponding to Zn²⁺ cations substituting for Al³⁺ cations at the

octahedral sites. The substituted surface Al^{3+} can more easily adsorb and fix the NCO complex of Zn.

The dual heterogeneous and homogeneous reaction mechanism can be extended to other ZnMe catalysts (Me = Co, Cr, Fe). The Zn_2Cr mixed oxide catalysts can achieve the highest reaction performance due to the contribution of reaction routes over both NCO complexes in the liquid phase and on the solid phase, while the $ZnFe_2$ (without NCO complexes) shows the slowest reaction rate.

6.2. Recommendations for future work

- The homogeneous reaction route can enhance significantly the reaction rate through the isocyanate complex of Zn or Co. However, the limitation of this reaction route is the separation of liquid products from the dissolved active sites after the reaction. Immobilization of isocyanate complex on a support can be a solution where the complexes will not dissolve into the liquid phase but still catalyze the reaction.

- The selectivity of the by-product (2) - 2,3-dihydroxypropyl carbamate of the reaction following the heterogeneous reaction route is high, which implies that the reaction from (2) to glycerol carbonate is the limited step of the whole reaction. Therefore, it's necessary to add an active site for the intramolecular chemical reaction to remove the ammonia group of (2) and form the cyclic glycerol carbonate. An acidic catalyst with a suitable strength can be the candidates for this reaction.

- Spinel structure is a large group with several options for the metallic cations in the lattice, such as Zn, Ni, Fe, Co, Cr, Al, Mg... There are potential research approaches to tune the surface properties (acidity, basicity...) of catalysts by changing the type of cations and monitoring the distribution of cations in the tetrahedral and octahedral sites of the spinel

structure. Other methods to prepare a porous & high surface area spinel catalyst with the desired surface properties can be studied more.

REFERENCES

- [1] The Global Risks Report 2019, 14th Edition, Geneva, 2019. <https://www.weforum.org/reports/the-global-risks-report-2019> (accessed October 20, 2019).
- [2] W.R.L. Anderegg, J.W. Prall, J. Harold, S.H. Schneider, *Proc. Natl. Acad. Sci. U. S. A.* 107 (2010) 12107–9.
- [3] F. Cherubini, N.D. Bird, A. Cowie, G. Jungmeier, B. Schlamadinger, S. Woess-Gallasch, *Resour. Conserv. Recycl.* 53 (2009) 434–447.
- [4] T.R. Karl, K.E. Trenberth, *Science* (80-.). 302 (2003) 1719–1723.
- [5] M.R. Raupach, G. Marland, P. Ciais, C. Le Quéré, J.G. Canadell, G. Klepper, C.B. Field, *Proc. Natl. Acad. Sci. U. S. A.* 104 (2007) 10288–93.
- [6] P.U. Clark, J.D. Shakun, S.A. Marcott, A.C. Mix, M. Eby, S. Kulp, A. Levermann, G.A. Milne, P.L. Pfister, B.D. Santer, D.P. Schrag, S. Solomon, T.F. Stocker, B.H. Strauss, A.J. Weaver, R. Winkelmann, D. Archer, E. Bard, A. Goldner, K. Lambeck, R.T. Pierrehumbert, G.-K. Plattner, *Nat. Clim. Chang.* 6 (2016) 360–369.
- [7] N. Abas, A. Kalair, N. Khan, *Futures* 69 (2015) 31–49.
- [8] N. Heidari, J.M. Pearce, *Renew. Sustain. Energy Rev.* 55 (2016) 899–908.
- [9] C.A.G. Quispe, C.J.R. Coronado, J.A. Carvalho Jr., *Renew. Sustain. Energy Rev.* 27 (2013) 475–493.
- [10] A. Abbaszaadeh, B. Ghobadian, M.R. Omidkhah, G. Najafi, *Energy Convers. Manag.* 63 (2012) 138–148.
- [11] I. Ambat, V. Srivastava, M. Sillanpää, *Renew. Sustain. Energy Rev.* 90 (2018) 356–369.
- [12] N.N.A.N. Yusuf, S.K. Kamarudin, Z. Yaakub, *Energy Convers. Manag.* 52 (2011) 2741–2751.
- [13] M. Johnston, T. Holloway, *Environ. Sci. Technol.* 41 (2007) 7967–7973.
- [14] N. Masoumifard, P.M. Arnal, S. Kaliaguine, F. Kleitz, *ChemSusChem* 8 (2015) 2093–2105.
- [15] A. Sivasamy, K.Y. Cheah, P. Fornasiero, F. Kemausuor, S. Zinoviev, S. Miertus, *ChemSusChem* 2 (2009) 278–300.
- [16] J.P.W. Scharlemann, W.F. Laurance, *Science* (80-.). 319 (2008) 43–44.
- [17] S.S. Yazdani, R. Gonzalez, *Curr. Opin. Biotechnol.* 18 (2007) 213–219.
- [18] M. Ayoub, A.Z. Abdullah, *Renew. Sustain. Energy Rev.* 16 (2012) 2671–2686.
- [19] Production Statistics - Biodiesel.org, U.S. Natl. Biodiesel Board. (2019).

- <http://biodiesel.org/production/production-statistics> (accessed December 25, 2019).
- [20] X. Fan, R. Burton, *Open Fuels Energy Sci. J.* 2 (2009) 100–109.
- [21] N. Dimitratos, J.A. Lopez-Sanchez, J.M. Anthonykutty, G. Brett, A.F. Carley, R.C. Tiruvalam, A.A. Herzing, C.J. Kiely, D.W. Knight, G.J. Hutchings, *Phys. Chem. Chem. Phys.* 11 (2009) 4952.
- [22] G.L. Brett, Q. He, C. Hammond, P.J. Miedziak, N. Dimitratos, M. Sankar, A.A. Herzing, M. Conte, J.A. Lopez-Sanchez, C.J. Kiely, D.W. Knight, S.H. Taylor, G.J. Hutchings, *Angew. Chemie Int. Ed.* 50 (2011) 10136–10139.
- [23] N. Dimitratos, J.A. Lopez-Sanchez, G.J. Hutchings, *Top. Catal.* 52 (2009) 258–268.
- [24] Y. Nakagawa, Y. Shinmi, S. Koso, K. Tomishige, *J. Catal.* 272 (2010) 191–194.
- [25] F. Frusteri, F. Arena, G. Bonura, C. Cannilla, L. Spadaro, O. Di Blasi, *Appl. Catal. A Gen.* 367 (2009) 77–83.
- [26] J.R. Ochoa-Gómez, O. Gómez-Jiménez-Aberasturi, C. Ramírez-López, M. Belsué, *Org. Process Res. Dev.* 16 (2012) 389–399.
- [27] Y. Chernyak, J.H. Clements, *J. Chem. Eng. Data* 49 (2004) 1180–1184.
- [28] M.O. Sonnati, S. Amigoni, E.P. Taffin de Givenchy, T. Darmanin, O. Choulet, F. Guittard, *Green Chem.* 15 (2013) 283–306.
- [29] W.K. Teng, G.C. Ngoh, R. Yusoff, M.K. Aroua, *Energy Convers. Manag.* 88 (2014) 484–497.
- [30] S. Christy, A. Noschese, M. Lomelí-Rodríguez, N. Greeves, J.A. Lopez-Sanchez, *Curr. Opin. Green Sustain. Chem.* 14 (2018) 99–107.
- [31] Q. Li, W. Zhang, N. Zhao, W. Wei, Y. Sun, *Catal. Today* 115 (2006) 111–116.
- [32] X. Song, D. Pan, Y. Wu, P. Cheng, R. Wei, L. Gao, J. Zhang, G. Xiao, *J. Alloys Compd.* 750 (2018) 828–837.
- [33] Y. Li, J. Liu, D. He, *Appl. Catal. A Gen.* 564 (2018) 234–242.
- [34] A. Takagaki, K. Iwatani, S. Nishimura, K. Ebitani, *Green Chem.* 12 (2010) 578.
- [35] M.S. Khayoon, B.H. Hameed, *Appl. Catal. A Gen.* 466 (2013) 272–281.
- [36] K. Shukla, V.C. Srivastava, *RSC Adv.* 6 (2016) 32624–32645.
- [37] W. Zhao, W. Peng, D. Wang, N. Zhao, J. Li, F. Xiao, W. Wei, Y. Sun, *Catal. Commun.* 10 (2009) 655–658.
- [38] A. Devarajan, S. Thiripuranthagan, R. Radhakrishnan, S. Kumaravel, *J. Nanosci. Nanotechnol.* 18 (2018) 4588–4599.
- [39] M. Aresta, A. Dibenedetto, F. Nocito, C. Pastore, *J. Mol. Catal. A Chem.* 257 (2006) 149–153.

- [40] H. Li, D. Gao, P. Gao, F. Wang, N. Zhao, F. Xiao, W. Wei, Y. Sun, *Catal. Sci. Technol.* 3 (2013) 2801.
- [41] C. Park, H. Nguyen-Phu, E.W. Shin, *Mol. Catal.* 435 (2017) 99–109.
- [42] F.D. Bobbink, P.J. Dyson, *J. Catal.* 343 (2016) 52–61.
- [43] J. Hu, Y. Gu, Z. Guan, J. Li, W. Mo, T. Li, G. Li, *ChemSusChem* 4 (2011) 1767–1772.
- [44] B. Gabriele, R. Mancuso, G. Salerno, L. Veltri, M. Costa, A. Dibenedetto, *ChemSusChem* 4 (2011) 1778–1786.
- [45] X. Song, Y. Wu, D. Pan, J. Zhang, S. Xu, L. Gao, R. Wei, G. Xiao, *J. CO₂ Util.* 28 (2018) 326–334.
- [46] J.-H. Park, J.S. Choi, S.K. Woo, S.D. Lee, M. Cheong, H.S. Kim, H. Lee, *Appl. Catal. A Gen.* 433–434 (2012) 35–40.
- [47] H. Nguyen-Phu, C. Park, E.W. Shin, *Catal. Commun.* 85 (2016) 52–56.
- [48] T.W. Turney, A. Patti, W. Gates, U. Shaheen, S. Kulasegaram, *Green Chem.* 15 (2013) 1925.
- [49] M.J. Climent, A. Corma, P. De Frutos, S. Iborra, M. Noy, A. Velty, P. Concepción, *J. Catal.* 269 (2010) 140–149.
- [50] H. Nguyen-Phu, C. Park, E.W. Shin, *Appl. Catal. A Gen.* 552 (2018) 1–10.
- [51] S.I. Fujita, Y. Yamanishi, M. Arai, *J. Catal.* 297 (2013) 137–141.
- [52] M. Aresta, A. Dibenedetto, F. Nocito, C. Ferragina, *J. Catal.* 268 (2009) 106–114.
- [53] L. Wang, Y. Ma, Y. Wang, S. Liu, Y. Deng, *Catal. Commun.* 12 (2011) 1458–1462.
- [54] F. Rubio-Marcos, V. Calvino-Casilda, M.A. Bañares, J.F. Fernandez, *J. Catal.* 275 (2010) 288–293.
- [55] Y.B. Ryu, J.H. Baek, Y. Kim, M.S. Lee, *J. Nanosci. Nanotechnol.* 15 (2015) 321–325.
- [56] C. Hammond, J.A. Lopez-Sanchez, M. Hasbi Ab Rahim, N. Dimitratos, R.L. Jenkins, A.F. Carley, Q. He, C.J. Kiely, D.W. Knight, G.J. Hutchings, *Dalt. Trans.* 40 (2011) 3927.
- [57] K. Jagadeeswaraiyah, C.R. Kumar, P.S.S. Prasad, S. Loidant, N. Lingaiah, *Appl. Catal. A Gen.* 469 (2014) 165–172.
- [58] M. Hasbi Ab Rahim, Q. He, J. a. Lopez-Sanchez, C. Hammond, N. Dimitratos, M. Sankar, A.F. Carley, C.J. Kiely, D.W. Knight, G.J. Hutchings, *Catal. Sci. Technol.* 2 (2012) 1914.
- [59] J. Li, T. Wang, *J. Chem. Thermodyn.* 43 (2011) 731–736.
- [60] W.M. Haynes, D.R. Lide, T.J. Bruno, *CRC Handbook of Chemistry and Physics : A Ready-Reference Book of Chemical and Physical Data.*, 97th ed., CRC Press, 2016.

- [61] C. Nguyen-Huy, V.H. Pham, D.K. Kim, D.-W. Kim, S.H. Oh, J.S. Chung, W.-J. Kim, E.W. Shin, *Appl. Catal. A Gen.* 468 (2013) 305–312.
- [62] K.C. Pratt, V. Christoverson, *Fuel* 61 (1982) 460–462.
- [63] E. Saputra, S. Muhammad, H. Sun, H.M. Ang, M.O. Tadé, S. Wang, *Catal. Today* 190 (2012) 68–72.
- [64] C. Nguyen-Huy, H. Kim, H. Kweon, D.K. Kim, D.W. Kim, S.H. Oh, E.W. Shin, *Chem. Eng. Technol.* 36 (2013) 1365–1370.
- [65] K.S.W. Sing, *Pure Appl. Chem.* 57 (1985) 603–619.
- [66] X. Zhao, L. Wang, X. Xu, X. Lei, S. Xu, F. Zhang, *AIChE J.* 58 (2012) 573–582.
- [67] L. Zhang, J. Yan, M. Zhou, Y. Yang, Y.-N.N. Liu, *Appl. Surf. Sci.* 268 (2013) 237–245.
- [68] V. Calvino-Casilda, G. Mul, J.F. Fernández, F. Rubio-Marcos, M.A. Bañares, J.F. Fernández, F. Rubio-Marcos, M. a. Bañares, *Appl. Catal. A Gen.* 409–410 (2011) 106–112.
- [69] M. Aresta, A. Dibenedetto, C. Devita, O.A. Bourova, O.N. Chupakhin, in: *Stud. Surf. Sci. Catal.*, Elsevier, 2004, pp. 213–220.
- [70] F.N. Pei, L. Li, S. Wang, Z. Zhu, G. Lu, Z. Yan, P.F. Ng, S. Wang, Z. Zhu, G. Lu, Z. Yan, *Environ. Sci. Technol.* 41 (2007) 3758–3762.
- [71] P. Liu, M. Derchi, E.J.M. Hensen, *Appl. Catal. B Environ.* 144 (2014) 135–143.
- [72] J.J. Woodford, J.-P. Dacquin, K. Wilson, A.F. Lee, *Energy Environ. Sci.* 5 (2012) 6145.
- [73] N.L. Finčur, J.B. Krstić, F.S. Šibul, D. V. Šojić, V.N. Despotović, N.D. Banić, J.R. Agbaba, B.F. Abramović, *Chem. Eng. J.* 307 (2017) 1105–1115.
- [74] L.T. Do, C. Nguyen-Huy, E.W. Shin, *Appl. Catal. A Gen.* 525 (2016) 23–30.
- [75] J.D. Martin, *DL GR 1001* (2004) 105.
- [76] X. Wu, M. Kang, Y. Yin, F. Wang, N. Zhao, F. Xiao, W. Wei, Y. Sun, *Appl. Catal. A Gen.* 473 (2014) 13–20.
- [77] H. Zou, J. Shen, *Thermochim. Acta* 351 (2000) 165–170.
- [78] J.R. Ochoa-Gómez, O. Gómez-Jiménez-Aberasturi, C. Ramírez-López, B. Maestro-Madurga, *Green Chem.* 14 (2012) 12–14.
- [79] D. Wang, X. Zhang, T. Cheng, J. Wu, Q. Xue, *AIMS Energy* 2 (2014) 399–409.
- [80] L. Wan, H. Liu, D. Skala, *Appl. Catal. B Environ.* 152–153 (2014) 352–359.
- [81] R.M. Taylor, A.J. Brock, *Pharmaceutical Compound Zinc Glycerolate Complex Prepared by Reacting Zinc Oxide and Glycerol*, US4544761 A, 1985.
- [82] F. da Silva Lisboa, F.R. da Silva, L.P. Ramos, F. Wypych, *Catal. Letters* 143 (2013) 1235–1239.

- [83] D.M. Reinoso, D.E. Damiani, G.M. Tonetto, *Appl. Catal. B Environ.* 144 (2014) 308–316.
- [84] R. Moleski, E. Leontidis, F. Krumeich, *J. Colloid Interface Sci.* 302 (2006) 246–253.
- [85] E. Radoslovich, M. Raupach, P. Slade, R. Taylor, *Aust. J. Chem.* 23 (1970) 1963.
- [86] H.G.M. Edwards, D.W. Farwell, I.R. Lewis, N. Webb, *J. Mol. Struct.* 271 (1992) 27–36.
- [87] F. Yin, A.L. Blumenfeld, V. Gruver, J.J. Fripiat, *J. Phys. Chem. B* 101 (1997) 1824–1830.
- [88] H. An, X. Zhao, L. Guo, C. Jia, B. Yuan, Y. Wang, *Appl. Catal. A Gen.* 433–434 (2012) 229–235.
- [89] P. Sharma, R. Dwivedi, R. Dixit, R. Prasad, *Ind. Eng. Chem. Res.* 52 (2013) 10977–10987.
- [90] H. Dong, C. Feldmann, *J. Alloys Compd.* 513 (2012) 125–129.
- [91] H. Nguyen-Phu, E.W. Shin, *Appl. Catal. A Gen.* 561 (2018) 28–40.
- [92] X. Duan, D. Yuan, F. Yu, *Inorg. Chem.* 50 (2011) 5460–5467.
- [93] V.G. Ivanov, M. V. Abrashev, M.N. Iliev, M.M. Gospodinov, J. Meen, M.I. Aroyo, *Phys. Rev. B* 82 (2010) 024104.
- [94] L. Chen, X. Sun, Y. Liu, K. Zhou, Y. Li, *J. Alloys Compd.* 376 (2004) 257–261.
- [95] H. Jung, T.-T. Pham, E.W. Shin, *Appl. Surf. Sci.* 458 (2018) 369–381.
- [96] X. Duan, D. Yuan, X. Wang, H. Xu, *J. Sol-Gel Sci. Technol.* 35 (2005) 221–224.
- [97] J.R. Jensen, T. Johannessen, S. Wedel, H. Livbjerg, *J. Nanoparticle Res.* 2 (2000) 363–373.
- [98] G. Del Piero, F. Trifiro, A. Vaccari, *J. Chem. Soc., Chem. Commun.* 0 (1984) 656–658.
- [99] E. Errani, F. Trifiro, A. Vaccari, M. Richter, G. Del Piero, *Catal. Letters* 3 (1989) 65–72.
- [100] M. Gomi, N. Oohira, K. Ozaki, M. Koyano, *Japanese J. Appl. Physics, Part 1 Regul. Pap. Short Notes Rev. Pap.* 42 (2003) 481–485.
- [101] T.C. Damen, S.P.S. Porto, B. Tell, *Phys. Rev.* 142 (1966) 570–574.
- [102] M. Koyano, P. QuocBao, L. thi ThanhBinh, L. HongHa, N. NgocLong, S. Katayama, *Phys. Status Solidi* 193 (2002) 125–131.
- [103] G. Xiong, U. Pal, J.G. Serrano, K.B. Ucer, R.T. Williams, *Phys. Status Solidi* 3 (2006) 3577–3581.
- [104] L. Pan, S. Wang, W. Mi, J. Song, J.-J. Zou, L. Wang, X. Zhang, *Nano Energy* 9 (2014) 71–79.

- [105] A.A. Da Silva, A. de Souza Gonçalves, M.R. Davolos, *J. Sol-Gel Sci. Technol.* 49 (2009) 101–105.
- [106] G. Busca, V. Lorenzelli, V.S. Escribano, R. Guidetti, *J. Catal.* 131 (1991) 167–177.
- [107] C. Morterra, G. Magnacca, *Catal. Today* 27 (1996) 497–532.
- [108] H. Song, D. Laudenschleger, J.J. Carey, H. Ruland, M. Nolan, M. Muhler, *ACS Catal.* 7 (2017) 7610–7622.
- [109] I.E. Wachs, K. Routray, *ACS Catal.* 2 (2012) 1235–1246.
- [110] K.G. Tshabalala, S.-H. Cho, J.-K. Park, S.S. Pitale, I.M. Nagpure, R.E. Kroon, H.C. Swart, O.M. Ntwaeaborwa, *J. Alloys Compd.* 509 (2011) 10115–10120.
- [111] P. Druska, U. Steinike, V. Šepelák, *J. Solid State Chem.* 146 (1999) 13–21.
- [112] J.H. Park, Y.C. Cho, J.M. Shin, S.-Y. Cha, C.R. Cho, H.S. Kim, S.J. Yoon, S.-Y. Jeong, S.E. Park, A.-R. Lim, *J. Korean Phys. Soc.* 51 (2007) 1968.
- [113] G. Moretti, *Surf. Interface Anal.* 17 (1991) 745–750.
- [114] D.S.Y. Jayathilake, T.A.N. Peiris, J.S. Sagu, D.B. Potter, K.G.U. Wijayantha, C.J. Carmalt, D.J. Southee, *ACS Sustain. Chem. Eng.* 5 (2017) 4820–4829.
- [115] M. Chen, X. Wang, Y.. Yu, Z.. Pei, X.. Bai, C. Sun, R.. Huang, L.. Wen, *Appl. Surf. Sci.* 158 (2000) 134–140.
- [116] C.-J. Ting, H.-Y. Lu, *J. Am. Ceram. Soc.* 82 (1999) 841–848.
- [117] Y.Y. Tay, S. Li, C.Q. Sun, P. Chen, *Appl. Phys. Lett.* 88 (2006) 173118.
- [118] I.A.P.S. Murthy, C.S. Swamy, *Catal. Letters* 27 (1994) 103–112.
- [119] G. Busca, V. Lorenzelli, G. Ramis, R.J. Willey, *Langmuir* 9 (1993) 1492–1499.
- [120] D.T. Lundie, A.R. McInroy, R. Marshall, J.M. Winfield, P. Jones, C.C. Dudman, S.F. Parker, C. Mitchell, D. Lennon, *J. Phys. Chem. B* 109 (2005) 11592–11601.
- [121] M. Trombetta, G. Busca, M. Lenarda, L. Storaro, R. Ganzerla, L. Piovesan, A. Jimenez Lopez, M. Alcantara-Rodriguez, E. Rodríguez-Castellón, *Appl. Catal. A Gen.* 193 (2000) 55–69.
- [122] K. Sohlberg, S.T. Pantelides, S.J. Pennycook, *J. Am. Chem. Soc.* 123 (2001) 26–29.
- [123] J.T. Mefford, W.G. Hardin, S. Dai, K.P. Johnston, K.J. Stevenson, *Nat. Mater.* 13 (2014) 726–732.
- [124] C. Drouilly, J.-M. Krafft, F. Averseng, H. Lauron-Pernot, D. Bazer-Bachi, C. Chizallet, V. Lecocq, G. Costentin, *Appl. Catal. A Gen.* 453 (2013) 121–129.
- [125] R. Rémiás, Á. Kukovecz, M. Darányi, G. Kozma, S. Varga, Z. Kónya, I. Kiricsi, *Eur. J. Inorg. Chem.* 2009 (2009) 3622–3627.
- [126] J. Das, D. Khushalani, *J. Phys. Chem. C* 114 (2010) 2544–2550.

- [127] O. Jankovský, D. Sedmidubský, P. Šimek, Z. Sofer, P. Ulbrich, V. Bartůněk, *Ceram. Int.* 41 (2015) 595–601.
- [128] L.-B. Zhang, J.-Q. Wang, H.-G. Wang, Y. Xu, Z.-F. Wang, Z.-P. Li, Y.-J. Mi, S.-R. Yang, *Compos. Part A Appl. Sci. Manuf.* 43 (2012) 1537–1545.
- [129] A. Auroux, A. Gervasini, C. Guimon, *J. Phys. Chem. B* 103 (1999) 7195–7205.
- [130] Y. Zhu, J. Hu, J. Wang, *J. Hazard. Mater.* 221–222 (2012) 155–161.
- [131] H. Nguyen-Phu, E.W. Shin, *J. Catal.* 373 (2019) 147–160.
- [132] G.. Kustova, E.. Burgina, G.. Volkova, T.. Yurieva, L.. Plyasova, *J. Mol. Catal. A Chem.* 158 (2000) 293–296.
- [133] D. Sibera, J. Kaszewski, D. Moszyński, E. Borowiak-Paleń, W. Łojkowski, U. Narkiewicz, *Phys. Status Solidi* 7 (2010) 1420–1423.
- [134] S. Chen, Y. Wu, P. Cui, W. Chu, X. Chen, Z. Wu, *J. Phys. Chem. C* 117 (2013) 25019–25025.
- [135] C. Xiangfeng, L. Xingqin, M. Guangyao, *Sensors Actuators B Chem.* 55 (1999) 19–22.
- [136] X. Song, Q. Ru, B. Zhang, S. Hu, B. An, *J. Alloys Compd.* 585 (2014) 518–522.
- [137] Y. Sharma, N. Sharma, G.V. Subba Rao, B.V.R. Chowdari, *Adv. Funct. Mater.* 17 (2007) 2855–2861.
- [138] F. Liu, X. Chu, Y. Dong, W. Zhang, W. Sun, L. Shen, *Sensors Actuators B Chem.* 188 (2013) 469–474.
- [139] J.-H. Kim, H.-M. Jeong, C.W. Na, J.-W. Yoon, F. Abdel-Hady, A.A. Wazzan, J.-H. Lee, *Sensors Actuators B Chem.* 235 (2016) 498–506.
- [140] K.E. Sickafus, J.M. Wills, N.W. Grimes, *J. Am. Ceram. Soc.* 82 (2004) 3279–3292.
- [141] J.K. Burdett, G.D. Price, S.L. Price, *J. Am. Chem. Soc.* 13 (1982) 92–95.
- [142] D. Makovec, A. Kodre, I. Arčon, M. Drogenik, *J. Nanoparticle Res.* 13 (2011) 1781–1790.
- [143] R.D. Shannon, *Acta Crystallogr. Sect. A* 32 (1976) 751–767.
- [144] J. Preudhomme, P. Tarte, *Spectrochim. Acta Part A Mol. Spectrosc.* 27 (1971) 1817–1835.
- [145] M. Samadi, H.A. Shivaee, M. Zanetti, A. Pourjavadi, A. Moshfegh, *J. Mol. Catal. A Chem.* 359 (2012) 42–48.
- [146] Š. Hajduk, V.D.B.C. Dasireddy, B. Likozar, G. Dražić, Z.C. Orel, *Appl. Catal. B Environ.* 211 (2017) 57–67.
- [147] M. Chen, J. Xu, F.-Z. Su, Y.-M. Liu, Y. Cao, H.-Y. He, K.-N. Fan, *J. Catal.* 256 (2008) 293–300.

- [148] J.C. Lavalley, *Catal. Today* 27 (1996) 377–401.
- [149] T. Sun, M.D. Fokema, J.Y. Ying, *Catal. Today* 33 (1997) 251–261.
- [150] T. Montanari, O. Marie, M. Daturi, G. Busca, *Appl. Catal. B Environ.* 71 (2007) 216–222.
- [151] H. -H Schmidtke, T. Schönherr, *ZAAC - J. Inorg. Gen. Chem.* 443 (1978) 225–230.
- [152] T. Schönherr, *Inorg. Chem.* 25 (1986) 171–175.
- [153] S. Gudyka, G. Grzybek, J. Gryboś, P. Indyka, B. Leszczyński, A. Kotarba, Z. Sojka, *Appl. Catal. B Environ.* 201 (2017) 339–347.

LIST OF PUBLICATIONS

- [1] **H. Nguyen-Phu**, C. Park, E.W. Shin, Activated red mud-supported Zn/Al oxide catalysts for catalytic conversion of glycerol to glycerol carbonate: FTIR analysis, *Catalysis communications* 85 (2016) 52–56.
- [2] **H. Nguyen-Phu**, C. Park, E.W. Shin, Dual catalysis over ZnAl mixed oxides in the glycerolysis of urea: Homogeneous and heterogeneous reaction routes, *Applied Catalysis A: General* 552 (2018) 1–10.
- [3] **H. Nguyen-Phu**, E.W. Shin, Investigating time-dependent Zn species over Zn-based catalysts in glycerol carbonylation with urea and their roles in the reaction mechanism, *Applied Catalysis A: General* 561 (2018) 28–40.
- [4] **H. Nguyen-Phu**, E.W. Shin, Disordered structure of ZnAl₂O₄ phase and the formation of a Zn NCO complex in ZnAl mixed oxide catalysts for glycerol carbonylation with urea, *Journal of Catalysis* 373 (2019) 147–160.
- [5] **H. Nguyen-Phu**, L.T. Do, E.W. Shin, Investigation of glycerolysis of urea over various ZnMeO (Me = Co, Cr, and Fe) mixed oxide catalysts, *Catalysis Today* (2019).
- [6] C. Park, **H. Nguyen-Phu**, E.W. Shin, Glycerol carbonation with CO₂ and La₂O₂CO₃/ZnO catalysts prepared by two different methods: Preferred reaction route depending on crystalline structure, *Molecular Catalysis* 435 (2017) 99–109.